Technische Universität München
Lehrstuhl I für Technische Chemie

Towards the Numerical Simulation of Multi-Scale Two-Phase Flows

Dipl.-Ing. Univ. Holger Marschall

Vollständiger Abdruck der von der Fakultät für Chemie der Technischen Universität München zur Erlangung des akademischen Grades eines Doktor-Ingenieurs (Dr.-Ing.) genehmigten Dissertation.

Vorsitzender:	Univ.-Prof. Dr. Karsten Reuter
Prüfer:	1. Univ.-Prof. Dr.-Ing. Kai-Olaf Hinrichsen
	2. Univ.-Prof. Dr.-Ing. Harald Klein
	3. Prof. Dr. sc. Hrvoje Jasak, Universität Zagreb / Kroatien

Die Dissertation wurde am 18.07.2011 bei der Technischen Universität München eingereicht und durch die Fakultät für Chemie am 05.12.2011 angenommen.

Technische Universität München
Lehrstuhl I für Technische Chemie

Towards the Numerical Simulation of Multi-Scale Two-Phase Flows

Zur Numerischen Simulation Mehrskaliger Zweiphasenströmungen

Dipl.-Ing. Univ. Holger Marschall

Vollständiger Abdruck der von der Fakultät für Chemie der Technischen Universität München zur Erlangung des akademischen Grades eines Doktor-Ingenieurs (Dr.-Ing.) genehmigten Dissertation.

Vorsitzender:	Univ.-Prof. Dr. Karsten Reuter
Prüfer:	1. Univ.-Prof. Dr.-Ing. Kai-Olaf Hinrichsen
	2. Univ.-Prof. Dr.-Ing. Harald Klein
	3. Prof. Dr. sc. Hrvoje Jasak, Universität Zagreb / Kroatien

Die Dissertation wurde am 18.07.2011 bei der Technischen Universität München eingereicht und durch die Fakultät für Chemie am 05.12.2011 angenommen.

Acknowledgements

This work has been accomplished at the Chair of Chemical Engineering (Catalysis Research Center, Technische Universität München) where the author had the position of a scientific assistant.

First and foremost, it is with immense gratitude that I acknowledge the support and help of Professor Dr.-Ing. Hinrichsen, my primary advisor. I wish to thank him expressly for his indispensable encouragement and scientific advice through the years. He has always been providing research opportunities being thoroughly characterized by freedom to pursue independent scientific work. I am also indebted to Prof. Polifke, Ph. D., for being available for very enjoyable discussions about forces exerted on fluid particles and interfaces (including their physical interpretation in an volume-averaged framework) as well as conceptual aspects modeling two-phase flows at multiple scales.

Furthermore, my research has always been accompanied by and benefited from numerous students being involved through term, Bachelor's, Diploma and Master's thesis. In particular, I would like to thank Robert Mornhinweg, Andreas Kossmann, Kim Langbein, Sebastian Oberhauser, Claude Labonte, Florian Kraus, Christian Albert, Karl Hupf, Anna Reif, Stephan Grünberger, Thomas Bartesch, Johanna Hable, Georg Rauch, Thomas Höllthaler, Florian Habla, Christian Schüler, Bruno Beban, Korbinian Hinterberger and Tomislav Marić. I am also indebted to my colleague Astrid Mahrla, who always has been available when I wanted to talk about something, and brought a lot of energy and enthusiasm in all common projects. Eventually, my special thanks go out to our invaluable secretary Heidi Holweck, who has made available her support in a number of ways. She was always prepared to help me in bureaucratic matters.

This thesis would not have been possible without the great support of Hrvoje Jasak. I owe my deepest gratitude to him for a telephone conversation we had in the beginning of this work and the initial direction and suggestions for my research. This thesis would never have taken this shape without his favourable attitude and conceptual guidance. My eternal gratitude goes also to him for providing me the opportunity to attend the NUMAP-FOAM (Numerical Modelling of Coupled Problems in Applied Physics with OpenFOAM®) summer school, which has expanded my numerics and programming skills significantly.

Of course, my research would have been impossible without the Open Source CFD toolbox OpenFOAM® providing a reliable and powerful framework for my work. It is OpenFOAM® that has enabled me to realize new conceptual approaches – efficiently transferring them from theory (physics & mathematics) to practice (numerics) in form of flexible models and solvers. Therefore my special thanks go to its principal

developers, Henry G. Weller and Prof. Dr. Hrvoje Jasak, for making it available to public and continuously maintaining its high quality. I further would like to thank all FOAMers: Thanks for your developments using OpenFOAM® technology and all support efforts within the community forums. This work would have been more difficult without your efforts. Special thanks go out to Alberto Passalacqua and Jaswinder Pal Singh for their invaluable input and help.

Finally I would like to express my deepest thanks to my family as well as to my fiancé Julia for putting up with all the times that being busy with research took priority over other activities. Thanks for sharing my joys and frustrations and encouraging me in turn. In particular, I warmly thank Julia for her companionship and great support. She unfailingly has been there for me throughout these years.

Preamble

Munich, February 2011 Holger Marschall

Contents

Acknowledgements V

List of Figures vii

List of Tables ix

Notation & Nomenclature xi

Theory and Development.

1. Introduction 1
- 1.1. Background . . . 1
  - 1.1.1. Interfacial Scale Averaging Techniques . . . 3
  - 1.1.2. Interfacial Scale Resolving Techniques . . . 3
- 1.2. State-of-the-Art & Motivation . . . 6
- 1.3. Scope and Objectives . . . 16

2. Theory 23
- 2.1. Local Instantaneous Bulk Conservation Equations . . . 24
  - 2.1.1. Single-phase Flow . . . 24
  - 2.1.2. Two-phase Flow . . . 28
- 2.2. Local Instantaneous Interfacial Jump Conditions . . . 31
- 2.3. Concept of Conditioning for Phase Discrimination . . . 32
  - 2.3.1. Conditioning and Conditioned Quantities . . . 32
  - 2.3.2. Phase Indicator Function and Phase Distribution Function . . . 33
  - 2.3.3. Interface Delta Function and Interface Transport Equation . . . 34
- 2.4. Averaging Procedures . . . 35
  - 2.4.1. Motivation of Averaging . . . 35
  - 2.4.2. Conceptual Approaches . . . 36
  - 2.4.3. Averaging Rules . . . 38
  - 2.4.4. State-of-the-Art – A critical Review . . . 40
  - 2.4.5. Conclusion, Scope & Objectives . . . 42
- 2.5. Concept of the Conditional Volume-Averaging Technique . . . 44
  - 2.5.1. Averaged Arbitrary General Quantities . . . 44

2.5.2. Analogy of Volume-Averaging Technique and Spatial Filtering in LES . . . 44
2.5.3. Averaged Products and Fluctuations . . . 46
2.5.4. Averaged Phase Indicator Function . . . 48
2.5.5. Averaged Differential Operators . . . 48
2.6. Conditional Volume-Averaged Bulk Conservation Equations . . . 53
2.7. Conditional Volume-Averaged Interfacial Jump Conditions . . . 55
2.8. Volume-averaged Interface Transport Equation . . . 56

3. Closure Framework **59**
3.1. Closure Strategy . . . 61
3.2. Conceptual Approaches . . . 64
3.2.1. Concept of Partially Penetrating Continua . . . 64
3.2.2. Concept of Interpenetrating Continua . . . 69
3.3. Momentum Transfer Closure . . . 71
3.3.1. Phase-interaction Terms . . . 71
3.3.2. Self-interaction Terms . . . 82
3.4. Interfacial Transport Closure . . . 84
3.5. Final Forms of Governing Equations . . . 85
3.5.1. Two-Field Equations . . . 85
3.5.2. Single-Field Equations . . . 88

4. Numerical Method **95**
4.1. Introduction . . . 96
4.2. Domain Discretization . . . 97
4.2.1. Spatial Discretization . . . 97
4.2.2. Temporal Discretion . . . 98
4.3. Equation Discretization . . . 98
4.3.1. Convection Term . . . 101
4.3.2. Diffusion Term . . . 106
4.3.3. Source Term . . . 108
4.3.4. Time Integration . . . 109
4.3.5. Boundary Conditions . . . 112
4.4. Discretization of Governing Equations . . . 114
4.4.1. Discetized Interface Transport Equation . . . 114
4.4.2. Discretized Momentum Equation . . . 118
4.5. Solution Method and Algorithm . . . 124
4.5.1. Solution Method . . . 124
4.5.2. Algorithm . . . 127

Results & Publications.

5. Gas-Liquid Flows in Bubble Columns – Part I **137**
5.1. Introduction . . . 138
5.1.1. State-of-the-Art . . . 138
5.1.2. Scope and Objectives . . . 142
5.2. Modeling . . . 143
5.2.1. Interfacial Interactions . . . 144
5.2.2. Turbulence . . . 149
5.2.3. Swarm Effects . . . 150
5.2.4. Polydispersity . . . 151
5.2.5. Mixing . . . 154
5.3. Summary . . . 155
5.A. References . . . 156

6. Gas-Liquid Flows in Bubble Columns – Part II **163**
6.1. Introduction . . . 164
6.1.1. Flow Domain Discrimination . . . 164
6.2. Numerical Simulation . . . 165
6.2.1. Rectangular Bubble Column (Pseudo-2D) . . . 166
6.2.2. Cylindrical Bubble Column (3D) . . . 167
6.3. Results . . . 168
6.3.1. Rectangular Bubble Column (Pseudo-2D) . . . 168
6.3.2. Cylindrical Bubble Column (3D) . . . 171
6.4. Summary and Outlook . . . 179
6.A. References . . . 180

7. Species Transfer across Fluid Interfaces **181**
7.1. Introduction . . . 182
7.2. Physical Background . . . 183
7.2.1. Bubble Dynamics . . . 183
7.2.2. Species Transfer . . . 186
7.3. Mathematical Model and Governing Equations . . . 187
7.3.1. Conceptual Approach and Methodology . . . 189
7.3.2. Assumptions . . . 192
7.3.3. Bubble Dynamics – Volume-of-Fluid Method . . . 192
7.3.4. Species Transfer – Continuous-Species-Transfer (CST) Method 196
7.4. Implementation . . . 198
7.5. Validation Studies . . . 202
7.5.1. Species Transfer across a Planar Interface in a Cube . . . 202
7.5.2. Species Transfer across a Deforming Bubble Surface . . . 203
7.6. Summary . . . 208
7.A. Conceptual Approach of Conditional Volume-Averaging . . . 209
7.B. Validation Study . . . 216

7.C. References 219

8. Numerical Simulation of Multi-scale Two-Phase Flows **227**
8.1. Introduction 228
8.2. Conceptual Approach of Conditional Volume-Averaging 232
8.2.1. Local Instantaneous Conservation Equation and Interfacial Jump Condition 232
8.2.2. Conditional Volume-averaged Conservation Equation and Interfacial Jump Condition 234
8.3. Multi-scale Two-Phase Methodology & Closure 240
8.3.1. Closure Strategy & Conceptual Approach 242
8.3.2. Momentum Closure 248
8.4. Simulation Results 254
8.4.1. Tangential Interfacial Coupling – Stratified Two-Phase Shear Flow 254
8.4.2. Normal Interfacial Coupling – Oscillating Viscous Cylinder . 257
8.4.3. Inertia-dominated – Dambreak with Obstacle 260
8.5. Conclusions & Outlook 261
8.A. Derivation of Analytical Validation Base 266

Closure.

9. Summary & Outlook **273**
9.1. Summary and Closing Comments 273
9.2. Outlook and Future Work 274

Appendix.

A. Subject Index **A – 1**

B. Declaration **B – 5**

C. List of Publications **C – 7**

List of Figures

1.1. Classification of two-phase flow types 2
1.2. Scale inconsistency of prevailing Eulerian multi-scale CMFD approaches 15

2.1. Control volume – Single-phase flow 24
2.2. Control volume – Two-phase flow 29
2.3. Sharp vs. continuous interface representation 43
2.4. Conceptual approach of the conditional volume-averaging procedure 45
2.5. Illustration of basic averaging techniques 49
2.6. Illustration of the interfacial surface averaging procedure 50

3.1. Principle of model closure – Dispersed flow type 62
3.2. Principle of model closure – Segregated flow type 63
3.3. Closure model for the interfacial morphology 66
3.4. Closure model for the interfacial averaged velocity 68
3.5. Interfacial forces in bubbly flows 70
3.6. Illustration of a fluctuating interface for an isotropic interfacial morphology 81

4.1. Control volume 98
4.2. Central differencing 102
4.3. Switching/Blending differencing schemes 103
4.4. Convection boundedness criterion in the NVD diagram 104
4.5. Family of Gamma differencing schemes in the NVD diagram 105
4.6. Non-orthogonal correction 108
4.7. Boundary control volume 113

5.1. Characteristic flow pattern in a bubble column 139
5.2. Concept of interpenetrating continua and principle of volume-averaging 143
5.3. Interfacial forces in bubbly flows 145
5.4. Swarm correction for the drag force coefficient 151
5.5. Basic bubble coalescence and break-up mechanisms 153
5.6. Principle of local vs. global polydispersity 154

6.1. Principle of flow domain discrimination 165
6.2. Domain and computational mesh for the pseudo-2D bubble column . 167

6.3. Domain and computational mesh for the pseudo-2D bubble column . 169
6.4. Simulation results for the pseudo-2D bubble column: volumetric gas-phase fraction 170
6.5. Evaluation of Results: change of the horizontal liquid velocity obtained in the center of the pseudo-2D bubble column 172
6.5. Evaluation of Results: change of the horizontal liquid velocity obtained in the center of the pseudo-2D bubble column 173
6.6. Simulation results for the 3D bubble column: gas phase velocity . . 174
6.7. Simulation results for the 3D bubble column: volumetric gas-phase fraction 175
6.8. Simulation results for the 3D bubble column: tracer distribution . . 176
6.9. Evaluation of Results: gas hold-up vs. superficial gas velocity obtained in a cylindrical bubble column 177
6.10. Evaluation of Results: tracer distribution subsequent to a stepwise dosing in a cylindrical bubble column 178

7.1. Flow structures and physico-chemical phenomena in bubble column reactors 182
7.2. Bubble shape depending on Reynolds, Eötvös and Morton number . 184
7.3. Bubble terminal rising velocity at different bubble (equivalent) diameters in air/water system 185
7.4. Bubble wake and rise trajectories at different bubble (equivalent) diameters 186
7.5. Schematic illustration of a characteristic concentration profile across a bubble surface for a transfer species 187
7.6. Conceptual approach of the conditional volume-averaging procedure and the immersed interface concept 191
7.7. Schematic illustration of the test case for species transfer across a planar interface in a cube 202
7.8. Quantitative comparison of normalized species concentration profiles across a planar interface in a cube – Exact reference solution (1D model) and numerical solution (CST method) 204
7.9. Schematic illustration of the test case for species transfer across a deforming bubble surface while rising through a quiescent liquid . . 205
7.10. Oxygen concentration wake behind a rising 6 mm bubble 206
7.11. Quantitative comparison of terminal rising velocities of single bubbles at different (equivalent) diameters rising in a quiescent liquid – results of numerical simulation and experimental data 207
7.12. Quantitative comparison of the trajectory (top view) of a 4 mm bubble rising in a quiescent liquid – results of numerical simulation and experimental data 207
7.13. Control volume – Two-phase flow 209
7.14. Illustration of the interfacial surface averaging procedure 213

7.15. Quantitative comparison of normalized species concentration profiles across a planar interface in a cube – Exact reference solution from 1D model and numerical solution from CST method 217

8.1. Control volume – Two-phase flow 232
8.2. Illustration of the interfacial surface averaging procedure 235
8.3. Principles of model closure 241
8.4. Closure model for the interfacial morphology 243
8.5. Closure model for the interfacial averaged velocity 245
8.6. Illustration of a fluctuating interface for an isotropic interfacial morphology 246
8.7. Stratified two-phase shear flow 254
8.8. Velocity profile over channel height for stratified two-phase shear flow scenario 256
8.9. Oscillating viscous droplet 257
8.10. Temporal evolution of distortion amplitude for an oscillating viscous droplet 259
8.11. Dambreak with obstacle 260
8.12. Qualitative comparison of numerical results with dambreak experiment 262
8.13. Qualitative comparison of numerical results at different spatial resolutions for the dambreak scenario 263
8.14. Quantitative assessment of numerical results for the dambreak scenario 264

List of Tables

0.1. Tensor Operations – Gibbs vs. Cartesian Notation xii
0.2. Finite Volume Notation according to Weller xv

2.1. Coefficients for the generic transport equation (single-phase flow) . . 26
2.2. Coefficients for the generic transport equation (two-phase flow) . . . 31

3.1. Forces exerted on a fluid particle 71
3.2. Overview – Closure terms for dispersed and segregated two-phase flow 87

4.1. Matrix contributions of discretized terms 126

5.1. Forces exerted on a fluid particle 146
5.2. Coefficients of the basic-mixture turbulence model 150
5.3. Bubble coalescence and break-up sources 153

7.1. Material and transport properties 203
7.2. Quantitative comparison of Sherwood numbers – experiments (Sherwood correlations) and numerical simulations (CST method) 208
7.3. Coefficients for the generic transport equation – species conservation 216

8.1. Coefficients for the generic transport equation (two-phase flow) – mass and momentum balance 237

Notation & Nomenclature

Tensor Notation

From the beginning it seems reasonable and rational to adopt a tensor notation which is compact yet unambitious, in order to *understand* tensors as entities in its own right, rather than a list of scalar components. Consequently, any tensor operation should be perceived as an operation on the entire tensor entity rather than a series of operations on its components [1].

That said, it is up to the tensor notation to encapsulate *and* actively support the concept of a tensor as an entity in its own right. Therefore, the following tensor notation shall be used henceforth and referred to as *Gibbs Tensor Notation* [2]: generally, lightface italic Roman symbols denote scalar quantities, whereas boldface symbols represent vector and tensor quantities[1]. Furthermore, it is convenient to distinguish boldface Roman symbols for vectors and boldface Greek symbols for tensor quantities wherever possible. However, this rule is not adhered to religiously [3].

The Gibbs notation is a compact and intuitive notation – as has been required initially. Moreover, it is devoid of any reference to the underlying coordinate system. A few examples shall suffice to accentuate the subtle distinction compared to another common notation – the Cartesian Tensor Notation (or Index Tensor Notation) – table 0.1. The interested reader is referred to [4, 5] for more details on tensor calculus.

Note in passing, that the author has omitted the use of parenthesis in the Gibbs Notation for the sake of readability: conveniently one could enclose any multiplication operation (or sums thereof) by parenthesis to indicate the type of quantity produced by the multiplication, i.e., $(\,) \mathrel{\widehat{=}}$ scalar, $[\,] \mathrel{\widehat{=}}$ vector and $\{\,\} \mathrel{\widehat{=}}$ tensor.

[1] Of course, scalar and vector quantities are to be regarded as zero-rank and first-rank tensors, respectively. However, a second-rank tensor is often colloquially termed 'tensor' since the occurrence of higher order tensors is fairly rare. Moreover, tensors of rank zero and one are commonly known as scalars and vectors [1]. Typical examples in fluid dynamics are: shear rate, energy and time (as examples for scalar quantities); velocity, momentum and acceleration (as examples for vector quantities); stress and rate-of-strain (as examples for tensor quantities). Hence, we shall stick to this differentiation throughout this thesis.

Table 0.1: Tensor Operations – Gibbs vs. Cartesian Notation [4].

Gibbs Notation	Expanded Notation in Terms of Unit Vectors & Unit Dyads	Cartesian Tensor Notation
$\mathbf{v}\bullet\mathbf{w}$	$\sum_i v_i w_i$	$v_i w_i$
$\mathbf{v}\times\mathbf{w}$	$\sum_i \sum_j \sum_k \epsilon_{ijk}\mathbf{e}_i v_j w_k$	$\epsilon_{ijk}\mathbf{e}_i v_j w_k$
$\nabla\mathbf{v} \equiv \nabla\otimes\mathbf{v}$ [(a)]	$\sum_i \sum_j \frac{\partial}{\partial x_i} v_j \mathbf{e}_i\mathbf{e}_j$	$\partial_i v_j$
$\nabla\bullet\boldsymbol{\tau}$	$\sum_i \sum_j \mathbf{e}_i \frac{\partial}{\partial x_j}\tau_{ji}$	$\partial_j \tau_{ji}$
$\nabla^2 s (= \Delta s)$ [(b)]	$\sum_i \frac{\partial^2}{\partial {x_i}^2} s$	$\partial_i\partial_i s$
$\nabla^2\mathbf{v} \equiv \nabla\bullet\nabla\mathbf{v}$	$\sum_j \mathbf{e}_j \left(\sum_i \frac{\partial^2}{\partial {x_i}^2} v_j\right)$	$e_j\partial_i\partial_i v_j$

[(a)] Note that the dyadic product sign in $\nabla\otimes\mathbf{v}$ will be dropped throughout this thesis denoting $\nabla\mathbf{v}$ instead. The vector differential operator ∇ is called Nabla operator and defined as $\nabla \equiv \mathbf{e}_1\frac{\partial}{\partial x_1} + \mathbf{e}_2\frac{\partial}{\partial x_2} + \mathbf{e}_3\frac{\partial}{\partial x_3}$.

[(b)] The vector differential operator $\nabla^2 = \Delta$ is called Laplacian operator and defined as $\nabla^2 \equiv \nabla\bullet\nabla = \frac{\partial^2}{\partial {x_1}^2} + \frac{\partial^2}{\partial {x_2}^2} + \frac{\partial^2}{\partial {x_3}^2}$.

Finite Volume Notation

The Finite Volume Method is a widely known and well-established method for the numerical solution of a variety of problems in continuum mechanics. However, the continuing increase in the complexity of these problems and the complexity of the corresponding numerical algorithms for their solution are found to cause severe problems when transferring ideas about details on the solution algorithm (e.g., discretization practices) between researchers in a clear yet compact way [6].

Hence, a concise, unambitious but still compact and intuitive notation to (re)present single finite-volume operations as well as entire solution algorithms is a severe need. As the Gibbs Notation for tensors is devoid of any reference to the underlying coordinate system, so should a Finite Volume Notation be made independent from the underlying code and mesh topology. In the following, the Finite Volume Notation of Weller shall be described in considerable detail, as it appears to fulfill the above requirements and is, thus, used in this thesis. His concept is set out below and repeated here for convenience; the interested reader is referred to [6, 7].

In the Finite Volume Method both *interpolating* fields from the cell-centers to the cell-faces and *averaging* fields over some computational region[2] are fundamental. Moreover, it appears necessary to introduce different methods in order to ensure boundedness and numerical stability. Thus, both interpolating and averaging procedures need to be denoted in a sufficiently detailed notation providing all specifications necessary for implementation:

face interpolations To support various differencing schemes a simple extensible notation is suggested, in order to specify the scheme itself along with all required parameters. Herein, the subscript f denotes the face interpolation. Other crucial information needed by the scheme – such as interpolation weighting factors (based on the face flux) or scheme-specific blending/switching coefficients – are provided in parentheses.
E.g., $\mathbf{\Phi}_f$ simply denotes the face value of $\mathbf{\Phi}$ obtained by central differencing, whereas $\mathbf{\Phi}_{f(F,S,\gamma)}$ generally describes the face value of $\mathbf{\Phi}$ obtained using scheme S, which utilizes the face flux F and a specific coefficient γ.

averaging procedures In order to specify the computational stencil ❑ over which the averaging is performed, a pertinent subscript is assigned to the averaging operator. It is convenient to *directly denote a particular operator* to indicate the *corresponding numerical stencil*. I.e., the averaging is performed on the basis of the computational stencil of the operator, provided as an subscript to the averaging operator.

[2] commonly referred to as computational stencil or molecule

E.g., in general the average of a field $\mathbf{\Phi}$ over the computational stencil $\square$ is denoted by $\langle \mathbf{\Phi} \rangle_{\square}$. If the average is to be based on the computational molecule of the ∇ operator, for instance, this is represented by $\langle \mathbf{\Phi} \rangle_{\nabla}$.

In the Finite Volume Method terms arising from differential operators generally can be treated either explicitly or implicitly. The Finite Volume Notation of Weller enables to distinguish between both treatments:

explicit differential operators In general, differential operators are denoted as prescribed by the Gibbs Tensor Notation without any further modification.

implicit differential operators The discretized expression $[\mathbf{\Phi}]$ that arises from an implicit differential operator $\mathcal{L}$ generally involves matrix coefficients (subscript A) and source contributions (subscript S). Being applied on $\mathbf{\Phi}$ the encapsulation of both is denoted as $[\![\mathcal{L}[\mathbf{\Phi}]]\!] \equiv [\![\mathcal{L}[\mathbf{\Phi}]]\!]_A \mathbf{\Phi} - [\![\mathcal{L}[\mathbf{\Phi}]]\!]_S$.
Similarly, the corresponding diagonal, upper and lower part of the matrix is denoted as $[\![\mathcal{L}[\mathbf{\Phi}]]\!]_D$, $[\![\mathcal{L}[\mathbf{\Phi}]]\!]_U$ and $[\![\mathcal{L}[\mathbf{\Phi}]]\!]_L$, respectively. Moreover, the 'H' part is defined as $[\![\mathcal{L}[\mathbf{\Phi}]]\!]_H \equiv [\![\mathcal{L}[\mathbf{\Phi}]]\!]_D \mathbf{\Phi} - [\![\mathcal{L}[\mathbf{\Phi}]]\!]$ (providing an approximate solution to $[\![\mathcal{L}[\mathbf{\Phi}]]\!] = 0$ by $\mathbf{\Phi} = [\![\mathcal{L}[\mathbf{\Phi}]]\!]_H / [\![\mathcal{L}[\mathbf{\Phi}]]\!]_D$ [3]).

A few examples shall suffice to accentuate the merits of this notation compared to the more common index notation – table 0.2. For more details the reader is referred to chapter 4.

[3] Note, that the inversion of the diagonal part of the matrix, $[\![\mathcal{L}[\mathbf{\Phi}]]\!]_D^{-1}$ has been denoted as $1/[\![\mathcal{L}[\mathbf{\Phi}]]\!]_D$ for reasons of a better readability.

Table 0.2: Finite Volume Notation according to Weller [6].

implicit differential operators	
rate of change	$\left[\!\left[\frac{\partial[\rho\phi]}{\partial t} \right]\!\right]$
convection term	$\left[\!\left[\nabla_{\bullet}\left(F[\phi]_{f(F,S,\gamma)} \right) \right]\!\right]$
diffusion term	$[\![\nabla_{\bullet}(\Gamma\nabla[\phi])]\!]$
linear part of source term	$[\![S_p\,[\phi]]\!]$
explicit differential operators	
temporal term	$\frac{\partial\rho\phi}{\partial t}$
divergence term	$\nabla_{\bullet}(\rho\mathbf{U}\phi_{f(\rho\mathbf{U},S,\gamma)})$
laplacian term	$\nabla_{\bullet}(\Gamma\nabla\phi)$
constant part of source term	S_u

Nomenclature

The following holds the nomenclature that has been adopted within this thesis. The list of used symbols is provided along with a short description. Dimensions are given in terms of SI units. Wherever the dimensions of an arbitrary quantity are found to be case-specific, the corresponding entry for its units has been left empty.

Roman Symbols

a	interfacial area density	$\frac{\mathrm{m}^2}{\mathrm{m}^3}$
a	matrix coefficient	
A	square matrix	
$\mathbf{a}$	general vector property	
c	molar species/component concentration	$\frac{\mathrm{kmole}}{\mathrm{m}^3}$
$\mathrm{c}\,, C$	constant/coefficient	
d	diameter	m
$\mathbf{d}$	delta vector, vector between P and N	m
D	molar diffusivity	$\frac{\mathrm{m}^2}{\mathrm{s}}$
$\mathbf{D}$	rate-of-deformation(strain) tensor	$\frac{1}{\mathrm{s}}$
$\mathbf{D}$	momentum drift-flux tensor	$\frac{\mathrm{m}^2}{\mathrm{s}^2}$
$\mathcal{E}$	event space	
f	face	
f	linear interpolation factor	
f	phase distribution function (signed distance function from the interface)	m
F	face mass flux	$\frac{\mathrm{kg}}{\mathrm{s}}$
$\mathbf{F}$	force	$\frac{\mathrm{kg\,m}}{\mathrm{s}^2}$

g	prescribed face normal gradient of quantity $\mathbf{\Phi}$	
$\mathbf{g}$	acceleration vector due to gravity	$\frac{\mathrm{m}}{\mathrm{s}^2}$
G	filter kernel (operator)	
I	indicator function	–
$\mathbf{I}$	identity tensor	–
l	length	m
L	length	m
$\mathbf{M}$	interfacial momentum transfer term (force density)	$\frac{\mathrm{kg}}{\mathrm{m}^2\,\mathrm{s}^2}$
n	number density	$\frac{1}{\mathrm{m}^3}$
$\mathbf{n}$	unit normal vector	–
N	control volume (neighboring to P)	
N	number/quantity	–
$\mathcal{O}$	order of truncation term	–
p	pressure	$\frac{\mathrm{kg}}{\mathrm{m}\,\mathrm{s}^2}$
P	control volume (usually subject of examination)	
$\mathcal{P}$	process	
$\mathbf{r}$	source	
$\mathbf{r}$	spatial position vector	m
$\mathbf{r}$	source vector	
R	molar reaction rate	$\frac{\mathrm{kmole}}{\mathrm{m}^3\,\mathrm{s}}$
$\mathbf{R}$	Reynolds stress tensor	$\frac{\mathrm{m}^2}{\mathrm{s}^2}$
$\mathcal{R}$	space domain	

S	control surface	m^2
S	source term	
$\mathcal{S}$	spatial terms (time integration)	
$\mathbf{S}$	face area vector	m^2
t	time	s
T	averaging time interval	s
$\mathbf{t}$	unit tangential vector	–
$\mathcal{T}$	time domain	
$\mathbf{U}$	velocity vector	$\frac{\mathrm{m}}{\mathrm{s}}$
V	(control/averaging) volume	m^3
x	mass fraction of a species/component	$\frac{\mathrm{kg}}{\mathrm{kg}}$
$\mathbf{x}$	spatial position vector	m

Greek Symbols

α	volumetric phase fraction / phase volume fraction	$\frac{\mathrm{m}^3}{\mathrm{m}^3}$
β	parameter in the Gamma differencing scheme	–
δ	interfacial width	m
$\boldsymbol{\eta}$	relative spatial position vector	m
γ	volumetric phase fraction / phase volume fraction of phase φ	$\frac{\mathrm{m}^3}{\mathrm{m}^3}$
γ	coefficient in differencing scheme	–
Γ	diffusivity	
κ	curvature	$\frac{1}{\mathrm{m}}$
μ	dynamic viscosity	$\frac{\mathrm{kg}}{\mathrm{m\,s}}$

μ	particular realization in an ensemble of events	–
ϕ	arbitrary general scalar quantity	
$\boldsymbol{\Phi}$	arbitrary general intensive quantity	
$\boldsymbol{\Psi}$	second arbitrary general intensive quantity	
ρ	density	$\frac{\mathrm{kg}}{\mathrm{m}^3}$
$\boldsymbol{\sigma}$	total stress tensor	$\frac{\mathrm{kg}}{\mathrm{m\,s}^2}$
σ	surface tension	$\frac{\mathrm{kg}}{\mathrm{s}^2}$
Σ	interfacial area density	$\frac{\mathrm{m}^2}{\mathrm{m}^3}$
$\boldsymbol{\tau}$	viscous stress tensor	$\frac{\mathrm{kg}}{\mathrm{m\,s}^2}$

Dimensionless Groups

Eo	Eötvos number
Fr	Froude number
He	distribution coefficient based on Henry's law
Mo	Morton number
π_ν	kinematic viscosity ratio
π_ρ	density ratio
Re	Reynolds number
We	Weber number

Others

Δ	spatial stencil in physical domain (often based on an averaging length scale)
❑	spatial stencil in computational domain

Subscripts

b	bubble phase
b	boundary
c	continuous phase
$char$	characteristic
d	diffusive
d	dispersed phase
d	drag (bubble force)
$\mathbf{d}$	projected face area vector, parallel to $\mathbf{d}$
D	downwind to P
$\boldsymbol{\Delta}$	delta face area vector
eff	effective
f	face
h	hydrodynamic
i, I	interfacial/interface
i	chemical species/component
k	phase k
l	lateral lift (bubble force)
l	liquid phase
lim	limiter,limiting
m	microscopic
M	macroscopic

n	normal
p	(fluid) particle
p	pressure
P	point in the center of the control volume (usually subject of examination)
p	linear part of the source term
N	point in the center of a neighboring control volume
φ	conditioned with respect to the generic phase φ (usually subject of examination)
ϕ	conditioned with respect to the generic phase ϕ (neighboring to phase φ)
$\varphi\phi$	from phase φ to phase ϕ
r	relative
S	control surface
σ	surface tension
td	turbulent dispersion (bubble force)
u	constant part of the source term
U	upwind to P
vm	virtual mass (bubble force)

Superscripts

n	at the new time step
o	at the old time step
oo	at the 'second' old time step
t	at time t

Oversymbols

$\overline{\boldsymbol{\Phi}} \equiv \overline{\boldsymbol{\Phi}}^{V}$	volume-average
$\overline{\boldsymbol{\Phi}}^{T}$	time-average
$\overline{\boldsymbol{\Phi}}^{E}$	ensemble-average
$\widetilde{\boldsymbol{\Phi}}$	weighted volume-average
$\overline{\boldsymbol{\Phi}}^{\varphi}$	conditional volume-average with respect to phase φ
$\widetilde{\boldsymbol{\Phi}}^{\varphi}$	conditional phase-weighted volume-average with respect to phase φ
$\widehat{\boldsymbol{\Phi}}$	interface-average
$\widehat{\widetilde{\boldsymbol{\Phi}}}^{\varphi}$	conditioned interface-average with respect to phase φ
$\boldsymbol{\Phi}'$ $(\boldsymbol{\Phi}'^{\varphi})$	(conditional) phasic/intrinsic fluctuation with respect to the averaging length scale
$\boldsymbol{\Phi}''$ $(\boldsymbol{\Phi}''^{\varphi})$	(conditional) phase-weighted fluctuation with respect to the averaging length scale
$\boldsymbol{\Phi}^{\sharp}$	surface fluctuation
$\widetilde{\phi}$	normalized scalar property

References

[1] http:www.foamcfd.org/Nabla/guides/ProgrammersGuidese2.html, January 2011. xi

[2] J. W. Gibbs. *Vector Analysis*. Dover Publications, 1960. xi

[3] H. G. Weller. Derivation, Modeling and Solution of the Conditionally Averaged Two-Phase Flow Equations. Technical report, OpenCFD Limited, 2005. xi

[4] R. B. Bird, R. C. Armstrong, and O. Hassager. *Dynamics of Polymeric Liquids*. Wiley, New York, 1st & 2nd edition, 1977. xi, xii

[5] R. B. Bird, W. E. Stewart, and E. N. Lightfoot. *Transport Phenomena*. Wiley, 2 edition, 2001. xi

[6] H. G. Weller. A Code Independent Notation for Finite Volume Algorithms. Technical report, OpenCFD Limited, 2005. xiii, xv

[7] H. Rusche. *Computational Fluid Dynamics of Dispersed Two-Phase Flows at High Phase Fractions*. PhD thesis, Imperial College of Science, Technology & Medicine London, 2002. xiii

Theory and Development

1

Introduction

1.1. Background – Scales, scales, scales ...

Many applications in chemical and process engineering involve two-phase flows. These can be categorised according to the phases present in the system as depicted in figure 1.1. Examples of industrial two-phase flow applications are found in chemical, petroleum, metallurgical and energy industries and cover liquid-phase oxidations, hydrogenations, chlorination, gas scrubbing, waste water treatment and various bio-technological applications.

However, as these types of flows often involve both a *continuous cascade of temporal and spatial scales* usually varying over orders of magnitude (multi-scale) and *multiple coupled phenomena* (multiphysics), their numerical treatment proves to be utmost complex. Thus, no general methodology or technique has evolved yet: finally the adopted approach severely depends upon the particular nature of the two-phase flow that is to be captured.

Nevertheless, the numerical simulation of two-phase systems using Computational Fluid Dynamics (CFD) has emerged as a powerful simulation tool for understanding these types of flow in two-phase apparatus. Therefore, throughout the last two decades different approaches have evolved and have been continuously developed leading to the field of Computational Multi-Fluid Dynamics (CMFD).

These CMFD approaches were motivated by a scale separation that is presumed for two-phase flows, given that the flow type (or flow regime) can be regarded as invariant throughout the simulation. Consequently, a classification of CMFD approaches can be done according to their ability of capturing interfacial scale regimes that characterize a two-phase flow:

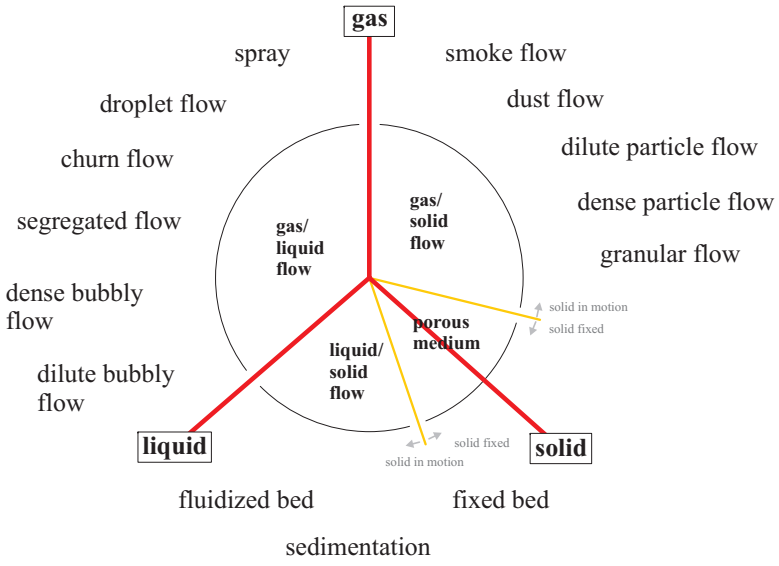

Figure 1.1: Classification of two-phase flow types.

- macroscopic scales, i.e., of mean/main flow features on the scales of the bounding flow domain
- mesoscopic scales, i.e., of major changes of the fluid dynamic phenomena on the scale of large eddies and recirculation regions
- microscopic scales, i.e., of flow features on the scale of bubble-bubble and bubble-turbulence interaction, or in the range of the thickness of the interfacial boundary layer

Several methodologies have evolved taking advantage of this presumed scale separation, two of which shall be considered more closely in the remainder of this section, namely

- interfacial scale averaging and
- interfacial scale resolving methods.

Both of them are well-established methodologies and have been successfully adopted to various two-phase flow types, capturing respective flow features by applying different resolutions. However, they are usually found to be restricted to one flow type being only valid for a narrow interfacial scale range characterizing this type.

1.1.1. Interfacial Scale Averaging Techniques

For simulation of industrial two-phase flow applications the scale to look at is typically rather large – in the order of several meters. In contrast, the smallest scale one might have to consider is that of a characteristic "dispersed phase element" (DPE[1]), which predominantly determines the fluid dynamics in an industrial two-phase flow application. The scales of DPEs surely vary from tens of microns to millimeters, depending on underlying process and material parameters under consideration.

Thus, there is a clear scale separation evident, which enables interfacial scale averaging CMFD approaches to be used for two-phase flow applications possessing dispersed flows (e.g., bubbly or droplet flows) occurring in industrial (large) scale domains. Advantageously, these CMFD approaches employ averaging techniques in which all interfacial scales under consideration are averaged – either spatially over an averaging volume[2], temporally over an averaging time interval, or ensemble-averaged over a set of realizations. In contrast to its single-phase counter-part, the averaging techniques for two-phase systems, however, need to be based upon *conditioning* [5], in the course of which an *indicator function* is introduced enabling to discriminate contributions to the balances of conserved quantities on a per-phase basis. In turn this states the basis of the so-called *concept of immersed interfaces* [7, 18] being a pivotal theme of interfacial scale averaging CMFD approaches. Its basic premise is that the interface between different immiscible fluids is embedded or immersed into the interior of the computational domain.

Consequently, *all* interfacial exchange phenomena are subject to modeling via (mostly empirical) closure models. Therefore the development, determination and choice of closure models is crucial for properly reproducing the desired interfacial physics. Moreover, this must be accomplished in a way that the closure restores the physical information that became non-resolved (and hence lost) due to the applied averaging procedure. Ultimately, the challenge clearly is to do this on a physically sound basis, rather than relying on empirical closures.

1.1.2. Interfacial Scale Resolving Techniques

On the other end of the scale range, i.e., at the molecular scale, an interfacial flow comprises the motion of molecules whereas the interface is represented by a transition region of finite thickness of typically a few tens of Ångströms. Over this region collections of molecules pertaining to one phase (out of the two phases) coexist at a

[1] generalized term for bubbles, drops or particles that will be used as general substitute throughout this thesis

[2] Due to its straightforward interpretability the volume-averaging technique mostly is employed in the context of two-phase flows.

certain probability promoting a smooth but rapid transition of the expected molecule number density from zero to the respective bulk values.

However, for the purpose of this thesis we will consider only interfacial flow situations for which two approximative but rather common assumptions apply:

1.) Continuum Hypothesis

Any fluid phase, a two-phase flow system under consideration might consist of, can be regarded as a continuum, where flow and material properties are well-defined spatio-temporal functions characterizing the phase and its flow.

2.) Manifold Hypothesis

The interface separating the two phases can be approximated as a mathematical surface of discontinuity (two-dimensional manifold having zero-thickness and no mass).

Note, these modeling hypotheses are most common and widely used. However, again the assumptions are based upon a clear scale separation that is the molecular scale is separated from the flow or interfacial scale (i.e., of a DPE) by orders of magnitude.

Conceptually, three methodologies are to be distinguished, each of which treats the characteristic interfacial jump (e.g., in flow properties) in a different, thus, specific manner. This special treatment of interfacial jump conditions becomes necessary, since there is no natural or straightforward representation to handle these sharp discontinuities in an (continuous) Eulerian framework.

1.) sharp interface (ghost fluid) methods

Sharp interface or ghost fluid methods are based upon numerical methods explicitly accounting for interfacial discontinuities within the discretization, which in effect fully retains the sharp characteristics of interfacial jumps in pressure and velocity.

2.) interface tracking methods

2.1.) mesh-based tracking

These class of methods either directly align the phase interface with edges of computation mesh cells (*moving mesh methods*) or the interface is represented by an additional two dimensional mesh being superimposed on a fixed three dimensional one (*front tracking methods*).

2.2.) marker-based tracking

Within this class the interface is *tracked* by directly marking it using (massless) marker particles.

3.) interface capturing methods

Generally there are two conceptual avenues

3.1.) marker-based capturing

The interface is *captured* by attaching marker particles to one of the two phases in order to gather information about the interfacial morphology from their distribution in the phase volume.

3.2.) indicator-based capturing

The interfacial morphology is *captured* by an order parameter (indicator) marking one out of the two phases advantageously employing the *concept of immersed interfaces*.

The concept of immersed interfaces is also a pivotal theme considering interfacial scale resolving CMFD methods. It in particular exhibits the advantage of decoupling the characteristic physical/interfacial scale (i.e., of a DPE) from the characteristic numerical/mesh scale (i.e., of a finite (control) volume) by 'spreading' the originally sharp interfacial jumps over several mesh cells transferring them into a smooth (regularized) yet approximative form.

There are two approaches to be distinguished:

- single-field (mixture) approach

  The two-phase system is treated as 'mixture' possessing one (center-of-mass) velocity and (mixture) pressure. Varying material properties as phase viscosities and densities are taken into account as mixture quantities by use of a smooth order parameter (indicator). This enforces the respective properties within the phases, while promoting a smooth transition across the interface.

- two-field (two-fluid or Eulerian-Eulerian) approach

  The two phases are treated separately – each with an own velocity and pressure field. The desired jump conditions at the interface (i.e., boundary conditions) are inherently involved: a field pertaining to one of the phases is *consistently* transferred to a fictitious field by use of a smooth order parameter (indicator), by means of which the field's physical significance is decreased when crossing the fluid interface. Eventually, the field has entirely lost its physical relevance on the fictitious side of the interface.

From the above description of methodologies, it is evident that the challenge for all interfacial scale resolving methods might be formulated as two-fold:

- flexibility and robustness (stability) for complex two-phase flow scenarios, e.g., changing interfacial morphology due to coalescence or break-up

- capability to handle multi-scale two-phase flow scenarios, i.e., capturing the mean interfacial evolution while under-resolving interfacial details as for instance the corresponding microscale curvature or interfacial boundary layer.

Being a priori neither restricted to a certain flow type or scale regime nor exhibiting features rendering its numerical treatment undue complex, it seems rational that the most promising and developable approach encompassing both requirements needs to be based upon the Eulerian-Eulerian two-fluid methodology.

1.2. State-of-the-Art & Motivation

Although two-phase flow systems and related interfacial transport phenomena commonly cover a wide range of physical scales, prevailing CMFD approaches presume a distinct scale range in narrow confines. E.g., DPEs being much larger than a characteristic length scale of the underlying averaging (control) volume are dealt with via interfacial scale *resolving* methods, whereas DPEs that are much smaller than a characteristic length scale of the underlying averaging volume are modeled using interfacial scale *averaging* techniques.

However, it needs to be emphasized that this assumption represents a substantial constraint imposing considerable restrictions on the concrete two-phase flow situations that can be treated using CMFD. For this reason, several groups have recently suggested to explicitly couple interfacial scale averaging and interfacial scale resolving methods in order to arrive at a more general two-phase flow model, that is capable of treating flow phenomena over a wider range of interfacial scales. In the following, these approaches are briefly discussed in order to gather an overview of the state-of-the-art. For convenience, the description shall stick to the respective notation and syntax of the original studies. Furthermore, only characteristics and features rendering the models unique shall be briefly set out. For the full sets of governing equations the reader is referred to the original publications as they are referenced in the remainder.

Černe et al. Černe et al. [27–33] suggests the coupling of the Volume-of-Fluid (VoF) method with the classical two-fluid model (TFM). This procedure has been motivated by the limitation of the VoF method regarding the local spatial resolution (i.e., mesh density), which must be chosen sufficiently small in order to allow the capturing of interfacial structures as the curvature, for instance. On the other hand, the TFM has been found more suitable for highly dispersed two-phase flows, where the VoF method would suffer from its need for computational resources. Moreover, the TFM – though in principle being capable of resolving interfacial scales – is assessed to be by far more reliable and developed for dispersed flows, where an interfacial scale averaging resolution is employed. Conceptually, the VoF method is adopted for parts of the domain, where the

mesh density allows the VoF method, as interfacial scale resolving approach, to capture detailed interfacial structures. In other parts of the domain, where the two-phase flow is too dispersed to properly resolve down to crucial interfacial scales, the TFM is applied.

The following model features and characteristics are found to be noteworthy:

- The coupled approach is capable of describing two-dimensional, incompressible two-phase flow of Newtonian fluids.
- Each method is associated to a certain part of the domain that is separated from each other. Consequently, a separate set of governing equations is used. Hence, the coupling approach moderates between the two-field formulation of the TFM and the single-field formulation of the VoF method

  $$\vec{u}_1^{\,(\mathrm{TFM})} = \vec{u}_2^{\,(\mathrm{TFM})} = \vec{u}^{\,(\mathrm{VoF})} \tag{1.1}$$

  and vice versa

  $$\vec{u}^{\,(\mathrm{VoF})} = f_1\,\vec{u}_1^{\,(\mathrm{TFM})} + f_2\,\vec{u}_2^{\,(\mathrm{TFM})}, \tag{1.2}$$

  where the subscripts 1 and 2 indicate the respective phases and f denotes their volumetric phase fraction.
- The coupling of the VoF and TFM approach is accomplished using the volumetric phase fraction of the liquid phase, since this quantity is used in both approaches underlying the same physical interpretation. The coupled approach is inherently based on the VoF single-field formulation and switches into the TFM two-field formulation relying on a specific *switch criterion*, which has either been based on the
  - interface reconstruction function of the LVIRA algorithm [29, 30, 32], or the
  - gradient of the volumetric phase fraction [28, 31, 33].
- For the interfacial scale resolving VoF approach, the surface tension has been disregarded, since it was assumed to play no important role for the model switching. Within the interfacial scale averaging TFM approach, only a simple interfacial friction (drag force) model has been employed in order to accomplish the coupling of the phase momenta equations for $\vec{u}_1^{\,(\mathrm{TFM})}$ and $\vec{u}_2^{\,(\mathrm{TFM})}$, respectively.

Summarizing, the coupled VoF-TFM approach suggested by Černe et al. alleviates restrictions of both the VoF and the TFM approach with respect to constraints of spatial resolution – i.e., an appropriate mesh density required for each approach to work properly. However, relying on a switch criterion, the coupled VoF-TFM approach involves another source of uncertainty, which has to be considered crucial for the achievable accuracy and reliability.

Tomiyama & Shimada In [20–25] Tomiyama and Shimada present their so-called NP2 (read N+2) model, which is based on a multifluid formulation encompassing two fields for the continuous gas phase (cG) and liquid phase (cL), respectively, and N fields for the dispersed bubble phase, which is classified into multiple groups of different bubble sizes. This approach is motivated by the difficulty of simultaneously capturing a continuous gas phase, a continuous liquid phase, a large scale gas-liquid interface separating the two continuous phases and many dispersed bubbles of non-uniform size, as it is found in bubble columns that usually operate in the heterogeneous bubble flow regime. The concept is based on the length scale ratio $d^\star$ of a sphere-volume equivalent bubble and a computational cell, $d^\star \equiv \frac{d_\mathrm{b}}{\Delta x}$ [20], which has been identified as crucial parameter to assess accurate predictions using multipurpose CMFD over a wide range of interfacial scales. Thus, if $d^\star \gg 1$, i.e., the characteristic interfacial length scale is much larger than the computational cell size, the two phases on each side of the interface are regarded as continuous gas and liquid phase, respectively. For $d^\star \leq 1$ the gas phase is classified into N groups in terms of bubble size. Consequently, for the sum of all volumetric phase fractions α, it is:

$$\alpha_\mathrm{cG} + \alpha_\mathrm{cL} + \sum_{m=1}^{N} \alpha_\mathrm{dm} \stackrel{!}{=} 1. \tag{1.3}$$

Following model features and characteristics are noteworthy:

- The NP2 model is based on the assumption that both the gas and the liquid phase can be considered as incompressible Newtonian fluids. Furthermore, it is assumed that there is no phase change due to condensation or evaporation. Moreover, viscous and turbulent stresses are neglected within the gas phase.
- The NP2 model employs the single-field formulation for the two continuous phases. Herein the mixture density ρ_c and viscosity μ_c are evaluated as

  $$\rho_c \equiv \frac{\alpha_\mathrm{cL}\rho_\mathrm{cL} + \alpha_\mathrm{cG}\rho_\mathrm{cL}}{\alpha_\mathrm{cL} + \alpha_\mathrm{cG}} \qquad \text{and} \qquad \mu_c \equiv \frac{\alpha_\mathrm{cL}\mu_\mathrm{cL} + \alpha_\mathrm{cG}\mu_\mathrm{cL}}{\alpha_\mathrm{cL} + \alpha_\mathrm{cG}} \tag{1.4}$$

  Similar to the VoF method, both the surface tension force and the viscous and turbulent stress is accounted for.
- For the dispersed phase a multitude of interfacial momentum transfer models is provided, as for the interfacial drag, lift, virtual mass and turbulent dispersion forces. Moreover, momentum transfer between the dispersed gas phase and the continuous liquid phase is found to be incorporated in the NP2 model.

Concluding the NP2 model by Tomiyama and Shimada has to be regarded as very flexible hybrid model combining interfacial capturing and Eulerian multifluid capabilities.

Alajbegovic Alajbegovic developed a hybrid method combining the multi-fluid and the Volume-of-Fluid approach [1], based on the work of Černe et al. [32] and Tomiyama and Shimada [25], and fully implemented in the commercial CFD code AVL FIRE/SWIFT. As the NP2 model of Tomiyama and Shimada, this method is applicable for two-phase flows where well-defined interfaces between different phases/fluids co-exist with small scale multiphase structures. It is motivated by the need for an efficient simulation method for complex flows with multiple phases/fluids on arbitrary unstructured meshes. According to Alajbegovic, examining a particular multiphase flow, a selection has to be made comparing the required spatial and temporal resolution to the available computational resources. However, as Alajbegovic claims, situations often exist where a comparison is not appropriate, since in many industrial multiphase flow applications relatively large-scale interfaces co-exist with much smaller multiphase structures. Conceptually, the method is similar to that of Černe et al. and Tomiyama and Shimada: The interfaces of relatively large scales are treated by the VoF method, whereas the small-scale multiphase flow structures are accounted for by using a multi-fluid approach, In order to provide more flexibility, any two of the phases treated by the multi-fluid approach can either have different velocities (two-field formulation) or share the same velocity (single-field formulation).

The following model characteristics and features have to be mentioned:

- The model treats isothermal multiphase flows. It is assumed that all fluids are incompressible and Newtonian.
- The hybrid model is based on the observation, that the mass conservation equation in the multi-fluid and the phase fraction conservation equation in the VoF approach are identical. It is concluded, that the only difference to be introduced for the hybrid model is the handling of the advection term: this is accomplished for the 'VoF phase' using the compressive discretization CICSAM developed by Ubbink and Issa [26], while for the 'multi-fluid' phase ordinary schemes as upwind or central discretization is utilized.

Concluding, the hybrid model has to be regarded as very flexible approach that features a robust and efficient numerical technique enabling to simulations of practical industrial multiphase problems. However, as Alajbegovic concludes as well, more efforts are necessary before the hybrid model mature enough to become a versatile simulation tool in industry.

Akimoto & Yoshida Akimoto and Yoshida present the capability of their *Advanced Two-Fluid Model* in [36–39]. The development of the advanced two-fluid model

has been based on the conventional two-fluid model: the VoF model is incorporated in the framework of the two-fluid model, that is interface structures larger than computational cells are simulated by the VoF method, while small bubbles and droplets are treated by the two-fluid model. Coming from thermo-hydraulic codes, the authors were motivated by the need for a more accurate and general multi-dimensional two-phase flow model that is not constrained by correlation representing geometry effects. Both the capability of simulating two-phase flow that includes large and small interface structures and the requirement to economize the computational resources have led to this development in the commercial CFD code ACE-3D. As already indicated, the conceptual approach of the advanced two-fluid model is around the incorporation of the VoF method into the two-fluid model framework. For this purpose, the information about the interface position is determined from the volumetric phase (void) fraction inside a computational cell only. Hence, three numerical regions are distinguished:

1.) droplet regions ($f = 1$) including droplets below the calculation cell size. The void fraction is larger than 0.5.

2.) bubble regions ($f = 0$) including bubbles below the calculation cell size. The void fraction is less than 0.5.

3.) interface regions ($0 < f < 1$) including the interface that is greater than the computational cell size. The interface is located between the bubble and droplet regions.

In order to calculate the two-phase flow in the bubble and droplet region ($f = 0$ and $f = 1$, respectively) individually and to adopt different empirical correlations for bubbles and droplets, the void fraction is expressed as

$$\alpha = f\alpha_b + (1 - f)\,\alpha_d. \tag{1.5}$$

Consequently, two conservation equations are necessary

- for the volumetric total fraction of the bubble region[3]

$$\frac{\partial f}{\partial t} + U_{L,k}\frac{\partial f}{\partial x_k} = 0. \tag{1.6}$$

- for the volumetric liquid fraction within the bubble region

$$\frac{\partial f\phi_b}{\partial t} + \frac{\partial f\phi_b U_{L,k}}{\partial x_k} = -\left(\Gamma_{\mathrm{ed}} - \Gamma_{\mathrm{dd}}\right), \tag{1.7}$$

[3] use of Piecewise-Linear Interface Construction (PLIC) algorithm for interface reconstruction.

where $\phi_b \equiv 1 - \alpha_b$ and Γ_{ed} and Γ_{dd} represent droplet entrainment and deposition rates, respectively. Within the interface region ($0 < f < 1$) $\phi_d \equiv 1 - \alpha_d$ is evaluated as

$$\phi_d = \frac{1 - \alpha - f\phi_b}{1 - f}. \tag{1.8}$$

- Similarly, for the droplet region the volumetric gas fraction is evaluated:

$$\frac{\partial \left(1 - f\right) \phi_d}{\partial t} + \frac{\partial \left(1 - f\right) \phi_d U_{G,k}}{\partial x_k} = \left(\Gamma_{\mathrm{ed}} - \Gamma_{\mathrm{dd}}\right). \tag{1.9}$$

Furthermore, it is worth noting additional model features and characteristics:

- The advanced two-fluid model can deal with incompressible two-phase flows with Newtonian fluids.
- Interfacial forces are considered for both bubbles and droplets encompassing the drag force, lift force and turbulent diffusion force. The surface tension force is accounted for by the Continuous-Surface-Force (CSF) model of Brackbill [4].
- A two-phase $k - \epsilon$ model is adopted to account for turbulence effects (turbulent energy production and dissipation) due to the presence of the gas-liquid interface, small bubbles and droplets.

As a conclusion, the advanced two-fluid model of Akimoto and Yoshida has to be regarded as efficient hybrid model capable of simulating two-phase flows with large and small scale interface structures. In particular, the necessary specific treatment of bubbles and droplets in the interfacial region within the hybrid TFM-VoF method is described in detail. However, little is known on entrainment and deposition rate modeling, which has to be considered as crucial.

Minato et al. Minato et al. demonstrate the capabilities of their so-called *Extended Two-Fluid Model* in [8–14]. This model realizes the combined merits of the two-fluid model and the Volume-of-Fluid approach. However, in contrast to the aforementioned methods this is entirely attempted within the two-fluid model framework. This means that the governing equations of the extended two-fluid model are those of the conventional two-fluid model, but the solution techniques differ dependent on the spatial resolution and the scale of the interface structure under consideration. This approach has been motivated by the need for an improved and verified simulation technique for three-dimensional, complex, heterogeneous and intermittent gas-liquid flows with the capability beyond that of the conventional two-fluid model. Conceptually the extended two-fluid model has been proposed as hybrid simulation method of

- macroscopic interface motion with a steep volumetric phase (void) fraction gradient
- microscopic dispersed phase motion as a continuous field of the volumetric gas fraction.

Thus, the extended two-fluid model treats macroscopic interface structures with a larger scale than the underlying mesh cells as intermittent and heterogeneous features, i.e., as discontinuous profiles of the volumetric phase (void) fraction. For this purpose, the transport of the 'step-wise' void profile is utilized using the downwind discretization scheme as long as the resultant void fraction is between zero and one, while the upwind discretization scheme is employed in order to maintain boundedness, i.e., in the limits of the void fraction being zero and one, respectively. On the other side, the extended two-fluid model treats microscopic interface structures with a scale smaller than the mesh cells in an averaged manner as in the conventional two-fluid model.

In particular, the following model features and characteristics have to be highlighted:

- The extended two-fluid model is capable of describing complex three-dimensional heterogeneous and intermittent flow of incompressible two-phase system with Newtonian fluids.
- As the extended two-fluid model is entirely based on governing equations known from the conventional two-fluid model, several model terms have been generalized to enable the treatment of gas-liquid interfaces:
  - In order to account for interfacial friction, a friction force is stated as

$$\mathbf{F}_{k,k'}^{(\mathrm{f})} = \frac{\alpha_g \alpha_l \left(\rho_l - \rho_g\right) g}{\bar{V}_{gj}^2} |\mathbf{u}_{k'} - \mathbf{u}_k| \left(\mathbf{u}_{k'} - \mathbf{u}_k\right), \tag{1.10}$$

    where the friction coefficient has been stated according to Andersen [2] on the basis of one-dimensional transient two-phase flow and the steady-state drift-flux theory. $\bar{V}_{gj}$ denotes the drift velocity, $\bar{V}_{gj} = \sqrt{2}\left[\sigma g \left(\rho_l - \rho_g\right)/\rho_l^2\right]^{1/4}$. Moreover, the model accounts for virtual mass and wall friction effects.
  - For turbulence modeling it is simply assumed that the eddy viscosity is proportional to the kinematic viscosity with a multiplier of 10. However, for the bubble-induced eddy-viscosity, a more sophisticated and generalized approach is attempted: the well-known model of Sato and Sekoguchi [19] is adapted to treat general features of the gas-liquid interface by replacing the bubble size and the relative velocity with the Taylor length and the drift-flux velocity, respectively:

$$\epsilon_i^{(\mathrm{generalized})} = 4 \alpha_g \alpha_l \, \lambda_{\mathrm{Taylor}} \, \bar{V}_{gj}, \tag{1.11}$$

where the Taylor length is calculated as $\lambda_{\text{Taylor}} = 2\pi\sqrt{\sigma/g\,(\rho_l - \rho_g)}$. This treatment is stabilizing and thus considered necessary, as the two-fluid model cannot account for surface tension.

As conclusion, the extended two-fluid model has to be considered as a first attempt to treat both heterogeneous/intermittent and dispersed two-phase flows employing a unified framework on the basis of the well-established governing equations of the two-fluid model. However, especially the adopted models suffer from a physical justification and lack of mathematical rigour.

Štrubelj et al. Štrubelj et al. suggest a *combined model* suitable for both stratified and dispersed flows [34, 35]. The underlying physical picture is based on the work of Černe et al. [27], that is stratified flows exhibit 'large' and dispersed flows 'small interfaces'. The underlying numerical grid spacing is assessed in order to distinguish 'small' from 'large' interface structures. However, Štrubelj et al. argue that the main shortcoming of Černe's coupled approach is the different number of governing equation in distinct regions of the same computational domain. As a remedy they suggest to utilize the two-fluid model in the whole domain and to implement an appropriate 'interface tracking/sharpening' algorithm, when stratified flow is encountered. To switch the 'interface tracking/sharpening' algorithm on and off, a transition criterion is suggested, which discriminates large interfacial length scales in stratified flows from small (sub-grid) interfacial length scales in dispersed flows.

Štrubelj et al. have identified four crucial sub-models stating the main features and characteristics of their combined approach. This covers a

- model for the surface tension force, which has to be split between the two phase momenta governed by the two-fluid model. Following Bartosiewicz et al. [3], this split in phase-contributions is suggested to take the form

$$\vec{F}_{S,k} = \beta_k \vec{F}_S, \tag{1.12}$$

where $\vec{F}_S$ and $\vec{F}_{S,k}$ represent the surface tension force density according to Brackbill et al. [4] and its contribution to the momentum of phase k, respectively. Consequently, $\sum_{k=1,2} \beta_k \stackrel{!}{=} 1$ must be fulfilled, as the sum of the two phase momenta eventually has to result in a force density due to surface tension being equivalent to $\vec{F}_S$. For the split factor β_k, several models have been considered by Štrubelj et al. .

  - According to Bartosiewicz et al. , an appropriate model can be based on a mass average

$$\beta_k \equiv \frac{\alpha_k \rho_k}{\sum\limits_{k=1,2} \alpha_k \rho_k} \tag{1.13}$$

or, alternatively, on a volume average

$$\beta_k \equiv \alpha_k. \tag{1.14}$$

  - Štrubelj et al. additionally proposed to add the surface tension force entirely to the momentum of the heavier phase $\beta_1 \equiv 1$, or alternatively, to the lighter one $\beta_2 \equiv 1$.

- interface 'tracking/sharpening' algorithm, which has been based on the so-called '*conservative level-set method*' by Olsson and Kreiss [15–17]. Originally, this approach traces back to the work of Harten [6]. The algorithm comprises two steps. In a first step the continuity equation is solved. Then, an additional equation is solved in order to counter-act the numerical diffusion utilizing artificial compression[4]:

$$\frac{\partial \alpha_1}{\partial \tau} + \nabla_\bullet \left(\alpha_1 \left(1 - \alpha_1\right) \vec{n}\right) = \epsilon \Delta \alpha_1, \tag{1.15}$$

  which is solved until steady-state is reached. In doing so, the interface representation is maintained as sharp as possible. τ represents an artificial time. Moreover, $\vec{n}$ denotes the interface normal vector $\vec{n} \equiv \frac{\nabla \alpha_1}{|\nabla \alpha_1|}$, which is evaluated only at the beginning of the artificial compression step.

- model for the interfacial drag force, which Štrubelj et al. suggests as follows:

$$\vec{F}_{D,1} = \alpha_1 \alpha_2 \left(\vec{u}_2 - \vec{u}_1\right) \rho_m \frac{c_D}{d}, \tag{1.16}$$

  where c_D, ρ_m and d denote the drag coefficient, mixture density and interfacial length scale, respectively. However, Štrubelj et al. concede that this model suffers from physical background and is adopted solely to 'more or less equalize' the phase velocities in vicinity to the interface. This is achieved by adjusting the interfacial length scale d such that it takes values that are sufficiently small to cause a strong coupling and, consequently, equal phase velocity.

- model for the transition criterion, which is supposed to locally distinguish between stratified flow with large interfacial length scales and dispersed flow with small interfacial length scales relative to the local grid size. Štrubelj et al. suggest a combination of two scalar criteria:
  - *curvature criterion*, which is based on a normalized surface tension force,

$$\gamma_\kappa \equiv \frac{\Delta x^2 |\vec{F}_S|}{\sigma} \overset{!}{>} \gamma_\kappa^* = 0.1, \tag{1.17}$$

    in order to switch-off the interface 'tracking/sharpening' algorithm for large curvatures (small radii of interfacial structures).

[4] Note in passing, that a closer examination of this equation reveals a inconsistency in the dimension of the compressive term.

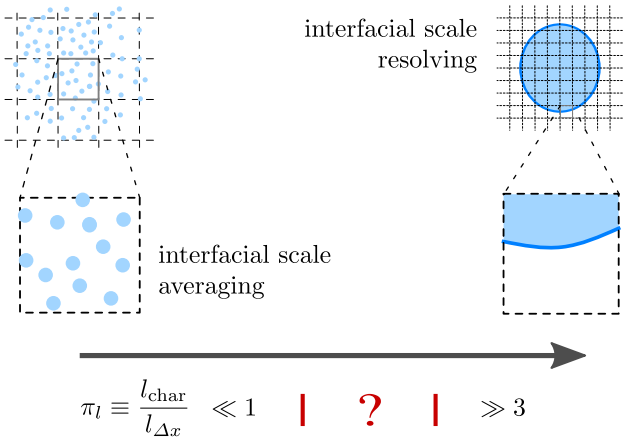

Figure 1.2: Scale inconsistency of prevailing Eulerian multi-scale CMFD approaches.

– *interfacial area density transition criterion*, which is based on the maximum interfacial area density on a computational stencil ❑ of 3x3 cells in a two-dimensional simulation. The interfacial area density transition criterion is used to recognize

$$\begin{aligned} &\text{dispersed flow} && \gamma_t \equiv \max_{❑}\left(|\nabla\alpha|\right)\Delta x \overset{!}{<} \gamma_t^* \quad \text{and} \\ &\text{stratified flow} && \gamma_t \equiv \max_{❑}\left(|\nabla\alpha|\right)\Delta x \overset{!}{>} \gamma_t^*, \end{aligned} \tag{1.18}$$

and then switch between drag force models for stratified and dispersed flows, respectively. Appropriate values for γ_t^* are found to be between 0.3 and 0.65.

Concluding, the combined model of Štrubelj et al. has to be regarded as a first approach to comprehensively incorporate capabilities of the Volume-of-Fluid method into the two-fluid model framework. However, Štrubelj et al. attempt to deduce crucial models for stratified flows from the established two-fluid model for dispersed flows mostly motivated by pure numerical considerations without a sound physical background. It is hardly surprising that this approach is associated with a severe scope of uncertainty.

All the aforementioned approaches attempt to explicitly couple the two-fluid model with the Volume-of-Fluid method or to partially mimic the Volume-of-Fluid method within the two-fluid model framework. It is Tomiyama [20], who enables to clearly recognize the issue around these approaches by introducing the dimensionless ratio $d^\star \equiv \frac{d_\text{b}}{\Delta x}$: if $d^\star \gg 1$, i.e., for the bubble diameter being much larger than the computational cell size, the VoF method is adopted, while for $d^\star \leq 1$, a two- or

multi-fluid approach is utilized. A generalization can be obtained when adopting a characteristic interfacial length scale l_{char} instead of the bubble diameter, which results in $\pi_l \equiv \frac{l_{char}}{l_{\Delta x}}$ instead of $d^\star$ as shown in figure 1.2. In consequence, there is still a gap in the scales, which renders the above hybrid methods inconsistent. It is not clear, to what extend the hybrid approaches suffer from this inconsistency. However, this does introduce another level of uncertainty and (at least) casts severe doubts on the applicability of these models to correctly capture transient multi-scale two-phase flows.

1.3. Scope and Objectives

A more general modeling framework is needed, that *not only inherently* encompasses both interfacial scale resolving and interfacial scale averaging approaches, *but also consistently* involves *intermediate* scale situations. Henceforth, such an approach based upon a consistent model capturing under-resolved interfacial features will be presented. For this purpose, the two-fluid approach states the pivotal subject of this thesis.

In the following, the consistent derivation of a novel comprehensive model framework shall be examined, starting from first principles that are the local instantaneous conservation equations for mass, momentum and chemical species as well as related interfacial jump conditions. This eventually will lead to a closed set of governing equations suitable for numerical simulations of two-phase multi-scale flows. I.e., the resulting model framework will encompass both interfacial scale resolving and averaging approaches enabling a smooth transition between these limiting cases.

The remainder of this thesis comprises two parts, the first of which covers the theoretical and numerical basics, while the second one sets out its concrete utilization. The first part is organized as follows:

Part I – Theory and Development

Chapter 2 provides the theoretical basis for the two-phase model framework, starting from first principles: the conditional volume-averaging technique is introduced and applied to both the local instantaneous generic transport equations for transport in a two-phase system and to the coupling interfacial jump conditions. As demonstrated, this enables us to treat the local instantaneous (microscopic) two-phase flow structures in a beneficial manner – i.e., representing the transport and interfacial jump of mass, momentum and chemical species in a two-phase system by use of generic equations and (moreover) of one arbitrary general intensive flow quantitity.

Chapter 3 In this chapter constitutive relations are suggested accomplishing a sound closure for interfacial scale resolving and interfacial scale averaging models. Finally, the framework is expanded to a multi-scale methodology. This results into a novel closure framework covering the intermediate interfacial scale range allowing for partially (un)resolved scales within the flow domain – which is deemed necessary for varying flow types exhibiting different characteristical interfacial scales as the flow evolves.

Chapter 4 presents a Finite Volume Method (FVM) being based on control volumes that exhibit an arbitrary shape. Consistent to chapter 2, the discretization of a generic transport equation for an arbitrary general intensive physical flow quantitity is examined – on a term by term basis. Comments are provided on the close relationship between the size and shape of the averaging volume stating the basis of the conditional volume-averaging technique (chapter 2) and the size and shape of a control or computational cell volume being considered within the FVM for arbitrarily unstructured meshes. Finally the algorithm being capable to the numerical solution of the governing model equations for a multi-scale two-phase flow is assembled.

Part II – Results & Publications

At the outset of this research, it has been clear that considering the immersed interface concept, one field of methods – namely the interfacial scale resolving methods – was alleged to be far less developed than the other – the interfacial scale averaging methods. However, it is the author's opinion that previous works have attempted to enhance interfacial scale averaging methods in a way, that surely is no longer in the original spirit of Ishii's two-fluid model. These enhancements attempt to provide information on details of the two-phase flow on a level significantly higher than the underlying methodology is able to provide. Consequently, this is done at the costs of additional models being necessary to compensate for this 'lack of compatibility'. Thus, within the framework of this work emphasize has been set upon the development of appropriate modeling approaches being compatible with each other.

The second part of this thesis covers papers that have been published during this research project. The topics therein encompass pivotal key aspects of Eulerian two-phase flow modeling being based upon the conditional volume-averaging procedure and the immersed interface concept, the theoretical and numerical basis of which has been set out in chapter 1-4: interfacial scale averaging techniques (chapter 5 and 6 – gas-liquid flow in bubble columns), interfacial scale (fully) resolving techniques (chapter 7 – single rising bubble & species transfer across fluid interfaces) and multi-scale gas-liquid flows (chapter 8 – hybrid interface-resolving two-fluid model).

Chapter 5 and 6 Chapter 5 aims at the exposure of the expected simulation quality considering *basic* models for two-fluid-model based simulations of dispersed gas-liquid flows in bubble columns at high gas fractions. As a subject of interest for these kind of gas-liquid reactors both the fluid dynamics and liquid mixing characteristics in bubble columns have been examined. For this purpose, solely models exhibiting conceptual proximity to the underlying two-fluid model approach (in the sense as stated above), have been ultimately applied.

Chapter 6 focuses on the evaluation of simulation results obtained by a selection of models as they were introduced in chapter 5. The results are further compared with those reported in literature. The main focus was set on capturing the characteristic process and design parameters of bubble columns.

Chapter 7 aims at the application of the methodology as set out in the chapters 2 and 3, however, fully resolving the interfacial scales and thus proving its usability for segregated flow types – using the example of a single bubble rising in quiescent liquid.

The methodology is demonstrated for the case of species transport across a fluid (bubble) interface. The derivation of the novel *Continuous-Species-Transfer (CST)* method is presented, which enables interface capturing techniques to deal with species transfer in a straightforward manner considering cases, where both steep concentration gradients (at high Schmidt numbers) and a sharp concentration jump (at high Henry coefficients due to different species' solubility) occur at the fluid interface. Thus, the main objective of this study was to establish the CST method for species transfer across fluid interfaces of arbitrary morphology in free-surface flows at high viscosity and density ratios.

For this purpose, detailed numerical simulations of single rising bubbles have been performed at high resolutions. Results were compared to experimental results and correlations derived thereof.

Chapter 8 presents the theoretical basis and application of a generalized multi-scale model framework based on the Eulerian-Eulerian two-fluid methodology, which has been derived in chapter 2 and 3. The main idea is based on the immersed interface concept and conditional volume-averaging (spatial filtering) of the fundamental conservation equations and a specific approach for closure modeling. The two-phase flow features are first divided into an unresolved portion (on sub-grid scale) and a resolved portion, and subsequently interpreted on a physical basis leading to sound closure relations.

The resulting hybrid interface-resolving two-fluid model (HIRES-TFM) enables to capture the mean interfacial evolution and allows for under-resolving interfacial details (microscale curvature and interfacial boundary layer) in a way

that enables to consider large-scale flow domains and, moreover, renders it compatible with the LES framework for turbulence modeling. Moreover, this multi-scale interface-capturing approach inherently bridges the gap in scales to the well-established two-fluid model for dispersed flows. For this purpose the concept of interpenetrating continua has been accomplished by the concept of partially penetrating continua. Hence, the presented multi-scale model framework generally enables to treat both dispersed and segregated flow types simultaneously in the same flow domain – just requiring distinct, type-specific closures.

The chapter provides results for various two-phase test cases, against which the model has been validated. Both experimental and analytical reference data are in a very good agreement with the results obtained by HIRES-TFM.

Chapter 9 summarizes this thesis and offers some suggestions and conclusions for future research work.

References

[1] A. Alajbegovic and J. Han. Simulation of multiphase flows in complex geometry using a hybrid method combining the multi-fluid and the Volume-Of-Fluid (VOF) approaches. In *ASME Joint U.S.-European Fluids Engineering Conf. (Fluids2002)*, pages 887–892, Montreal, Quebec, Canada, July 14-18 2002. 9

[2] J. G. M. Andersen. Interfacial shear for two-fluid models. *Trans. Am. Nucl. Soc.*, 41:669–671, 1982. 12

[3] Y. Bartosiewicz, J. Lavieville, and J.-M. Seynhaeve. A first assessment of the NEPTUNE_CFD code: Instabilities in a stratified flow comparison between the VOF method and a two-field approach. *Int. J. Heat Fluid Flow*, 29(2):460–478, 2008. 13

[4] J. U. Brackbill, D. B. Kothe, and C. Zemach. A continuum method for modeling surface tension. *J. Comput. Phys.*, 100(2):335–354, 1992. 11, 13

[5] C. Dopazo. On conditioned averages for intermittent turbulent flows. *J. Fluid Mech.*, 81(03):433–438, 1977. 3

[6] A. Harten. The artificial compression method for computation of shocks and contact discontinuities. I – Single conservation laws. *Comm. Pure Appl. Math.*, 30:611–638, 1977. 14

[7] R. J. Leveque and Z. Li. The immersed interface method for elliptic equations with discontinuous coeffcients and singular sources. *SIAM J. Numer. Anal.*, 31:1019–1044, 1994. 3

[8] A. Minato, T. Nagayoshi, M. Misawa, A. Suzuki, H. Ninokato, and S. Koshizuka. Numerical simulation method of complex 3d gas-liquid two-phase flow. In *5th Int. Conf. Multiphase Flow, ICMF 2004*, pages 1–11, May 30 - June 4 2004. No. 170. 11

[9] A. Minato, T. Nagayoshi, K. Takamori, I. Harada, M. Mase, and K. Otani. Numerical simulation of gas-liquid two-phase flow in siphon outlets of pumping plants. available online at `http://www.hitachi-pt.com/products/si/pump/pdf/pump_04.pdf`, January 2008. 11

[10] A. Minato, N. Nakajima, and T. Nagahara. Simulation of two-phase flow in pumping stations. In *Advances in the Modeling Methodologies of Two-Phase Flows*, 2004. 11

[11] A. Minato, N. Nakajima, and T. Nagahara. Simulation of two-phase flow in pumping stations. *La Houille Blaunche*, 1:59–64, 2006. 11

[12] A. Minato, N. Nakajima, T. Nagahara, and K. Kariya. Three-dimensional two-phase flow simulation of siphon self-priming in pumping stations. In *23rd IAHR Symp. Hydraulic Machinery and Systems*, pages 1–6, 2006. 11

[13] A. Minato, K. Takamori, and N. Ishida. An extended two-fluid model for interface behavior in gas-liquid two-phase flow. In *8th Int. Conf. Nuclear Engineering, ICONE 8*, volume 6 of *Part A*, pages 27–35, April 2-6 2000. 11

[14] T. Nagayoshi, A. Minato, M. Misawa, A. Suzuki, M. Kuroda, and N. Ichikawa. Simulation of multi-dimensional heterogeneous and intermittent two-phase flow by using an

extended two-fluid model. *J. Nucl. Sci. Technol.*, 40(10):827–833, 2003. 11

[15] E. Olsson. *Mass Conserving Simulations of Two Phase Flow.* PhD thesis, KTH School of Computer Science and Communication, Stockholm, Sweden, 2006. 14

[16] E. Olsson and G. Kreiss. A conservative level set method for two phase flow. *J. Comput. Phys.*, 210(1):225–246, 2005. 14

[17] E. Olsson, G. Kreiss, and S. Zahedi. A conservative level set method for two phase flow II. *J. Comput. Phys.*, 225(1):785–807, 2007. 14

[18] C. S. Peskin. Numerical analysis of blood flow in the heart. *J. Comput. Phys.*, 25:220–252, 1977. 3

[19] Y. Sato and K. Sekoguchi. Liquid velocity distribution in two-phase bubble flow. *Int. J. Multiphase Flow*, 2(1):79, 1975. 12

[20] A. Tomiyama, K. Sakoda, K. Hayashi, A. Sou, N. Shimada, and S. Hosokawa. Modeling and hybrid simulation of bubbly flow. In *Japan-US Sem. Two-Phase Flow Dynamics*, December 6-11 2004. 8, 15

[21] A. Tomiyama, K. Sakoda, K. Hayashi, A. Sou, N. Shimada, and S. Hosokawa. Modeling and hybrid simulation of bubbly flow. *Multiphase. Sci. Tech.*, 18(1):73–110, 2006. 8

[22] A. Tomiyama and N. Shimada. A numerical method for bubbly flow simulation based on a multi-fluid model. *J. of Pressure Vessel Technology*, 123(4):510–516, 2001. 8

[23] A. Tomiyama and N. Shimada. (N+2)-field modeling for bubbly flow simulation. *Comp. Fluid Dyn. J.*, 9(4):418–426, 2001. 8

[24] A. Tomiyama, N. Shimada, and H. Asano. Application of number density transport equation for the recovery of consistency in multi-fluid model. In *4th ASMER-JSME Joint Fluids Engineering Conference (CD-ROM)*, pages 1–7, 2003. FEDSM'03 No.45168. 8

[25] A. Tomiyama, N. Shimada, I. Zun, T. Noguchi, and T. Yakawa. NP2-3D: An (N+2)-field model for computing mesoscale and macroscale multiphase flows. In *ASME FEDSM2001-18191*, 2001. 8, 9

[26] O. Ubbink and R. I. Issa. A method for capturing sharp fluid interfaces on arbitrary meshes. *J. Comput. Phys.*, 153(1):26–50, 1999. 9

[27] G. Černe. *Two-Fluid Flow Simulation with the Coupling of Volume-Of-Fluid Model and Two-Fluid Model.* PhD thesis, University of Ljubljana, Faculty of Mathematics and Physics (Department of Physics), 2001. 6, 13

[28] G. Černe, S. Petelin, and I. Tiselj. Simulation of the instability in the stratified two-fluid system. In *Int. Conf. Nuclear Energy in Central Europe*, 1999. 6, 7

[29] G. Černe, S. Petelin, and I. Tiselj. Model for the simulation of the interface dispersion. In *Int. Conf. Nuclear Energy in Central Europe*, September 11-14 2000. 6, 7

[30] G. Černe, S. Petelin, and I. Tiselj. Upgrade of the VOF method for the simulation of the dispersed flow. In *ASME Fluids Engineering Division Summer Meeting*, Boston, Massachusetts, 2000. 6, 7

[31] G. Černe, S. Petelin, and I. Tiselj. Analysis of the interface tracking errors. In *Int. Conf. Nuclear Energy in Central Europe*, September 10-13 2001. 6, 7

[32] G. Černe, S. Petelin, and I. Tiselj. Coupling of the interface tracking and the two-fluid models for the simulation of incompressible two-phase flow. *J. Comput. Phys.*, 171(2):776–804, 2001. 6, 7, 9

[33] G. Černe, S. Petelin, and I. Tiselj. Numerical errors of the volume-of-fluid interface tracking algorithm. *Int. J. Numer. Meth. Fluids*, 38:329–350, 2002. 6, 7

[34] L. Štrubelj. *Numerical Simulations of Stratified Two-Phase Flows with Two-Fluid Model and Interface Sharpening*. PhD thesis, University of Ljubljana, Faculty of Mathematics and Physics (Department of Physics), 2009. 13

[35] L. Štrubelj, I. Tiselj, and B. Mavko. Simulations of free surface flows with implementation of surface tension and interface sharpening in the two-fluid model. *Int. J. Heat Fluid Flow*, 30(4):741–750, 2009. 13

[36] H. Yoshida. Draft Report – Development of analytical procedures on two-phase flow in tight-lattice fuel bundles for innovative water reactor for flexible fuel cycle (FLWR). Personal communication, July 2007. 9

[37] H. Yoshida, A. Ohnuki, T. Misawa, K. Takase, and H. Akimoto. Development of analytical procedures on two-phase flow in tight-lattice fuel bundles for innovative water reactor for flexible fuel cycle (FLWR). In *Int. Congress on Advances in Nuclear Power Plants – ICAPP 2006*, pages 1593–1600. American Nuclear Society, 555 North Kensington Avenue, La Grange Park, IL 60526 (United States), American Nuclear Society - ANS, La Grange Park (United States), 2006. 9

[38] H. Yoshida, A. Ohnuki, K. Takase, M. Kureta, H. Akimoto, H. Okada, and K. Yamamoto. Development of mechanistic boiling transition model in rod bundles. In *11th Int. Conf. Nuclear Engineering*, April 20–23 2003. ICONE-11-36097. 9

[39] H. Yoshida, H. Tamai, K. Takase, T. Nagayoshi, and H. Akimoto. Development of predictable technology for thermal/hydraulic performance of reduced-moderation water reactors (3) – Current status of development of three-dimensional two-phase flow simulation method. In *Int. Congr. Advances in Nuclear Power Plants – ICAPP 2004*, 2004. 9

2

Theory

While mathematical correctness does not imply physical validity, the latter cannot be obtained without the former.

D.A. Drew & S.L. Passman [1]

Abstract

This chapter provides the consistent derivation of the governing equations for two-phase flows, on the basis of which computational simulations in the field of Computational Multi-Fluid Dynamics (CMFD) are routinely accomplished.

We start from first principles, that are instantaneous conservation equations and interfacial jump relations for mass, momentum and chemical species. Conditioning and averaging eventually results in fundamental yet unclosed two-phase model equations suitable for evaluation.

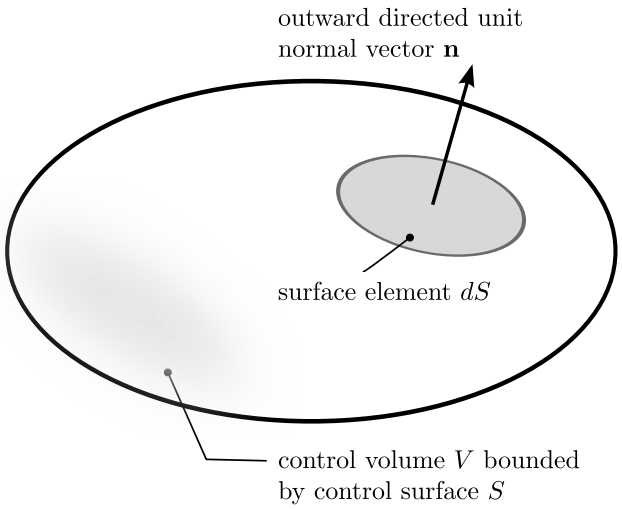

Figure 2.1: Control volume – Single-phase flow.

The central approach both in CFD for single-phase and in CMFD for two- and multiphase flows is to balance generally conserved quantities such as mass, momentum and chemical species. These quantities are assumed to change continuously within each phase, whereas discontinuous jumps might be observed at the phase interface(s). Thus, for the following it is instructive to distinguish the single-phase from the two-phase situation considering the associated transport of mass, momentum and species separately – first *within the bulk* and hereafter *across the interface* of a phase under consideration.

As a presumption but without loss of generality we shall focus and restrict ourself to isothermal two-phase flows of immiscible and incompressible Newtonian fluids.

2.1. Local Instantaneous Bulk Conservation Equations

2.1.1. Single-phase Flow

In a first step, consider a control volume V that is arbitrary in its shape and spatially fixed within an Eulerian framework as illustrated in figure 2.1. Over this control volume balances shall be formulated in the following. For this, suppose that one fluid of density ρ crosses the control volume's surface S at an infinitesimal surface element dS with a velocity $\mathbf{U}$.

Let $\mathbf{\Phi}(\mathbf{x}, t)$[1] be an arbitrary general intensive physical quantitity, e.g. a fluid property (scalar or tensor of any rank) being transported within a spatio-temporal domain. Note that the transport quantity $\mathbf{\Phi}$ represents the intensive equivalent of extensive balance quantities, e.g., mass, momentum and energy, on the basis of which balance equations are stated commonly.

According to these balances the rate of change of $\mathbf{\Phi}$ in time within an arbitrary control volume V is generally constituted from different contributions, that are either volume or surface sources and thus can be assembled accordingly as:

$$\begin{aligned}\frac{d}{dt}\int_{V(t)} \rho\mathbf{\Phi}\, dV = &- \oint_{S(t)} \mathbf{n}_\bullet \left(\rho\mathbf{\Phi}\mathbf{U}\right)\, dS \\ &- \oint_{S(t)} \mathbf{n}_\bullet \left(-\mathit{\Gamma}_{\mathbf{\Phi},d}\nabla\mathbf{\Phi}\right)\, dS \\ &+ \int_{V(t)} S_{\mathbf{\Phi}}(\mathbf{\Phi})\, dV. \end{aligned} \tag{2.1}$$

The general balance given by equation 2.1 states that the total amount of $\mathbf{\Phi}$ will change within the control volume V if a diffusive or convective net flux across the bounding control surface S takes place, or a source/sink within the control volume V itself causes an increase/decrease of $\mathbf{\Phi}$. ρ and $\mathbf{U}$ represent the phase density and velocity, respectively. $S_{\mathbf{\Phi}}$ denotes a generic volumetric source term. $\mathit{\Gamma}_{\mathbf{\Phi},d}$ represents a generic transport coefficient for the diffusive transport of the quantity $\mathbf{\Phi}$.

In order to assort the terms of equation 2.1, commonly two differential geometry theorems are employed, that are valid for any material control volume $V(t)$. For an arbitrary vector $\mathbf{a}$ it is:

- Leibniz' theorem

$$\frac{d}{dt}\int_{V(t)} \mathbf{a}\, dV = \int_{V(t)} \frac{\partial \mathbf{a}}{\partial t}\, dV + \oint_{S(t)} \mathbf{n}_\bullet \mathbf{U}_S \mathbf{a}\, dS. \tag{2.2}$$

  Being arbitrary in shape but fixed in space and time, the displacement velocity of the control surface S becomes $\mathbf{U}_S = \mathbf{0}$, such that the last term of equation 2.2 can be omitted henceforth.

- Gauss' theorem

$$\int_{V(t)} \nabla_\bullet \mathbf{a}\, dV = \oint_{S(t)} \mathbf{n}_\bullet \mathbf{a}\, dS, \tag{2.3}$$

$$\int_{V(t)} \nabla \mathbf{a}\, dV = \oint_{S(t)} \mathbf{n}\mathbf{a}\, dS, \tag{2.4}$$

[1] In order to accentuate that a flow quantitity can be a scalar, vector or tensor, henceforth $\mathbf{\Phi}(\mathbf{x}, t)$ shall be used, denoting an arbitrary intensive physical quantity – instead of the more common and conversant notation $\phi(\mathbf{x}, t)$.

Table 2.1: Coefficients for the generic transport equation (single-phase flow).

balance	$\boldsymbol{\Phi}$	$\Gamma_{\boldsymbol{\Phi},d}$	$S_{\boldsymbol{\Phi}}$
mass	1	0	0
momentum	$\mathbf{U}$	μ	$\rho\mathbf{g} - \nabla p$
species	x_i	ρD_i	$\hat{R}_i$
	$M/\rho\, c_i$	$M\, D_i$	$M\, R_i$

where tantamount to $\mathbf{n}\, dS$ the surface area vector $d\mathbf{S} = \mathbf{n}\, dS$ (both of which pointing outwards in normal direction on the surface $S(t)$ of the material control volume $V(t)$) shall be introduced for the further course of this thesis.

Using Leibniz' theorem according to equation 2.2 the l.h.s. of equation 2.1 might be rearranged bringing the time derivative inside the integral, which is feasible since the control volume V is spatially fixed:

$$\frac{d}{dt}\int_{V(t)} \rho\boldsymbol{\Phi}\, dV = \int_{V(t)} \frac{\partial}{\partial t}\left(\rho\boldsymbol{\Phi}\right)\, dV. \tag{2.5}$$

Next, applying Gauss' theorem according to equations 2.3 and 2.4 both surface integrals, i.e., the convective and diffusive terms on the r.h.s. of equation 2.1, can be rewritten in terms of volume integrals:

$$\oint_{S(t)} \mathbf{n}_\bullet \left(\rho\boldsymbol{\Phi}\mathbf{U}\right)\, dS = \int_{V(t)} \nabla_\bullet \left(\rho\boldsymbol{\Phi}\mathbf{U}\right)\, dV \quad \text{and} \tag{2.6}$$

$$\oint_{S(t)} \mathbf{n}_\bullet \left(\Gamma_{\boldsymbol{\Phi},d}\nabla\boldsymbol{\Phi}\right)\, dS = \int_{V(t)} \nabla_\bullet \left(\Gamma_{\boldsymbol{\Phi},d}\nabla\boldsymbol{\Phi}\right)\, dV. \tag{2.7}$$

Then, substituting equation 2.5, 2.6 and 2.7 into equation 2.1 gives

$$\int_{V(t)} \left[\frac{\partial}{\partial t}\left(\rho\boldsymbol{\Phi}\right) + \nabla_\bullet \left(\rho\boldsymbol{\Phi}\mathbf{U}\right) - \nabla_\bullet \left(\Gamma_{\boldsymbol{\Phi},d}\nabla\boldsymbol{\Phi}\right) - S_{\boldsymbol{\Phi}}(\boldsymbol{\Phi})\right]\, dV = 0. \tag{2.8}$$

As the control volume V can be chosen arbitrarily – it just needs to be fixed spatially as a constraint – tantamount to the integral on the l.h.s. of equation 2.8 its integrand may be set to zero, resulting in the so-called *generic transport equation* for $\boldsymbol{\Phi}$,

$$\frac{\partial}{\partial t}\left(\rho\boldsymbol{\Phi}\right) + \nabla_\bullet \left(\rho\boldsymbol{\Phi}\mathbf{U}\right) - \nabla_\bullet \left(\Gamma_{\boldsymbol{\Phi},d}\nabla\boldsymbol{\Phi}\right) - S_{\boldsymbol{\Phi}}(\boldsymbol{\Phi}) = 0. \tag{2.9}$$

As transport equations mostly exhibit this generic mathematical structure, one simply has to replace the transport quantity, coefficients and source terms in equation

2.9 according to table 2.1 in order to arrive at the well-known local-instantaneous governing equations of continuum mechanics, representing the principles of

- conservation of mass (local instantaneous continuity equation)

$$\frac{\partial \rho}{\partial t} + \nabla\bullet\left(\rho\mathbf{U}\right) = 0. \tag{2.10}$$

Note for an incompressible fluid ($\rho = \text{const}$) equation 2.10 reduces to

$$\nabla\bullet\mathbf{U} = 0, \tag{2.11}$$

rendering the flow divergence-free with a solenoidal velocity field.

- conservation of linear momentum (henceforth local instantaneous momentum equation)

$$\frac{\partial \rho\mathbf{U}}{\partial t} + \nabla\bullet\left(\rho\mathbf{U}\mathbf{U}\right) - \nabla\bullet\left(\mu\nabla\mathbf{U}\right) = \rho\mathbf{g} - \nabla p. \tag{2.12}$$

Note in passing that equation 2.12 can be rewritten into a more common form by reformulation of the diffusive term for incompressible Newtonian flows decomposing the velocity gradient tensor $\nabla\mathbf{U}$ into a symmetric ($\mathbf{D}$) and antisymmetric ($\mathbf{S}$) part:

$$\nabla\bullet\left(\mu\nabla\mathbf{U}\right) = \mu\nabla\bullet\left(\nabla\mathbf{U}\right) = \mu\nabla\bullet\left(-\left(\mathbf{D}+\mathbf{S}\right)\right) \tag{2.13}$$
$$\text{with } \mathbf{D} \equiv -\frac{1}{2}\left(\nabla\mathbf{U} + \left(\nabla\mathbf{U}\right)^T\right) \text{ and } \mathbf{S} \equiv -\frac{1}{2}\left(\nabla\mathbf{U} - \left(\nabla\mathbf{U}\right)^T\right),$$

representing the rate-of-strain (or rate-of-deformation) tensor, being positive for compressive contributions, and the vorticity (or spin) tensor, which does not contribute to viscous shear and/or compression.

Then by defining[2] the total momentum flux tensor (or total stress tensor) as

$$\boldsymbol{\sigma} \equiv p\mathbf{I} + \boldsymbol{\tau} \quad \text{where} \quad \boldsymbol{\tau} = 2\mu\mathbf{D}, \tag{2.14}$$

[2] In most treatises on mechanical engineering or fluid mechanics a different convention is chosen, that is the negative transposed of $\boldsymbol{\sigma}$. As the total stress tensor for a Newtonian fluid is symmetric a transposition is not particularly worrisome ($\boldsymbol{\sigma} = \boldsymbol{\sigma}^T$, due to angular momentum conservation); however the sign convention is interesting: Throughout this thesis the total stress tensor is defined such that $-\int_S \left(\boldsymbol{\sigma}\bullet\mathbf{n}\right) dS$ can be interpreted as rate of increase of momentum due to *external* forces acting on the fluid *inside* the control volume V – constituted of both the body force exerted by gravity and the surface force exerted by the surrounding fluid [2]. Hence the total momentum within the control volume V will increase for a net influx of momentum across the bounding surface S (and vice versa). Doing so leads to two benefits regarding consistency: (i) For one-dimensional heat conduction (Fourier's law, $q_y = -\lambda\frac{dT}{dy}$) and one-dimensional species diffusion (Fick's law, $j_i = -D_i\frac{dc_i}{dy}$) the heat/species flux is positive when heat/species is moving in the positive y-direction. It is felt that in analogy for a simple shear flow of a Newtonian fluid (Newton's law, $\sigma_{yx} = -\mu\frac{du}{dy}$) the viscous flux σ_{yx} should be defined positive if the momentum flux moves in positive y-direction (direction of decreasing velocity). (ii) If the total stress tensor $\boldsymbol{\sigma}$ is decomposed into an isotropic (static) pressure part and a deviatoric (dynamic) viscous part as given by equation 2.14, both contributions have the same sign. I.e., compression is positive in both contributions – in accordance with the sign convention commonly employed in thermodynamics.

the momentum equation becomes

$$\frac{\partial \rho \mathbf{U}}{\partial t} + \nabla\bullet\left(\rho \mathbf{U}\mathbf{U}\right) = \rho\mathbf{g} - \nabla\bullet\boldsymbol{\sigma}. \tag{2.15}$$

Similarly, for an incompressible fluid

$$\frac{\partial \mathbf{U}}{\partial t} + \nabla\bullet\left(\mathbf{U}\mathbf{U}\right) = \mathbf{g} - \nabla\bullet\boldsymbol{\sigma}/\rho. \tag{2.16}$$

- conservation of chemical species
  As for the total mass, also the components i of a particular phase give rise to conserved quantities. Generally this can either be expressed mass-based (mass fraction x_i) or volume-based (molar concentration c_i). Thus, for a constant mixture density $\rho = const$ (assuming incompressible flow and dilute species concentration) it is

$$\frac{\partial x_i}{\partial t} + \rho\nabla\bullet\left(x_i\mathbf{U}\right) - \nabla\bullet\left(D_i\nabla x_i\right) - \hat{R}_i/\rho = 0, \quad \text{and} \tag{2.17}$$

$$\frac{\partial c_i}{\partial t} + \nabla\bullet\left(c_i\mathbf{U}\right) - \nabla\bullet\left(D\nabla c_i\right) - R_i = 0. \tag{2.18}$$

2.1.2. Two-phase Flow

In order to extend the consideration towards a two- or multiphase case, it is instructive to immerse an assemblage of interfaces separating the phases of the system within the control volume V (see *immersed interface concept* – page 5) [3–5]. Note that the control volume as depicted in figure 2.2 is still spatially fixed and arbitrary in its shape, but contrary to the single-phase situation it is now constituted by several phase volumes $V_k \subseteq V \bigcup_{k=\varphi,\phi,\ldots} V_k$, each possessing an interface S_I separating it from its neighboring phase. In consequence, the control surface S is composed of phase surfaces $S_k \subseteq S \bigcup_{k=\varphi,\phi,\ldots} S_k$ that come into existence where the control volume V cuts the phase volumes V_k. Note further that generally more phases, i.e., a third phase κ, might be present within the control volume. However, without loss of generality[3] these will be dropped in the remainder of this thesis when discussing the interaction of two arbitrary phases φ and ϕ. In the following, the former phase, i.e., phase φ, shall be examined, whereas the latter phase ϕ is considered as an arbitrary phase neighbor.

Generic Transport Equation in a Two-Phase System

Owed to the presence of two or more phases within the control volume V, it is now necessary to distinguish among the contributions of phases to the transport

[3] One or more additional phases would be treated analogously without imposing additional complexity.

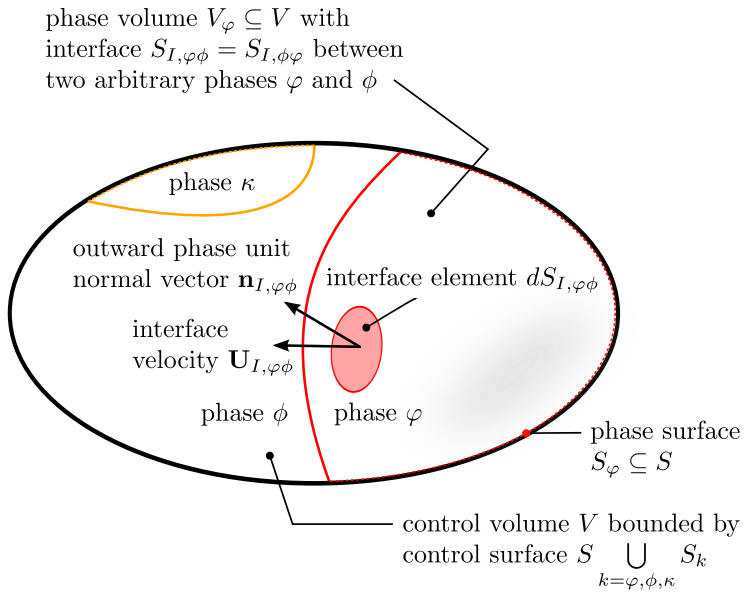

Figure 2.2: Control volume – Two-phase flow.

quantity $\mathbf{\Phi}$. For this purpose the balances have to be considered over the *phase* surfaces S_k and the *phase* volumes V_k – with $k \in [\varphi, \phi]$.

Examining the transport of $\mathbf{\Phi}$ within the control volume V, one has to bear in mind that due to the presence of two phases, *interfacial contributions* have to be taken into account that stem from both phases φ and ϕ. As will be seen, these in effect couple the bulk phase transport equations derived in the antecedent of this section. The overall balance equation for $\mathbf{\Phi}$ within the control volume V holding two phases φ and ϕ reads:

$$\begin{aligned}\sum_{k=\varphi,\phi}\left(\frac{d}{dt}\int_{V_k(t)}\rho\mathbf{\Phi}\,dV\right) = &-\sum_{k=\varphi,\phi}\int_{S_k(t)}\mathbf{n}_{k\bullet}\left(\rho\mathbf{\Phi}\mathbf{U}\right)\,dS\\ &-\sum_{k=\varphi,\phi}\int_{S_k(t)}\mathbf{n}_{k\bullet}\left(-\Gamma_{\mathbf{\Phi},d}\nabla\mathbf{\Phi}\right)\,dS\\ &+\sum_{k=\varphi,\phi}\int_{V_k(t)}S_{\mathbf{\Phi}}\left(\mathbf{\Phi}\right)\,dV\\ &+\frac{1}{2}\sum_{k=\varphi,\phi}\sum_{j=\varphi,\phi}\left(1-\delta_{jk}\right)\int_{S_{I,jk}(t)}S_{\mathbf{\Phi},I}\left(\mathbf{\Phi}\right)\,dS. \quad (2.19)\end{aligned}$$

The first three terms hold the already introduced bulk (phase interior) contributions *within* the phases φ and ϕ, respectively. The last term on the r.h.s. of equation

2.19 represents the *coupling interfacial* source term. δ_{jk} herein denotes Kronecker's delta.

Again applying Leibniz' theorem according to equation 2.2, e.g., for phase φ, yields

$$\frac{d}{dt}\int_{V_\varphi(t)} \rho\mathbf{\Phi}\, dV = \int_{V_\varphi(t)} \frac{\partial}{\partial t}\left(\rho\mathbf{\Phi}\right)\, dV + \int_{S_{I,\varphi\phi}(t)} \mathbf{n}_{I,\varphi\phi} \bullet \mathbf{U}_{I,\varphi\phi}\left(\rho\mathbf{\Phi}\right)\, dS, \tag{2.20}$$

where the last term on the r.h.s. arises since the surface displacement velocity $\mathbf{U}_{I,\varphi\phi}$ of the phase interface $S_{I,\varphi\phi}$ usually is non-zero.

The Gauss' theorem according to equations 2.3 and 2.4, for instance resulting for phase φ results in

$$\int_{S_\varphi(t)} \mathbf{n}_{\varphi\bullet}\left(\rho\mathbf{\Phi}\mathbf{U}\right)\, dS = \int_{V_\varphi(t)} \nabla\bullet\left(\rho\mathbf{\Phi}\mathbf{U}\right)\, dV - \int_{S_{I,\varphi\phi}(t)} \mathbf{n}_{I,\varphi\phi}\bullet\left(\rho\mathbf{\Phi}\mathbf{U}\right)\, dS \qquad \text{and} \tag{2.21}$$

$$\int_{S_\varphi(t)} \mathbf{n}_{\varphi\bullet}\left(-\mathit{\Gamma}_{\mathbf{\Phi},d}\nabla\mathbf{\Phi}\right)\, dS = \int_{V_\varphi(t)} \nabla\bullet\left(-\mathit{\Gamma}_{\mathbf{\Phi},d}\nabla\mathbf{\Phi}\right)\, dV - \int_{S_{I,\varphi\phi}(t)} \mathbf{n}_{I,\varphi\phi}\bullet\left(-\mathit{\Gamma}_{\mathbf{\Phi},d}\nabla\mathbf{\Phi}\right)\, dS. \tag{2.22}$$

Hence, the balance equation 2.19 can be compacted as

$$0 = \sum_{k=\varphi,\phi}\int_{V_k(t)}\left[\frac{\partial}{\partial t}\left(\rho\mathbf{\Phi}\right) + \nabla\bullet\left(\rho\mathbf{\Phi}\mathbf{U}\right) - \nabla\bullet\left(\mathit{\Gamma}_{\mathbf{\Phi},d}\nabla\mathbf{\Phi}\right) - S_{\mathbf{\Phi}}\left(\mathbf{\Phi}\right)\right] dV - \frac{1}{2}\sum_{k=\varphi,\phi}\sum_{j=\varphi,\phi}\left(1-\delta_{jk}\right)\int_{S_{I,kj}(t)}\left[\rho\mathbf{\Phi}\left(\mathbf{U}-\mathbf{U}_{I,kj}\right)\bullet\mathbf{n}_{I,kj} - \left(\mathit{\Gamma}_{\mathbf{\Phi},d}\nabla\mathbf{\Phi}\right)\bullet\mathbf{n}_{I,kj} + S_{\mathbf{\Phi},I}\right] dS. \tag{2.23}$$

As equation 2.23 is valid for arbitrary phase volumes V_k and arbitrary configurations of phase interfaces $S_{I,\varphi\phi}$ within V, the two terms and therein the integrands can be set to zero interchangeably. Thus, the local instantaneous generic transport equation can be deduced from the first integrand (representing the bulk phase contributions). I.e., for phase φ it might be stated

$$\frac{\partial\rho\mathbf{\Phi}}{\partial t} + \nabla\bullet\left(\rho\mathbf{\Phi}\mathbf{U}\right) - \nabla\bullet\left(\mathit{\Gamma}_{\mathbf{\Phi},d}\nabla\mathbf{\Phi}\right) - S_{\mathbf{\Phi}}\left(\mathbf{\Phi}\right) = 0, \tag{2.24}$$

as it has already been the result for the single phase case (equation 2.9). However, considering the two- or multi-phase case, there is always coupling with (at least) another transport equation of the same type due to the presence of a neighboring phase ϕ. Hence, interfacial jump conditions have to be specified from the second term of equation 2.23 in order to close the system, as professed in the next section.

Table 2.2: Coefficients for the generic transport equation (two-phase flow).

balance	$\boldsymbol{\Phi}$	$\Gamma_{\boldsymbol{\Phi},d}$	$S_{\boldsymbol{\Phi}}$	$S_{\boldsymbol{\Phi},I}$
mass	1	0	0	0
momentum	$\mathbf{U}$	μ	$\rho\mathbf{g} - \nabla p$	$\|p\mathbf{n}_I\| - \sigma\kappa_{I,\varphi\phi}\,\mathbf{n}_{I,\varphi\phi} - \nabla_{I,\varphi\phi}\sigma$
species	x_i	ρD_i	$\hat{R}_i$	0
	$M/\rho\, c_i$	$M\, D_i$	$M\, R_i$	0

2.2. Local Instantaneous Interfacial Jump Conditions

As a consequence of different phases being present in the control volume V, coupling relations have to be specified. This results in local instantaneous jump conditions for a generic transport quantity $\boldsymbol{\Phi}$. Note that the generic condition as set out in the second term of equation 2.23 is independent of the particular choice of the phases φ and ϕ. φ and ϕ are interchangeable, i.e., $\mathbf{n}_{I,\varphi\phi} = -\mathbf{n}_{I,\phi\varphi}$. Hence, this symmetry can be utilized to simplify the derivation. Introducing a jump notation, where $\|\cdot\|$ shall denote a jump across the interface S_I as $\|f\| \equiv f_{I,\varphi} - f_{I,\phi}$, the second term in equation 2.23 reveals

$$\|\rho\boldsymbol{\Phi}\,(\mathbf{U} - \mathbf{U}_I)\,\bullet\mathbf{n}_I - (\Gamma_{\boldsymbol{\Phi},d}\nabla\boldsymbol{\Phi})\,\bullet\mathbf{n}_I\| = -S_{\boldsymbol{\Phi},I}, \tag{2.25}$$

where the subscript I in $S_{\boldsymbol{\Phi},I}$ has been adopted as a short form of $I, \varphi\phi$ for the sake of readability.

Now equation 2.25 enables to formulate the local instantaneous jump conditions for mass, momentum and chemical species. It follows by use of table 2.2:

- local instantaneous interfacial jump condition for mass

  $$\|\rho\,(\mathbf{U} - \mathbf{U}_I)\,\bullet\mathbf{n}_I\| = 0. \tag{2.26}$$

  Equation 2.26 simply states that mass transfered from phase φ to phase ϕ is the same in its value but opposite in direction with respect to the mass transfered from phase ϕ to phase φ. Hence, no mass is lost.

- local instantaneous interfacial jump condition for momentum

  $$\|\rho\mathbf{U}\,(\mathbf{U} - \mathbf{U}_I)\,\bullet\mathbf{n}_I - \boldsymbol{\sigma}\bullet\mathbf{n}_I\| = \sigma\kappa_{I,\varphi\phi}\,\mathbf{n}_{I,\varphi\phi} + \nabla_I\sigma, \tag{2.27}$$

  where $\nabla_I \equiv (\mathbf{I} - \mathbf{n}_{I,\varphi\phi}\,\mathbf{n}_{I,\varphi\phi})\,\bullet\nabla$ denotes the interface gradient operator. This becomes relevant solely when the interfacial tension σ generally depends on the

interface composition or temperature. However, considering σ to be uniform this term might be neglected henceforth. Thus, the surface tension is assumed to be constant, not varying along the interface.

Now, decomposing the total stress tensor $\boldsymbol{\sigma}$ in its isotropic (static) and deviatoric (dynamic) component according to equation 2.14, yields the *dynamic condition*:

$$\| \rho \mathbf{U} \left(\mathbf{U} - \mathbf{U}_I \right) \bullet \mathbf{n}_I - \left(p \mathbf{n}_I + \boldsymbol{\tau} \bullet \mathbf{n}_I \right) \| = \sigma \kappa_{I,\varphi\phi} \, \mathbf{n}_{I,\varphi\phi} \, . \tag{2.28}$$

From this, it is evident that in the absence of interfacial mass transfer, the surface tension force is solely balanced by pressure and stress forces.

- local instantaneous interfacial jump condition for chemical species

$$\| \left(-D_i \nabla c_i \right) \bullet \mathbf{n}_I \| = 0. \tag{2.29}$$

In most cases the species i transfered across the interface will be exposed to different solubilities in the phases pertaining to each side of the interface. In consequence, another interfacial jump relation is needed in order to account for an interfacial concentration jump of transferred species. It is common practice to do so by means of a simple distribution relation known as Henry's law, which reads

$$\| c_i \| = c_{i;I,\varphi} \cdot (1 - He) \quad \Leftrightarrow \quad He = \frac{c_{i;I,\phi}}{c_{i;I,\varphi}}. \tag{2.30}$$

2.3. Concept of Conditioning for Phase Discrimination

In order to *realize* the immersed interface concept, i.e., to derive governing equations that are valid throughout the entire flow domain of a two-phase system, one needs to discriminate one phase from each other selectively. This is accomplished by making the local instantaneous equations *conditional* on the presence of a particular phase before examining the balance of conserved quantities over the control volume. In doing so, it is achieved that only those parts within the control volume, that do contain the particular phase under consideration, contribute to the (conditional) conservation equation.

2.3.1. Conditioning and Conditioned Quantities

Conditioning of the arbitrary general local instantaneous quantity $\boldsymbol{\Phi}$ is provided by multiplication with the so-called *phase indicator function* I_φ, that takes the value one within phase φ and zero elsewhere. The product $I_\varphi \boldsymbol{\Phi}$ is generally entitled *conditioned quantity* and is denoted $\boldsymbol{\Phi}_\varphi$ in the remainder of this thesis, $\boldsymbol{\Phi}_\varphi \equiv I_\varphi \boldsymbol{\Phi}$.

In this view, the terms *conditioning* and *conditional* are used henceforth in the meaning: use of the phase indicator function in order to pick out an arbitrary property pertaining to the phase of interest while ignoring this property in other phases. It has however to be stressed that both $\mathbf{\Phi}$ and $\mathbf{\Phi}_\varphi$ are defined throughout the domain, and, thus, are promoting the immersed interface concept consistently and to the full extent, if the phase indicator function is chosen properly – as set forth in the following.

2.3.2. Phase Indicator Function and Phase Distribution Function

The definition of the phase indicator function $I_\varphi(\mathbf{x}, t;\, \mu)$[4] is given by equation 2.31.

$$I_\varphi(\mathbf{x}, t;\, \mu) = \begin{cases} 1 & \text{if } \mathbf{x} \in \varphi \text{ at time } t \text{ in realization } \mu \\ 0 & \text{otherwise,} \end{cases} \tag{2.31}$$

where μ denotes the realization of interest in an ensemble of possible interface configurations within the control volume. However, aiming at a deterministic (rather than probabilistic) framework to describe phenomena within a two-phase system, we might restrict ourself to one realization – thus, $\mu = 1$. Mathematically the phase indicator function I_φ may be expressed as Heaviside unit step function $\mathbb{H}$ operating on the so-called *phase distribution function* – a continuous scalar property, that exhibits the local instantaneous position of the interface. This phase distribution function, denoted as f_φ henceforth, might be stated more precisely as the signed distance function from the interface that is found to be positive within phase φ of interest, negative in the other phase(s) and zero at the interface itself. Thus,

$$I_\varphi(\mathbf{x},\, t) \equiv \mathbb{H}\left(f_\varphi(\mathbf{x},\, t)\right). \tag{2.32}$$

While in a multiphase system (arbitrary number of phases) the phase distribution function needs to be defined for each phase present, the situation considerably simplifies in the particular case of a two-phase flow, because $I_\varphi = \mathbb{H}(f_\varphi)$ and $I_\phi = \mathbb{H}(-f_\varphi)$. This directly implies that $I_\varphi + I_\phi = 1$, meaning that only one phase distribution f_φ and subsequently one phase indicator function I_φ needs to be considered in order to completely describe the local-instantaneous position of the interface(s) and phases within a two-phase system.

Note further that I_φ is piecewise continuous, hence, its integral as well as its spatial and temporal derivatives are clearly defined.

[4] Note that Weller [6, 7] uses an inconsistent notation: generally employing conditional ensemble-averaging but denoting the phase indicator function as $I_\varphi(\mathbf{x},\, t)$ implies the existence of only one realization. Ensemble-averaging would not be necessary at all in that case.

2.3.3. Interface Delta Function and Interface Transport Equation

Since after conditioning temporal and spatial derivatives of the phase indicator function are to be found in the local instantaneous conservation equations and jump conditions, a closer look on their interpretation seems to be of avail.

spatial The spatial derivative of the phase indicator function, ∇I_φ, can be expressed as

$$\begin{aligned}\nabla I_\varphi(\mathbf{x},t) &= -\delta_I\left(f_\varphi(\mathbf{x},t)\right)\nabla f_\varphi(\mathbf{x},t)\\ &= -\delta_I\left(f_\varphi(\mathbf{x},t)\right)\left|\nabla f_\varphi(\mathbf{x},t)\right|\mathbf{n}_{I,\varphi\phi}\\ &= -\delta_I\left(f_\varphi(\mathbf{x},t)\right)\mathbf{n}_{I,\varphi\phi}\,,\end{aligned} \tag{2.33}$$

since the eikonal identity $\left|\nabla f_\varphi\right| = 1$ holds for the signed distance function. This allows the interpretation of an *interface delta function* $\nabla I_\varphi(\mathbf{x},t)$. As can be seen, this function clearly excises the interface, on which it becomes the Dirac delta function[5]of the phase distribution function $\delta_I\left(f_\varphi(\mathbf{x},t)\right)$ in the direction normal to the interface pointing towards phase φ by $(-\mathbf{n}_{I,\varphi\phi})$. Elsewhere (within the phases) $\nabla I_\varphi(\mathbf{x},t)$ becomes zero.

temporal For the temporal derivative of the phase indicator function it is instructive to consider the temporal evolution of I_φ by following it along its path while moving with a – generally space and time dependent – velocity field that is the interfacial velocity $\mathbf{U}_I$:

$$\frac{\partial I_\varphi}{\partial t} + \mathbf{U}_{I,\varphi\phi}\bullet\nabla I_\varphi = 0, \tag{2.34}$$

revealing the simple physical fact that the phase interface travels with the interfacial velocity. Tantamount to this, the phase indicator function can be interpreted as Lagrangian invariant propagating according to the *interface transport equation*[6] 2.34.

[5] Note in passing that δ will be used purposively with two different meanings: On the one hand δ will hold as a Dirac delta function – as used above:

$$\delta_I \equiv \delta(\mathbf{x}-\mathbf{x}_I,\,t)\,,$$

denoting any point on the phase interface. Subsequently, $\mathbf{\Phi}_{I,\varphi} \equiv \delta_I\mathbf{\Phi}_\varphi$ represents the contribution from the general arbitrary quantity $\mathbf{\Phi}$ on the φ-side of the interface [8]. On the other hand δ is used as Kronecker's delta as well:

$$\delta_{\varphi\phi} \equiv \begin{cases}1 & \text{if } \varphi = \phi\\ 0 & \text{if } \varphi \neq \phi.\end{cases}$$

Note that from a mathematical point of view, the Dirac delta function might be seen as a continuous analog of Kronecker's delta, which is used in a discrete manner, i.e., in order to account for alternating phase contributions.

[6] also: topological equation

2.4. Averaging Procedures

The last section has been devoted to the detailed derivation of a local instantaneous set of governing equations for mass, momentum and chemical species in a two-phase system, starting from first principles that are the local instantaneous conservation (bulk phase) and interfacial jump relations (phase interface). Now we have to turn to the development of a sound averaging technique, the issue around which is a long-standing one in CMFD.

Hence, beforehand some aspects might be worth mentioning for comprehension in the further course of this thesis. Thus, a rather comprehensive yet necessary discussion about averaging in general is provided in the following.

2.4.1. Motivation of Averaging

Several numerical methods have been developed in order to solve the local instantaneous conservation equations at a local instantaneous (microscopic) level – often being referred to as Direct Numerical Simulation (DNS) methods. However, the 'exact' numerical solution of the detailed (local instantaneous – microscopic) evolution of interfacial structures in two-phase flow systems is utmost complex and thus a quite challenging task. This is owed to both physical and numerical aspects [9] – corollary note 2.1.

Corollary Note 2.1

- numerical restrictions:
  Despite their efficiency it is evident that DNS methods need a substantial amount of computation even for simple and small cases, while especially the interfacial boundary treatment needs considerable care. Hence, the numerical algorithm is often difficult and tedious. Therefore application of these methods is restricted to a very limited number of problems, aiming at a basic understanding of physics in proximity of interfaces.
- physical restriction:
  The idealization of interfaces being geometrical surfaces over which the fluids' properties change abruptly – resulting in intermittent structures with sharp discontinuities – is generally problematic, too. Numerical methods based upon this idealizing assumption encounter a severe problem when aiming at the simulation of so-called topological changes (e.g., coalescence and breakup) in two-phase systems or phase formation (e.g., nucleation in boiling flows) in initially single-phase systems. In these cases the model becomes singular.

Owing to the complexity in both physics (modeling singularities due topological changes or phase change) and numerics (computational costs and complex algorithms for interfacial boundary treatment) DNS methods are often disapproved. The exact solution approaching *all details* of the two-phase flow for most cases of practical interest is neither possible nor deemed to be necessary enough to be desirable [10]: it is rather well-established practice for most practical purposes to apply some sort of averaging procedure to the local instantaneous conservation equations and related jump conditions. This results into averaged governing equations for a broad class of two-phase flow problems avoiding the aforementioned problems at the cost of introducing the necessity of modeling and resolution constraints – as set out in the following.

2.4.2. Conceptual Approaches

In general, averaging can be seen as a low-pass filter procedure applied on a field at the scale of its fluctuating structures, by means of which solely high-wavenumber portions of the field under consideration are selectively removed. In consequence, this considerably reduces complexity and computational efforts when solving for averaged (instead of local instantaneous) equations.

However, as already intimated, averaged equations have become unclosed due to the applied averaging by means of additional *a priori* unknown terms stemming from the averaging procedure itself. Hence, averaging is always at the expense of the necessity of introducing sound closure models (relations for these a priori unknown terms). The closure in turn needs to account for the physics of those portions that have been filtered away and recover lost informations on an appropriate and physically sound basis.

There is a multitude of various model frameworks in which averaging is performed temporally (over an averaging time interval), spatially (over an averaging volume based upon an averaging length scale), statistically (over an ensemble representing a set of realizations) or by some combinations of these. Hence one could categorize averaging techniques basically into

- time-averaging,
- volume-averaging and
- ensemble-averaging.

It is widely recognized that the particular choice of an averaging technique *solely* affects the physical meaning of terms constituting the averaged governing equations and in consequence impair the physical interpretation of the subsequent closure models [11]. Nonetheless the mathematical rigour and the general structure is

retained – independent from the chosen averaging technique. However, as stated before, one generally has to comply with certain restrictions on the applied temporal and spatial resolution when employing averaging to local-instantaneous conservation equations. This clearly is related to the conceptual approach chosen for averaging.

Now before expatiating upon averaging approaches, it is advisable first to have a look at prevalent definitions for disambiguity [3]: Let $\mathcal{R}$ (often also Ω) be a space domain with $\mathbf{x} \in \mathcal{R}$ being a position vector; further denote $\mathcal{T}$ as a time domain and $\mathcal{E}$ as event space respectively, with $t \in \mathcal{T}$ being the time and $\mu \in \mathcal{E}$ being a particular realization of the process $\mathcal{P}$ under consideration. Then, let $\boldsymbol{\Phi}(\mathbf{x}, t;\, \mu)$ be an arbitrary general local instantaneous quantity, i.e., fluid property, any other scalar, vector or tensor of any rank at point ($\mathbf{x}$, t) in realisation μ. $\boldsymbol{\Phi}$ shall be defined in the entire fluid domain.

Henceforth the aforementioned basic averaging approaches shall be defined as follows when being applied on $\boldsymbol{\Phi}$:

- volume-averaging:

$$\overline{\boldsymbol{\Phi}}^{V} \equiv \frac{1}{V} \int_{V} \boldsymbol{\Phi}(\mathbf{x} + \boldsymbol{\eta}, t;\, \mu)\, d\mathbf{x}_{\boldsymbol{\eta}} \quad \text{with} \quad V \subset \mathcal{R}, \tag{2.35}$$

  where V denotes the averaging volume based on an averaging length scale Δ, which is invariant in time and space. The location vector $\mathbf{x}$ points to the centroid of V, whereas $\boldsymbol{\eta}$ is used as relative position vector to locate any position within V relative to its centroid.

  Volume-averaging is subject to the restrictions [3, 5, 12]

$$L_m \ll \Delta \ll L_M, \tag{2.36}$$

  where L_m denotes the length scale of the local instantaneous (microscopic fluctuating) structures, i.e., length scales of particles within a two-phase system, whereas L_M represents the characteristic macroscopic length scale of the system, i.e., the dimension of the flow domain.

  This means on the one hand, that it must be ensured that V is sufficiently large and infinitesimal translations do not bias the magnitude of the averaged quantities within the volume V. On the other hand, V must be chosen much smaller than the characteristic dimension of the system under consideration in order to ensure that using averaged quantities still represents local variations within the system sufficiently. Thus, the pivotal requirement for the choice of the size of the averaging volume V is to be still *representative*.

- time-averaging:

$$\overline{\mathbf{\Phi}}^{T} \equiv \frac{1}{T}\int_{T} \mathbf{\Phi}\left(\mathbf{x}, t;\, \mu\right) dt_{\tau} \quad \text{with} \quad T \subset \mathcal{T}, \tag{2.37}$$

  where, analogously to the volume averaging procedure, T denotes an averaging time interval over which $\mathbf{\Phi}$ is averaged temporally.

  In a uniform manner as for the averaging volume, restrictions are imposed on the averaging time scale T as well [3, 5, 12]:

$$T_m \ll T \ll T_M \tag{2.38}$$

  Essentially the inequalities 2.38 reflect the requirements that the time averaging period needs to be significantly larger than microscopic (fluctuating) time scales T_m, but smaller than the characteristic time scale of the flow T_M.

- ensemble-averaging:

$$\begin{aligned}\overline{\mathbf{\Phi}}^{E} &\equiv \lim_{N\to\infty} \frac{1}{N}\sum_{\mu=1}^{N} \mathbf{\Phi}\left(\mathbf{x},\, t;\, \mu\right) \quad \text{with } N \subset \mathcal{E}(\mathcal{P}) \\ &= \int_{\mathcal{E}} \mathbf{\Phi}\left(\mathbf{x},\, t;\, \mu\right) dm(\mu),\end{aligned} \tag{2.39}$$

  where $\mathcal{E}$ denotes the set of all possible realizations of the system, N being its size (total number of possible realizations) and μ representing a concrete realization observed during the process $\mathcal{P}$.

  As indicated by $dm(\mu)$ – the probability density on the set of all events $\mathcal{E}$ – the ensemble-average view of a physical process allows for an interpretation in terms of statistical repeatability. I.e., all observed realizations μ might be only seen as approximations of the ideal one: the expectation considering a very large set of realizations. Thus the ensemble average solely requires $N \to \infty$ to be representative; in particular, it is not subject to any spatial or temporal restrictions.

2.4.3. Averaging Rules

The three averaging approaches[7], as defined in the preceding discussion, have been established as rigour and sound mathematical procedures. Thus, they obey certain averaging rules, namely the Leibniz' and Gauss' rules (commutation) and the

[7] For the sake of brevity and ease of reading, the averaging operator shall further be denoted with a simple overbar not distinguishing between different averaging approaches as long as generally valid characteristics are subject of discussion.

Reynolds' rules (linearity and idempotence). Let $\boldsymbol{\Psi}(\mathbf{x}, t)$ be a second general arbitrary quantity – scalar or tensor of any rank – beside $\boldsymbol{\Phi}(\mathbf{x}, t)$; then averaging obeys the following averaging rules [4, 13]

commutation:

$$\overline{\frac{\partial \overline{\boldsymbol{\Phi}}}{\partial t}} = \frac{\partial \overline{\boldsymbol{\Phi}}}{\partial t}, \tag{2.40}$$

$$\overline{\nabla \overline{\boldsymbol{\Phi}}} = \nabla \overline{\boldsymbol{\Phi}}, \tag{2.41}$$

linearity:

$$\overline{\overline{\boldsymbol{\Phi}} + \overline{\boldsymbol{\Psi}}} = \overline{\boldsymbol{\Phi}} + \overline{\boldsymbol{\Psi}}, \tag{2.42}$$

$$\overline{\mathrm{c}\,\overline{\boldsymbol{\Phi}}} = \mathrm{c}\,\overline{\boldsymbol{\Phi}} \quad \text{and} \tag{2.43}$$

idempotence:

$$\overline{\overline{\boldsymbol{\Phi}}\,\overline{\boldsymbol{\Psi}}} = \overline{\boldsymbol{\Phi}}\,\overline{\boldsymbol{\Psi}}, \tag{2.44}$$

where c denotes an arbitrary constant scalar being both temporally and spatially fixed.

Note that for the above equalities to render generally valid, specific constraints on the averaging operation have to be fulfilled. Clearly, a spatial averaging operator being constant in time will commute with time derivatives. Moreover, a spatial averaging operator that is constant in space commutes with spatial derivatives. I.e., in case of volume-averaging the Gauss' rule is only valid, if the underlying spatial averaging operator is based upon a spatially homogeneous filter, that is the spatial filter width (e.g., size of the averaging volume) does not depend on the spatial position. Obviously, an analog constraint certainly applies to the Leibniz' rule and temporal filtering (time-averaging).

Considering volume-averaging, however, non-homogeneous spatial filters are surely interesting for adequately capturing relevant scales, that often vary significantly at different locations of the flow domain. As non-homogeneous spatial filtering does not commute with the spatial derivative, this does introduce a so-called commutation error or – from another point of view – an additional term to model. For single-phase Large Eddy Simulations (LES) this is a well known issue, for instance discussed in [14]. However, the situation for a general (turbulent) two-phase system is found to be more complex compared to single-phase phase turbulence: turbulence near phase interfaces exhibits distinct vortical structures rendering it anisotropic – backscatter of energy from unresolved to resolved scales [15, 16] (not considered in [17], for instance).

The undue modeling complexity that would result when employing a non-uniform spatial filter surely overweights its use. Hence for the remainder of this thesis, the averaging is performed assuming a constant uniform spatial filter. Moreover, particularly for two-phase flows being the pivotal topic of this study, the commutation

error might be assumed negligible – especially compared to modeling uncertainties surely introducing the main source of possible errors in this context. Hence, this issue shall not be addressed further within this study. Nevertheless, it is emphasized that in some cases the commutation error should have perceivable influence, that has yet not been in the focus of scientific research.

2.4.4. State-of-the-Art – A critical Review

It is commonly accepted that averaged model equations based on local instantaneous conservation equations for two-phase flows are far less developed and less reliable to catch up physical reality than their single-phase counter-parts, that employ the same averaging techniques in order to model turbulence [18]. At a first sight, this is surely caused by the lack of a clear mathematical framework *some of these models* suffer from. Moreover, there are considerable difficulties in both physical interpretation and (thus) the concrete modeling of many terms of the averaged governing equation.

Over the last two decades time- and volume-averaging have been widely adopted by many workers due to their straightforward, physical meaningful and direct interpretability of unclosed terms. However, there are difficulties when considering the modeling of these a priori unknown terms for cases of practical interest. This is caused by a lack of sound examination and thus the conclusions drawn from the interpretation of these terms. For instance, considering volume-averaging in detail, the problem class seems to be two-fold:

1.) The most serious problem with both time- and volume-averaging concerns the presupposition that one has to obey certain conditions imposed upon the resolution of the time or space domain for a *meaningful* time- or volume-average.

However, considering the volume-averaging technique, the prerequisite of a clear scale separation within the spatial domain cannot be observed in many cases of practical interest. The characteristic spatial dimension of a two-phase flow might approach the macroscopic scale of the system as the flow evolves. Nigmatulin [19] recognizes this problem of changing scale regimes in both directions emphasizing the need of a:

> "elementary macrovolume... the characteristic linear dimension of which are many times greater than the nonuniformities..., but *at the same time* much less than the characteristic macrodimension of a problem."

2.) To make it worse, for the most practical cases length and time scales are inherently related to each other. As a matter of fact, a characteristic linear dimension of a two-phase flow most certainly corresponds to its characteristic

time and thus can not be regarded in a decomposed manner. The presumption of decoupling of temporal and spatial scales is seldom satisfied.

Consequently, volume-averaged conservation equations are usually sought to be applicable in the case of highly transient flows since they are 'instantaneous' that is they do not base on time-averaging. But restrictions on spatial scales concomitantly affect the effective temporal resolution of the resulting equations when applied to flow under consideration, which is rather seldom addressed.

Therefore, in a strict sense, a volume-average should only be applied on model systems that clearly provide a scale separation within the spatial domain and ensure that the spatio-temporal state of the system can be decomposed and regarded as decoupled throughout the process under consideration.

Now, if one moves further from this model system to a realistic flow scenario of practical interest, two questions arise: 1.) As utilizing either time- or volume-averaging on its own seems to be troublesome, does a combination of these well-established approaches overcome the aforementioned problem? and 2.) Does the more general ensemble-averaging technique state an alternative?

1.) Many authors address the shortcoming issued under the first question by repeatedly applying volume- *and* time-averaging on the microscopic equations. Usually the first averaging technique being imposed is the volume-average. The resulting instantaneous volume-averaged equations however, are subject to temporal fluctuations caused by turbulence. Therefore, the second average that is commonly applied is the time-average. The result of this so-called *double-averaging* process is believed to yield governing equations that exhibit smooth transitions in both the temporal and spatial domain.

However, double-averaging introduces terms, that are complex to interpret and thus less than straightforward to model. Moreover, considering two-phase flows specifically against the background of intrinsically tied temporal and spatial scales it is simply impossible to separate two-phase (temporal) unsteadiness and (spatial) intermittence from corresponding characteristics in turbulence – as it initially has been intended by those authors when introducing the double-averaging. Hence, to the author's point of view, it is rather evident that double-averaging looses its ground of validity for many practical cases; that is in the event that volume-average and time-average domain are found to overlap or to be close to each other.

2.) Another avenue that is suggested by some workers is to employ the more fundamental and mathematical rigour ensemble-averaging procedure, because this technique is not subject to any spatial or temporal restrictions while remaining the physical significance and interpretability of resulting unclosed

terms. This in turn alleviates modeling. Moreover, it is argued that both the time- and the volume-average might be seen as special case of the ensemble average (ergodic hypothesis[8]).

Considering the ensemble-average, the problem has its seeds in the experimental validation base being very rarely. Despite the advantages and benefits that might be expedient from a theoretical point of view, to the author's opinion, it is a questionable practice to perform simulations based upon ensemble-averaged governing equations without the option of a sound validation study, which has to provide ensemble-averaged data from statistically representative experiments.

2.4.5. Conclusion, Scope & Objectives

In view of the antecendent discussion, the above approaches are abandoned while the central approach exposed in the remainder of this thesis is entirely based on *conditional volume-averaging* (section 2.5) [21]. The two-phase flow model resulting from this averaging procedure shall possess two characteristics:

- generality and flexibility

  The underlying concept is required to be independent of the specific nature of the two-phase flow under consideration. I.e., the derivation of the governing flow equations is independent from the particular flow type, the influence of which is transferred and grouped into closure terms being modeled appropriately.

- stability and robustness

  As a consequence of conditioning and volume-averaging, each phase is considered as independently interpenetrating each other (Eulerian-Eulerian two-fluid framework), while exchanging mass, momentum and species, which is modeled according to the underlying flow type.

  Moreover, the local-instantaneous governing equations are transferred into their conditional volume-averaged counter-parts, which in effect translates the originally sharp interfacial jump conditions into volume-averaged interfacial conditions, that consistently promote a smooth but still rapid transition of material and flow properties – as depicted in figure 2.3 for a demanding (segregated) two-phase flow scenario. The interfacial surface is replaced by an interfacial transition region. This in turn alleviates the shortcoming of sharp interface methods and facilitates both stability and robustness of the underlying numerical solution procedure.

[8] The interested reader is referred to [20] by A. Patrascioiu.

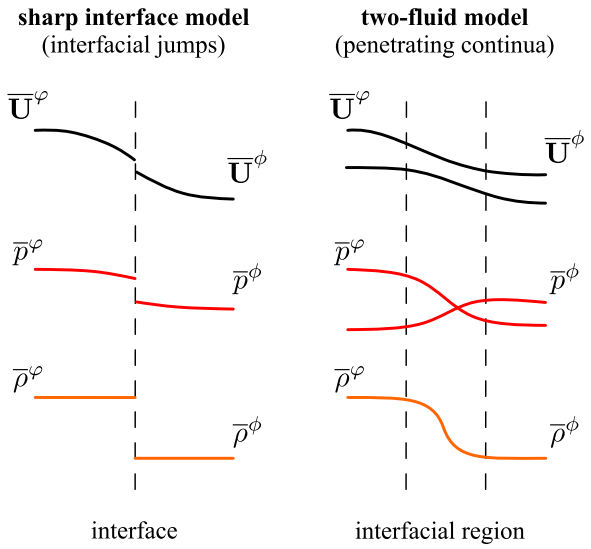

Figure 2.3: Sharp vs. continuous interface representation.

The choice of conditional volume-averaging seems beneficial and reasonable to the author for three reasons:

1.) the aforementioned advantages with respect to both generality and flexibility and to stability and robustness.

2.) the possibility to validate against experimental data being consistent (and thus comparable) to numerical results obtained from a conditional volume-averaged two-phase flow model.

3.) the conceptual proximity to the Large Eddy Simulation (LES) approach – as set out in the following section. This enables to the consistent treatment of turbulent two-phase flows, which certainly states the common case in industrial two-phase apparatus.

The next section exposes in considerable detail the consistent derivation of this modeling framework that will further be applied to various flow types at different scales. Therefore, a straightforward derivation of a general set of conditional-averaged governing equations based upon already derived local instantaneous conservation equations is presented in the remainder. This is found to be useful and instructive approaching the physical origin, and thereby the numerical treatment of model terms stemming from the averaging procedure.

2.5. Concept of the Conditional Volume-Averaging Technique

2.5.1. Averaged Arbitrary General Quantities

Starting from an unconditioned arbitrary general quantity $\mathbf{\Phi}$, which represents any physical property, scalar or tensor of any rank, conditioning and subsequent volume-averaging yields

$$\overline{I_\varphi \mathbf{\Phi}} = \overline{\mathbf{\Phi}}_\varphi = \frac{1}{V} \int_V I_\varphi \left(\mathbf{x} + \boldsymbol{\eta},\, t\right) \mathbf{\Phi} \left(\mathbf{x} + \boldsymbol{\eta},\, t\right) d\mathbf{x}_{\boldsymbol{\eta}}. \tag{2.45}$$

Since I_φ exhibits compact support, that is it takes the value unity within phase φ while it is zero elsewhere, equation 2.45 can be rewritten as

$$\begin{aligned} \overline{I_\varphi \mathbf{\Phi}} = \overline{\mathbf{\Phi}}_\varphi &\equiv \frac{1}{V} \int_{V_\varphi} \mathbf{\Phi} \left(\mathbf{x} + \boldsymbol{\eta},\, t\right) d\mathbf{x}_{\boldsymbol{\eta}} \\ &= \frac{V_\varphi}{V} \frac{1}{V_\varphi} \int_{V_\varphi} \mathbf{\Phi} \left(\mathbf{x} + \boldsymbol{\eta},\, t\right) d\mathbf{x}_{\boldsymbol{\eta}} \\ &= \alpha_\varphi \overline{\mathbf{\Phi}}^\varphi, \end{aligned} \tag{2.46}$$

where α_φ has been defined as *volumetric phase fraction* or *phase volume fraction*, $\alpha_\varphi \equiv V_\varphi / V$, and the so-called *phasic or intrinsic average* has been found to be defined according to

$$\overline{\mathbf{\Phi}}^\varphi \equiv \frac{1}{V_\varphi} \int_{V_\varphi} \mathbf{\Phi} \left(\mathbf{x} + \boldsymbol{\eta},\, t\right) d\mathbf{x}_{\boldsymbol{\eta}}. \tag{2.47}$$

As can be seen, $\overline{I_\varphi \mathbf{\Phi}} = \overline{\mathbf{\Phi}}_\varphi = \alpha_\varphi \overline{\mathbf{\Phi}}^\varphi$[9] clearly relates the phasic average $\overline{\mathbf{\Phi}}^\varphi$ of quantity $\mathbf{\Phi}$ with the volume average of the conditioned quantity $\overline{\mathbf{\Phi}}_\varphi$ – linearly over α_φ.

This gives rise to the physical view of conditional volume-averaging, that is of a procedure that *spreads* the contribution of phase φ uniformly over the entire averaging volume V as illustrated in figure 2.4a and 2.4b, superposing with the contribution of phase ϕ being averaged alike. Thus, $\overline{I_\varphi \rho} = \alpha_\varphi \overline{\rho}^\varphi$, for instance.

2.5.2. Analogy of Volume-Averaging Technique and Spatial Filtering in LES

Examining equation 2.47, a clear conceptual relation between the conditional volume-averaging procedure and the spatial filtering process becomes evident. The latter is

[9] Note that, in contrary to Weller [6, 7], the phasic average is denoted by an superscript, i.e., attached to the averaging operator. It has to be emphasized, that Weller's notation certainly leads to confusion, since it does not allow to distinguish a conditioned average $I_\varphi \overline{\mathbf{\Phi}} = \overline{\mathbf{\Phi}}_\varphi = \left(\overline{\mathbf{\Phi}}\right)_\varphi$ from the phasic average $\overline{I_\varphi \mathbf{\Phi}} = \overline{\mathbf{\Phi}}^\varphi$, however $\overline{\mathbf{\Phi}}_\varphi \neq \overline{\mathbf{\Phi}}^\varphi$.

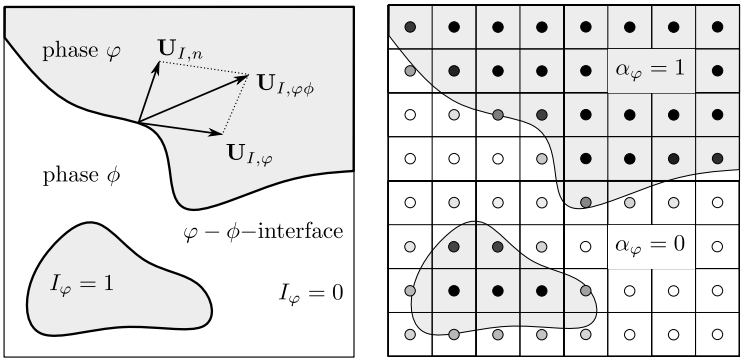

(a) physical domain Ω (local-instantaneous).

(b) computational domain (volume-averaged).

Figure 2.4: Conceptual approach of the conditional volume-averaging procedure.

well-known and commonly applied in the Large Eddy Simulation (LES) for single-phase turbulence modeling:

$$\overline{I_\varphi \boldsymbol{\Phi}}^G(\mathbf{x},\, t) = \int_\Omega G(\mathbf{r}, \Delta)\, I_\varphi(\mathbf{x}+\mathbf{r}, t)\, \boldsymbol{\Phi}(\mathbf{x}+\mathbf{r}, t)\; d\mathbf{r}, \tag{2.48}$$

with $G(\mathbf{x}+\boldsymbol{\eta}, \Delta)$ denoting the filter kernel (operator) corresponding to a three-dimensional box (or top-hat) filter, that exhibits a compact support[10] according to

$$\begin{aligned} G(\mathbf{r}, \Delta) \equiv & \frac{1}{\Delta^3} \mathbb{H}\left(\frac{\Delta}{2} - |\mathbf{r}|\right) \\ = & \begin{cases} \frac{1}{V} & \text{if } \mathbf{r} \in V \\ 0 & \text{otherwise} \end{cases} \qquad \text{with} \int_\Omega G(\mathbf{r}, \Delta)\, d\mathbf{r} \overset{!}{=} 1. \end{aligned} \tag{2.49}$$

By revisiting equations 2.35 and comparing to 2.47 (with $\boldsymbol{\eta} = \mathbf{x}+\mathbf{r}$), the conclusion can be drawn that $\overline{\boldsymbol{\Phi}_\varphi}^V$ and $\overline{\boldsymbol{\Phi}_\varphi}^G$ are to be taken identical, i.e., $\overline{\boldsymbol{\Phi}_\varphi}^V = \overline{\boldsymbol{\Phi}_\varphi}^G$.

However, note that this is only valid for G being a three-dimensional box filter kernel. For instance, employing any other filter kernel that might be commonly used in LES modeling, e.g., a Gaussian filter according to

$$G_G(\mathbf{r}, \Delta) = \sqrt{\frac{6}{\pi\Delta^2}} \exp \frac{6\mathbf{r}^2}{\Delta^2}, \tag{2.50}$$

would result in far-field contributions to the filtered quantity. Consequently, a filtered phase indicator function could no longer be *interpreted* as volumetric phase fraction

[10] G shall represent a localized filter function being only large for small $\mathbf{r}$'s.

within the control volume V. Thus, the physical view as depicted in figure 2.4 would loose its significance.

It is further important to stress the fact, that the spatial filter to choose within the context of two-phase flow modeling needs to be a homogeneous one – as already has been postulated for the averaging rules (section 2.4.3) as a necessity for the derivation of conditional volume-averaged governing equations. The reason for this rests in the two-phase flow exhibiting non-uniformity and anisotropy near a fluid interface. Consequently, a homogeneous spatial filter needs to be employed in order to avoid unduly complicated modeling.

Moreover, as will be seen through the course of chapter 4, there is an intimate relationship between the averaging length scale (filter width Δ) used for volume-averaging (spatial filtering) in physical space and the characteristic length scale ❑ of a finite volume in computational domain. If not taken into account, the governing equations (more exactly the closure) loose validity and thus the numerical procedure unavoidably leads to an unphysical solution. Hence, it has to be emphasized that this relationship inherently ties together the mathematical representation and the numerical solution methodology of the physical (continuum mechanical) problem.

For the remainder of this thesis a sufficiently well-behaved spatial filter (homogeneous with finite support) will be presumed when switching between the wordings *spatial filtering* and *volume-averaging*.

2.5.3. Averaged Products and Fluctuations

Generally the averaging of a term containing the product of local instantaneous (thus, on an averaging scale fluctuating) quantities $\boldsymbol{\Phi}$ and $\boldsymbol{\Psi}$ gives rise to correlations between their corresponding fluctuations.

E.g., for a single local instantaneous (fluctuating) quantity $\boldsymbol{\Phi}(\mathbf{x}, t)$ one may separate its average from fluctuating parts by *Reynolds decomposition* according to

$$\boldsymbol{\Phi}(\mathbf{x}, t) = \overline{\boldsymbol{\Phi}(\mathbf{x}, t)} + \boldsymbol{\Phi}'(\mathbf{x}, t), \tag{2.51}$$

where $\boldsymbol{\Phi}'(\mathbf{x}, t)$ denotes the fluctuating part with respect to the applied averaging scale. It is $\overline{\boldsymbol{\Phi}'(\mathbf{x}, t)} \stackrel{!}{=} 0$.

Now, for the average of the product $\overline{\boldsymbol{\Psi}\boldsymbol{\Phi}}$ one obtains

$$\begin{aligned}\overline{\boldsymbol{\Psi}\boldsymbol{\Phi}} &= \overline{\left(\overline{\boldsymbol{\Psi}}+\boldsymbol{\Psi}'\right)\left(\overline{\boldsymbol{\Phi}}+\boldsymbol{\Phi}'\right)} = \overline{\overline{\boldsymbol{\Psi}}\,\overline{\boldsymbol{\Phi}}+\overline{\boldsymbol{\Psi}}\,\boldsymbol{\Phi}'+\boldsymbol{\Psi}'\,\overline{\boldsymbol{\Phi}}+\boldsymbol{\Psi}'\boldsymbol{\Phi}'} \\ &= \underbrace{\overline{\boldsymbol{\Psi}}\,\overline{\boldsymbol{\Phi}}}_{\text{since } \overline{\overline{\boldsymbol{\Psi}}\,\overline{\boldsymbol{\Phi}}}=\overline{\boldsymbol{\Psi}}\,\overline{\boldsymbol{\Phi}}} + \underbrace{\overline{\boldsymbol{\Psi}}\,\overline{\boldsymbol{\Phi}'}+\overline{\boldsymbol{\Phi}}\,\overline{\boldsymbol{\Psi}'}}_{=0,\text{ since } \overline{\boldsymbol{\Phi}'}=\overline{\boldsymbol{\Psi}'}=\mathbf{0}} + \overline{\boldsymbol{\Psi}'\boldsymbol{\Phi}'} \\ &= \overline{\boldsymbol{\Psi}}\,\overline{\boldsymbol{\Phi}}+\overline{\boldsymbol{\Psi}'\boldsymbol{\Phi}'} \end{aligned} \tag{2.52}$$

As can be seen, the last term represents the average of the product of two fluctuating properties and thus needs modeling in order to arrive at a closed expression.

However, one may avoid this unclosed term by a more appropriate (weighted) decomposition of $\overline{\boldsymbol{\Phi}(\mathbf{x},\,t)}$ based on the average of $\boldsymbol{\Psi}\boldsymbol{\Phi}$:

$$\overline{\boldsymbol{\Phi}(\mathbf{x},\,t)} = \frac{\overline{\boldsymbol{\Psi}\boldsymbol{\Phi}}}{\overline{\boldsymbol{\Psi}}} - \frac{\overline{\boldsymbol{\Psi}'\boldsymbol{\Phi}'}}{\overline{\boldsymbol{\Psi}}} \equiv \widetilde{\boldsymbol{\Phi}} + \boldsymbol{\Phi}'', \tag{2.53}$$

where $\boldsymbol{\Phi}''(\mathbf{x},\,t)$ represents the fluctuation with respect to the weighted average, with $\overline{\boldsymbol{\Phi}''} \overset{!}{\neq} 0$ but $\widetilde{\rho\boldsymbol{\Phi}''} \overset{!}{=} 0$ (for the weight $\boldsymbol{\Psi}=\rho$, for instance). Now the average of the above product is found to be

$$\overline{\boldsymbol{\Psi}\boldsymbol{\Phi}} = \overline{\boldsymbol{\Psi}}\,\widetilde{\boldsymbol{\Phi}} \quad \text{, since } \widetilde{\boldsymbol{\Phi}} \equiv \frac{\overline{\boldsymbol{\Psi}\boldsymbol{\Phi}}}{\overline{\boldsymbol{\Psi}}}, \tag{2.54}$$

obviously omitting the additional correlation term while remaining the physical significance of all constituting terms, if the weight $\boldsymbol{\Psi}$ is chosen appropriately.

For the course of following-up derivations, it is advisable to introduce an appropriately weighted average on this basis, namely the so-called *phase-weighted average*[11] or *density-weighted (Favre) average*, with the weight being chosen as $\boldsymbol{\Psi} = I_\varphi\rho = \rho_\varphi$:

$$\widetilde{\boldsymbol{\Phi}}^{\varphi} \equiv \frac{\overline{I_\varphi\rho\boldsymbol{\Phi}}}{\alpha_\varphi\,\overline{\rho}^{\varphi}}. \tag{2.55}$$

In this view, both phasic (intrinsic) and phase-weighted conditional fluctuations are introduced according to

$$\boldsymbol{\Phi}'^{\varphi} \equiv \boldsymbol{\Phi} - \overline{\boldsymbol{\Phi}}^{\varphi} \quad \text{and} \tag{2.56}$$

$$\boldsymbol{\Phi}''^{\varphi} \equiv \boldsymbol{\Phi} - \widetilde{\boldsymbol{\Phi}}^{\varphi}, \tag{2.57}$$

that are the differences between the local instantaneous and corresponding phasic or phase-weighted volume-averages of the property $\boldsymbol{\Phi}$[12].

[11] not phasic average!

[12] Note that φ is used as superscript to indicate that the fluctuation occurs around their corresponding averages, contrary to the notation of Weller [6,7].

Hence, for the conditional volume-average of products one obtains

$$\overline{I_\varphi \boldsymbol{\Psi}\boldsymbol{\Phi}} = \alpha_\varphi \, \overline{\boldsymbol{\Psi}\boldsymbol{\Phi}}^\varphi = \alpha_\varphi \, \overline{\boldsymbol{\Psi}}^\varphi \, \overline{\boldsymbol{\Phi}}^\varphi + \alpha_\varphi \, \overline{\boldsymbol{\Psi}'^\varphi \boldsymbol{\Phi}'^\varphi}^\varphi \qquad \text{and} \tag{2.58}$$

$$\overline{I_\varphi \rho \boldsymbol{\Psi}\boldsymbol{\Phi}} = \alpha_\varphi \, \overline{\rho \boldsymbol{\Psi}\boldsymbol{\Phi}}^\varphi = \alpha_\varphi \, \overline{\rho}^\varphi \widetilde{\boldsymbol{\Psi}\boldsymbol{\Phi}}^\varphi = \alpha_\varphi \, \overline{\rho}^\varphi \widetilde{\boldsymbol{\Psi}}^\varphi \widetilde{\boldsymbol{\Phi}}^\varphi + \alpha_\varphi \, \overline{\rho}^\varphi \widetilde{\boldsymbol{\Psi}''^\varphi \boldsymbol{\Phi}''^\varphi}^\varphi. \tag{2.59}$$

2.5.4. Averaged Phase Indicator Function

Considering mass as transport quantity, and substituting $\boldsymbol{\Phi} = 1$ in equation 2.46 (compare to table 2.2) reveals

$$\overline{I_\varphi} \equiv \alpha_\varphi, \tag{2.60}$$

where α_φ denotes the *volumetric phase fraction* or *phase volume fraction* pertaining to phase φ within V[13] – as depicted schematically in figure 2.5a.

Similarly to the phasic volume-average $\overline{\boldsymbol{\Phi}}^\varphi$, it is further common to define the phase-weighted (density-weighted) average. From the equations 2.54 and 2.58 it follows:

$$\begin{aligned} \overline{I_\varphi \rho \boldsymbol{\Phi}} &= \alpha_\varphi \, \overline{\rho \boldsymbol{\Phi}}^\varphi = \alpha_\varphi \, \overline{\rho}^\varphi \, \overline{\boldsymbol{\Phi}}^\varphi + \alpha_\varphi \, \overline{\rho' \boldsymbol{\Phi}'}^\varphi \\ &= \alpha_\varphi \, \overline{\rho}^\varphi \widetilde{\boldsymbol{\Phi}}^\varphi. \end{aligned} \tag{2.61}$$

In the same line, the *density-weighted volume fraction* or *phase mass fraction* $\widetilde{\alpha_\varphi}$ can be defined as

$$\widetilde{\alpha_\varphi} \equiv \frac{\alpha_\varphi \, \overline{\rho}^\varphi}{\rho}, \tag{2.62}$$

where ρ denotes the mixture density in the averaging volume V.

2.5.5. Averaged Differential Operators

As the local instantaneous conservation equations hold spatial and temporal derivatives of their dependent variable, it is instructive to have a closer look at these derivatives when being conditioned and averaged.

[13] Other averages evidently have to be *interpreted* in a different way. E.g., $\alpha_\varphi = \overline{I_\varphi}^T$ stemming from a time-averaging procedure expresses the *phase residence time fraction* of phase φ that alternately passes a point competing with the other phase ϕ – for a two-phase scenario (figure 2.5b). The same holds for ensemble-averaging where $\overline{I_\varphi}^E$ denotes a *phase fraction* representing the expectation (probability) of phase φ being present at the sampling point $(\mathbf{x}, t)$ under consideration (figure 2.5c).

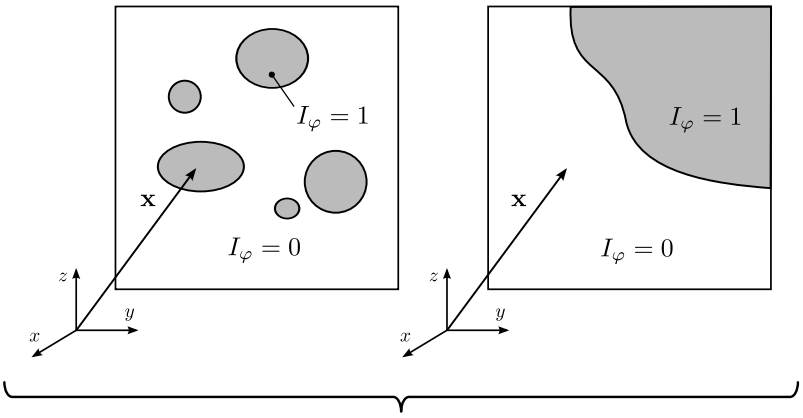

instantaneous volume-average – I_φ as phase indicator at time t

(a) volume-averaging technique.

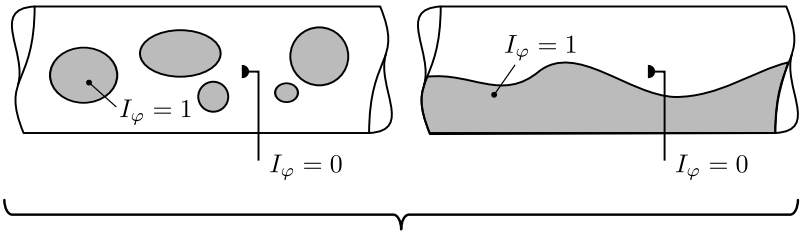

local time-average – I_φ as 'phase sensor' at point $\mathbf{x}$

(b) time-averaging technique.

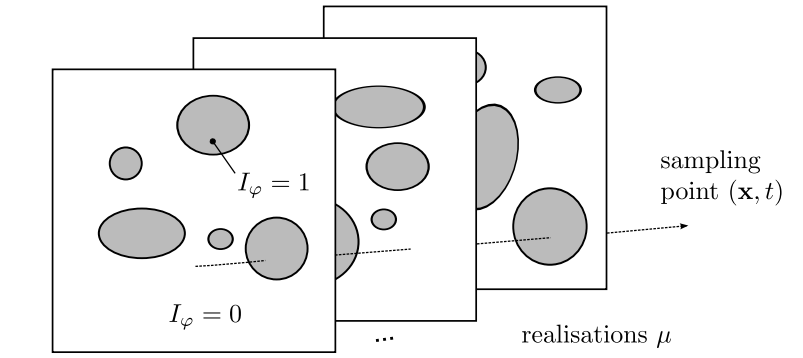

representative ensemble-average – I_φ as phase sample at $(\mathbf{x}, t)$

(c) ensemble-averaging technique.

Figure 2.5: Illustration of basic averaging techniques.

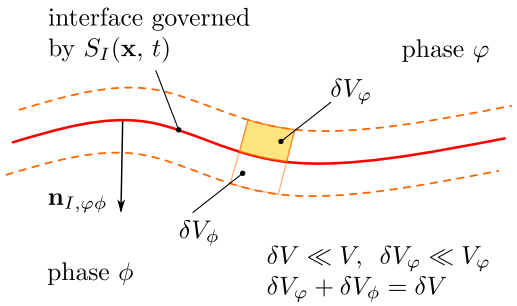

Figure 2.6: Illustration of the interfacial surface averaging procedure.

spatial Conditioning and volume-averaging of $\nabla\mathbf{\Phi}$ yields using equation 2.33:

$$\begin{aligned}\overline{I_\varphi \nabla\mathbf{\Phi}} &= \overline{\nabla I_\varphi \mathbf{\Phi}} - \overline{\mathbf{\Phi}\nabla I_\varphi} = \nabla\,\overline{I_\varphi\mathbf{\Phi}} + \overline{\delta_I \mathbf{\Phi}\mathbf{n}_{I,\varphi\phi}} \\ &= \nabla\left(\alpha_\varphi\,\overline{\mathbf{\Phi}}^{\varphi}\right) + \overline{\mathbf{\Phi}_I \mathbf{n}_{I,\varphi\phi}}\end{aligned} \tag{2.63}$$

Moreover, conditioning and volume-averaging of $\nabla\bullet\mathbf{\Phi}$ becomes

$$\begin{aligned}\overline{I_\varphi \nabla\bullet\mathbf{\Phi}} &= \nabla\bullet\,\overline{I_\varphi\mathbf{\Phi}} - \overline{\mathbf{\Phi}\bullet\nabla I_\varphi} = \nabla\bullet\left(\alpha_\varphi\,\overline{\mathbf{\Phi}}^{\varphi}\right) + \overline{\delta_I \mathbf{\Phi}\bullet\mathbf{n}_{I,\varphi\phi}} \\ &= \nabla\bullet\left(\alpha_\varphi\,\overline{\mathbf{\Phi}}^{\varphi}\right) + \overline{\mathbf{\Phi}_I\bullet\mathbf{n}_{I,\varphi\phi}}\,,\end{aligned} \tag{2.64}$$

as the average and differentiation operator commute (equation 2.41).

From both equation 2.63 and equation 2.64 it is evident that the second term on the r.h.s. depicts the averaged interfacial contribution as indicated by the use of the interfacial delta function $\nabla I_\varphi = -\mathbf{n}_{I,\varphi\phi}\,\delta_I$, while the first term represents the bulk contribution.

According to Weller [6, 7], who follows Dopazo [21], a further analysis can be done, when integrating each term in equation 2.63 and 2.64 over an infinitesimal volume element δV. However, Weller does not define his volume element δV.

Therefore, consider the volume element $\delta V = \delta V_\varphi + \delta V_\phi$ as illustrated in figure 2.6 being composed of two infinitesimal volume elements adjacent to the interface – δV_φ on the φ-side and δV_ϕ on the ϕ-side. Then, integrating over δV_φ, when examining $\overline{I_\varphi\nabla\mathbf{\Phi}}$ and $\overline{I_\varphi\nabla\bullet\mathbf{\Phi}}$, has no net effect on the first terms in the equations 2.63 and 2.64, respectively, since the bulk (phase interior) contributions can be regarded constant over δV_φ. However, the second terms can

be transfered into surface integrals (as they contain the Dirac delta function), and then read:

$$\begin{aligned}\overline{\boldsymbol{\Phi}\nabla I_\varphi} &= -\lim_{\delta V_\varphi \to 0} \overline{\frac{1}{\delta V_\varphi} \int_{\delta V_\varphi(\mathbf{x},t)} \boldsymbol{\Phi}_I \mathbf{n}_{I,\varphi\phi}\, dV} \\ &= -\lim_{\delta V_\varphi \to 0} \overline{\frac{1}{\delta V_\varphi} \int_{S_I(\mathbf{x},t)} \boldsymbol{\Phi}\mathbf{n}_{I,\varphi\phi}\; dS},\end{aligned} \tag{2.65}$$

where $S_I(\mathbf{x},\, t)$ is the equation for the interface. Note further that the two volume-average operations have been interchanged since they commute. Similarly, one obtains

$$\begin{aligned}\overline{\boldsymbol{\Phi}\bullet\nabla I_\varphi} &= -\lim_{\delta V_\varphi \to 0} \overline{\frac{1}{\delta V_\varphi} \int_{\delta V_\varphi(\mathbf{x},t)} \boldsymbol{\Phi}_I\bullet\mathbf{n}_{I,\varphi\phi}\, dV} \\ &= -\lim_{\delta V_\varphi \to 0} \overline{\frac{1}{\delta V_\varphi} \int_{S_I(\mathbf{x},t)} \boldsymbol{\Phi}\bullet\mathbf{n}_{I,\varphi\phi}\; dS}.\end{aligned} \tag{2.66}$$

To omit this rather ponderous (yet illustrative) representation, it is useful to introduce the definition of a *conditioned interface-average* $\widetilde{\overline{\boldsymbol{\Phi}}}^{\varphi}$:

$$\widetilde{\overline{\boldsymbol{\Phi}}}^{\varphi} \equiv \frac{1}{\Sigma} \lim_{\delta V_\varphi \to 0} \overline{\frac{1}{\delta V_\varphi} \int_{\delta V_\varphi} \boldsymbol{\Phi}_I dV} = \frac{1}{\Sigma} \lim_{\delta V_\varphi \to 0} \overline{\frac{1}{\delta V_\varphi} \int_{S_I(\mathbf{x},t)} \boldsymbol{\Phi}\, dS}, \tag{2.67}$$

$$\text{with} \qquad \Sigma \equiv \lim_{\delta V \to 0} \overline{\frac{1}{\delta V} \int_{S_I(\mathbf{x},t)} dS}, \tag{2.68}$$

where Σ denotes the *interfacial area density* – the interfacial surface area per unit volume. Note that the interface average $\widetilde{\boldsymbol{\Phi}}$ as defined by Weller [6,7], being the surface integral per unit volume divided by the interfacial area density,

$$\widetilde{\boldsymbol{\Phi}} \equiv \frac{1}{\Sigma} \lim_{\delta V \to 0} \overline{\frac{1}{\delta V} \int_{S_I(\mathbf{x},t)} \boldsymbol{\Phi}\,(\mathbf{x},\, t)\; dS}, \tag{2.69}$$

can be transferred into $\widetilde{\overline{\boldsymbol{\Phi}}}^{\varphi}$ – considering the limiting value of $\boldsymbol{\Phi}$ after conditioning and approaching the interface from the φ-side:

$$\begin{aligned}\widetilde{\overline{\boldsymbol{\Phi}}}^{\varphi} &= \widetilde{\overline{\boldsymbol{\Phi}_{I,\varphi}}} \\ \text{with} \qquad \boldsymbol{\Phi}_{I,\varphi} &= \delta_I \boldsymbol{\Phi}_\varphi,\end{aligned} \tag{2.70}$$

which is fully compatible with equation 2.47 for the bulk analog $\overline{\boldsymbol{\Phi}}^{\varphi}$. Note in passing, that Hill [12] has enforcedly introduced the notation as set out on the r.h.s. of equation 2.70, since he has *interpreted* the surface average of a quantity (equation 2.69) as surface area weighted value of $\boldsymbol{\Phi}_\varphi$ *at the interface*. Hence, his final form was identical to the r.h.s. of equation 2.70 – without introducing the corresponding l.h.s. as necessary definition. For the sake of brevity and ease of reading, both notations shall be used purposively henceforth.

For interfacial quantities that are inherently defined *on the interface* it is

$$\overbrace{\boldsymbol{\Phi}_{I,\varphi\phi}}^{\varphi} = \overbrace{\boldsymbol{\Phi}_{I,\varphi\phi}}. \tag{2.71}$$

Eventually this leads to the final forms of the equations 2.63 and 2.64:

$$\overline{I_\varphi \nabla \boldsymbol{\Phi}} = \nabla \left(\alpha_\varphi \, \overline{\boldsymbol{\Phi}}^{\varphi} \right) + \overbrace{\boldsymbol{\Phi}\mathbf{n}_I}^{\varphi} \Sigma \quad \text{and} \tag{2.72}$$

$$\overline{I_\varphi \nabla \boldsymbol{\cdot} \boldsymbol{\Phi}} = \nabla \boldsymbol{\cdot} \left(\alpha_\varphi \, \overline{\boldsymbol{\Phi}}^{\varphi} \right) + \overbrace{\boldsymbol{\Phi} \boldsymbol{\cdot} \mathbf{n}_I}^{\varphi} \Sigma. \tag{2.73}$$

Note in passing that of course the last terms again might be decomposed into surface averages and surface fluctuation correlations denoted by the superscript $\sharp$. Hence

$$\overbrace{\boldsymbol{\Phi}\mathbf{n}_I}^{\varphi} = \overbrace{\boldsymbol{\Phi}}^{\varphi} \overbrace{\mathbf{n}_{I,\varphi\phi}} + \overbrace{\boldsymbol{\Phi}^\sharp \mathbf{n}_I^\sharp}^{\varphi} \tag{2.74}$$

$$\overbrace{\boldsymbol{\Phi} \boldsymbol{\cdot} \mathbf{n}_I}^{\varphi} = \overbrace{\boldsymbol{\Phi}}^{\varphi} \boldsymbol{\cdot} \overbrace{\mathbf{n}_{I,\varphi\phi}} + \overbrace{\boldsymbol{\Phi}^\sharp \boldsymbol{\cdot} \mathbf{n}_I^\sharp}^{\varphi}, \tag{2.75}$$

where akin to the already introduced fluctuations with respect to the phasic and phase-weighted averages, also the surface fluctuation products generally needs to be modeled, if they are neither zero nor negligible.

temporal Conditioning and volume-averaging of $\frac{\partial \boldsymbol{\Phi}}{\partial t}$ leads to

$$\begin{aligned} \overline{I_\varphi \frac{\partial \boldsymbol{\Phi}}{\partial t}} &= \frac{\partial \overline{I_\varphi \boldsymbol{\Phi}}}{\partial t} - \overline{\boldsymbol{\Phi} \frac{\partial I_\varphi}{\partial t}} \\ &= \frac{\partial \overline{I_\varphi \boldsymbol{\Phi}}}{\partial t} - \overline{\boldsymbol{\Phi} \frac{\partial I_\varphi}{\partial t}}. \end{aligned} \tag{2.76}$$

Using the identity 2.34 yields

$$\overline{I_\varphi \frac{\partial \boldsymbol{\Phi}}{\partial t}} = \frac{\partial \overline{I_\varphi \boldsymbol{\Phi}}}{\partial t} - \overline{\boldsymbol{\Phi} \frac{\partial I_\varphi}{\partial t}} = \frac{\partial \overline{I_\varphi \boldsymbol{\Phi}}}{\partial t} + \overline{\boldsymbol{\Phi} \left(\mathbf{U}_{I,\varphi\phi} \boldsymbol{\cdot} \nabla I_\varphi \right)}, \tag{2.77}$$

the last term of which again can be rewritten making use of the interfacial delta function $\nabla I_\varphi = -\mathbf{n}_{I,\varphi\phi} \, \delta_I$:

$$\begin{aligned} \overline{\boldsymbol{\Phi} \left(\mathbf{U}_{I,\varphi} \boldsymbol{\cdot} \nabla I_\varphi \right)} &= - \lim_{\delta V_\varphi \to 0} \overline{\frac{1}{\delta V_\varphi} \int_{\delta V_\varphi(\mathbf{x},t)} \boldsymbol{\Phi} \left(\mathbf{U}_{I,\varphi\phi} \boldsymbol{\cdot} \mathbf{n}_{I,\varphi\phi} \, \delta_I \right) dV} \\ &= - \lim_{\delta V_\varphi \to 0} \overline{\frac{1}{\delta V_\varphi} \int_{S_I(\mathbf{x},t)} \boldsymbol{\Phi} \left(\mathbf{U}_{I,\varphi\phi} \boldsymbol{\cdot} \mathbf{n}_{I,\varphi\phi} \right) \, dS} \\ &= - \overbrace{\boldsymbol{\Phi} \left(\mathbf{U}_{I,\varphi\phi} \boldsymbol{\cdot} \mathbf{n}_I \right)}^{\varphi} \Sigma = \overbrace{\boldsymbol{\Phi}\mathbf{n}_I \boldsymbol{\cdot} \mathbf{U}_{I,\varphi\phi}}^{\varphi} \Sigma. \end{aligned} \tag{2.78}$$

Finally, it is

$$\overline{I_\varphi \frac{\partial \boldsymbol{\Phi}}{\partial t}} = \frac{\partial \alpha_\varphi \, \overline{\boldsymbol{\Phi}}^{\varphi}}{\partial t} - \overbrace{\boldsymbol{\Phi}_{I,\varphi} \mathbf{n}_{I,\varphi\phi} \boldsymbol{\cdot} \mathbf{U}_{I,\varphi\phi}} \Sigma. \tag{2.79}$$

2.6. Conditional Volume-Averaged Bulk Conservation Equations

In order to obtain the averaged arbitrary generic transport equation, its local instantaneous counter-part (2.24) is conditional volume-averaged, which reads

$$\overline{I_\varphi \frac{\partial \rho \boldsymbol{\Phi}}{\partial t}} + \overline{I_\varphi \nabla\bullet \left(\rho \boldsymbol{\Phi} \mathbf{U}\right)} - \overline{I_\varphi \nabla\bullet \left(\Gamma_{\boldsymbol{\Phi},d} \nabla \boldsymbol{\Phi}\right)} - \overline{I_\varphi S_{\boldsymbol{\Phi}}} = \mathbf{0}. \tag{2.80}$$

Now recalling equations 2.46, 2.72, 2.73 and 2.79 yields, when neglecting mass transfer:

$$\frac{\partial \alpha_\varphi \, \overline{\rho \boldsymbol{\Phi}}^\varphi}{\partial t} + \nabla\bullet \left(\alpha_\varphi \, \overline{\rho \boldsymbol{\Phi} \mathbf{U}}^\varphi\right) - \nabla\bullet \left(\alpha_\varphi \, \overline{\Gamma_{\boldsymbol{\Phi},d} \nabla \boldsymbol{\Phi}}^\varphi\right) = \overline{I_\varphi S_{\boldsymbol{\Phi}}} + \overbrace{\left(\Gamma_{\boldsymbol{\Phi},d} \nabla \boldsymbol{\Phi}\right) \bullet \mathbf{n}_I}^{\varphi} \Sigma. \tag{2.81}$$

By replacing the generic transport quantity as well as corresponding coefficients and source terms according to table 2.1 we arrive at the

- conditional volume-averaged continuity equation:

$$\frac{\partial \alpha_\varphi \, \overline{\rho}^\varphi}{\partial t} + \nabla\bullet \left(\alpha_\varphi \, \overline{\rho \mathbf{U}}^\varphi\right) = 0. \tag{2.82}$$

  By use of an appropriate (density-weighted) decomposition according to equation 2.55, this results in:

$$\frac{\partial \alpha_\varphi \, \overline{\rho}^\varphi}{\partial t} + \nabla\bullet \left(\alpha_\varphi \, \overline{\rho}^\varphi \widetilde{\mathbf{U}}^\varphi\right) = 0. \tag{2.83}$$

  Considering incompressible flows with constant densities $\overline{\rho}^\varphi$ and $\overline{\rho}^\phi$ *in both phases* φ and ϕ, e.g., it is $\widetilde{\boldsymbol{\Phi}}^\varphi \overset{!}{=} \overline{\boldsymbol{\Phi}}^\varphi$, since $I_\varphi \rho = \overline{\rho}^\varphi = \text{const}$ within phase φ. Then, the conditional volume-averaged continuity equation reads:

$$\frac{\partial \alpha_\varphi}{\partial t} + \nabla\bullet \left(\alpha_\varphi \, \overline{\mathbf{U}}^\varphi\right) = 0. \tag{2.84}$$

- conditional volume-averaged momentum equation:

$$\frac{\partial \alpha_\varphi \, \overline{\rho \mathbf{U}}^\varphi}{\partial t} + \nabla\bullet \left(\alpha_\varphi \, \overline{\rho \mathbf{U}\mathbf{U}}^\varphi\right) - \nabla\bullet \left(\alpha_\varphi \, \overline{\mu \nabla \mathbf{U}}^\varphi\right) = -\nabla \left(\alpha_\varphi \, \overline{p}^\varphi\right) + \alpha_\varphi \, \overline{\rho}^\varphi \mathbf{g} - \overbrace{p \mathbf{n}_I}^{\varphi} \Sigma + \overbrace{\left(\mu \nabla \mathbf{U}\right) \bullet \mathbf{n}_I}^{\varphi} \Sigma. \tag{2.85}$$

The non-linear second term on the l.h.s. of equation 2.85, needs appropriate (density-weighted) decomposition according to equation 2.55:

$$\begin{aligned}\overline{\rho\mathbf{U}\mathbf{U}}^{\varphi} &= \overline{\rho}^{\varphi}\widetilde{\widetilde{\mathbf{U}}^{\varphi}\widetilde{\mathbf{U}}^{\varphi}}^{\varphi} + \underbrace{2\,\overline{\rho}^{\varphi}\widetilde{\widetilde{\mathbf{U}}^{\varphi}\mathbf{U}''^{\varphi}}^{\varphi}}_{=\mathbf{0}} + \overline{\rho}^{\varphi}\underbrace{\widetilde{\mathbf{U}''^{\varphi}\mathbf{U}''^{\varphi}}^{\varphi}}_{\equiv\widetilde{\mathbf{R}}^{\varphi}} \\ &= \overline{\rho}^{\varphi}\widetilde{\mathbf{U}}^{\varphi}\widetilde{\mathbf{U}}^{\varphi} + \overline{\rho}^{\varphi}\widetilde{\mathbf{R}}^{\varphi}, \end{aligned} \tag{2.86}$$

with $\widetilde{\mathbf{R}}^{\varphi}$ representing the density-weighted Reynolds stress tensor, by means of which velocity fluctuations, which may be introduced by interface motion and turbulence, are accounted for.

Eventually, by use of equation 2.13 and 2.14, the conditional volume-averaged momentum equation becomes:

$$\begin{aligned}&\frac{\partial\alpha_{\varphi}\,\overline{\rho}^{\varphi}\widetilde{\mathbf{U}}^{\varphi}}{\partial t} + \nabla\bullet\left(\alpha_{\varphi}\,\overline{\rho}^{\varphi}\widetilde{\mathbf{U}}^{\varphi}\widetilde{\mathbf{U}}^{\varphi}\right) + \nabla\bullet\left(\alpha_{\varphi}\,\overline{\rho}^{\varphi}\widetilde{\mathbf{R}}^{\varphi}\right) \\ &= -\nabla\left(\alpha_{\varphi}\,\overline{p}^{\varphi}\right) - \nabla\bullet\left(\alpha_{\varphi}\,\overline{\boldsymbol{\tau}}^{\varphi}\right) + \alpha_{\varphi}\,\overline{\rho}^{\varphi}\mathbf{g} + \mathbf{M}_{\varphi}, \end{aligned} \tag{2.87}$$

where the last term in the r.h.s. has been summarized as:

$$\begin{aligned}\mathbf{M}_{\varphi} &\equiv -\widetilde{(p\mathbf{I}+\boldsymbol{\tau})\bullet\mathbf{n}_I}^{\varphi}\,\Sigma = \overline{(p\mathbf{I}+\boldsymbol{\tau})_{I,\varphi}\bullet\nabla I_{\varphi}} \\ &= -\widetilde{\boldsymbol{\sigma}\bullet\mathbf{n}_I}^{\varphi}\,\Sigma = \overline{\boldsymbol{\sigma}_{I,\varphi}\bullet\nabla I_{\varphi}}\,, \end{aligned} \tag{2.88}$$

denoting the *interfacial momentum transfer* term.

For incompressible two-phase flows, i.e., $\widetilde{\boldsymbol{\Phi}}^{\varphi} \overset{!}{=} \overline{\boldsymbol{\Phi}}^{\varphi}$, the conditional volume-averaged momentum equation becomes

$$\begin{aligned}&\frac{\partial\alpha_{\varphi}\,\overline{\mathbf{U}}^{\varphi}}{\partial t} + \nabla\bullet\left(\alpha_{\varphi}\,\overline{\mathbf{U}}^{\varphi}\,\overline{\mathbf{U}}^{\varphi}\right) + \nabla\bullet\left(\alpha_{\varphi}\,\overline{\mathbf{R}}^{\varphi}\right) \\ &= -\frac{\nabla\left(\alpha_{\varphi}\,\overline{p}^{\varphi}\right)}{\overline{\rho}^{\varphi}} - \frac{\nabla\bullet\left(\alpha_{\varphi}\,\overline{\boldsymbol{\tau}}^{\varphi}\right)}{\overline{\rho}^{\varphi}} + \alpha_{\varphi}\mathbf{g} + \frac{\mathbf{M}_{\varphi}}{\overline{\rho}^{\varphi}}. \end{aligned} \tag{2.89}$$

- conditional volume-averaged chemical species conservation equation:

$$\frac{\partial\alpha_{\varphi}\,\overline{\rho x_i}^{\varphi}}{\partial t} + \nabla\bullet\left(\alpha_{\varphi}\,\overline{\rho x_i\mathbf{U}}^{\varphi}\right) - \nabla\bullet\left(\alpha_{\varphi}\,\overline{\rho D_i\nabla x_i}^{\varphi}\right) - \alpha_{\varphi}\,\overline{\hat{R}_i}^{\varphi} = \widetilde{(\rho D_i\nabla x_i)\bullet\mathbf{n}_I}^{\varphi}\,\Sigma. \tag{2.90}$$

By substituting $c_i = x_i \cdot c = x_i \cdot \rho/M$ – where c, ρ and M denote the mean mixture concentration, density and molar mass, respectively – it follows for a diluted species i (c = const, ρ = const and M = const, even for varying c_i) from equation 2.90:

$$\frac{\partial\alpha_{\varphi}\,\overline{c_i}^{\varphi}}{\partial t} + \nabla\bullet\left(\alpha_{\varphi}\,\overline{c_i\mathbf{U}}^{\varphi}\right) - \nabla\bullet\alpha_{\varphi}\,\overline{D_i\nabla c_i}^{\varphi} - \alpha_{\varphi}\,\overline{R_i}^{\varphi} = \widetilde{(D_i\nabla c_i)\bullet\mathbf{n}_I}^{\varphi}\,\Sigma, \tag{2.91}$$

which becomes

$$\frac{\partial \alpha_\varphi \, \overline{c_i}^{\varphi}}{\partial t} + \nabla\!\bullet\left(\alpha_\varphi \, \overline{c_i \mathbf{U}}^{\varphi}\right) - \nabla\!\bullet\alpha_\varphi \, \overline{D_i}^{\varphi} \nabla \, \overline{c_i}^{\varphi} - \alpha_\varphi \, \overline{R_i}^{\varphi} = \overbrace{\left(D_i \nabla c_i\right) \bullet \mathbf{n}_I}^{\varphi} \Sigma, \tag{2.92}$$

given that $D_i'^{\varphi} \stackrel{!}{=} 0$.

2.7. Conditional Volume-Averaged Interfacial Jump Conditions

From equation 2.25, representing the local-instantaneous jump condition for a generic transport quantity $\mathbf{\Phi}$, we arrive at the corresponding volume-averaged interface balance by conditioning and subsequently volume-averaging. Conditioning is accomplished by multiplication with $\delta_I\left(\mathbf{x} - \mathbf{x}_I,\, t\right)$, which represents the interface delta function. Taking into account the symmetry, $\mathbf{n}_{I,\varphi\phi} = -\mathbf{n}_{I,\phi\varphi}$, and neglecting mass transfer, it is:

$$\begin{aligned}
& \overline{\| \left(\Gamma_{\mathbf{\Phi},d} \nabla \mathbf{\Phi}\right) \bullet \mathbf{n}_I \| \delta_I} = - \overline{S_{\mathbf{\Phi},I} \delta_I} \\
\Leftrightarrow \quad & \overline{\left(\Gamma_{\mathbf{\Phi},d} \nabla \mathbf{\Phi}\right)_{I,\varphi} \bullet \nabla I_\varphi} + \overline{\left(\Gamma_{\mathbf{\Phi},d} \nabla \mathbf{\Phi}\right)_{I,\phi} \bullet \nabla I_\phi} = - \overline{S_{\mathbf{\Phi},I} \delta_I} \\
\Leftrightarrow \quad & \overbrace{\left(\Gamma_{\mathbf{\Phi},d} \nabla \mathbf{\Phi}\right) \bullet \mathbf{n}_{I,\varphi\phi}}^{\varphi} \Sigma + \overbrace{\left(\Gamma_{\mathbf{\Phi},d} \nabla \mathbf{\Phi}\right) \bullet \mathbf{n}_{I,\phi\varphi}}^{\phi} \Sigma = \overline{S_{\mathbf{\Phi},I} \delta_I} \, .
\end{aligned} \tag{2.93}$$

Again replacing the generic transport quantity $\mathbf{\Phi}$ and corresponding coefficients and source terms, one can state the following for the

- conditional volume-averaged interfacial mass jump condition:
  In absence of mass transfer (e.g., due to phase change) the generic jump condition as provided in equation 2.93 degenerates to the trivial identity $0 = 0$, indicating that no additional condition has to be taken into account.

- conditional volume-averaged interfacial momentum jump condition:

$$\begin{aligned}
& \overline{\left(\mu \nabla \mathbf{U}\right)_{I,\varphi} \bullet \nabla I_\varphi} + \overline{\left(\mu \nabla \mathbf{U}\right)_{I,\phi} \bullet \nabla I_\phi} \\
& \quad = \overline{-p_{I,\varphi} \mathbf{n}_{I,\varphi\phi} \, \delta_I - p_{I,\phi} \mathbf{n}_{I,\phi\varphi} \, \delta_I - \sigma \kappa_{I,\varphi\phi} \, \mathbf{n}_{I,\varphi\phi} \, \delta_I} \\
& \quad = \overline{p_{I,\varphi} \nabla I_\varphi} + \overline{p_{I,\phi} \nabla I_\phi} + \sigma \, \overline{\kappa_{I,\varphi\phi} \, \nabla I_\varphi}
\end{aligned} \tag{2.94}$$

$$\begin{aligned}
\Leftrightarrow \quad & - \overbrace{\left(p\mathbf{I} + \boldsymbol{\tau}\right) \bullet \mathbf{n}_{I,\varphi\phi}}^{\varphi} \Sigma - \overbrace{\left(p\mathbf{I} + \boldsymbol{\tau}\right) \bullet \mathbf{n}_{I,\phi\varphi}}^{\phi} \Sigma = \sigma \, \overbrace{\kappa_{I,\varphi\phi} \mathbf{n}_{I,\varphi\phi}}^{\varphi} \Sigma \\
& - \overbrace{\boldsymbol{\sigma} \bullet \mathbf{n}_{I,\varphi\phi}}^{\varphi} \Sigma - \overbrace{\boldsymbol{\sigma} \bullet \mathbf{n}_{I,\phi\varphi}}^{\phi} \Sigma = \sigma \, \overbrace{\kappa_{I,\varphi\phi} \mathbf{n}_{I,\varphi\phi}}^{\varphi} \Sigma.
\end{aligned} \tag{2.95}$$

  By use of equation 2.13 and 2.14 and taking into account the definition of the interfacial momentum transfer term $\mathbf{M}_\varphi$ (and for $\mathbf{M}_\phi$) according to equation 2.88, we arrive at the shorthand notation for the conditional volume-averaged

momentum jump condition. In the absence of mass transfer and neglecting any variations of the surface tension σ along the interface (e.g., no Marangoni effect $\nabla_I(\sigma) = \mathbf{0}$), it is:

$$\mathbf{M}_\varphi + \mathbf{M}_\phi = \mathbf{M}_\sigma, \tag{2.96}$$

where $\mathbf{M}_\sigma$ on the r.h.s. of equation 2.96 denotes the averaged interfacial momentum source due to surface tension:

$$\mathbf{M}_\sigma \equiv -\sigma\,\overline{\kappa_{I,\varphi\phi}\,\nabla I_\varphi} = \sigma\,\overbrace{\kappa_{I,\varphi\phi}\,\mathbf{n}_{I,\varphi\phi}}\,\Sigma. \tag{2.97}$$

- conditional volume-averaged interfacial species jump conditions

$$\overbrace{(\rho D_i \nabla x_i)\bullet\mathbf{n}_{I,\varphi\phi}}^{\varphi}\,\Sigma + \overbrace{(\rho D_i \nabla x_i)\bullet\mathbf{n}_{I,\phi\varphi}}^{\phi}\,\Sigma = 0. \tag{2.98}$$

Then, from equation 2.98 for the corresponding jump condition, it follows:

$$\overbrace{(D_i \nabla c_i)\bullet\mathbf{n}_{I,\varphi\phi}}^{\varphi}\,\Sigma + \overbrace{(D_i \nabla c_i)\bullet\mathbf{n}_{I,\phi\varphi}}^{\phi}\,\Sigma = 0. \tag{2.99}$$

2.8. Volume-averaged Interface Transport Equation

In order to arrive at the volume-averaged interface transport equation, its local-instantaneous counter-part as set out in equation 2.34 is volume-averaged:

$$\overline{\frac{\partial I_\varphi}{\partial t}} + \overline{\mathbf{U}_{I,\varphi}\bullet\nabla I_\varphi} = 0 \qquad \Leftrightarrow \qquad \frac{\partial \alpha_\varphi}{\partial t} - \overbrace{\mathbf{U}_{I,\varphi}\bullet\mathbf{n}_{I,\varphi\phi}}\,\Sigma = 0, \tag{2.100}$$

where the substitution $\mathbf{U}_{I,\varphi\phi} = \mathbf{U}_{I,\varphi}$ has been made. This is valid in the *absence of mass transfer* due to condensation or evaporation – as it is assumed throughout this study. Note in passing that this result is also achieved by simply substituting $\mathbf{\Phi} = 1$ into equation 2.79.

Some progress towards a more exploitable form of the second term on the l.h.s. of equation 2.100 is achieved by decomposing $\mathbf{U}_{I,\varphi}$ into an interfacial average and interfacial fluctuating velocity as

$$\mathbf{U}_{I,\varphi} = \widetilde{\mathbf{U}}^{\varphi} + \mathbf{U}^{\sharp}_{I,\varphi}. \tag{2.101}$$

Then, substituting of equation 2.101 in 2.100 results in

$$\frac{\partial \alpha_\varphi}{\partial t} - \overbrace{\widetilde{\mathbf{U}}^{\varphi}\bullet\mathbf{n}_{I,\varphi\phi}}\,\Sigma - \overbrace{\mathbf{U}^{\sharp}_{I,\varphi}\bullet\mathbf{n}_{I,\varphi\phi}}\,\Sigma = 0, \tag{2.102}$$

$$\Leftrightarrow \qquad \frac{\partial \alpha_\varphi}{\partial t} - \widetilde{\mathbf{U}}^{\varphi}\bullet\overbrace{\mathbf{n}_{I,\varphi\phi}}\,\Sigma - \overbrace{\mathbf{U}^{\sharp}_{I,\varphi}\bullet\mathbf{n}_{I,\varphi\phi}}\,\Sigma = 0. \tag{2.103}$$

By use of equation 2.72 (substituting $\mathbf{\Phi} = 1$) it follows

$$\frac{\partial \alpha_\varphi}{\partial t} + \widetilde{\mathbf{U}}^{\varphi} \bullet \nabla \alpha_\varphi - \overbrace{\mathbf{U}^{\sharp}_{I,\varphi} \bullet \mathbf{n}_{I,\varphi\phi}} \, \Sigma = 0, \tag{2.104}$$

which represents the final form of the averaged interface transport equation, with two interfacial averaged terms allowing for a further inspection on a physical basis.

3

Closure Framework

Reality is that which, when you stop believing in it, doesn't go away.

Philip K. Dick

Abstract

This chapter considers modeling approaches for closure. For this purpose, different two-phase flow types in varying scale regimes are examined in order to obtain a consistent multi-scale model framework. This model framework shall cover both well-established Eulerian CMFD methods for resolved (microscale) and unresolved (macroscale) interfacial scale regimes. Moreover, it encompasses a more general novel CMFD approach for two-phase flow situations being partially resolved (mesoscale) – intrinsically including the above cases as its limits of applicability.

The equations 2.84, 2.89 and 2.104 constitute a two-phase flow model, which is generally valid, thus applicable for quite different flow types that might occur in a two-phase system. However, in this form the two-phase flow model is not solvable. It is said to be unclosed, since there are terms present within its governing equations that need further modeling in order to express them as functions of conditional volume-averaged quantities – only these are accessible within a solution procedure. This modeling process is called closure. The model equations accomplishing the closure in terms of averaged quantities are called constitutive or (straightforward) closure models.

Traditionally, the unclosed terms in the two-phase flow model equations might be categorized[1] into three groups, that are

- phase-interaction terms: interfacial momenta transfer terms $\mathbf{M}_\varphi$ and $\mathbf{M}_\phi$ along with the interfacial momentum source term due to surface tension $\mathbf{M}_\sigma$
- self-interaction terms: averaged shear stress terms $\overline{\boldsymbol{\tau}}^\varphi$ and $\overline{\boldsymbol{\tau}}^\phi$
- turbulence terms: averaged Reynolds stress tensors $\overline{\mathbf{R}}^\varphi$ and $\overline{\mathbf{R}}^\phi$.

However, the modeling of the latter group of terms, i.e., turbulence modeling of two- and multiphase systems, is still an open research area on its own, that requires detailed knowledge of the interaction between turbulent and morphological interfacial structures. The interested reader might be referred to the work of Toutant et al. [22–25], who examine the interplay of under-resolved discontinuous interfaces and turbulence structures, employing spatial filtering as central tool. Thus, their work appears to be fully compatible with both the LES concept and this study. Hence, the present thesis will further focus on the first two groups concerning interfacial momenta transfer and shear stress modeling.

Eventually, all of these (at this stage) unclosed terms will differ when considering different flow types, e.g., dispersed and segregated flows, respectively. It seems reasonable that the concrete form of a closure relation might vary dependent upon the length scale down to which the two-phase flow under consideration is *resolved*, which finally is a matter of the size of the averaging volume chosen. Accordingly, we might refer to the resulting two-phase flow models as *interfacial scale averaging* or *interfacial scale resolving* (compare to page 3 in the introductory chapter 1). The latter group can be split up further into *fully* and *partially* resolving interfacial scales of a two-phase flow at hand – as will be set out below.

[1] However, as will be seen, this categorization looses somewhat ground, since as for the generic transport equation for a two-phase flow, there will be coupling terms accounting for the presence of the respective second phase. In particular, the wording *self-interaction* is no longer clear for this reason. However, for convenience we might stick to that common nomenclature for now, as this at least points to the physical origin the unclosed terms stem from – the corresponding mathematical model for single-phase flows.

In the remainder of this section closure relations for different two-phase flow types shall be examined. Main scope is put upon the 'information loss' due to averaging that occurs beyond the averaging scale. It is attempted to provide reasonable avenues towards a physical meaningful interpretation of unclosed terms within this non-resolved scale range, in turn enabling to formulate closure relations on a sound basis.

Finally, for the sake of completeness, comments are made on commonly used and widely accepted simplifications of the previously derived general two-phase model. However, as this does not lead to a general model framework for different two-phase flow types (thus not being the objective of this work), solely the underlying assumptions, the resulting governing equations and the corresponding specific field of applicability shall be briefly highlighted.

3.1. Closure Strategy

In order to develop a sound and consistent closure it is first advisable to have a closer look on the 'conceptual picture' that can be drawn from the applied averaging procedure and its physical interpretation, which is examined in the forthcoming sections. For this purpose it is of use to distinguish between two specific flow types, namely

1.) dispersed flows (figure 3.1), e.g., bubbly or droplet flows, and

2.) segregated flows (figure 3.2), e.g., stratified or wavy free-surface flows,

as limiting cases of a rather general two-phase flow scenario of mixed type, that is bubbles and droplets exist in the liquid and the gaseous phase, respectively, as this might be achieved by superposition of both cases. Consequently, for the purpose of a consistent and general closure, the use of a *scale similarity hypothesis* is proposed – analogous to LES modeling for single-phase flows:

> The smallest resolved scales of a two-phase flow are assumed to exhibit similar characteristics as the largest non-resolved ones.

Following this hypothesis, it is reasonable and advantageous to consider dispersed flows within an interfacial scale averaging closure framework and segregated flows within an interfacial resolving closure framework. However, the latter is allowed to only partially resolve interfacial details. Doing so, ensures that both conceptual frameworks are fully compatible with each other, that is the characteristic length scales of both underlying flow types are inherently aligned. This allows the utilization of one uniform closure framework that holds the influence of different flow types in its closure terms and provides a decent avenue to model mixed flow types as well.

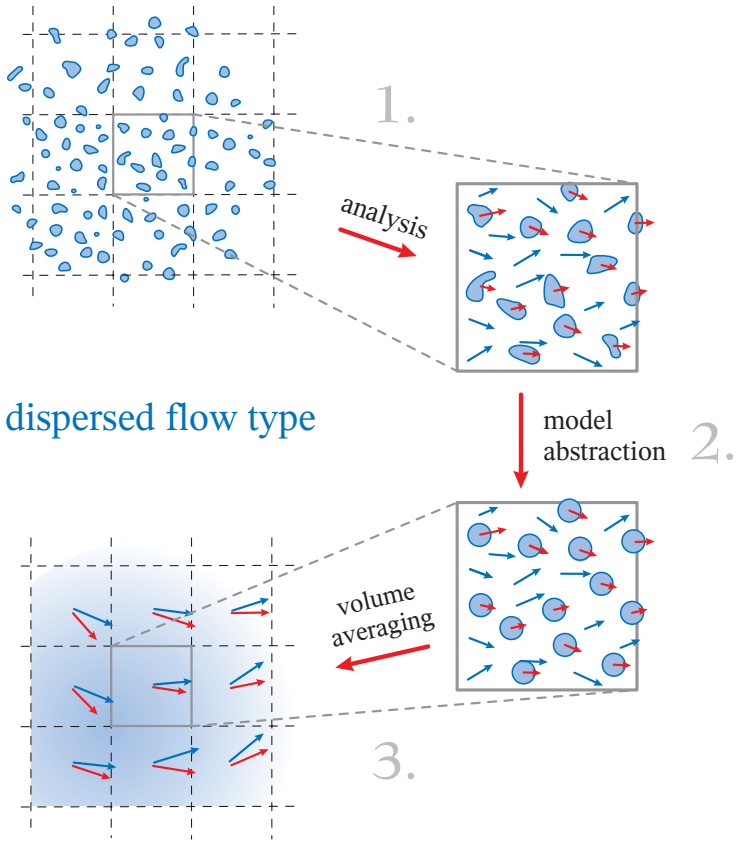

Figure 3.1: Principle of model closure – Dispersed flow type.

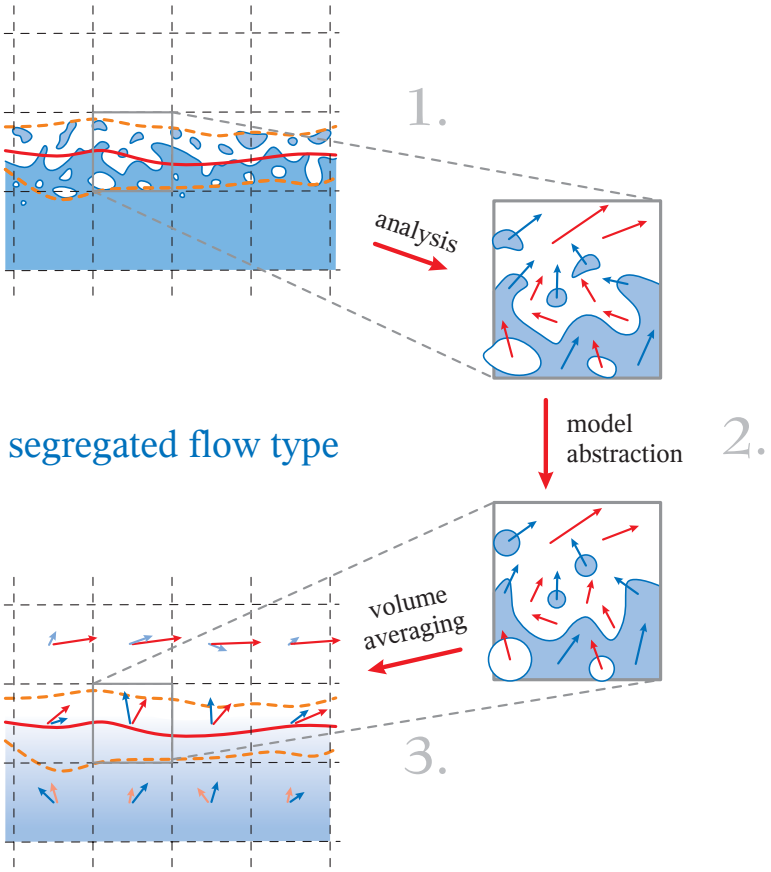

Figure 3.2: Principle of model closure – Segregated flow type.

ad 1.) interfacial scale averaging closure framework – figure 3.1

Closure models for the first two phase-flow type (dispersed flows) are well-established and widely used. Modeling is commonly accomplished employing two-fluid model frameworks, that are based on the *concept of interpenetrating continua* [26]: The actual interface morphology and motion is not explicitly resolved, i.e., the averaging volume is chosen much larger than the characteristic length scale of the dispersed phase (e.g., the equivalent diameter of the (fluid) particle). As a consequence, all interactions between the phases have to be modeled appropriately within the averaging framework – in an average sense.

ad 2.) interfacial scale resolving closure framework – figure 3.2

A closure for the second two-phase flow type under consideration (segregated flow) needs to be accomplished consistently, meaning also *in the same manner*. As a pivotal aspect of closure, a conceptual framework has to be formulated that is *compatible and in the same spirit* as the concept of interpenetrating continua for dispersed flow types. Such a conceptual framework has been developed through the course of this study and will henceforth be entitled *concept of partially penetrating continua* in the interfacial transition region: The interfacial morphology is partially resolved, i.e., the averaging volume is chosen sufficiently in its size to capture the main (mean) dynamics of the interfacial flow, whereas non-resolved interfacial morphologies and phase interactions again must be accounted for in the underlying averaging framework by appropriate (physical meaningful) closure models. As a consequence, the interface is represented as an interfacial transition region of certain characteristic width, which is determined by the averaging length scale.

Note that both concepts are based upon the same 'physical picture' directly evolving from the conditional volume-averaging procedure employed, that is each phase is treated separately and is assumed to coexist within the averaging volumes, possessing characteristic properties and an own velocity and pressure field.

3.2. Conceptual Approaches

3.2.1. Concept of Partially Penetrating Continua

Figure 3.2 schematically illustrates the 'conceptual picture' arising from the conditional volume-averaging procedure if a segregated flow is present within the averaging volume. This enables to decompose the morphological structure of the interface into a resolved mean and a non-resolved local one. Consequently, this separation into resolved mesoscale and non-resolved microscale allows for the same modeling approach that already has been established and is well-known within the concept of interpenetrating continua for dispersed two-phase flows – that is to model all

non-resolved scales employing *closure relations in the underlying averaging framework* while resolving the other scales by means of *numerically solving for averaged conservation equations.*

Hence, to be consistent within this framework and thus through the course of the forthcoming derivations of closure relations, it is rational to formulate models for both the interfacial averaged and the interfacial fluctuation parts of a conditioned generic flow quantity at the interface

$$\mathbf{\Phi}_{I,\varphi} = \widetilde{\mathbf{\Phi}}^{\varphi} + \mathbf{\Phi}^{\sharp}_{I,\varphi}, \tag{3.1}$$

as functions of averaged (thus accessible) quantities, being separated into contributions stemming from the non-resolved microscale and the resolved mesoscale, respectively.

However, for this purpose a model representation of the interface morphology is needed. This can be illustrated along three quantities representing pivotal features of two-phase flows, the interfacial averaged curvature $\widetilde{\kappa_I}$ and unit normal vector $\widetilde{\mathbf{n}_I}$, and the interfacial averaged velocity $\widetilde{\mathbf{U}}^{\varphi}$ – characterizing the interface morphology and its transport.

interfacial morphology The *local* interface morphology is entirely characterized by the *local* curvature $\kappa_{I,\varphi\phi}$, and the local unit vector normal to the microscale interface, $\mathbf{n}_{I,\varphi\phi}$. By use of the phase indicator function I_φ, it is

$$\kappa_{I,\varphi\phi} = \nabla_\bullet \mathbf{n}_{I,\varphi\phi} \qquad \text{and} \qquad \mathbf{n}_{I,\varphi\phi} = \frac{\nabla I_\varphi}{|\nabla I_\varphi|}, \tag{3.2}$$

henceforth shortly denoted as κ_I and $\mathbf{n}_I$ instead $\kappa_{I,\varphi\phi}$ and $\mathbf{n}_{I,\varphi\phi}$, respectively. However, the evaluation of the corresponding interfacial averaged counter-parts,

$$\widetilde{\kappa_I} \equiv \frac{\overline{\kappa_I \nabla I_\varphi}}{\overline{|\nabla I_\varphi|}} \qquad \text{and} \qquad \widetilde{\mathbf{n}_I} \equiv \frac{\overline{\mathbf{n}_I \nabla I_\varphi}}{\overline{|\nabla I_\varphi|}}, \tag{3.3}$$

requires detailed knowledge of the microscopic interfacial morphology, which is a priori unknown – figure 3.3. The frontier might be pushed somewhat further by taking advantage of equation 2.72 and substituting $\mathbf{\Phi} = 1$, which results in $\widetilde{\mathbf{n}_I}\Sigma = -\nabla\alpha_\varphi$. Thus, it is:

$$\widetilde{\mathbf{n}_I} = -\frac{\nabla\alpha_\varphi}{\Sigma} \qquad \text{and} \qquad \widetilde{\kappa_I} = \widetilde{\nabla_\bullet \mathbf{n}_I} = \nabla_\bullet \widetilde{\mathbf{n}_I} = -\nabla_\bullet \left(\frac{\nabla\alpha_\varphi}{\Sigma}\right). \tag{3.4}$$

It has to be emphasized that Σ herein comprises two contributions, that are the averaged (mesoscale, resolved) curvatures and the fluctuating (microscale, non-resolved) curvature, both of which are fully governing the entire interfacial area density.

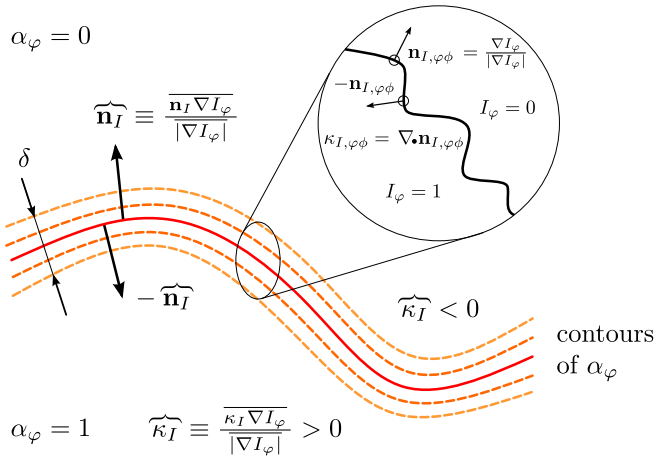

Figure 3.3: Closure model for the interfacial morphology.

To make progress, a closure model for the interfacial area density Σ is needed – see corollary note 3.1.

Corollary Note 3.1

From equation 2.72 a model for the interfacial area density Σ might be derived:

$$|\widehat{\mathbf{n}_I}|\Sigma = |\nabla\alpha_\varphi| \overset{|\widehat{\mathbf{n}_I}|\approx 1}{\Longleftrightarrow} \Sigma \equiv \overline{|\nabla I_\varphi|} \approx |\nabla \overline{I_\varphi}| = |\nabla\alpha_\varphi|. \tag{3.5}$$

As can be seen, this model is justified under one specific assumption that is $|\widehat{\mathbf{n}_{I,\varphi\phi}}| \approx 1$ stating that the interfacial area density is allowed to vary only across the interfacial transition region normal to $\widehat{\mathbf{n}_{I,\varphi\phi}}$ – but not along contours of constant α_φ. This means that Σ is assumed to be dominated by contributions from the non-resolved interfacial morphology within the interfacial transition region, while macroscopic contributions (e.g., from the resolved mean curvature) play a much lesser role.
Note that assuming such a local instantaneous *isotropic interfacial morphology* fully complies with the requirement of phase invariance, since $\nabla\alpha_\varphi = -\nabla\alpha_\phi$.

For the interfacial averaged interface morphology it follows:

$$\widehat{\mathbf{n}_I} = -\frac{\nabla\alpha_\varphi}{|\nabla\alpha_\varphi|} \qquad \text{and} \qquad \widehat{\kappa_I} = -\nabla\bullet\left(\frac{\nabla\alpha_\varphi}{|\nabla\alpha_\varphi|}\right), \tag{3.6}$$

which enables to a further analysis of $\widetilde{\kappa_I}$ resulting in the desired separation of non-resolved microscopic and resolved macroscopic contributions:

$$\begin{aligned}\widetilde{\kappa_I} &= -\nabla\bullet\left(\frac{\nabla\alpha_\varphi}{|\nabla\alpha_\varphi|}\right) = -\frac{1}{|\nabla\alpha_\varphi|}\left[\nabla\bullet\nabla\alpha_\varphi + \nabla\left(\frac{1}{|\nabla\alpha_\varphi|}\right)\bullet\nabla\alpha_\varphi\right] \\ &= -\frac{1}{|\nabla\alpha_\varphi|}\left[\nabla^2\alpha_\varphi - \underbrace{\frac{\nabla\alpha_\varphi}{|\nabla\alpha_\varphi|}\bullet\nabla|\nabla\alpha_\varphi|}_{=\widetilde{\mathbf{n}_I}\bullet\nabla\Sigma}\right].\end{aligned} \tag{3.7}$$

Since Σ only varies across the interfacial transition region normal to $\widetilde{\mathbf{n}_I}$, it is

$$\widetilde{\kappa_I} = -\frac{\nabla^2\alpha_\varphi}{|\nabla\alpha_\varphi|} + \frac{d\Sigma}{d\alpha_\varphi}, \tag{3.8}$$

with the second contribution consequently being identified as contribution from the microscopic non-resolved curvature to $\widetilde{\kappa_I}$ – stemming from local fluctuations *inside* the interfacial transition region.

interface transport The decomposition of the instantaneous velocity at the interface into an interfacial averaged velocity and local interfacial velocity fluctuation yields

$$\mathbf{U}_{I,\varphi} = \widetilde{\mathbf{U}}^\varphi + \mathbf{U}^\sharp_{I,\varphi}. \tag{3.9}$$

Stating that the non-resolved velocity profile shall be continuous across the interface – which essentially is an interfacial no-slip condition – a closure model for the interfacial averaged velocity $\widetilde{\mathbf{U}}^\varphi$ can be deduced (corollary note 3.2):

Corollary Note 3.2

Illustratively, the interfacial situation is depicted in figure 3.4 for a shear flow scenario. From elementary geometry (intercept theorem) it can be easily seen, that for a simple case where $\overline{\mu}^\varphi = \overline{\mu}^\phi$:

$$\frac{\widetilde{\mathbf{U}}^\varphi - \overline{\mathbf{U}}^\phi}{\overline{\mathbf{U}}^\varphi - \widetilde{\mathbf{U}}^\varphi} = \frac{I_\phi}{I_\varphi} \qquad \Leftrightarrow \qquad \widetilde{\mathbf{U}}^\varphi = I_\phi\,\overline{\mathbf{U}}^\varphi + I_\varphi\,\overline{\mathbf{U}}^\phi, \tag{3.10}$$

and with a correction for the general case where $\overline{\mu}^\varphi \neq \overline{\mu}^\phi$:

$$\frac{\overline{\mu}^\phi}{\overline{\mu}^\varphi}\frac{\widetilde{\mathbf{U}}^\varphi - \overline{\mathbf{U}}^\phi}{\overline{\mathbf{U}}^\varphi - \widetilde{\mathbf{U}}^\varphi} = \frac{I_\phi}{I_\varphi} \qquad \Leftrightarrow \qquad \widetilde{\mathbf{U}}^\varphi = \frac{I_\phi\,\overline{\mu}^\varphi\,\overline{\mathbf{U}}^\varphi + I_\varphi\,\overline{\mu}^\phi\,\overline{\mathbf{U}}^\phi}{I_\varphi\,\overline{\mu}^\phi + I_\phi\,\overline{\mu}^\varphi}. \tag{3.11}$$

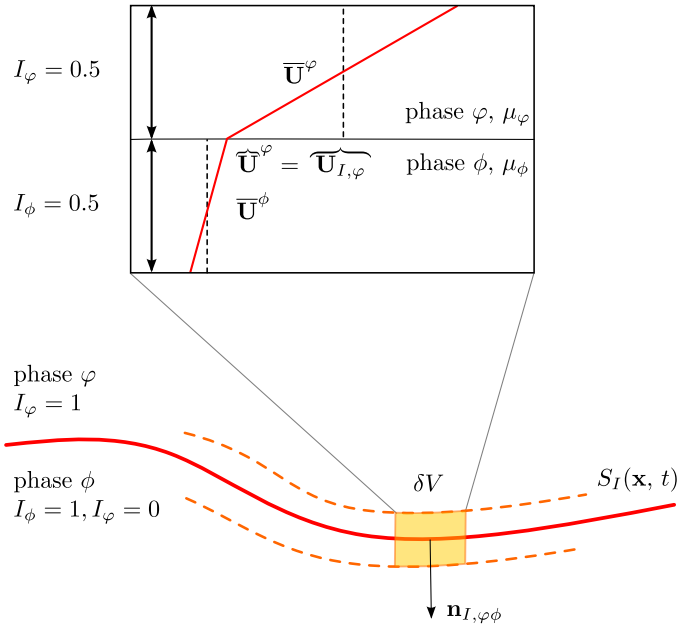

Figure 3.4: Closure model for the interfacial averaged velocity.

Consequently, equation 3.11 results in the final closure relation for $\widetilde{\overline{\mathbf{U}}}^{\varphi}$ (for $I_\varphi = I_\phi \overset{!}{=} 1/2$ at the interface):

$$\widetilde{\overline{\mathbf{U}}}^{\varphi} = \widetilde{\overline{\mathbf{U}}_{I,\varphi}} = \frac{\overline{\mu}^{\varphi}\,\overline{\mathbf{U}}^{\varphi} + \overline{\mu}^{\phi}\,\overline{\mathbf{U}}^{\phi}}{\overline{\mu}^{\varphi} + \overline{\mu}^{\phi}}. \tag{3.12}$$

Note that the phase symmetry is still preserved, e.g., φ and ϕ are interchangeable. Furthermore, the closure according to equation 3.12 is generally applicable, i.e., it can be assumed valid for different viscosity ratios $\overline{\mu}^{\phi}/\overline{\mu}^{\varphi}$. Moreover, considering limiting cases, this closure yields physically reasonable results. If we choose phase φ as liquid phase and ϕ as gaseous phase, that is in case of a free-surface flow flow where $\overline{\mu}^{\phi} \ll \overline{\mu}^{\varphi}$, it follows $\widetilde{\overline{\mathbf{U}}}^{\varphi} = \overline{\mathbf{U}}^{\varphi}$, which clearly is a physically plausible outcome.

For comprehension, it shall be emphasized that the concept of partially penetrating continua does not rely upon fully resolving both the interfacial morphology and the interfacial boundary layer – as for instance DNS methods do requiring a sufficiently small averaging volume. In fact the challenge now rests in the necessity to find appropriate (physically sound) closure models in order to account for non-resolved interfacial scales.

Moreover, in contrast to conventional diffuse interface models, this approach is fluid dynamically motivated, rather than thermodynamically: while diffuse interface models consider the fluctuating scale on a molecular level – considering the interface as region of coexisting molecules pertaining to both phases – the concept of partially penetrating continua considers the fluctuating scale being shifted by several orders of magnitude to the scale of wavy structures; thus it closes the gab between sharp interface models (relying on the full resolution of interfacial morphologies and boundary layers) and the conventional two-fluid model based upon the concept of interpenetrating continua for dispersed flows (resolving no interfacial scales at all). In consequence, this means a paradigm shift, similar to LES (from DNS or RANS) for turbulence modeling.

3.2.2. Concept of Interpenetrating Continua

Figure 3.1 depicts the 'conceptual picture' arising from the conditional volume-averaging procedure imposed on a dispersed flow type being present in the underlying averaging volume. The dispersed two-phase flow is considered as two constituent pseudo-continuum, with each phase being treated separatly. As already indicated, the interfacial morphology is not resolved at all. Hence, generally one has to act on specific assumptions regarding the flow morphology (e.g., spherical or ellipsoidal particles, drops or bubbles) when modeling phase interactions via closure relations within the averaging framework. As a consequence of modeling, interfacial exchange processes have to be accounted for explicitly. This is usually done for the most general case, that is for a fluid particle of arbitrary shape moving in a potentially non-uniform flow field. The fluid dynamic forces, generally acting upon a fluid particle in such a flow type, can be categorized into *drag* and *non-drag* forces as

$$\mathbf{F}_p = \underbrace{\mathbf{F}_d}_{\text{drag-force}} + \underbrace{\mathbf{F}_l + \mathbf{F}_{vm} + \mathbf{F}_{td}}_{\text{non-drag forces}} . \tag{3.13}$$

The fluid dynamic origin of these forces is set out in table 3.1 and illustrated in figure 3.5 for bubbly flows. Their modeling will be examined in considerable detail in the closure section below and depends on a multitude of parameters and factors, mostly being grouped in dimensionless numbers, as it is established practice in engineering: the bubble Reynolds number[2] $Re_b \equiv d_b|\mathbf{U}_r|/\nu_l$ representing the ratio of inertia to viscous forces, the Eötvos number $Eo \equiv g(\rho_l - \rho_b)d_b^2/\sigma$ representing the ratio of buoyancy to surface tension forces and $Mo \equiv g(\rho_l - \rho_b)\eta_l^4/\rho_l^2\sigma^3$, the Morton number by means of which the ratio of viscous to surface tension forces is taken into account. Note that this is not a complete set fully describing bubbly flows. E.g., dimension analysis reveals two more dimensionless numbers, the density ratio $\Pi_\rho \equiv \rho_l/\rho_b$ and viscosity ratio $\Pi_\nu \equiv \nu_l/\nu_b$. Also the system purity plays a central

[2] Note that the disperse bubble phase has been denoted as $\varphi = b$, whereas $\phi = l$ represents the continuous liquid phase.

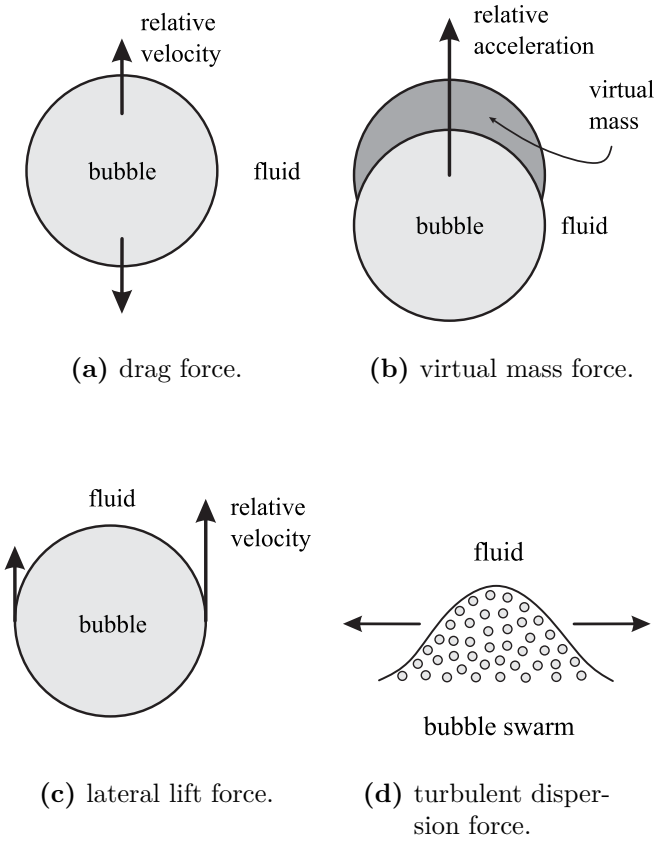

(a) drag force.

(b) virtual mass force.

(c) lateral lift force.

(d) turbulent dispersion force.

Figure 3.5: Interfacial forces in bubbly flows.

Table 3.1: Forces exerted on a fluid particle.

$\mathbf{F}_d$	The drag force acts on particles when they move with a relative (slip) velocity $\mathbf{U}_r$ with respect to an underlying flow. Consequently, a fluid particle is exerted to a resisting force which is opposed to the direction of its movement.
$\mathbf{F}_l$	The lateral lift force is a shear-induced force on the fluid particle due to a non-uniform incident flow of the continuous phase. For bubbly flows this is the most important non-drag force, since the lateral lift force acts perpendicular to the drag force and as such makes a pivotal contribution in capturing the evolution of typical bubbly flow characteristics.
$\mathbf{F}_{vm}$	The virtual mass force accounts for the effect that accelerating particles always entrain a certain amount of surrounding fluid.
$\mathbf{F}_{td}$	The turbulent dispersion force accounts for turbulent fluctuations in the flow field acting with the fluid particles. These turbulent eddies in the continuous phase usually tend to scatter a swarm of dispersed phase particles.

role. Furthermore, other dimensionless groups might be used in a complementary manner, i.e., $We = Re^2\sqrt{Mo/Eo}$ or $Fr = \sqrt{We/Eo}$. Additionally, there are parameters explicitly taking into account particular flow properties and conditions that are imposed on bubbles: E.g., the vorticity of the continuous liquid phase velocity, $\nabla \times \overline{\mathbf{U}}^{\phi}$, its density $\overline{\rho}^{\phi}$ and effective viscosity $\nu_{eff,\phi}$ (including liquid phase *and* bubble-induced turbulence).

3.3. Momentum Transfer Closure

3.3.1. Phase-interaction Terms – M_{φ} and M_{ϕ}

The first phase-interaction term to be analyzed for closure is the interfacial momentum transfer term $\mathbf{M}_{\varphi}$ as defined in equation 2.88. In effect, the momentum equations 2.89 for phase φ and ϕ are coupled through the conditional volume-averaged momentum jump condition set out in equation 2.96. Hence, a careful analysis of the physical nature of this coupling is crucial for a reasonable closure and plausible solution. As can be seen from equation 2.88, the integral of the instantaneous pressure and viscous stress distribution needs to be expressed as constitutive equation. In order to examine this integral it is useful to decompose the instantaneous pressure

in a static contribution (mean interfacial pressure) and a dynamic one (fluctuating pressure). This *pressure split* thus reads

$$p_{I,\varphi} = \widetilde{p}^{\varphi} + p^{\sharp}_{I,\varphi}, \tag{3.14}$$

and results for the interfacial momentum transfer term in:

$$\begin{aligned}\mathbf{M}_{\varphi} &= \overline{\widetilde{p}^{\varphi}\mathbf{I}\bullet\nabla I_{\varphi}} + \overline{\left(p^{\sharp}\mathbf{I}+\boldsymbol{\tau}\right)_{I,\varphi}\bullet\nabla I_{\varphi}} = \overline{\widetilde{p}^{\varphi}\mathbf{I}\bullet\nabla I_{\varphi}} - \overbrace{\left(p^{\sharp}\mathbf{I}+\boldsymbol{\tau}\right)\bullet\mathbf{n}_I}^{\varphi}\,\Sigma \\ &= \widetilde{p}^{\varphi}\nabla\alpha_{\varphi} + \mathbf{M}_{\varphi,h},\end{aligned} \tag{3.15}$$

since

$$\overline{\widetilde{p}^{\varphi}\nabla I_{\varphi}} = -\overbrace{\delta_I\,\widetilde{p}^{\varphi}\mathbf{n}_I}^{\varphi}\,\Sigma = -\overbrace{\widetilde{p}^{\varphi}}^{\varphi}\,\widetilde{\mathbf{n}}_I^{\varphi}\Sigma = \widetilde{p}^{\varphi}\nabla\alpha_{\varphi}. \tag{3.16}$$

The last term on the r.h.s. of equation 3.15 is defined as

$$\mathbf{M}_{\varphi,h} \equiv \overline{\left(p^{\sharp}\mathbf{I}+\boldsymbol{\tau}\right)_{I,\varphi}\bullet\nabla I_{\varphi}} = -\overbrace{\left(p^{\sharp}\mathbf{I}+\boldsymbol{\tau}\right)\bullet\mathbf{n}_I}^{\varphi}\,\Sigma. \tag{3.17}$$

Illustratively, the first term on the r.h.s. of equation 3.15 represents a net force contribution from the interfacial averaged pressure $\widetilde{p}^{\varphi}$ in case there is a gradient in the volumetric phase fraction of phase φ, $\nabla\alpha_{\varphi}$, whereas the second term holds the unbalanced interfacial pressure and shear (viscous) stress contribution $\overbrace{(p^{\sharp}\mathbf{I}+\boldsymbol{\tau})\bullet\mathbf{n}_I}^{\varphi}\Sigma$. For both dispersed and segregated two-phase flows the closure model for $\mathbf{M}_{\varphi,h}$ is a crucial one, since it couples both momenta explicitly. With some evidence, constitutive models for both contributions are expected to differ significantly for different flow types. Hence, these contributions are to be analyzed for both dispersed and segregated flow type.

Mean interfacial pressure contribution

In order to examine the interfacial averaged pressure contribution to $\mathbf{M}_{\varphi}$ and to formulate an appropriate closure, it is important to note that there are two constituents, that *generally* cause the 'mean interfacial' pressure $\widetilde{p}^{\varphi}$ to be different from the 'mean bulk' pressure $\overline{p}^{\varphi}$:

- phase slip,

  i.e., relative motion between the phases, reducing the mean pressure in vicinity to the interface (Bernoulli effect). For closure an expression would be of use, that clearly relates the pressure distribution over the interface to the bulk mean pressure. Subsequent averaging over the interface would result in a closure relation.

- surface tension,

  manifesting in an interfacial force balance with a force contribution due to interfacial averaged pressure (Young-Laplace effect).

For the first constituent (that is due to phase slip) it is rational to examine the conditional volume-averaged interfacial momentum jump condition while disregarding surface tension. From equations 2.96 and 3.15, it follows:

$$\widetilde{p}^{\varphi}\nabla\alpha_{\varphi} + \mathbf{M}_{\varphi,h} + \widetilde{p}^{\phi}\nabla\alpha_{\phi} + \mathbf{M}_{\phi,h} = \mathbf{0}. \tag{3.18}$$

In order to examine the second constituent (that is due to surface tension) the conditional volume-averaged interfacial momentum jump condition has to be considered for a case without flow:

$$\widetilde{p}^{\varphi}\nabla\alpha_{\varphi} + \widetilde{p}^{\phi}\nabla\alpha_{\phi} = \mathbf{M}_{\sigma}. \tag{3.19}$$

Moreover, this needs to be examined for both dispersed and segregated flows.

Dispersed Flows

- contribution from phase slip

  According to Stuhmiller [27] the interfacial averaged pressure can be related to the phasic averaged one by

  $$\widetilde{p}^{\varphi} = \overline{p}^{\varphi} - 0.37\,\overline{\rho}^{\phi} C_d |\,\overline{\mathbf{U}}^{\phi} - \overline{\mathbf{U}}^{\varphi}|^2, \tag{3.20}$$

  where φ represents the dispersed phase while ϕ was taken to denote the continuous one. This closure model is based upon an approximate expression for the pressure distribution over a bubble's surface underlying an inviscid flow solution. However, it shall be assumed valid for bubble Reynolds numbers outside the inviscid limit henceforth [12]. The factor C_d in the above expression denotes the drag coefficient, which needs to be modeled as well, as set out in the following (page 77).

- contribution from surface tension

  Since the size of the averaging volume has been chosen significantly larger than the characteristic length scale of the dispersed phase – e.g., the equivalent diameter of the fluid particles – it is justified to neglect fluid particles that intersect the control volume's surface, which in turn means that the replacement

  $$\widetilde{(\ldots)\,\mathbf{n}_{I,\varphi\phi}}\,\Sigma \approx \frac{1}{V}\sum_{N_p}\oint_{S_p}(\ldots)\,\mathbf{n}_{I,\varphi\phi}\,dS \tag{3.21}$$

  is approximately valid. Hence, it follows from equation 2.97:

  $$\mathbf{M}_{\sigma} = \sigma\,\widetilde{\kappa_I\mathbf{n}_I}\,\Sigma \approx \frac{\sigma}{V}\sum_{N_p}\oint_{S_p}\kappa_I\mathbf{n}_I dS = \mathbf{0}. \tag{3.22}$$

Subsequently equation 3.19 results into

$$\left(\widetilde{p}^{\varphi} - \widetilde{p}^{\phi}\right)\nabla\alpha_{\varphi} = \mathbf{0}, \tag{3.23}$$

stating that there is no net force that has to be explicitly taken into account. Claiming phase-symmetry and with $\mathbf{M}_{\varphi,\sigma} \equiv \widetilde{p}^{\varphi}\nabla\alpha_{\varphi}$ (and $\mathbf{M}_{\phi,\sigma} \equiv \widetilde{p}^{\phi}\nabla\alpha_{\phi}$) it follows:

$$\mathbf{M}_{\varphi,\sigma} = \mathbf{0} \qquad \text{and} \qquad \mathbf{M}_{\phi,\sigma} = \mathbf{0}. \tag{3.24}$$

Segregated Flows

- contribution from phase slip

  For segregated flows it is suggested to relate the 'interfacial mean' and the 'bulk mean' pressure as

  $$\widetilde{p}^{\varphi} = \overline{p}^{\varphi} - \frac{\alpha_{\varphi}\alpha_{\phi}\,\overline{\rho}^{\varphi}\,\overline{\rho}^{\phi}}{\alpha_{\varphi}\,\overline{\rho}^{\phi} + \alpha_{\phi}\,\overline{\rho}^{\varphi}}|\,\overline{\mathbf{U}}^{\phi} - \overline{\mathbf{U}}^{\varphi}|^2 \tag{3.25}$$

  simply following Bestion [28], who introduced this term in the CATHARE CODE without physical argumentation, however resulting in a form expected by Drew and Lahey [1]. It is interesting to note that this expression vanishes for stagnant fluids, while at the same time preserving hyperbolicity at least when there exists a phase slip [29].

- contribution from surface tension

  Since closure relations obviously are related to an interfacial force density due to surface tension, that is assumed to be dominated by non-resolved (microscopic/local) curvature, i.e., the inner morphological structure of the interfacial transition region, it is advisable to revisit the underlying assumption of an *isotropic interfacial topology*: According to equation 3.8 the interfacial averaged curvature $\widetilde{\kappa_I}$ can be decomposed into a resolved mesoscopic contribution and a dominant non-resolved microscopic contribution $d\Sigma/d\alpha_{\varphi}$, where the interfacial area density Σ is only allowed to vary across the interfacial transition region, that is in the direction of $\widetilde{\mathbf{n}_I}$ – perpendicular to contours of constant α_{φ}.

  As set out for equation 3.19 closure models are needed for the terms $\mathbf{M}_{\varphi,\sigma}$ and $\mathbf{M}_{\phi,\sigma}$ as well as for $\mathbf{M}_{\sigma}$. Considering the adoption of this assumption in the context of interfacial surface tension modeling it is proposed that

  $$\mathbf{M}_{\varphi,\sigma} = \alpha_{\varphi}\cdot 4\alpha_{\varphi}\alpha_{\phi}\mathbf{M}_{\sigma} \qquad \text{and} \qquad \mathbf{M}_{\phi,\sigma} = \alpha_{\phi}\cdot 4\alpha_{\varphi}\alpha_{\phi}\mathbf{M}_{\sigma}, \tag{3.26}$$

  where $4\alpha_{\varphi}\alpha_{\phi}$ represents a regularization term. This is clearly stating that the essential contribution of the interfacial force density due to surface tension to

the momentum equation of a particular phase is to be *localized in a part of the interfacial transition region that does feature the inner curvature*: on the adjacent sites of the interface (from the respective "phases' view point").

It is left to formulate a closure relation for $\mathbf{M}_\sigma$ being defined as $\sigma\widetilde{\kappa_I\mathbf{n}_I}\Sigma$ according to equation 2.97: This might be decomposed in the usual way into an interfacial average and an interfacial fluctuating contribution:

$$\mathbf{M}_\sigma = \sigma\widetilde{\kappa_I\mathbf{n}_I}\Sigma = \sigma\left(\widetilde{\kappa_I}\,\widetilde{\mathbf{n}_I} + \widetilde{\kappa_I^\sharp\mathbf{n}_I^\sharp}\right)\Sigma. \tag{3.27}$$

With equation equation 2.72 (substituting $\mathbf{\Phi} = 1$) and 3.8 it can be seen that underlying an isotropic interfacial morphology equation 3.27 can be rewritten as

$$\Rightarrow \qquad \mathbf{M}_\sigma = -\sigma\left(-\frac{\nabla^2\alpha_\varphi}{|\nabla\alpha_\varphi|} + \frac{d\Sigma}{d\alpha_\varphi}\right)\nabla\alpha_\varphi + \sigma\widetilde{\kappa_I^\sharp\mathbf{n}_I^\sharp}\Sigma. \tag{3.28}$$

As already has been set out for equation 3.8, $d\Sigma/d\alpha_\varphi$ states the contribution of the microscopic non-resolved curvature stemming from local fluctuations inside the interfacial transition region. Thus, it seems rational to assume the same form for $\widetilde{\kappa_I^\sharp\mathbf{n}_I^\sharp}\Sigma$. Consequently, we propose the model

$$\widetilde{\kappa_I^\sharp\mathbf{n}_I^\sharp}\Sigma \sim \frac{d\Sigma}{d\alpha_\varphi}\nabla\alpha_\varphi. \tag{3.29}$$

In order to arrive at an exploitable form of relation 3.29 an algebraic expression for the interfacial area density Σ is needed. Moreover, the relation must be transferred into an equation. For this purpose, it is suggested to adopt the following phase-invariant formulation for Σ:

$$\Sigma = 4\alpha_\varphi\alpha_\phi\,\Sigma_0, \tag{3.30}$$

where Σ_0 depends on the presumed non-resolved interfacial morphology and shall (for now) be assumed to be constant. Using the equations 3.6 and incorporating the proportionality factor (q.v. relation 3.29) into Σ_0 (equation 3.30), we can rewrite equation 3.27:

$$\begin{aligned}\mathbf{M}_\sigma &= \sigma\,\widetilde{\kappa_I}\,\widetilde{\mathbf{n}_I}\Sigma + \sigma\frac{d\Sigma}{d\alpha_\varphi}\nabla\alpha_\varphi \\ &\approx \sigma\left(\nabla\bullet\left(\frac{\nabla\alpha_\varphi}{|\nabla\alpha_\varphi|}\right) + 4\Sigma_0\,(1-2\alpha_\varphi)\right)\nabla\alpha_\varphi.\end{aligned} \tag{3.31}$$

Note that the model assumption according to equation 3.29 is rational, since $d\Sigma/d\alpha_\varphi$ is identified to provide the contribution from the microscopic non-resolved curvature that remains even for a macroscopically flat interfacial

transition region and $\widetilde{\kappa_I^\sharp \mathbf{n}_I^\sharp}\,\Sigma$ can be interpreted as the mean effect of this microscopic non-resolved curvature. Thus, finally it is:

$$\mathbf{M}_{\varphi,\sigma} \approx \alpha_\varphi \cdot 4\alpha_\varphi\alpha_\phi\,\sigma\left(\nabla\bullet\left(\frac{\nabla\alpha_\varphi}{|\nabla\alpha_\varphi|}\right)+4\Sigma_0\left(1-2\alpha_\varphi\right)\right)\nabla\alpha_\varphi \qquad \text{and}$$
$$\mathbf{M}_{\phi,\sigma} \approx \alpha_\phi \cdot 4\alpha_\varphi\alpha_\phi\,\sigma\left(\nabla\bullet\left(\frac{\nabla\alpha_\varphi}{|\nabla\alpha_\varphi|}\right)+4\Sigma_0\left(1-2\alpha_\varphi\right)\right)\nabla\alpha_\varphi. \tag{3.32}$$

Taking advantage of the product rule, the term $\nabla\left(\alpha_\varphi\,\overline{p}^\varphi\right)$ in the conditional volume-averaged momentum equation 2.89 might be expanded towards $\alpha_\varphi\nabla\,\overline{p}^\varphi + \overline{p}^\varphi\nabla\alpha_\varphi$. This enables to isolate a net interfacial pressure force density $\mathbf{M}_{\varphi,p} \equiv \left(\widetilde{p}^\varphi - \overline{p}^\varphi\right)\nabla\alpha_\varphi$, accounting for the pressure difference $\widetilde{p}^\varphi - \overline{p}^\varphi$ due to phase slip. It follows for dispersed flow from equation 3.20

$$\mathbf{M}_{\varphi,p} = -0.37\,\overline{p}^\phi C_d|\,\overline{\mathbf{U}}^\phi - \overline{\mathbf{U}}^\varphi|^2\,\nabla\alpha_\varphi, \tag{3.33}$$

and for segregated flow from equation 3.25

$$\mathbf{M}_{\varphi,p} = -\frac{\alpha_\varphi\alpha_\phi\,\overline{\rho}^\varphi\,\overline{p}^\phi}{\alpha_\varphi\,\overline{p}^\phi + \alpha_\phi\,\overline{\rho}^\varphi}|\,\overline{\mathbf{U}}^\phi - \overline{\mathbf{U}}^\varphi|^2\,\nabla\alpha_\varphi. \tag{3.34}$$

Then, the conditional volume-averaged momentum equation reads:

$$\frac{\partial\alpha_\varphi\,\overline{\mathbf{U}}^\varphi}{\partial t} + \nabla\bullet\left(\alpha_\varphi\,\overline{\mathbf{U}}^\varphi\,\overline{\mathbf{U}}^\varphi\right) = -\frac{\alpha_\varphi\nabla\,\overline{p}^\varphi}{\overline{\rho}^\varphi} - \frac{\nabla\bullet\left(\alpha_\varphi\,\overline{\boldsymbol{\tau}}^\varphi\right)}{\overline{\rho}^\varphi} + \alpha_\varphi\mathbf{g} + \frac{\mathbf{M}_{\varphi,h}+\mathbf{M}_{\varphi,p}+\mathbf{M}_{\varphi,\sigma}}{\overline{\rho}^\varphi}, \tag{3.35}$$

where according to the flow type under consideration, $\mathbf{M}_{\varphi,p}$ is modelled using equations 3.33 and 3.34, and $\mathbf{M}_{\varphi,\sigma}$ is modeled adopting equations 3.24 and 3.32 for dispersed and segregated flow, respectively.

It is left to consider the unbalanced interfacial pressure and shear stress contribution, $\mathbf{M}_{\varphi,h}$.

Unbalanced interfacial pressure and shear stress contribution

Dispersed flows For the same reasons as already discussed for equation 3.21, it is justified to do the replacement

$$\widetilde{(\ldots)\bullet\mathbf{n}_{I,\varphi\phi}}\,\Sigma = \frac{1}{V}\sum_{N_p}\oint_{S_p}(\ldots)\bullet\mathbf{n}_{I,\varphi\phi}\,dS, \tag{3.36}$$

since for the closure the averaging volume has been chosen significantly larger than the characteristic length scale of the flow. Thus, particles intersecting the control volume's surface might be neglected.

Assuming particles of one specific (representative) size within the control volume it is

$$\begin{aligned}\mathbf{M}_{\varphi,h} &= -\overbrace{\left(p^\sharp \mathbf{I} + \boldsymbol{\tau}\right) \bullet \mathbf{n}_I}^{\varphi} \Sigma \\ &= -\frac{1}{V} \sum_{N_p} \oint_{S_p} \left(p^\sharp \mathbf{I} + \boldsymbol{\tau}\right)_{I,\varphi} \bullet \mathbf{n}_{I,\varphi\phi}\, dS \\ &= -n_p \mathbf{F}_p, \end{aligned} \tag{3.37}$$

where $n_p \equiv N_p/V$ denotes the particle number density that is the number of particles per control volume and $\mathbf{F}_p$ represents the sum of fluid dynamic forces exerted to a particle

$$\mathbf{M}_{\varphi,h} = -\frac{N_p}{V}\mathbf{F}_p = -\frac{N_p}{V}\frac{V_p}{V_p}\mathbf{F}_p = -\frac{\alpha_\varphi}{V_p}\mathbf{F}_p. \tag{3.38}$$

Note that again the choice of phase φ being the dispersed phase was made – inherently. Moreover, from the conditional volume-averaged interfacial momentum jump condition, it follows subsequently that $\mathbf{M}_{\varphi,h}$ and $\mathbf{M}_{\phi,h}$ balance each other:

$$\mathbf{M}_{\varphi,h} + \mathbf{M}_{\phi,h} = \mathbf{0} \qquad \Leftrightarrow \qquad \mathbf{M}_{\varphi,h} = -\mathbf{M}_{\phi,h}. \tag{3.39}$$

Equation 3.38 can be further analyzed, when splitting up the fluid dynamic forces $\mathbf{F}_p$ into two categories, namely drag and non-drag forces as already set out in equation 3.13, and repeated here for convenience:

$$\mathbf{M}_{\varphi,h} = -\frac{\alpha_\varphi}{V_p}\Big(\underbrace{\mathbf{F}_d}_{\text{drag-force}} + \underbrace{\mathbf{F}_l + \mathbf{F}_{vm} + \mathbf{F}_{td}}_{\text{non-drag forces}} \Big). \tag{3.40}$$

drag force As is well known, the drag force exerted on a particle reads

$$\mathbf{F}_d = -\frac{1}{2}\,\overline{\rho}^{\phi} A_p C_d |\,\overline{\mathbf{U}}^{\phi} - \overline{\mathbf{U}}^{\varphi}|\left(\overline{\mathbf{U}}^{\phi} - \overline{\mathbf{U}}^{\varphi}\right). \tag{3.41}$$

Consequently, the corresponding drag force density is

$$\mathbf{M}_{\varphi,d} = \frac{1}{2}\alpha_\varphi \frac{A_p}{V_p}\,\overline{\rho}^{\phi} C_d |\,\overline{\mathbf{U}}^{\phi} - \overline{\mathbf{U}}^{\varphi}|\left(\overline{\mathbf{U}}^{\phi} - \overline{\mathbf{U}}^{\varphi}\right). \tag{3.42}$$

Presuming solely spherical particles, the ratio A_p/V_p can be evaluated and becomes $A_p/V_p = 3/(2d_p)$. Then, the drag-force density within the two-fluid model approach eventually reads in its final functional form

$$\mathbf{M}_{\varphi,d} = \frac{3}{4}\alpha_\varphi C_d \frac{\overline{\rho}^{\phi}}{d_p} |\,\overline{\mathbf{U}}^{\phi} - \overline{\mathbf{U}}^{\varphi}|\left(\overline{\mathbf{U}}^{\phi} - \overline{\mathbf{U}}^{\varphi}\right). \tag{3.43}$$

The drag coefficient C_d herein is a function of the bubble Reynolds number:

$$Re \equiv \frac{d_p |\mathbf{U}_r|}{\overline{\nu}^{\phi}}, \tag{3.44}$$

where d_p denotes a characteristic, i.e., representative, diameter of fluid particles of the dispersed phase φ.
This procedure can be adopted to non-drag forces as well. Note that deviations from a spherical particle shape are usually accounted for only within the models for the force coefficients, that are then a function of several dimensionless groups taking into account inertia, viscous, buoyancy and surface tension effects. Moreover, these models for the force coefficients are based on (mostly) empirical correlations.

lateral lift force There are various model formulations aiming at the description of the lateral lift force density. The following is found to be widely used:

$$\mathbf{M}_{\varphi,l} = \alpha_{\varphi}\, \overline{\rho}^{\phi} C_l \left(\overline{\mathbf{U}}^{\phi} - \overline{\mathbf{U}}^{\varphi} \right) \times \bar{\boldsymbol{\omega}}_{\phi} \qquad \text{with } \bar{\boldsymbol{\omega}}_{\phi} = \nabla \times \overline{\mathbf{U}}^{\phi}. \tag{3.45}$$

The lateral lift force coefficient C_l is modeled as a function of the bubble Reynolds and the Eötvös number,

$$Eo \equiv \frac{\left(\overline{\rho}^{\phi} - \overline{\rho}^{\varphi} \right) g\, d_p^2}{\sigma}. \tag{3.46}$$

turbulent dispersion force The turbulent dispersion force density is usually introduced into the momentum balance by a term that is proportional to the gradient of the dispersed phase volume fraction. Examining the concrete model formulation, however, particularly the turbulent dispersion force models exhibit various forms. The following is found to be widely used [30]:

$$\mathbf{M}_{\varphi,td} = C_{td}\, \overline{\rho}^{\phi}\, \overline{k}\, \nabla \alpha_{\varphi}. \tag{3.47}$$

Henceforth the dispersion coefficient C_{td} shall be assumed constant, taking a value between 0.1 and 1.0 [31]. Thus, the turbulent dispersion force is assumed to be proportional to the product of the mean kinetic energy and the gradient of the volumetric gas phase fraction.

virtual mass force The virtual mass force density is accounted for by the following model term:

$$\mathbf{M}_{\varphi,vm} = C_{vm} \alpha_{\varphi}\, \overline{\rho}^{\phi} \left(\frac{D_{\varphi}\, \overline{\mathbf{U}}^{\varphi}}{Dt} - \frac{D_{\phi}\, \overline{\mathbf{U}}^{\phi}}{Dt} \right) \tag{3.48}$$
$$\text{with} \qquad \frac{D_i}{Dt} \equiv \frac{\partial}{\partial t} + \overline{\mathbf{U}}^{i} \bullet \nabla.$$

For spherical single bubbles the virtual mass force coefficient reads $C_{vm} = 0.5$ [32, 33]. For bubbles with altering shapes this value is usually found to be

smaller. However, there are not many reliable correlations, which mostly has been stated to be the reason for neglecting the virtual mass force so far. Sokolichin and Eigenberger [34] propose a constant virtual mass force coefficient of $C_{vm} = 0.25$ for these bubbles with variable shapes.

wall lubrication force At this stage, the so-called wall lubrication force shall only be mentioned as well for completeness. The corresponding force density has first been introduced by Antal [35] in order to account for the repulsive effect, which bubbles are exerted to in the vicinity of the column's wall as a consequence of an asymmetric incident flow near the wall boundary layer.
However, as models for the wall lubrication force are subject to various restrictions and constraints, it is neglected in the further course of this study.

A summary of model correlations for both drag and non-drag force coefficients can be found in [33, 36].

Segregated flows In the concept of partially penetrating continua $\mathbf{M}_{\varphi,h}$ in the interfacial transition region might be identified as interfacial force density due to unbalanced pressures and viscous stresses, which manifests itself in a dissipative drag due to interfacial friction in the presence of phase slip.

With $\widetilde{\overline{\mu}}^{\varphi} = \overline{\mu}^{\varphi}$ the following relation is proposed for the interfacial force density accounting for viscous drag:

$$\mathbf{M}_{\varphi,h} \sim \frac{\Sigma}{\delta}\,\overline{\mu}^{\varphi}\left(\overline{\mathbf{U}}^{\varphi} - \widetilde{\overline{\mathbf{U}}}^{\varphi}\right), \tag{3.49}$$

where Σ denotes the interfacial area density according to equation 3.5 that varies across the interfacial transition region of width δ. As for Σ, a closure model has to be found for the interfacial width δ.

However, first the relation 3.49 needs to be rewritten by use of equation 3.12 (model for $\widetilde{\overline{\mathbf{U}}}^{\varphi}$) and 3.5 (model for Σ):

$$\mathbf{M}_{\varphi,h} \sim \frac{|\nabla\alpha_{\varphi}|}{\delta}\,\frac{\overline{\mu}^{\varphi}\,\overline{\mu}^{\phi}}{\overline{\mu}^{\varphi} + \overline{\mu}^{\phi}}\left(\overline{\mathbf{U}}^{\varphi} - \overline{\mathbf{U}}^{\phi}\right), \tag{3.50}$$

which further might be written into a more exploitable form:

$$\mathbf{M}_{\varphi,h} = \lambda\left(Re_I, \pi_{\mu}\right)\frac{|\nabla\alpha_{\varphi}|}{\delta}\,\frac{\overline{\mu}^{\varphi}\,\overline{\mu}^{\phi}}{\overline{\mu}^{\varphi} + \overline{\mu}^{\phi}}\left(\overline{\mathbf{U}}^{\varphi} - \overline{\mathbf{U}}^{\phi}\right), \tag{3.51}$$

where the proportionality factor has been denoted as $\lambda\left(Re_I, \pi_{\mu}\right)$, representing a dimensionless friction coefficient which holds (unbalanced) tangential inertia and tangential shear contributions:

$$\lambda\left(Re_I, \pi_{\mu}\right) = m\,Re_I + n\,\pi_{\mu}, \tag{3.52}$$

where the parameters m and n have to be chosen appropriate; $m = 0.1 \ldots 1.5$ and $n \approx 8$ have proven adequate. From this, it is evident that the dissipative drag is a function of the relative phase velocity, that is the averaged slip velocity between the phases. Note that the interfacial Reynolds number has been defined as

$$Re_I \equiv \frac{\rho\, \delta\, |\, \overline{\mathbf{U}}^{\varphi} - \overline{\mathbf{U}}^{\phi}|}{\alpha_{\varphi}\alpha_{\phi}\; \overline{\mu}^{\varphi}\, \overline{\mu}^{\phi} / (\, \overline{\mu}^{\varphi} + \overline{\mu}^{\phi})}. \tag{3.53}$$

Moreover, for the dimensionless group π_{μ} (viscous shear contribution), it is suggested:

$$\pi_{\mu} \equiv \frac{\alpha_{\varphi}\alpha_{\phi}\, \overline{\mu}^{\varphi}\, \overline{\mu}^{\phi} / \left(\alpha_{\phi}\, \overline{\mu}^{\varphi} + \alpha_{\varphi}\, \overline{\mu}^{\phi}\right)}{\overline{\mu}^{\varphi}\, \overline{\mu}^{\phi} / \left(\, \overline{\mu}^{\varphi} + \overline{\mu}^{\phi}\right)}. \tag{3.54}$$

Note in passing that – in the view of the underlying microscopic shear flow scenario for closure – the numerator of the above expression has been chosen as the harmonic mean of the phase viscosities weighted with the respective volumetric phase fractions. This in fact is the correct viscosity value when the flow velocity is parallel to the interface. For the denominator, the corresponding local instantaneous analogue at the interface ($I_{\varphi} = I_{\phi} = 0.5$) has been chosen as dimensionless viscosity term. Note that this term is also present within our ansatz as given by equation 3.51.

As first attempt for a closure model for δ, it is suggested that

$$\delta \approx \frac{1}{\Sigma} = \frac{1}{|\nabla \alpha_{\varphi}|}, \tag{3.55}$$

which inversely relates interfacial width δ and interfacial area density Σ, and is motivated from the closure for the *flame brush thickness* of an unwrinkled flamelet [37]. However, it is necessary to adapt the conceptual framework to gas-liquid flows of segregated type (see corollary note 3.3).

Corollary Note 3.3

Consider the simple gedankenexperiment as illustrated in figure 3.6a. Herein, a flat surface element of the gas-liquid interface is assumed to oscillate vertically within the interfacial transition region. The boundaries in-between which this happens is characterized by the root-mean-squared position deviation of interfacial fluctuations from the interface mean position. The resulting distance shall be entitled interfacial width and henceforth be denoted as δl_I.
This scenario is completely compatible with the model representation of an isotropic interfacial morphology as illustrated in figure 3.3 and set out for the interfacial area density Σ on page 65. The interfacial surface element shall move with a (for now) constant interfacial fluctuation velocity $\mathbf{U}_I^{\sharp}$ – back and forth in the presumed horizontal direction. Furthermore, the

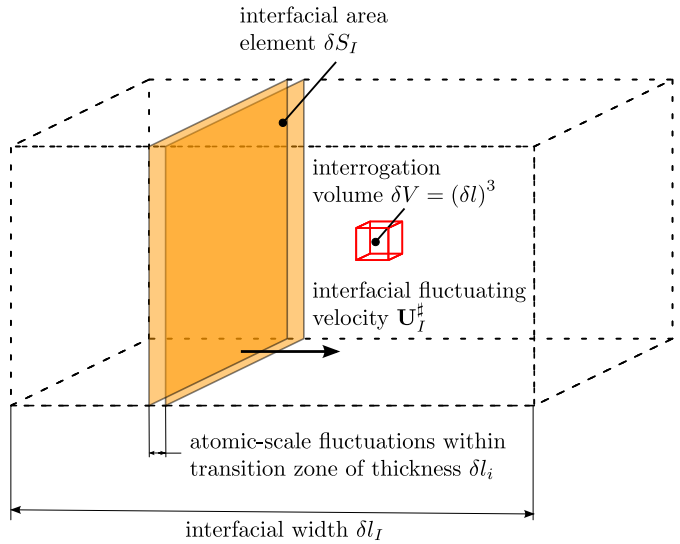

(a) fluctuating interface within the interfacial transition region.

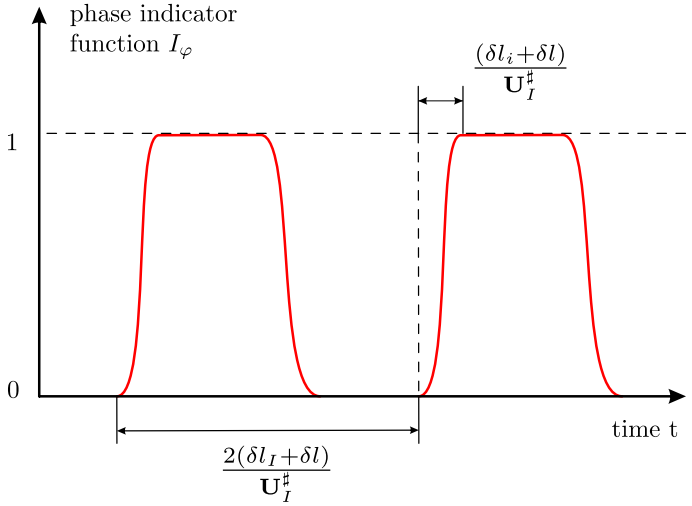

(b) time history of the phase indicator function.

Figure 3.6: Illustration of a fluctuating interface for an isotropic interfacial morphology.

phase indicator function I_φ shall vary smoothly between its limiting values of unity and zero within a thin transition zone, where on a molecular scale fluctuations occur governing the inner atomic-scale structure of the *diffuse interface* (as it is commonly described by diffuse interface or phase-field methods). The width δl_i of this thin transition zone is usually assumed to be in the order of several nanometers.
To approach a more exploitable expression for the interfacial area density Σ consider an infinitesimal 'interrogation' volume δV in the limiting case where $\delta V \to 0$. Then, the *local* interfacial area density reads:

$$\Sigma = \lim_{\delta V \to 0} \frac{\delta S_I}{\delta V} = \lim_{\delta l \to 0} \frac{\delta S_I}{(\delta l)^3}, \tag{3.56}$$

where δl represents the edge length of the 'interrogation' volume δV, and δS_I denotes the interfacial area density, in case the interface is found to be in the 'interrogation' volume $(\delta l)^2$ multiplied by the time fraction, that it is effectively present within δV considering the whole fluctuation in progress. With the help of figure 3.6b showing the time history of the phase indicator function averaged over δV, it follows

$$\Sigma = \lim_{\delta l \to 0} (\delta l)^2 \frac{2\left(\delta l_i + \delta l\right)/\mathbf{U}_I^\sharp}{2\left(\delta l_I + \delta l\right)/\mathbf{U}_I^\sharp} \frac{1}{(\delta l)^3}. \tag{3.57}$$

As a clear scale separation applies,

$$\delta l \ll \delta l_I \qquad \text{and} \qquad \delta l \gg \delta l_i, \tag{3.58}$$

which is regarded fulfilled by orders of magnitude, equation 3.57 reduces to

$$\Sigma = \frac{1}{\delta l_I}, \tag{3.59}$$

and thus for the desired closure of the interfacial width, it follows from equation 3.5

$$\delta_I (= \delta) = \frac{1}{|\nabla \alpha_\varphi|}. \tag{3.60}$$

3.3.2. Self-interaction Terms – $\overline{\boldsymbol{\tau}}^{\varphi}$ and $\overline{\boldsymbol{\tau}}^{\phi}$

A closure model for the conditional volume-averaged (viscous) shear stress tensor $\overline{\boldsymbol{\tau}}^{\varphi}$ as a function of other (accessible) averaged quantities can be obtained by examining the conditional volume-averaged constitutive equation of the *local* shear stress tensor

as given by equation 2.14. This is repeated here for convenience for incompressible Newtonian fluids:

$$\boldsymbol{\tau} = -\mu \left(\nabla \mathbf{U} + (\nabla \mathbf{U})^T \right). \tag{3.61}$$

Conditional volume-averaging of equation 3.61 yields for phase φ:

$$\begin{aligned} \alpha_\varphi \, \overline{\boldsymbol{\tau}}^\varphi &= -\overline{I_\varphi \mu \left(\nabla \mathbf{U} + (\nabla \mathbf{U})^T \right)} = -\overline{I_\varphi \mu \nabla \mathbf{U}} - \overline{I_\varphi \mu \nabla \mathbf{U}^T} \\ &= -\nabla \left(\alpha_\varphi \, \overline{\mu \mathbf{U}}^\varphi \right) - \overbrace{(\mu \mathbf{U})\, \mathbf{n}_I}^{\varphi} \Sigma - \nabla \left(\alpha_\varphi \, \overline{\mu \mathbf{U}}^\varphi \right)^T - \overbrace{\mathbf{n}_I \, (\mu \mathbf{U})}^{\varphi} \Sigma. \end{aligned} \tag{3.62}$$

Thus, it follows with the decomposition for the local-instantaneous velocity into an interfacial averaged and an interface fluctuating velocity (as set out in equation 3.9) and by taking advantage of the product rule

$$\begin{aligned} \alpha_\varphi \, \overline{\boldsymbol{\tau}}^\varphi = &- \overline{\mu}^\varphi \nabla \left(\alpha_\varphi \, \overline{\mathbf{U}}^\varphi \right) - \overline{\mu}^\varphi \nabla \left(\alpha_\varphi \, \overline{\mathbf{U}}^\varphi \right)^T \\ &- \overbrace{\left(\mu \left(\widetilde{\mathbf{U}}^\varphi + \mathbf{U}^\sharp_{I,\varphi} \right) \right) \mathbf{n}_I}^{\varphi} \Sigma - \overbrace{\mathbf{n}_I \left(\mu \left(\widetilde{\mathbf{U}}^\varphi + \mathbf{U}^\sharp_{I,\varphi} \right) \right)}^{\varphi} \Sigma, \end{aligned} \tag{3.63}$$

where the last two terms on the r.h.s. needs to be analyzed further. For instance, for the first term it is

$$\begin{aligned} \overbrace{\left(\mu \left(\widetilde{\mathbf{U}}^\varphi + \mathbf{U}^\sharp_{I,\varphi} \right) \right) \mathbf{n}_I}^{\varphi} \Sigma &= \overbrace{\mu \, \widetilde{\mathbf{U}}^\varphi}^{\varphi} \widetilde{\mathbf{n}_I} \Sigma + \underbrace{\overbrace{\mu \mathbf{U}^\sharp_{I,\varphi}}^{\varphi}}_{=\mathbf{0}} \widetilde{\mathbf{n}_I} \Sigma \\ &= -\widetilde{\mu}^\varphi \, \widetilde{\mathbf{U}}^\varphi \nabla \alpha_\varphi. \end{aligned} \tag{3.64}$$

Hence, finally it is

$$\begin{aligned} \alpha_\varphi \, \overline{\boldsymbol{\tau}}^\varphi = &- \alpha_\varphi \, \overline{\mu}^\varphi \nabla \, \overline{\mathbf{U}}^\varphi - \overline{\mu}^\varphi \, \overline{\mathbf{U}}^\varphi \nabla \alpha_\varphi - \alpha_\varphi \, \overline{\mu}^\varphi \nabla \, \overline{\mathbf{U}}^{\varphi T} - \nabla \alpha_\varphi \, \overline{\mu}^\varphi \, \overline{\mathbf{U}}^\varphi \\ &+ \widetilde{\mu}^\varphi \, \widetilde{\mathbf{U}}^\varphi \nabla \alpha_\varphi + \widetilde{\mu}^\varphi \nabla \alpha_\varphi \, \widetilde{\mathbf{U}}^\varphi \\ \Rightarrow \quad \alpha_\varphi \, \overline{\boldsymbol{\tau}}^\varphi = &- \left(\alpha_\varphi \, \overline{\mu}^\varphi \left(\nabla \, \overline{\mathbf{U}}^\varphi + \nabla \, \overline{\mathbf{U}}^{\varphi T} \right) \right) \\ &- \left(\left(\overline{\mu}^\varphi \, \overline{\mathbf{U}}^\varphi - \widetilde{\mu}^\varphi \, \widetilde{\mathbf{U}}^\varphi \right) \nabla \alpha_\varphi + \nabla \alpha_\varphi \left(\overline{\mu}^\varphi \, \overline{\mathbf{U}}^\varphi - \widetilde{\mu}^\varphi \, \widetilde{\mathbf{U}}^\varphi \right) \right). \end{aligned} \tag{3.65}$$

By substituting closure models for $\widetilde{\mathbf{U}}^\varphi$ and with $\widetilde{\mu}^\varphi = \overline{\mu}^\varphi$, the conditional volume-averaged shear stress tensor $\overline{\boldsymbol{\tau}}^\varphi$ might be completely expressed in terms of averaged flow quantities for different flow types.

Segregated Flows Substituting equation 3.12 for $\widetilde{\mathbf{U}}^\varphi$ into equation 3.65 yields

$$\begin{aligned} \alpha_\varphi \, \overline{\boldsymbol{\tau}}^\varphi = &- \left(\alpha_\varphi \, \overline{\mu}^\varphi \left(\nabla \, \overline{\mathbf{U}}^\varphi + \nabla \, \overline{\mathbf{U}}^{\varphi T} \right) \right) \\ &- \frac{\overline{\mu}^\varphi \, \overline{\mu}^\phi}{\overline{\mu}^\varphi + \overline{\mu}^\phi} \left(\left(\overline{\mathbf{U}}^\varphi - \overline{\mathbf{U}}^\phi \right) \nabla \alpha_\varphi + \nabla \alpha_\varphi \left(\overline{\mathbf{U}}^\varphi - \overline{\mathbf{U}}^\phi \right) \right). \end{aligned} \tag{3.66}$$

Examining this reveals that the first term holds the viscous stress contributions of the phase φ to itself, while the second parts account for phase slip, inducing viscous stress in phase φ due to relative motion with respect to phase ϕ. Note that $\nabla\alpha_\varphi$ ensures the second contribution to be only non-zero inside the interfacial region.

It is moreover interesting to note that Sun and Beckermann [38] found a similar term. However, it seems neither rational nor plausible that their phase slip contribution is proportional to the phase fraction α_φ, since strictly decomposing into terms $\sim \alpha_\varphi$ (i.e., bulk contribution) and terms $\sim \nabla\alpha_\varphi$ (i.e., a interfacial contribution) – as shown in equation 3.65 and its derivation – does not result in such an outcome. Furthermore, it is worth noting that Drew and Passman [1] proposed another closure for $\overline{\boldsymbol{\tau}}^\varphi$. However, their approach is deemed quite case-sensitive, as it holds several *effective viscosities* for different flow scenarios, which is rather ponderous and avoided by the above approach.

Dispersed Flows It remains to model the velocity averaged over the interfacial surface of the fluid particles being possessed within a dispersed two-phase flow system. In this case it is justified and reasonable to assume $\widetilde{\mathbf{U}}^\varphi = \overline{\mathbf{U}}^\varphi$ with φ being chosen to denote the dispersed phase. It follows by substitution into equation 3.65 for the dispersed phase φ:

$$\alpha_\varphi\,\overline{\boldsymbol{\tau}}^\varphi = -\left(\alpha_\varphi\,\overline{\mu}^\varphi\left(\nabla\,\overline{\mathbf{U}}^\varphi + \nabla\,\overline{\mathbf{U}}^{\varphi T}\right)\right), \tag{3.67}$$

and similarly for the continuous phase ϕ:

$$\begin{aligned}\alpha_\phi\,\overline{\boldsymbol{\tau}}^\phi = &-\left(\alpha_\phi\,\overline{\mu}^\phi\left(\nabla\,\overline{\mathbf{U}}^\phi + \nabla\,\overline{\mathbf{U}}^{\phi T}\right)\right)\\ &-\overline{\mu}^\phi\left(\left(\overline{\mathbf{U}}^\phi - \overline{\mathbf{U}}^\varphi\right)\nabla\alpha_\phi + \nabla\alpha_\phi\left(\overline{\mathbf{U}}^\phi - \overline{\mathbf{U}}^\varphi\right)\right).\end{aligned} \tag{3.68}$$

Note that the last term on the r.h.s. of equation 3.68 is non-zero only in the presence of a gradient of the volumetric phase fraction $\nabla\alpha_\varphi$, while an analog counterpart is not appearing at all in equation 3.67. Thus, the second contribution can be interpreted as net shear stress in the continuous phase being induced by the dispersed phase due to phase slip.

3.4. Interfacial Transport Closure

Assuming an isotropic interfacial morphology for segregated flows (as described in section 3.2.1) and taking into account equation 3.36 for dispersed flows, the volume-averaged interfacial transport equation 2.104 reduces for both cases to

$$\frac{\partial\alpha_\varphi}{\partial t} + \widetilde{\mathbf{U}}^\varphi\bullet\nabla\alpha_\varphi = 0. \tag{3.69}$$

Thus, in order to arrive at a closed governing equation, a model for $\widetilde{\mathbf{U}}^\varphi$ needs to be involved – both for segregated and for dispersed flow types.

Dispersed Flow As it already has been described for the conditional volume-averaged shear stress, it is justified and physically reasonable to presume

$$\widetilde{\overline{\mathbf{U}}}^{\varphi} = \overline{\mathbf{U}}^{\varphi}. \tag{3.70}$$

Hence, the volume-averaged interfacial transport is governed by

$$\frac{\partial \alpha_{\varphi}}{\partial t} + \overline{\mathbf{U}}^{\varphi} \bullet \nabla \alpha_{\varphi} = 0. \tag{3.71}$$

Segregated Flow According to equation 3.12, the interfacial averaged velocity can be modeled as

$$\widetilde{\overline{\mathbf{U}}}^{\varphi} = \frac{\overline{\mu}^{\varphi}\,\overline{\mathbf{U}}^{\varphi} + \overline{\mu}^{\phi}\,\overline{\mathbf{U}}^{\phi}}{\overline{\mu}^{\varphi} + \overline{\mu}^{\phi}}. \tag{3.72}$$

Consequently, the volume-averaged interfacial transport equation for segregated flows reads

$$\frac{\partial \alpha_{\varphi}}{\partial t} + \left[\frac{\overline{\mu}^{\varphi}\,\overline{\mathbf{U}}^{\varphi} + \overline{\mu}^{\phi}\,\overline{\mathbf{U}}^{\phi}}{\overline{\mu}^{\varphi} + \overline{\mu}^{\phi}} \right] \bullet \nabla \alpha_{\varphi} = 0. \tag{3.73}$$

For free-surface flows ($\overline{\mu}^{\phi} \ll \overline{\mu}^{\varphi}$) the interfacial averaged velocity reduces to

$$\widetilde{\overline{\mathbf{U}}}^{\varphi} = \overline{\mathbf{U}}^{\varphi}. \tag{3.74}$$

Thus, equation 3.73 and 3.71, i.e., the volume-averaged interfacial transport equation for dispersed and free-surface segregated flow, are found to take identical forms:

$$\frac{\partial \alpha_{\varphi}}{\partial t} + \overline{\mathbf{U}}^{\varphi} \bullet \nabla \alpha_{\varphi} = 0. \tag{3.75}$$

3.5. Final Forms of Governing Equations

3.5.1. Two-Field Equations

From the conditional volume-averaged continuity equation 2.84, it follows by summing up for both phase φ and ϕ and taking into account $\alpha_{\phi} = 1 - \alpha_{\varphi}$:

$$\nabla \bullet \left(\alpha_{\varphi}\,\overline{\mathbf{U}}^{\varphi} + \alpha_{\phi}\,\overline{\mathbf{U}}^{\phi} \right) = 0 \quad \Leftrightarrow \quad \nabla \bullet \mathbf{U} \overset{!}{=} 0. \tag{3.76}$$

The volume-averaged interfacial transport equation 3.69 reads

$$\frac{\partial \alpha_{\varphi}}{\partial t} + \widetilde{\overline{\mathbf{U}}}^{\varphi} \bullet \nabla \alpha_{\varphi} = 0. \tag{3.77}$$

The conditional volume-averaged momentum equations eventually take the following form:

$$\frac{\partial \alpha_\varphi \, \overline{\mathbf{U}}^\varphi}{\partial t} + \nabla\!\bullet \left(\alpha_\varphi \, \overline{\mathbf{U}}^\varphi \, \overline{\mathbf{U}}^\varphi \right) = - \frac{\alpha_\varphi \nabla \, \overline{p}^\varphi}{\overline{\rho}^\varphi} - \frac{\nabla\!\bullet \left(\alpha_\varphi \, \overline{\boldsymbol{\tau}}^\varphi \right)}{\overline{\rho}^\varphi} + \alpha_\varphi \mathbf{g} + \frac{\mathbf{M}_{\varphi,h} + \mathbf{M}_{\varphi,p} + \mathbf{M}_{\varphi,\sigma}}{\overline{\rho}^\varphi}, \tag{3.78}$$

and

$$\frac{\partial \alpha_\phi \, \overline{\mathbf{U}}^\phi}{\partial t} + \nabla\!\bullet \left(\alpha_\phi \, \overline{\mathbf{U}}^\phi \, \overline{\mathbf{U}}^\phi \right) = - \frac{\alpha_\phi \nabla \, \overline{p}^\phi}{\overline{\rho}^\phi} - \frac{\nabla\!\bullet \left(\alpha_\phi \, \overline{\boldsymbol{\tau}}^\phi \right)}{\overline{\rho}^\phi} + \alpha_\phi \mathbf{g} + \frac{\mathbf{M}_{\phi,h} + \mathbf{M}_{\phi,p} + \mathbf{M}_{\phi,\sigma}}{\overline{\rho}^\phi}. \tag{3.79}$$

The corresponding closure terms are summarized in table 3.2. The respective derivations and underlying assumptions have been described in considerable detail in the above sections.

		segregated flow type	dispersed flow type
momentum transfer	phase-interaction	mean interfacial pressure contribution	
		$\mathbf{M}_{\varphi,p} = -\frac{\alpha_\varphi \alpha_\phi \, \overline{\rho}^{\varphi} \, \overline{\rho}^{\phi}}{\alpha_\varphi \, \overline{\rho}^{\phi} + \alpha_\phi \, \overline{\rho}^{\varphi}} \lvert \, \overline{\mathbf{U}}^{\phi} - \, \overline{\mathbf{U}}^{\varphi} \rvert^2 \, \nabla \alpha_\varphi$	$\mathbf{M}_{\varphi,p} = -0.37 \, \overline{\rho}^{\phi} C_d \lvert \, \overline{\mathbf{U}}^{\phi} - \, \overline{\mathbf{U}}^{\varphi} \rvert^2 \, \nabla \alpha_\varphi$
		$\mathbf{M}_{\varphi,\sigma} = \alpha_\varphi \; 4 \alpha_\varphi \alpha_\phi \, \sigma \left(\nabla \bullet \left(\frac{\nabla \alpha_\varphi}{\lvert \nabla \alpha_\varphi \rvert} \right) + 4 \Sigma_0 \left(1 - 2 \alpha_\varphi \right) \right) \nabla \alpha_\varphi$	$\mathbf{M}_{\varphi,\sigma} = \mathbf{0}$
		unbalanced interfacial pressure and shear stress contribution	
		$\mathbf{M}_{\varphi,h} = \lambda \left(Re_I \right) \frac{\lvert \nabla \alpha_\varphi \rvert}{\delta} \frac{\overline{\mu}^{\varphi} \, \overline{\mu}^{\phi}}{\overline{\mu}^{\varphi} + \, \overline{\mu}^{\phi}} \left(\overline{\mathbf{U}}^{\varphi} - \, \overline{\mathbf{U}}^{\phi} \right)$	$\mathbf{M}_{\varphi,h} = -\frac{\alpha_\varphi}{V_p} (\underbrace{\mathbf{F}_d}_{\text{drag-force}} + \underbrace{\mathbf{F}_l + \mathbf{F}_{vm} + \mathbf{F}_{td}}_{\text{non-drag forces}})$
	self-interaction	$\alpha_\varphi \, \overline{\boldsymbol{\tau}}^{\varphi} = - \left(\alpha_\varphi \, \overline{\mu}^{\varphi} \left(\nabla \, \overline{\mathbf{U}}^{\varphi} + \nabla \, \overline{\mathbf{U}}^{\varphi T} \right) \right) - \frac{\overline{\mu}^{\varphi} \, \overline{\mu}^{\phi}}{\overline{\mu}^{\varphi} + \, \overline{\mu}^{\phi}} \left(\left(\overline{\mathbf{U}}^{\varphi} - \, \overline{\mathbf{U}}^{\phi} \right) \nabla \alpha_\varphi + \nabla \alpha_\varphi \left(\overline{\mathbf{U}}^{\varphi} - \, \overline{\mathbf{U}}^{\phi} \right) \right)$	dispersed phase φ : $\alpha_\varphi \, \overline{\boldsymbol{\tau}}^{\varphi} = - \left(\alpha_\varphi \, \overline{\mu}^{\varphi} \left(\nabla \, \overline{\mathbf{U}}^{\varphi} + \nabla \, \overline{\mathbf{U}}^{\varphi T} \right) \right)$ continuous phase ϕ : $\alpha_\phi \, \overline{\boldsymbol{\tau}}^{\phi} = - \left(\alpha_\phi \, \overline{\mu}^{\phi} \left(\nabla \, \overline{\mathbf{U}}^{\phi} + \nabla \, \overline{\mathbf{U}}^{\phi T} \right) \right) - \overline{\mu}^{\phi} \left(\left(\overline{\mathbf{U}}^{\phi} - \, \overline{\mathbf{U}}^{\varphi} \right) \nabla \alpha_\phi + \nabla \alpha_\phi \left(\overline{\mathbf{U}}^{\phi} - \, \overline{\mathbf{U}}^{\varphi} \right) \right)$
interfacial transport		$\widetilde{\mathbf{U}}^{\varphi} = \frac{\overline{\mu}^{\varphi} \, \overline{\mathbf{U}}^{\varphi} + \overline{\mu}^{\phi} \, \overline{\mathbf{U}}^{\phi}}{\overline{\mu}^{\varphi} + \, \overline{\mu}^{\phi}}$	$\widetilde{\mathbf{U}}^{\varphi} = \, \overline{\mathbf{U}}^{\varphi}$

Table 3.2: Overview – Closure terms for dispersed and segregated two-phase flow.

3.5.2. Single-Field Equations

Further insights might be gained, considering the so-called single-field equations, which are obtained by summing up the two-field equations for each phase φ and ϕ, respectively. In doing so, the two mass and momentum conservation equations will be replaced by one conservation equation for mass and momentum of the system's center-of-mass [8, 39–42].

For further derivations, it is useful to define mixture quantities in order to arrive at a more compact form after summing up the respective equations:

- The *mixture density and viscosity* are defined as

$$\rho \equiv \alpha_\varphi \, \overline{\rho}^\varphi + \alpha_\phi \, \overline{\rho}^\phi \qquad \text{and} \qquad \mu \equiv \alpha_\varphi \, \overline{\mu}^\varphi + \alpha_\phi \, \overline{\mu}^\phi \tag{3.80}$$

- The *center-of-mass velocity* and *phase relative velocity* are defined as

$$\mathbf{U}_m \equiv \frac{\alpha_\varphi \, \overline{\rho}^\varphi \, \overline{\mathbf{U}}^\varphi + \alpha_\phi \, \overline{\rho}^\phi \, \overline{\mathbf{U}}^\phi}{\alpha_\varphi \, \overline{\rho}^\varphi + \alpha_\phi \, \overline{\rho}^\phi} \qquad \text{and} \tag{3.81}$$

$$\mathbf{U}_r \equiv \overline{\mathbf{U}}^\varphi - \overline{\mathbf{U}}^\phi. \tag{3.82}$$

  These provide local measures for the system's mean velocity with respect to its center-of-mass and for the system's mean velocity difference between the phases, respectively.

- We further assume a *mixture pressure* that is shared by both phases:

$$\overline{p}^\varphi = \overline{p}^\phi = p. \tag{3.83}$$

  This is a commonly adopted assumption. Nevertheless, aside from numerical reasons (q.v. pg. 121), a physical justification for assuming a mixture pressure is rarely provided. However, looking into diffuse interface or phase-field methods, which are based on thermodynamic considerations, a physical foundation of this assumption might be postulated: Sun and Beckermann, who conceptually link phase-field methods and conditional volume-averaging on the microscopic (atomistic) scale in [38], state in the absence of phase-change

$$\overline{p}^\varphi - \overline{p}^\phi = -\delta \; \mathbf{M}_\sigma \bullet \frac{\nabla \alpha_\varphi}{|\nabla \alpha_\varphi|}. \tag{3.84}$$

  Consequently, the two phasic pressures are equivalent in the so-called *sharp interface limit*, that is in the limit when the interfacial thickness tends to zero ($\delta \to 0$). In turn, a condensed notation which holds the mixture pressure p instead of the phasic ones is physically justified if a sharp interface representation can be ensured.

With this, the conditional volume-averaged phase velocities can be rewritten in terms of the center-of-mass velocity and phase relative velocity:

$$\overline{\mathbf{U}}^{\varphi} = \mathbf{U}_m + \frac{\alpha_\phi\,\overline{\rho}^{\phi}}{\rho}\mathbf{U}_r \qquad \text{and} \tag{3.85}$$

$$\overline{\mathbf{U}}^{\phi} = \mathbf{U}_m - \frac{\alpha_\varphi\,\overline{\rho}^{\varphi}}{\rho}\mathbf{U}_r, \tag{3.86}$$

Defining $\gamma \equiv \alpha_\varphi$ and eliminating $\overline{\mathbf{U}}^{\varphi}$ in the conditional volume-averaged continuity equation 2.84 using equation 3.85 yields in terms of mixture quantities:

$$\frac{\partial \gamma}{\partial t} + \nabla\!\bullet\left(\gamma \mathbf{U}_m\right) = -\nabla\!\bullet\left(\frac{\gamma\left(1-\gamma\right)\,\overline{\rho}^{\phi}}{\rho}\mathbf{U}_r\right). \tag{3.87}$$

However, note that by underlying the conditional volume-averaged continuity equation 2.84 instead of the volume-averaged interfacial transport equation 3.69, the assumption of a free-surface flow has been made inherently. As $\alpha_\phi = (1-\alpha_\varphi) = (1-\gamma)$, the same procedure for phase ϕ results in

$$-\frac{\partial \gamma}{\partial t} + \nabla\!\bullet\left(\left(1-\gamma\right)\mathbf{U}_m\right) = \nabla\!\bullet\left(\frac{\gamma\left(1-\gamma\right)\,\overline{\rho}^{\varphi}}{\rho}\mathbf{U}_r\right). \tag{3.88}$$

Summing up the interfacial transport equations for both phases φ and ϕ, finally yields

$$\begin{aligned} &\nabla\!\bullet\mathbf{U}_m = \nabla\!\bullet\left(\gamma\left(1-\gamma\right)\frac{\overline{\rho}^{\varphi} - \overline{\rho}^{\phi}}{\rho}\mathbf{U}_r\right) \\ \Leftrightarrow &\nabla\!\bullet\mathbf{U} = 0, \qquad \text{with} \qquad \mathbf{U} \equiv \alpha_\varphi\,\overline{\mathbf{U}}^{\varphi} + \alpha_\phi\,\overline{\mathbf{U}}^{\phi} = \gamma\mathbf{U}_\gamma + (1-\gamma)\mathbf{U}_{1-\gamma}. \end{aligned} \tag{3.89}$$

As can be seen, the center-of-mass velocity field $\mathbf{U}_m$ is only solenoidal if the phase densities are equal, i.e., $\overline{\rho}^{\varphi} = \overline{\rho}^{\phi}$, or the relative velocity vanishes, whereas the *volumetric mixture velocity* field $\mathbf{U}$ is always found to be solenoidal (for constant phase densities). Moreover, if we multiply the conditional volume-averaged continuity equations 2.84 for both phases φ and ϕ by their respective phase density and subsequently sum up, this results in the *mixture continuity equation*, which takes the following form:

$$\frac{\partial \rho}{\partial t} + \nabla\!\bullet\left(\rho\mathbf{U}_m\right) = 0 \qquad \Leftrightarrow \qquad \frac{D\rho}{Dt} = \frac{\partial \rho}{\partial t} + \mathbf{U}_m\!\bullet\nabla\rho = -\rho\nabla\!\bullet\mathbf{U}_m. \tag{3.90}$$

Note, that this equation has the same form as for single-phase flows. However, in contrast to the single-phase case, the local velocity and density have been replaced by the center-of-mass velocity and the mixture density, respectively. Hence, the mixture continuity equation reveals that the mixture is compressible inside the interfacial transition region, since generally $\nabla\!\bullet\mathbf{U}_m \neq 0 \Rightarrow \frac{D\rho}{Dt} \neq 0$.

Finally, in order to arrive at the *mixture momentum equation*, the same procedure is to be adopted: the momentum equations for both phases φ and ϕ, i.e., equations 3.78 and 3.79, needs to be summed up.

$$\begin{aligned}&\frac{\partial\left(\alpha_\varphi\,\overline{\rho}^{\varphi}\,\overline{\mathbf{U}}^{\varphi}+\alpha_\phi\,\overline{\rho}^{\phi}\,\overline{\mathbf{U}}^{\phi}\right)}{\partial t}+\nabla\bullet\left(\alpha_\varphi\,\overline{\rho}^{\varphi}\,\overline{\mathbf{U}}^{\varphi}\,\overline{\mathbf{U}}^{\varphi}+\alpha_\phi\,\overline{\rho}^{\phi}\,\overline{\mathbf{U}}^{\phi}\,\overline{\mathbf{U}}^{\phi}\right)\\&=-\left(\alpha_\varphi\nabla\,\overline{p}^{\varphi}+\alpha_\phi\nabla\,\overline{p}^{\phi}\right)-\nabla\bullet\left(\alpha_\varphi\,\overline{\boldsymbol{\tau}}^{\varphi}+\alpha_\phi\,\overline{\boldsymbol{\tau}}^{\phi}\right)+\left(\alpha_\varphi\,\overline{\rho}^{\varphi}+\alpha_\phi\,\overline{\rho}^{\phi}\right)\mathbf{g}+\mathbf{M}_\sigma,\end{aligned}\tag{3.91}$$

since $\mathbf{M}_\varphi+\mathbf{M}_\phi=\mathbf{M}_\sigma$ according to equation 2.96.

The divergence term on the r.h.s. of equation 3.91 can be rewritten in terms of mixture quantities using equations 3.85 and 3.86:

$$\begin{aligned}\alpha_\varphi\,\overline{\rho}^{\varphi}\,\overline{\mathbf{U}}^{\varphi}\,\overline{\mathbf{U}}^{\varphi}+\alpha_\phi\,\overline{\rho}^{\phi}\,\overline{\mathbf{U}}^{\phi}\,\overline{\mathbf{U}}^{\phi}&=\alpha_\varphi\,\overline{\rho}^{\varphi}\mathbf{U}_m\mathbf{U}_m+2\frac{\alpha_\varphi\alpha_\phi\,\overline{\rho}^{\varphi}\,\overline{\rho}^{\phi}}{\rho}\mathbf{U}_m\mathbf{U}_r\\&\quad+\alpha_\varphi\,\overline{\rho}^{\varphi}\frac{\alpha_\phi\,\overline{\rho}^{\phi}}{\rho}\frac{\alpha_\phi\,\overline{\rho}^{\phi}}{\rho}\mathbf{U}_r\mathbf{U}_r+\alpha_\phi\,\overline{\rho}^{\phi}\mathbf{U}_m\mathbf{U}_m-2\frac{\alpha_\varphi\alpha_\phi\,\overline{\rho}^{\varphi}\,\overline{\rho}^{\phi}}{\rho}\mathbf{U}_m\mathbf{U}_r\\&\quad+\alpha_\phi\,\overline{\rho}^{\phi}\frac{\alpha_\varphi\,\overline{\rho}^{\varphi}}{\rho}\frac{\alpha_\varphi\,\overline{\rho}^{\varphi}}{\rho}\mathbf{U}_r\mathbf{U}_r\\&=\rho\mathbf{U}_m\mathbf{U}_m+\frac{\alpha_\varphi\alpha_\phi\,\overline{\rho}^{\varphi}\,\overline{\rho}^{\phi}}{\rho^2}\left(\alpha_\varphi\,\overline{\rho}^{\varphi}+\alpha_\phi\,\overline{\rho}^{\phi}\right)\mathbf{U}_r\mathbf{U}_r\\&=\rho\mathbf{U}_m\mathbf{U}_m+\underbrace{\frac{\alpha_\varphi\alpha_\phi\,\overline{\rho}^{\varphi}\,\overline{\rho}^{\phi}}{\rho}\mathbf{U}_r\mathbf{U}_r}_{\equiv\mathbf{D}_i\ \text{(momentum drift-flux term)}}.\end{aligned}\tag{3.92}$$

Moreover, it follows for the divergence term on the l.h.s. of equation 3.91 using equation 3.66:

$$\begin{aligned}\alpha_\varphi\,\overline{\boldsymbol{\tau}}^{\varphi}+\alpha_\phi\,\overline{\boldsymbol{\tau}}^{\phi}&=-\alpha_\varphi\,\overline{\mu}^{\varphi}\left(\nabla\,\overline{\mathbf{U}}^{\varphi}+\nabla\,\overline{\mathbf{U}}^{\varphi T}\right)-\alpha_\phi\,\overline{\mu}^{\phi}\left(\nabla\,\overline{\mathbf{U}}^{\phi}+\nabla\,\overline{\mathbf{U}}^{\phi T}\right)\\&=\underbrace{-\mu\left(\nabla\mathbf{U}_m+\nabla\mathbf{U}_m^T\right)}_{\equiv\boldsymbol{\tau}_m}\\&\quad\underbrace{-\left[\alpha_\varphi\,\overline{\mu}^{\varphi}\left(\nabla\frac{\alpha_\phi\,\overline{\rho}^{\phi}}{\rho}\mathbf{U}_r+\left(\nabla\frac{\alpha_\phi\,\overline{\rho}^{\phi}}{\rho}\mathbf{U}_r\right)^T\right)\right.}_{\equiv\boldsymbol{\tau}_i\ \text{(interfacial friction tensor)}}\\&\quad\underbrace{\left.-\alpha_\phi\,\overline{\mu}^{\phi}\left(\nabla\frac{\alpha_\varphi\,\overline{\rho}^{\varphi}}{\rho}\mathbf{U}_r+\left(\nabla\frac{\alpha_\varphi\,\overline{\rho}^{\varphi}}{\rho}\mathbf{U}_r\right)^T\right)\right]}_{\equiv\boldsymbol{\tau}_i\ \text{(interfacial friction tensor)}}.\end{aligned}\tag{3.93}$$

Finally, equation 3.91 takes the form:

$$\frac{\partial\rho\mathbf{U}_m}{\partial t}+\nabla\bullet\rho\mathbf{U}_m\mathbf{U}_m=-\nabla p-\nabla\bullet\left(\boldsymbol{\tau}_m+\boldsymbol{\tau}_i\right)-\nabla\bullet\left(\rho\mathbf{D}_i\right)+\rho\mathbf{g}+\mathbf{M}_\sigma.\tag{3.94}$$

It is important to note that these governing equations are not widely employed to study segregated flows, though the set of equations looks quite similar compared to the set underlying the well-known Volume-Of-Fluid Method, for instance. The central discrepancy, however, is found in the fact that the VoF model relies on *local* Navier-Stokes and continuity equations, and the *local* interface transport equation, while the above single-field equations have actually been volume-averaged. In consequence, additional terms are present, which needs to be discussed further:

momentum drift-flux term $\mathbf{D}_i$ as defined in equation 3.92 expresses the differences between the fully resolved momentum flux (involving contributions from the relative phase velocity) and the averaged momentum due to the center-of-mass velocity. Therefore, this term is called *momentum drift-flux term* (MDF term) henceforth.

interfacial friction tensor $\boldsymbol{\tau}_i$ as defined in equation 3.93 clearly arises from viscous forces and is non-zero only within the interfacial transition region. Hence, this term can be referred to as *interfacial friction tensor*.

Since both $\mathbf{D}_i$ and $\boldsymbol{\tau}_i$ depend on $\mathbf{U}_r$, further modeling is necessary, in order to close the mixture momentum equation. The easiest closure might be to assume $\mathbf{U}_r = \mathbf{0}$. This is commonly referred to as *homogeneous mixture assumption*, which is only found to be fulfilled under specific constraints: I.e., this is only valid for systems where the difference between the characteristic velocities of the two phases is small. For instance, in cases where the interfacial boundary layer is not sufficiently resolved, each phase velocity differs from the center-of-mass velocity in the interfacial transition region. In consequence, the spatial resolution, i.e., the characteristic length scale of the averaging volume (spatial filter width) must be carefully assessed before adopting the homogeneous mixture assumption. One has to bear in mind that the averaging/control volume has been implicitly defined through the adopted conditional volume-averaging procedure. Thus, underlying the homogeneous mixture assumption, inherently involves neglecting the scales beneath that of the control volume.

However, if the homogeneous mixture assumption is justified (e.g., for vanishingly small $\mathbf{U}_r$), the above single-field equations properly reduce to that of the local VoF method, as it is well-known and widely used in literature.

References

[1] D. A. Drew and S. L. Passman. *Theory of Multicomponent Fluids*. Number 135 in Applied mathematical sciences. Springer, New York, NY [u.a.], 1999. 23, 74, 84

[2] R. B. Bird, R. C. Armstrong, and O. Hassager. *Dynamics of Polymeric Liquids*. Wiley, New York, 1st & 38; 2nd ed edition, 1977. 27

[3] S. Bove. *Computational Fluid Dynamics of Gas-Liquid Flows including Bubble Population Balances*. PhD thesis, Aalborg University Esbjerg – Esbjerg Institute of Engineering, 2005. 28, 37, 38

[4] D. L. Marchisio and R. O. Fox, editors. *Multiphase Reacting Flows: Modelling and Simulation*. Number 492 in @CISM International Centre for Mechanical Sciences. CISM, Udine, Vienna, 2007. 28, 39

[5] H. A. Jakobsen. *Chemical Reactor Modeling*. Springer, Berlin, Heidelberg, 2008. 28, 37, 38

[6] H. G. Weller. The Development of a New Flame Area Combustion Model Using Conditional Averaging. Technical report, Thermo-Fluids Section Report TF 9307, Imperial College of Science, Technology and Medicine, 1993. 33, 44, 47, 50, 51

[7] H. G. Weller. Derivation, Modelling and Solution of the Conditionally Averaged Two-Phase Flow Equations. Technical report, OpenCFD Limited, 2005. 33, 44, 47, 50, 51

[8] M. Wörner. Volume-averaged Volume-Of-Fluid method. Private communication, September 2008. 34, 88

[9] D. Jamet. Diffuse Interface Models in Fluid Mechanics. GdR CNRS documentation, see http://pmc.polytechnique.fr/mp/GDR/docu/Jamet.pdf. 35

[10] G. H. Yeoh and J. Tu. *Computational Techniques for Multi-Phase Flows*. Butterworth-Heinemann, Oxford, 2010. 36

[11] D. A. Drew. Mathematical modeling of two-phase flow. *Annu. Rev. Fluid. Mech.*, 15(1):261–291, 1983. 36

[12] D. P. Hill. *The Computer Simulation of Dispersed Two-Phase Flows*. PhD thesis, Imperial College of Science, Technology & Medicine – Department of Mechanical Engineering, 1998. 37, 38, 51, 73

[13] A. Kaufmann. *Toward Eulerian-Eulerian Large-Eddy Simulation of Reactive Two-Phase Flows*. PhD thesis, Institut National Polytechnique de Toulouse, 2004. 39

[14] P. Sagaut and C. Meneveau. *Large Eddy Simulation for Incompressible Flows*. Scientific computation. Springer, Berlin [u.a.], 3. ed. edition, 2006. 39

[15] R. Nagaosa. Direct numerical simulation of vortex structures and turbulent scalar transfer across a free surface in a fully developed turbulence. *Phys. Fluids*, 11(6):1581, 1999. 39

[16] L. Shen and D. K. P. Yue. Large-Eddy Simulation of free-surface turbulence. *J. Fluid Mech.*, 440:75–116, 2001. 39

[17] T. Kawamura, S. Mayer, A. Garapon, and L. Sorensen. Large eddy simulation of a flow past a free surface piercing circular cylinder. *J. Fluid Eng.*, 124(1):91–101, March 2002. 39

[18] A. Prosperetti and G. Tryggvason. *Computational Methods for Multiphase Flow*. Cambridge University Press, 1 edition, May 2007. 40

[19] R. I. Nigmatulin. Spatial averaging in the mechanics of heterogeneous and dispersed systems. *Int. J. Multiphase Flow*, 5(5):353–385, 1979. 40

[20] A. Patrascioiu. The ergodic-hypothesis, a complicated problem in mathematics and physics. *Los Alamos Science*, 15:263, 1987. 42

[21] C. Dopazo. On conditional averages for intermittent turbulent flow. *J. Fluid Mech.*, 81(3):433–438, 1977. 42, 50

[22] A. Toutant. *Physical Modelling of Interactions between Interfaces and Turbulence*. PhD thesis, CEA-Grenoble and IMF-Toulouse, 2006. 60

[23] A. Toutant, E. Labourasse, O. Lebaigue, and O. Simonin. DNS of the interaction between a deformable buoyant bubble and a spatially decaying turbulence: A priori tests for LES two-phase flow modelling. *Comput. Fluids*, 37(7):877–886, 2008. 60

[24] A. Toutant, M. Chandesris, D. Jamet, and O. Lebaigue. Jump conditions for filtered quantities at an under-resolved discontinuous interface. Part 1: Theoretical development. *Int. J. Multiphase Flow*, 35(12):1100–1118, 2009. 60

[25] A. Toutant, M. Chandesris, D. Jamet, and O. Lebaigue. Jump conditions for filtered quantities at an under-resolved discontinuous interface. Part 2: A priori tests. *Int. J. Multiphase Flow*, 35(12):1119–1129, 2009. 60

[26] M. Ishii. Two-fluid model for two-phase flow. *Multiphase. Sci. Tech.*, 5(1-4):1–63, 1990. 64

[27] J. H. Stuhmiller. The influence of interfacial pressure forces on the character of two-phase flow model equations. *Int. J. Multiphase Flow*, 3(6):551–560, 1977. 73

[28] D. Bestion. The physical closure laws in the CATHARE code. *Nucl. Eng. Des.*, 124(3):229–245, 1990. 74

[29] S. T. Munkejord. *Analysis of the Two-Fluid Model and the Drift-Flux Model for Numerical Calculation of Two-Phase Flow*. PhD thesis, Norwegian University of Science and Technology, 2005. 74

[30] F. J. Moraga, A. E. Larreteguy, D. A. Drew, and R. T. Lahey. Assessment of turbulent dispersion models for bubbly flows in the low Stokes number limit. *Int. J. Multiphase Flow*, 29(4):655–673, 2003. 78

[31] R. T. Lahey Jr. and D. A. Lahey. An analysis of two-phase flow and heat transfer using a multidimensional, multi-field, two-fluid computational fluid dynamics (CFD) model. In *Japan/US Sem. Two-Phase Flow Dynamics, Santa Barbara, Kalifornien*, 2000. 78

[32] D. A. Drew and S. L. Passman. *Theory of Multicomponent Fluids*. Springer, New York, 1998. 78

[33] O. Kramer. Forces Acting on Bubbles. Technical report, University of Twente, Faculty of Chemical Technology, 2000. 78, 79

[34] A. Sokolichin, G. Eigenberger, and A. Lapin. Simulation of buoyancy driven bubbly flow: Established simplifications and open questions. *AIChE J.*, 50:24–45, 2004. 79

[35] S. P. Antal, R. T. Lahey Jr., and J. E. Flaherty. Analysis of phase distribution in fully developd laminar bubbly two-phase flow. *Int. J. Multiphase Flow*, 17:635–652, 1991. 79

[36] T. Frank. A Review on Advanced Eulerian Multiphase Flow Modelling for Gas-Liquid Flows. Technical report, AEA Technology GmbH / ANSYS CFX, 2003. 79

[37] J. M. Donbar, J. F. Driscoll, and C. D. Carter. Reaction zone structure in turbulent nonpremixed jet flames. *Combustion and Flame*, 122:1–19, 2000. 80

[38] Y. Sun and C. Beckermann. Diffuse interface modeling of two-phase flows based on averaging: Mass and momentum equations. *Physica D: Nonlinear Phenomena*, 198(3-4):281–308, 2004. 84, 88

[39] M. Wörner, W. Sabisch, G. Grötzbach, and D. G. Cacuci. Volume-averaged conservation equations for volume-of-fluid interface tracking. In *4th Int. Conf. Multiphase Flow, ICMF 2001*, New Orleans, Louisiana, U.S.A, May 27 – June 1 2001. E.E. Michaelides. CD-ROM. 88

[40] W. Sabisch. *Dreidimensionale Numerische Simulation der Dynamik von Aufsteigenden Einzelblasen und Blasenschwärmen mit einer Volume-of-Fluid-Methode*. PhD thesis, Universität Karlsruhe, 2000. 88

[41] A. A. Onea. *Numerical Simulation of Mass Transfer with and without First Order Chemical Reaction in Two-Fluid Flows*. PhD thesis, Universität Karlsruhe, 2006. 88

[42] S. M. Mitran. Closure Models for the Computation of Dilute Bubbly Flows. Forschungszentrum Karlsruhe, Wissenschaftliche Berichte, FZKA 6357, 2000. pp. 1-121. 88

4

Numerical Method

If you think dogs can't count, try putting three dog biscuits in your pocket and then giving Fido only two of them.

Phil Pastoret

Numerical quantities focus on expected *values...*

John Tukey

Abstract

As set out in chapters 2 and 3, the mathematical model to describe two-phase flows takes the form of a set of partial differential equations along with corresponding boundary and initial conditions. These fully describe a two-phase problem; however, the mathematical model can not be solved analytically. Thus, an approximative (numerical) solution procedure is needed.

The present chapter deals with the numerical solution methodology which transfers the continuous physical domain into a discretized computational domain enabling to numerically solve for a system of algebraic equations instead of partial differential equations.

4.1. Introduction

The basic premise of an approximative numerical method is that the solution is sought for the discretized computational domain, which comprises a finite number of computational nodes in space and time. In general, the aim is to provide an adequate representation of the solution for the continuous physical domain. This concerns both *accuracy* and correctness (*conservation, continuity, boundedness and realisability*) of the approximative numerical solution. Moreover, for *consistency*, in increasing the number of computational nodes (up to infinity) the approximative numerical solution must approach the exact one – and finally exactly meet it.

The numerical solution methodology can be categorized into three consecutive steps:

1.) Domain Discretization

The domain discretization encompasses the sub-division of the continuous physical domain into sub-entities both in space (spatial discretization) and in time (temporal discretization). Consequently, the spatial sub-entities are referred to as control volumes (CV, or simply cell), the collection of which defines and bounds the spatial solution domain. Similarly, the temporal sub-entities are referred to as time steps (or time intervals) henceforth.

2.) Equation Discretization

Having at hand a discretized solution domain, the governing transport equations, stating the mathematical model, are to be discretized as well. They are first integrated over each control volume. Then, the resulting volume integrals are translated into surface integrals applying Gauss' theorem. By use of interpolation (differencing schemes) the values of dependent variables on the CV surfaces are rewritten in terms of cell-centered values. These values are needed for the evaluation of the surface integrals and eventually enable to assemble a set of algebraic equations for the dependent variables in each cell written in terms of neighboring cell values. Finally, the set of algebraic equations for a particular dependent variable under consideration is ready for its numerical evaluation.

3.) Solution Method and Algorithm

The solution procedure generally needs to be seen on two distinct levels in a bottom-up approach:

3.1.) the core-level, covering the solution methods for solving a system of algebraic equations

3.2.) the top-level, covering the steps of the solution algorithm, which handles multiple (possibly coupled) discretized governing equations. This step must further ensure the accuracy and correctness of the result – as already requested before.

Each of the above levels exhibits two solution strategies:

ad 3.1) On the core-level, solution methods might be grouped according to their use of either direct solvers or iterative solvers.

ad 3.2) On the top-level, solution algorithms might be categorized into simultaneous/block or segregated top-level approaches.

For efficiency reasons, solely iterative solvers and the segregated approach shall be considered in this study for solving the system of algebraic equations (core-level) and the overall set of coupled discretized governing equations (top-level), respectively.

As it is set out below, the current implementation and numerical simulations were accomplished by use of the Open Source CFD toolbox OpenFOAM®. This is a versatile C++ library suitable for all kinds of continuum problems [1,2]. OpenFOAM is based on an unstructured mesh formulation with a collocated cell-centered variable arrangement featuring unstructured boundary-fitted meshes (including topological mesh changes) for arbitrary complex geometries. Along with its spatial and temporal discretization being of second order accuracy, OpenFOAM enables to examine continuum problems in a generalized and flexible manner.

4.2. Domain Discretization

4.2.1. Spatial Discretization

Figure 4.1 depicts a typical *control volume* (CV) stating the sub-entity evolving from the sub-division of the spatial solution domain (spatial discretization). Here, the CV represents a computational cell, which is allowed to possess an arbitrary shape, i.e., a convex polyhedron. The CV's centroid P represents a computational node and is located in $\mathbf{x}_P$, such that $\int_{V_P} (\mathbf{x} - \mathbf{x}_P)\, dV \stackrel{!}{=} 0$, where V_P denotes the cell's volume.

The CV is bounded by a set of *faces* f that are likewise allowed to be of arbitrary shape, i.e., convex polygons, the geometrical centroid of which is located in $\mathbf{x}_f$, being defined as $\int_f d\mathbf{S}_f\, (\mathbf{x} - \mathbf{x}_f) \stackrel{!}{=} 0$.

A representative (again arbitrary) CV, adjacent to P, shall be denoted as N with the *delta vector* $\mathbf{d}$ connecting the centroids of P and N, $\mathbf{d} \equiv \mathbf{x}_P - \mathbf{x}_N = \overline{PN}$.

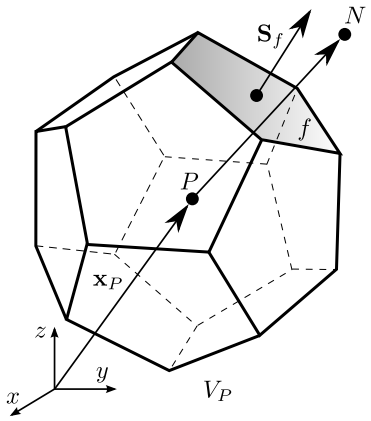

Figure 4.1: Control volume.

Furthermore, in this generalized nomenclature, $\mathbf{S}_f$ represents the outward pointing *face area vector* normal to the face f between P and N. The magnitude of the face area vector is equal to the face area itself, $S_f \equiv |\mathbf{S}_f|$. Henceforth the case $\mathbf{d} \parallel \mathbf{S}_f$ shall be referred to as orthogonal, whereas $\mathbf{d} \nparallel \mathbf{S}_f$ is denoted as non-orthogonal.

4.2.2. Temporal Discretion

For transient problems temporal discretization is to be considered. This involves subdividing the temporal solution domain into *time steps* covering certain time intervals of a specific size Δt – which itself might be uniform or non-uniform (adaptive time-stepping).

4.3. Equation Discretization

Having discretized the solution domain both in space and in time, the governing transport equations, i.e., the mathematical model (in the form of a system of partial differential equations), needs to be discretized correspondingly.

In order to examine the details of the discretization practice in a generic manner it is rational to reconsider governing equations in form of the generic transport equation for an arbitrary general flow quantity ϕ – as already introduced in chapter 2 and repeated here for the sake of convenience:

$$\frac{\partial}{\partial t}(\rho\phi) + \nabla\bullet(\rho\phi\mathbf{U}) - \nabla\bullet(\Gamma_{\phi,d}\nabla\phi) - S_\phi(\phi) = 0. \tag{4.1}$$

Note however, that in contrast to chapter 2, these equations expediently refer to the volume-averaged, i.e., the spatially (box-) filtered, state – as it has been the result

of chapter 3 after conditional volume-averaging and closure modeling. However, for readability the overbar-notation indicating the volume-average shall be dropped in the remainder. Hence, it is remarkable that the generic transport equation 4.1 still comprises the same structure, that we have derived for the local-instantaneous case for single-phase flows. This in turn renders Eulerian two-phase flow models suitable to be treated with the same numerical solvers that were originally developed for single-phase flows. However, compared to single-phase flows, different constraints have to be considered for two-phase flow models in order to ensure consistency – see corollary note 4.1.

Corollary Note 4.1

The requirement of consistency for the numerical solution methodology – that is the numerical solution must approach the physical one when decreasing the size of the underlying control volumes (increasing their number up to infinity) – needs to be reconsidered: a meaningful evaluation of the closure terms relies upon the volume-averaged phase-indicator function being interpretable as volumetric phase fraction. Thus, the size of the averaging volume, i.e., the spatial filter width, needs to be identical to the size of the control volume. Moreover, as the form of the closure relies upon an appropriate choice of the size of the control volume – dependent on the concrete two-phase flow scale to be captured – it is required that the control volume size (cell size) is not freely reducible, but has a lower limit constrained by the interfacial structure under consideration and the closure model, the validity of which needs to be preserved. This in consequence states the pivotal difference compared to the single-phase case, that one has to bear in mind when examining the equation discretization for a system of volume-averaged governing equations corresponding to a two-phase flow: the spatial resolution is not freely reducible.

In the framework of the FVM, equation 4.1 has to be integrated over the control volume yielding its integral form:

$$\begin{aligned} &\int_{V_P} \frac{\partial}{\partial t}\left(\rho\phi\right)\, dV + \int_{V_P} \nabla\bullet\left(\rho\phi\mathbf{U}\right)\, dV - \int_{V_P} \nabla\bullet\left(\Gamma_{\phi,d}\nabla\phi\right)\, dV = \int_{V_P} S_\phi(\phi)\, dV \\ \Leftrightarrow\; &\int_{V_P} \frac{\partial}{\partial t}\left(\rho\phi\right)\, dV + \oint_S \rho\phi\left(\mathbf{n}\bullet\mathbf{U}\right)\, dS - \oint_S \Gamma_{\phi,d}\left(\mathbf{n}\bullet\nabla\phi\right)\, dS = \int_{V_P} S_\phi(\phi)\, dV \end{aligned} \tag{4.2}$$

As equations 4.1 and 4.2 involve a second order derivative of ϕ in space that is the diffusion term, these equations are of second order. For accuracy and consistency the underlying discretization method must be of the same or higher order than the equation being discretized. This requirement is fulfilled when presuming a linear

variation of $\phi(\mathbf{x}, t)$ both in space (around P) and in time (around t), which is accomplished via a Taylor Series expansion according to:

$$\phi(\mathbf{x}) = \phi_P + (\mathbf{x} - \mathbf{x}_P) \bullet (\nabla\phi)_P + \mathcal{O}\left(|\mathbf{x} - \mathbf{x}_P|^2\right) \qquad \text{and} \tag{4.3}$$

$$\phi(t + \Delta t) = \phi^t + \Delta t \left(\frac{\partial\phi}{\partial t}\right)^t + \mathcal{O}\left(\Delta t^2\right), \tag{4.4}$$

where $\phi_P = \phi(\mathbf{x}_P)$ and $\phi^t = \phi(t)$. Note that $\mathcal{O}(|\mathbf{x} - \mathbf{x}_P|^2)$ and $\mathcal{O}\left(\Delta t^2\right)$ denote the truncation terms indicating the second order accuracy. Henceforth these truncation terms are dropped for readability.

As set out in equation 4.2, each term in the integral form of the generic transport equation, upon which the finite volume discretization is based, contains either volume or surface integrals. These can be evaluated in a second order manner by substitution of the prescribed variation of ϕ in space (equation 4.3):

- volume integral

$$\begin{aligned}\int_{V_P} \phi \, dV &= \int_{V_P} \left[\phi_P + (\mathbf{x} - \mathbf{x}_P) \bullet (\nabla\phi)_P\right] dV \\ &= \phi_P \int_{V_P} dV + (\nabla\phi)_P \bullet \int_{V_P} (\mathbf{x} - \mathbf{x}_P) \, dV = \phi_P V_P.\end{aligned} \tag{4.5}$$

- surface integral

$$\begin{aligned}\oint_S \mathbf{n}\phi \, dS &= \sum_f \int_{S_f} \mathbf{n} \left(\phi(\mathbf{x})\right)_f \, dS_f \\ &= \sum_f \int_{S_f} \mathbf{n} \left[\phi_f + (\mathbf{x} - \mathbf{x}_f) \bullet (\nabla\phi)_f\right] dS_f = \sum_f \mathbf{S}_f \phi_f.\end{aligned} \tag{4.6}$$

Moreover, for the approximative evaluation of the volume integrals of gradient and divergence terms, we might rewrite Gauss' theorem in its discretized form (compare to equations 2.3 and 2.4):

$$\int_{V_P} \nabla \bullet \mathbf{a} \, dV = \int_S d\mathbf{S} \bullet \mathbf{a} = \sum_f \int_{S_f} d\mathbf{S} \bullet \mathbf{a} = \sum_f \mathbf{S}_f \bullet \mathbf{a}_f \tag{4.7}$$

$$\int_{V_P} \nabla \mathbf{a} \, dV = \int_S d\mathbf{S}\mathbf{a} = \sum_f \int_{S_f} d\mathbf{S}\mathbf{a} = \sum_f \mathbf{S}_f \mathbf{a}_f, \tag{4.8}$$

which now enables to consider the discretization of equation 4.2 on a term-by-term basis. Obviously, the solution procedure basically might be broken down to the evaluation of the face values of ϕ.

However, in the context of Eulerian two-phase flow models being the central subject of this thesis, it has to be emphasized that any discretization practice needs to meet

prerequisites with respect to *phase boundedness*: small errors in the volume fraction will correspond to large ones in mass fraction due to a typically high density ratio. Hence, in the following, comments shall be provided on this central issue along with the description of the discretization practice of each term in equation 4.2.

4.3.1. Convection Term

The finite volume discretization of the convection term is accomplished by first converting it into a sum over the faces by use of Gauss' theorem according to equation 4.7 and then approximating it numerically as

$$\begin{aligned}\int_{V_P} \nabla\bullet\left(\rho\phi\mathbf{U}\right)\,dV &= \sum_f \mathbf{S}_f\bullet\left(\rho\phi\mathbf{U}\right)_f \\ &\approx \sum_f \mathbf{S}_f\bullet\left(\rho\mathbf{U}\right)_f\,\phi_f = \sum_f F\,\phi_f,\end{aligned} \tag{4.9}$$

where $F \equiv \mathbf{S}_f\bullet\left(\rho\mathbf{U}\right)_f$ shall be denoted as *face mass flux* henceforth. The face mass flux needs to be provided directly from the algorithm (section 4.5) to ensure continuity for every CV, i.e., it is for incompressible flows

$$\int_{V_P} \nabla\bullet\left(\rho\mathbf{U}\right)\,dV = \sum_f \mathbf{S}_f\bullet\left(\rho\mathbf{U}\right)_f = \sum_f F \stackrel{!}{=} 0. \tag{4.10}$$

The cell face average values ϕ_f are approximated from the cell center values using an appropriate face interpolation scheme or *differencing scheme*.

Differencing Schemes

Generally, the choice of differencing schemes is a matter of boundedness and accuracy the scheme needs to ensure for the solution, and further a matter of stability and computational efficiency the scheme needs to guarantee for the overall solution procedure. Both aspects are discussed thoroughly by Jasak in [3].

In what follows a brief overview is given over both basic (central and upwind) and more sophisticated (blending or switching) differencing schemes.

- Central Differencing (CD) – linear face interpolation

  The face-centered value is found by linearly interpolating between the cell-centered values at P and N – as illustrated in figure 4.2:

  $$\phi_f = f_x\phi_P + \left(1 - f_x\right)\phi_N, \tag{4.11}$$

  where the linear interpolation factor f_x is defined as

  $$f_x \equiv \frac{|\mathbf{x}_f - \mathbf{x}_N|}{|\mathbf{d}|} = \frac{\overline{fN}}{\overline{PN}}. \tag{4.12}$$

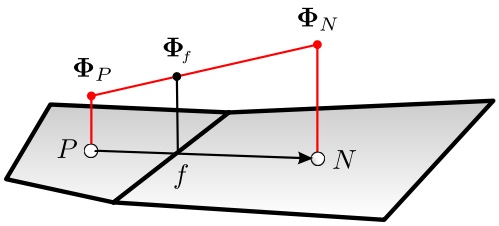

Figure 4.2: Central differencing.

While central differencing is second order accurate, it does not ensure boundedness – especially being a problem with increasing convection dominance causing non-physical oscillation of the solution.

- Upwind Differencing (UD) – flux-direction dependent face interpolation
  A simple remedy for the aforementioned shortcoming of the CD scheme might comprise of taking into account the direction of the face flux. In the upwind differencing scheme the face value is determined from the cell value in upstream flow direction:

$$\begin{aligned}\phi_f &= \max(F,0)\,\phi_P + \min(F,0)\,\phi_N \\ &= \begin{cases}\phi_P & \text{for } F \geq 0 \\ \phi_N & \text{for } F < 0\end{cases}.\end{aligned} \tag{4.13}$$

  Upwind differencing ensures unconditional boundedness at the cost of numerical diffusion, i.e., the leading term of the truncation error is a function of $(\mathbf{x}_f - \mathbf{x}_P) \bullet (\nabla\phi)_P$ – a diffusion-like term.

- Switching/Blending Schemes – superposition of UD and CD
  These schemes attempt to preserve boundedness while maintaining a reasonable accuracy. This is accomplished by superposing CD and UD as

$$\phi_f = \phi_{f(F,UD)} + \gamma\left(\phi_{f(CD)} - \phi_{f(F,UD)}\right), \tag{4.14}$$

  where the switching/blending criterion is chosen $0 \leq \gamma \leq 1$. $\gamma = 1$ leads to a CD and $\gamma = 0$ to a full upwind discretization practice. There are different evaluation procedures for γ dependent on distinct boundedness criteria, e.g., the cell Peclet number $\gamma(Pe_c)$ or the local shape of the solution $\gamma(\phi)$. The values of γ are either evaluated for all faces of the mesh as a constant or on a face-by-face basis. Nowadays one of the most sophisticated approaches appears

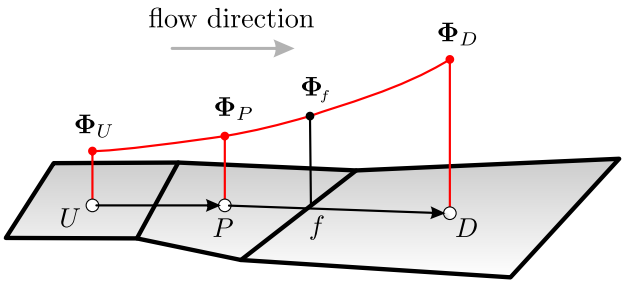

Figure 4.3: Switching/Blending differencing schemes – Variation of ϕ around the face f.

to be based on the *Normalised Variable Approach* (NVD) of Leonard [4] and Gaskell et al. [5] where normalized variables are defined as

$$\widetilde{\phi_P} = \frac{\phi_P - \phi_U}{\phi_D - \phi_U} \qquad \text{and} \qquad \widetilde{\phi_f} = \frac{\phi_f - \phi_U}{\phi_D - \phi_U}, \tag{4.15}$$

with the subscripts U and D denoting the cells upwind and downwind to P, respectively – dependent on the flow direction as depicted in figure 4.3.

In order to avoid unphysical oscillations local boundedness is required:

$$\phi_U \overset{!}{\leq} \phi_P \overset{!}{\leq} \phi_D \qquad \text{or vice versa} \qquad \phi_U \overset{!}{\geq} \phi_P \overset{!}{\geq} \phi_D, \tag{4.16}$$

or as *convection boundedness criterion* (CBC) in terms of $\widetilde{\phi_P}$:

$$0 \overset{!}{\leq} \widetilde{\phi_P} \overset{!}{\leq} 1. \tag{4.17}$$

It is shown in [3] that the boundedness criterion according to equation 4.17 can be illustrated within the so-called NVD diagram as given in figure 4.4 depicting $\widetilde{\phi_f}$ as a function of $\widetilde{\phi_P}$:

- The convection boundedness criterion $0 \leq \widetilde{\phi_P} \leq 1$ is fulfilled within the shaded area, bounded by $\widetilde{\phi_f} = \widetilde{\phi_P}$ as lower limit and $\widetilde{\phi_f} = 1$ as upper one.
- For unboundedness ($\widetilde{\phi_P} < 0$ or $\widetilde{\phi_P} > 1$) it is $\widetilde{\phi_f} = \widetilde{\phi_P}$.

As can be seen from the NVD diagram, the choice of the discretization practice to ensure boundedness is more or less free for $0 \leq \widetilde{\phi_P} \leq 1$.

Note that for the purpose of applicability to arbitrary meshes $\widetilde{\phi_P}$ has to be modified according to Jasak [3]

$$\widetilde{\phi_P} = 1 - \frac{(\nabla\phi)_f \bullet \mathbf{d}}{2\,(\nabla\phi)_P \bullet \mathbf{d}}, \tag{4.18}$$

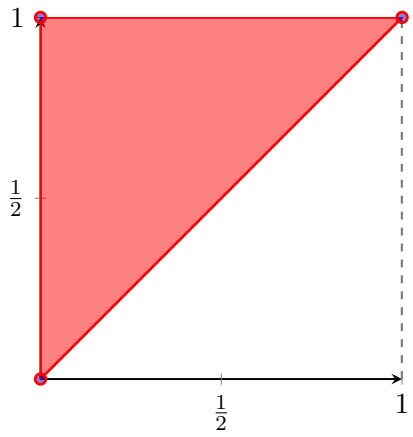

Figure 4.4: Convection boundedness criterion in the NVD diagram.

where P must be chosen upwind to the face f; and $\mathbf{d} = \mathbf{x}_D - \mathbf{x}_P$.

Depending on the normalized variable $\widetilde{\phi_P}$ the blending factor γ might now be evaluated, e.g., using the auxiliary β_m according to the *Gamma scheme* [6]:

$$\gamma\left(\widetilde{\phi_P}\right) = \begin{cases} 0 & \text{for } \widetilde{\phi_P} \leq 0 \\ \widetilde{\phi_P}/\beta_m & \text{for } 0 < \widetilde{\phi_P} < \beta_m \\ 1 & \text{for } \beta_m \leq \widetilde{\phi_P} < 1 \\ 0 & \text{for } \widetilde{\phi_P} \geq 1 \end{cases}, \tag{4.19}$$

or equivalent in terms of $\widetilde{\phi_f}$ being calculated from $\widetilde{\phi_P}$:

$$\widetilde{\phi_f}\left(\widetilde{\phi_P}\right) = \begin{cases} \widetilde{\phi_P} & \text{for } \widetilde{\phi_P} \leq 0 \\ -\frac{\widetilde{\phi_P}^2}{2\beta_m} + \left(1 + \frac{1}{2\beta_m}\right)\widetilde{\phi_P} & \text{for } 0 < \widetilde{\phi_P} < \beta_m \\ 1/2 + 1/2\widetilde{\phi_P} & \text{for } \beta_m \leq \widetilde{\phi_P} < 1 \\ \widetilde{\phi_P} & \text{for } \widetilde{\phi_P} \geq 1 \end{cases}. \tag{4.20}$$

Thus the NVD diagram of the Gamma differencing scheme results as shown in figure 4.5a.

A variant of the Gamma scheme being utilised in this work along with Eulerian interface capturing, is the inter-Gamma scheme [7] as set out below.

$$\gamma\left(\widetilde{\phi_P}\right) = \begin{cases} 0 & \text{for } \widetilde{\phi_P} \leq 0 \\ 4\widetilde{\phi_P} & \text{for } 0 < \widetilde{\phi_P} < 1/2 \\ 2 & \text{for } 1/2 \leq \widetilde{\phi_P} < 1 \\ 0 & \text{for } \widetilde{\phi_P} \geq 1 \end{cases}, \tag{4.21}$$

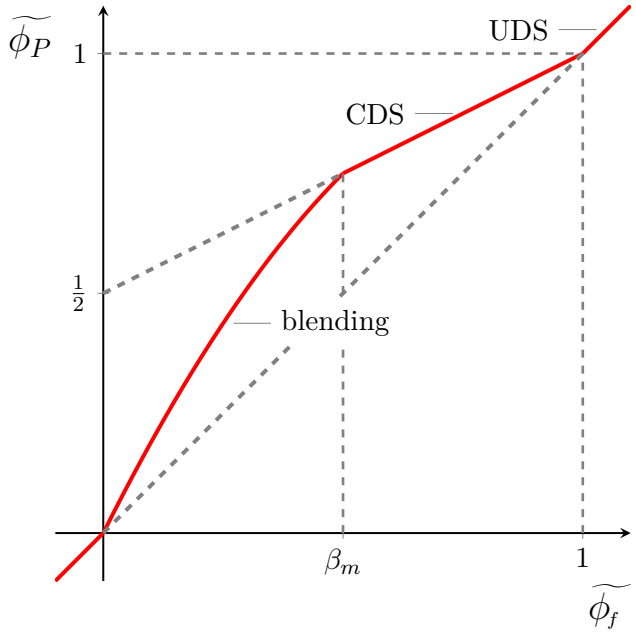

(a) Gamma scheme, [6].

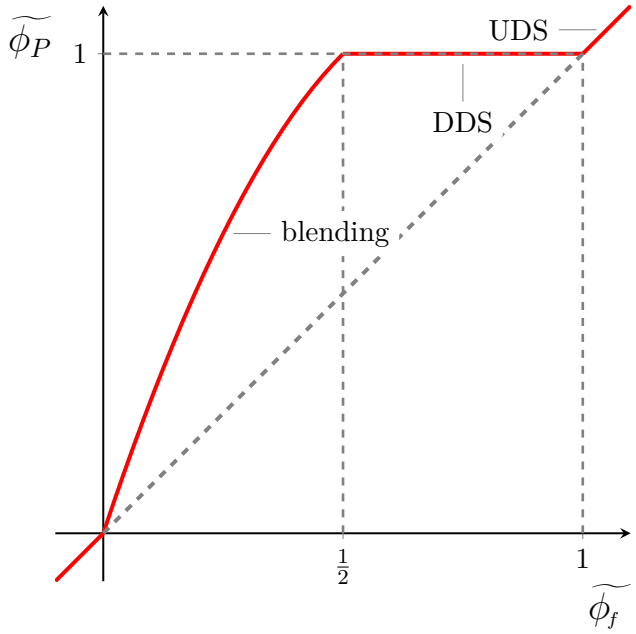

(b) inter-Gamma scheme, [7].

Figure 4.5: Family of Gamma differencing schemes in the NVD diagram.

or in terms of $\widetilde{\phi_f}$

$$\widetilde{\phi_f}\left(\widetilde{\phi_P}\right) = \begin{cases} \widetilde{\phi_P} & \text{for } \widetilde{\phi_P} \leq 0 \\ -2\widetilde{\phi_P}^2 + 3\widetilde{\phi_P} & \text{for } 0 < \widetilde{\phi_P} < 1/2 \\ 1 & \text{for } 1/2 \leq \widetilde{\phi_P} < 1 \\ \widetilde{\phi_P} & \text{for } \widetilde{\phi_P} \geq 1 \end{cases}, \tag{4.22}$$

resulting in the representation of the inter-Gamma scheme in the NVD diagram as depicted in figure 4.5b.

As can be seen, the objective when developing the inter-Gamma scheme certainly was to create a smooth transition from upwind (UDS) to downwind differencing (DDS) for $0 < \widetilde{\phi_P} < 1/2$ and to use downwind differencing for $1/2 \leq \widetilde{\phi_P} < 1$. Otherwise, i.e., for $\widetilde{\phi_P} \geq 1$ and $\widetilde{\phi_P} \leq 0$, upwind differencing is utilized in order to preserve boundedness. In doing so, the inter-Gamma scheme effectively introduces an anti-diffusion term by downwind differencing which counteracts numerical diffusion due to upwind differencing. Thus this discretization practice does not overly 'diffuse' the interface (maintaining the interface profile as sharp as possible), while preserving the boundedness of the transport quantity (volumetric phase fraction between zero and unity). However, due to this compressive characteristics (and for time accuracy) a Courant number limit has to be taken into account, $1/5 \leq Co_{\max} \leq 1/3$.

4.3.2. Diffusion Term

The diffusion term can be discretized in the same manner as before using Gauss' theorem. This yields

$$\int_{V_P} \nabla\bullet\left(\Gamma_{\phi,d}\nabla\phi\right)\, dV = \sum_f \mathbf{S}_f\bullet\left(\Gamma_{\phi,d}\nabla\phi\right)_f \approx \sum_f \left(\Gamma_{\phi,d}\right)_f \mathbf{S}_f\bullet\left(\nabla\phi\right)_f, \tag{4.23}$$

where both $\left(\Gamma_{\phi,d}\right)_f$ and $\mathbf{S}_f\bullet\left(\nabla\phi\right)_f$ needs further examination:

1.) face interpolation of $\Gamma_{\phi,d}$

Face interpolation of $\Gamma_{\phi,d}$ can either be done as set out by equation 4.11 that is by use of linear interpolation $\left(\Gamma_{\phi,d}\right)_{f(CD)}$ (single-phase flow) or by taking into account the interface / cell-face orientation (two-phase flow), since $\Gamma_{\phi,d}$ usually takes different values within the interiors of different phases.

Following Patankar [8] and Kothe [9] the latter is accomplished appropriately as

$$\left(\Gamma_{\phi,d}\right)_f = \eta_f \left(\Gamma_{\phi,d}\right)_f^p + \left(1-\eta_f\right)\left(\Gamma_{\phi,d}\right)_f^s, \tag{4.24}$$

where the superscripts p and s denote the parallel (harmonic) and the serial (geometric) average, respectively. η_f represents an interpolation factor accounting for an appropriate weighting of geometric and harmonic contributions to $(\Gamma_{\phi,d})_f$ according to the relative interface / cell-face orientation:

$$\eta_f \equiv \left| \left(\frac{(\nabla\alpha_\varphi)_f}{|(\nabla\alpha_\varphi)_f|} \right) \bullet \frac{\mathbf{S}_f}{|\mathbf{S}_f|} \right|, \tag{4.25}$$

which approaches zero or unity for extreme orientations, that are the face-interpolated mean interface unit normal $(\nabla\alpha_\varphi)_f/|(\nabla\alpha_\varphi)_f|$ being perpendicular or parallel to the unit cell face normal $\mathbf{S}_f/|\mathbf{S}_f|$. In between these extremes η_f is varying smoothly between zero and unity.

2.) approximation of the face normal gradient $\mathbf{S}_f \bullet (\nabla\phi)_f$

The evaluation of the face normal gradient $\mathbf{S}_f \bullet (\nabla\phi)_f$ for *orthogonal meshes*, that is for $\mathbf{S}_f \parallel \mathbf{d}$, reads

$$\mathbf{S}_f \bullet (\nabla\phi)_f = |\mathbf{S}_f| \frac{\phi_N - \phi_P}{|\mathbf{d}|}, \tag{4.26}$$

representing the component of the gradient in the direction of $\mathbf{d}$. Furthermore, note the compact computational molecule compared to simply interpolating the cell-centered gradients linearly:

$$\mathbf{S}_f \bullet (\nabla\phi)_f = \mathbf{S}_f \bullet \left[f_x \, (\nabla\phi)_P + (1 - f_x) \, (\nabla\phi)_N \right], \tag{4.27}$$

$$\text{where} \qquad (\nabla\phi)_P = \frac{1}{V_P} \sum_f \mathbf{S}_f \phi_f.$$

However, for *non-orthogonal meshes*, i.e., for $\mathbf{S}_f \nparallel \mathbf{d}$ – which states the general case in CFD as shown in figure 4.6, for instance – the compact evaluation according to equation 4.26 is no longer valid. Hence to make use of the higher accuracy the following split renders necessary:

$$\mathbf{S}_f \bullet (\nabla\phi)_f = |\mathbf{S_d}| \frac{\phi_N - \phi_P}{|\mathbf{d}|} + \mathbf{S_\Delta} \bullet \left(f_x \, (\nabla\phi)_P + (1 - f_x) \, (\nabla\phi)_N \right), \tag{4.28}$$

where $\mathbf{S_d}$ is chosen parallel to $\mathbf{d}$ allowing the use of equation 4.26 for a more accurate evaluation of the orthogonal contribution to the face normal gradient $\mathbf{S}_f \bullet (\nabla\phi)_f$, while limiting the less accurate method according to equation 4.27 to the evaluation of the non-orthogonal contribution. For consistency, $\mathbf{S_\Delta}$ must satisfy:

$$\mathbf{S}_f = \mathbf{S_d} + \mathbf{S_\Delta}. \tag{4.29}$$

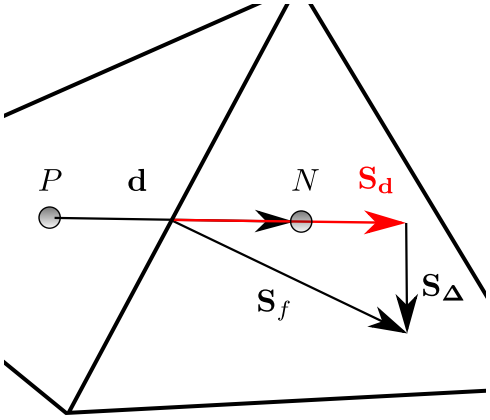

Figure 4.6: Non-orthogonal correction.

As can be seen, this constraint leaves some scope of variability for the concrete choice of $\mathbf{S}_{\boldsymbol{\Delta}}$. In [3] Jasak identified the so-called 'over-relaxed' approach as the most robust and convergent. It reads

$$\mathbf{S}_{\boldsymbol{\Delta}} = \frac{\mathbf{d}}{\mathbf{d}\bullet\mathbf{S}_f}|\mathbf{S}_f|^2. \tag{4.30}$$

However, this formulation might give rise to unboundedness, especially on highly non-orthogonal meshes. In such cases it might become necessary to limit the magnitude of the non-orthogonal contribution decreasing the formal accuracy in order to preserve boundedness. One way of limiting the non-orthogonal contribution comprises of imposing a limiter such that its magnitude is not allowed to exceed the magnitude of the orthogonal contribution [10].

4.3.3. Source Term

All terms that cannot be considered as convection, diffusion or temporal terms in the generic transport equation are to be loosely classified as source and sink terms, $S_\phi(\phi)$.

In general the source term $S_\phi(\phi)$ is allowed to be a function of time, space, other variables and the solution ϕ itself. In order to promote both stability and boundedness typically linearisation with respect to ϕ is performed before the actual discretization is applied to the source term $S_\phi(\phi)$:

$$S_\phi(\phi) = S_u + S_p\phi \qquad \text{with} \qquad S_p = \frac{\partial S_\phi(\phi)}{\partial\phi}, \tag{4.31}$$

where both S_u and S_p are allowed to be a function of ϕ. Integration of equation 4.31 over the control volume then yields

$$\int_{V_p} S_\phi(\phi)\, dV = S_u V_P + S_p V_P \phi_P. \tag{4.32}$$

As might be evident and has been intimated before, there is some scope of variability in the concrete form of a particular source term. Generally it is advisable to examine its interaction with other terms as well as its influence on accuracy and boundedness of the solution. It is further certainly wise to treat the source 'as implicit as possible' – as will become clear in the sequel.

4.3.4. Time Integration

Before describing the temporal derivative and the time integration of the generic transport equation in detail, we shall first define the time levels needed therefore. Underlying the prescribed temporal derivation, and thus the time-step size Δt, enables to define these time levels as

$$t^n = t^o + \Delta t \qquad \text{and} \qquad t^o = t^{oo} + \Delta t, \tag{4.33}$$

with the superscript n, o and oo denoting the new, the first old and the second old time levels, respectively.

Presuming that the control volumes do not change in time, the temporal term can be treated using the same rationale as for the source terms. Applying the Leibniz' theorem, it is:

$$\int_t^{t+\Delta t} \left[\int_{V_P} \frac{\partial \rho\phi}{\partial t}\, dV \right] dt = \int_t^{t+\Delta t} \frac{\partial}{\partial t} \left[\int_{V_P} \rho\phi\, dV \right] dt = \int_t^{t+\Delta t} V_P \frac{\partial}{\partial t} (\rho_P \phi_P)\, dt. \tag{4.34}$$

With this, time integration of the generic transport equation can be performed yielding its so-called semi-discretized form:

$$\begin{aligned} &\int_t^{t+\Delta t} \left[\left(\frac{\partial \rho\phi}{\partial t} \right) V_P + \sum_f F\phi_f - \sum_f (\Gamma_{\phi,d})_f \, \mathbf{S}_f \bullet (\nabla\phi)_f \right] dt \\ =&\int_t^{t+\Delta t} [S_u V_P + S_p V_P \phi_P]\, dt. \end{aligned} \tag{4.35}$$

Rearrangement of equation 4.35 to

$$\begin{aligned} &\int_t^{t+\Delta t} \left(\frac{\partial \rho\phi}{\partial t} \right) V_P\, dt \\ =&\int_t^{t+\Delta t} \left[-\sum_f F\phi_f + \sum_f (\Gamma_{\phi,d})_f \, \mathbf{S}_f \bullet (\nabla\phi)_f + (S_u V_P + S_p V_P \phi_P) \right] dt, \end{aligned} \tag{4.36}$$

reveals that the temporal discretization can be thought of in two parts:

1.) approximation of the temporal derivative on the l.h.s. of equation 4.36 in terms of ϕ_P at different time levels as they have been defined above.

2.) approximation of the r.h.s. of equation 4.36 containing all (time-intergrated) spatial terms.

For convenience and ease of reading this r.h.s. comprising all spatial terms shall be denoted in a short-hand notation henceforth:

$$\mathcal{S} \equiv \int_t^{t+\Delta t} \left[-\sum_f F\phi_f + \sum_f \left(\Gamma_{\phi,d}\right)_f \mathbf{S}_f \bullet \left(\nabla\phi\right)_f + \left(S_u V_P + S_p V_P \phi_P\right) \right] dt. \tag{4.37}$$

ad 1) By expressing ϕ^o, that is the first old time level of ϕ, and ϕ^{oo}, i.e., the second old time level of ϕ, as Taylor Series expansion around the new time level n:

$$\phi^o = \phi^n - \left(\frac{\partial\phi}{\partial t}\right)^n \Delta t + \frac{1}{2}\left(\frac{\partial^2(\phi)}{\partial t^2}\right)^n \Delta t^2 + \mathcal{O}\left(\Delta t^3\right) \qquad \text{and} \tag{4.38}$$

$$\phi^{oo} = \phi^n - 2\left(\frac{\partial\phi}{\partial t}\right)^n \Delta t + 2\left(\frac{\partial^2(\phi)}{\partial t^2}\right)^n \Delta t^2 + \mathcal{O}\left(\Delta t^3\right), \tag{4.39}$$

and combining them, yields a second order approximation of the desired temporal derivative at the new time level n. For constant Δt it is:

$$\begin{aligned} \left(\frac{\partial\phi}{\partial t}\right)^n &= \frac{\frac{3}{2}{\phi_P}^n - 2{\phi_P}^o + \frac{1}{2}{\phi_P}^{oo}}{\Delta t} \qquad \text{and} \\ \left(\frac{\partial\rho\phi}{\partial t}\right)^n &= \frac{\frac{3}{2}{\rho_P}^n{\phi_P}^n - 2{\rho_P}^o{\phi_P}^o + \frac{1}{2}{\rho_P}^{oo}{\phi_P}^{oo}}{\Delta t}. \end{aligned} \tag{4.40}$$

Alternatively by rearranging equation 4.4 one arrives at a first order approximation of the temporal derivative at the new time level n:

$$\begin{aligned} \left(\frac{\partial\phi}{\partial t}\right)^n &= \frac{{\phi_P}^n - {\phi_P}^o}{\Delta t} \qquad \text{and} \\ \left(\frac{\partial\rho\phi}{\partial t}\right)^n &= \frac{{\rho_P}^n{\phi_P}^n - {\rho_P}^o{\phi_P}^o}{\Delta t}. \end{aligned} \tag{4.41}$$

ad 2) It has become customary to neglect the temporal variation of the face values. This means, that the cell values, the face values are evaluated from for approximating the spatial terms in $\mathcal{S}$, are considered constant during a time step. In consequence, either their determination is performed explicitly (exclusively from the cell values at the old time level), implicitly (exclusively from the cell values at the new time level) or time-centered (from the cell values at both the old and the new time levels).

Underlying a first order approximation of the temporal derivative (equation 4.41 for the l.h.s. of equation 4.36) one refers to the

- Euler explicit method,

  if all face values in $\mathcal{S}$ are determined from the values at the old time level t^o. Moreover, the linear part of the source term is evaluated from the old time level. Hence:

$$\begin{aligned} &\mathcal{S} = \mathcal{S}\left(t^o\right) \\ \Rightarrow &\int_t^{t+\Delta t} \frac{\partial \rho\phi}{\partial t} V_P \, dt = \frac{{\rho_P}^n {\phi_P}^n - {\rho_P}^o {\phi_P}^o}{\Delta t} V_P = \mathcal{S}\left(t^o\right). \end{aligned} \tag{4.42}$$

  In doing so, ${\phi_P}^n$ at the new time level can be *determined directly* – i.e., without solving for a system of linear equations. However, in order to ensure stability the solution procedure has to obey the Courant number limit:

$$Co \equiv \frac{\mathbf{U}_f \bullet \mathbf{d}}{\Delta t} \overset{!}{<} 1, \tag{4.43}$$

  stating a severe restriction for the choice of the time step size – especially for steady-state problems, whereas for transient cases time-accuracy (being actually promoted by the Courant number limit) is of major importance.

- Euler implicit method,

  if all face values in $\mathcal{S}$ and the linear part in the source term are determined from the values at the new time level t^n:

$$\begin{aligned} &\mathcal{S} = \mathcal{S}\left(t^n\right) \\ \Rightarrow &\int_t^{t+\Delta t} \frac{\partial \rho\phi}{\partial t} V_P \, dt = \frac{{\rho_P}^n {\phi_P}^n - {\rho_P}^o {\phi_P}^o}{\Delta t} V_P = \mathcal{S}\left(t^n\right), \end{aligned} \tag{4.44}$$

  which yields a system of linear equations. In consequence, the resultant implicitness causes a stronger coupling within the system and hence removes the Courant number limit, which results in unconditional stability. Furthermore, this method guarantees boundedness of the solution – provided that the non-orthogonal correction is treated explicitly.

- time-centered Crank-Nicholson method,

  if the face values and the linear part of the source terms are determined as arithmetic mean from the cell values at both the old and the new time levels. Hence, centering the spatial terms in time yields:

$$\begin{aligned} &\mathcal{S} = \frac{1}{2}\left[\mathcal{S}\left(t^o\right) + \mathcal{S}\left(t^n\right)\right] \\ \Rightarrow &\int_t^{t+\Delta t} \frac{\partial \rho\phi}{\partial t} V_P \, dt = \frac{{\rho_P}^n {\phi_P}^n - {\rho_P}^o {\phi_P}^o}{\Delta t} V_P = \frac{1}{2}\left[\mathcal{S}\left(t^o\right) + \mathcal{S}\left(t^n\right)\right]. \end{aligned} \tag{4.45}$$

This method is unconditionally stable but generally does not guarantee boundedness.

Underlying the second order approximation for the temporal derivative (equation 4.40 for the l.h.s. of equation 4.36) one refers to the

- backward differencing method,
  if all face values and the linear part of the source term are evaluated from cell values at the new time level:

$$\begin{aligned} &\mathcal{S} = \mathcal{S}\left(t^n\right) \\ \Rightarrow &\int_t^{t+\Delta t} \frac{\partial \rho\phi}{\partial t} V_P \, dt = \frac{\frac{3}{2}\rho_P{}^n \phi_P{}^n - 2\rho_P{}^o \phi_P{}^o + \frac{1}{2}\rho_P{}^{oo}\phi_P{}^{oo}}{\Delta t} V_P = \mathcal{S}\left(t^n\right). \end{aligned} \tag{4.46}$$

  However, again boundedness is not guaranteed.

As shown in [11], both the Euler explicit and the Euler implicit method are of first order accuracy in time, while the time-centered Crank-Nicholson and the backward differencing methods are of second order accuracy.

Note in passing, that in order to achieve second order accuracy in time, time-centering the spatial terms (r.h.s.) can be avoided when choosing a second order accurate representation of the time derivative (l.h.s.).

4.3.5. Boundary Conditions

Up to now the examination of the discretization practice of the finite volume method has been restricted to *internal mesh faces*. Face-centered values have been determined by use of cell-centered ones obtained from cells pertaining to each side of the face under consideration. For *boundary faces*, however, these values have to be evaluated from the *boundary condition*.

In general there are two basic types of boundary conditions, namely the *Dirichlet boundary condition* (fixed value prescribing the value of ϕ at the boundary) and the *von Neumann boundary condition* (prescribing the gradient of ϕ at the boundary).

Before expatiating upon the discrete representation of these basic boundary conditions in more detail, it is advisable to first examine the nomenclature associated with an arbitrary control volume with one boundary face b – as shown in figure 4.7.

As described for the treatment of the non-orthogonality, a distance vector $\mathbf{d}$ is introduced. However, in absence of a neighboring cell, it is redefined to connect

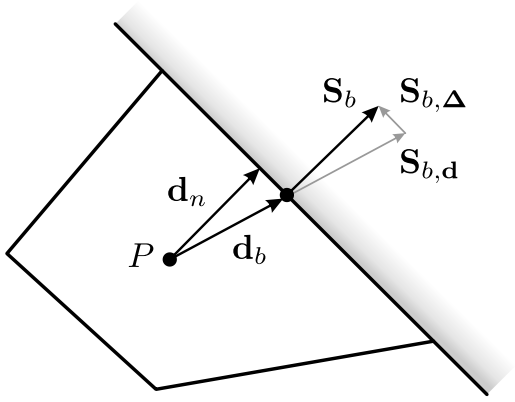

Figure 4.7: Boundary control volume.

the boundary cell center with the corresponding boundary face center – thus it is denoted as $\mathbf{d}_b$. With the vector $\mathbf{d}_n$ being parallel to the boundary face area vector $\mathbf{S}_b$, $\mathbf{d}_n \parallel \mathbf{S}_b$, it is

$$\mathbf{d}_n \equiv \frac{\mathbf{S}_b}{|\mathbf{S}_b|}\frac{\mathbf{d}_b \bullet \mathbf{S}_b}{|\mathbf{S}_b|}. \tag{4.47}$$

Basic Boundary Conditions

- Dirichlet boundary condition (fixed value)
  The value of ϕ at the boundary is prescribed to be $\phi = \phi_b$. This means for the *convection term* if it is discretized involving a boundary face b:

  $$\int_{V_P} \nabla \bullet \rho\phi\mathbf{U}\, dV = \sum_f F\phi_f + F_b\phi_b, \tag{4.48}$$

  where F_b is the prescribed flux across the boundary face. The *diffusion term* is discretized as

  $$\int_{V_P} \nabla \bullet \Gamma_{\phi,d}\nabla\phi\, dV = \sum_f \left(\Gamma_{\phi,d}\right)_f \mathbf{S}_f \bullet \left(\nabla\phi\right)_f + \left(\Gamma_{\phi,d}\right)_b \mathbf{S}_b \bullet \left(\nabla\phi\right)_b . \tag{4.49}$$

  The normal gradient at the boundary face is evaluated as

  $$\mathbf{S}_b \bullet \left(\nabla\phi\right)_b = |\mathbf{S}_{b,\mathbf{d}}|\frac{\phi_b - \phi_P}{|\mathbf{d}_n|} + \mathbf{S}_{b,\boldsymbol{\Delta}} \bullet \left(\nabla\phi\right)_P , \tag{4.50}$$

  where the explicit second component is calculated from the cell-centered value in P instead of the interpolated face gradient.

- von Neumann boundary condition (fixed gradient)
  The normal gradient of ϕ is prescribed at the boundary face to be $\mathbf{S}_b \bullet (\nabla\phi)_b = g_b$. Hence, the *convection term* reads

$$\int_{V_P} \nabla \bullet \rho\phi\mathbf{U}\, dV = \sum_f F\phi_f + F_b\phi_b = \sum_f F\phi_f + F_b\left(\phi_P + |\mathbf{d}_n| g_b\right), \tag{4.51}$$

  where ϕ_b has been evaluated from the normal gradient d_b at the boundary. Further, the discretized *diffusion term* can be calculated directly as

$$\mathbf{S}_b \bullet (\nabla\phi)_b = g_b \tag{4.52}$$

4.4. Discretization of Governing Equations

Considering appropriate strategies for discretization and numerical solution of the governing equations as they are provided in section 3.5, we shall restrict ourself to those equations describing two-phase flows of segregated flow type. The discretization of governing equations describing dispersed two-phase flows has been set out in considerable detail by Weller in [12, 13]. The route followed here is understood as complementary, in the sense that it provides the details for two-phase flows of segregated flows in an analogous manner. Eventually this clearly points out the avenue towards a *'full'* methodology covering both dispersed and segregated two-phase flow types, which does not impose any additional arduousness with respect to discretization.

4.4.1. Discetized Interface Transport Equation

Equation Formulation

One critical issue in the numerical treatment of two-phase flow is around phase-conservation and boundedness of the volumetric phase fraction, since small errors in the volume fraction correspond to large ones in mass fraction due to a typically high density ratio.

Therefore, each numerical approach being adopted needs to ensure both phase conservation and boundedness in the full range of volumetric phase fractions. In order to arrive at such an approach for the interface transport, we might start from the volume-averaged interfacial transport equation 3.77, which is repeated here for convenience:

$$\frac{\partial \alpha_\varphi}{\partial t} + \widehat{\mathbf{U}}^{\varphi} \bullet \nabla\alpha_\varphi = 0.$$

From this it is evident that the transport of the volumetric phase fraction α_φ is non-conservative per se – irrespective of the choice of closure for $\widetilde{\mathbf{U}}^\varphi$ (cf. section 3.4). Thus, it is clear that in order to achieve a more expedient (but equivalent) form any closed volume-averaged interfacial transport equation (based on 3.77) must first be rearranged. With the volumetric phase fraction being a conserved quantity, it is felt that as a guidance the rearrangement should be accomplished such that an established (conservative) form of governing equations is recovered as much as possible. This, of course, is expected to hold both conservative and non-conservative transport terms, however, with the latter being either interpretable on a physical basis or assessable from modeling assumptions that have been introduced in the course of model derivation. It is then expected (yet hoped) to establish a form more suitable for numerical evaluation, i.e., meeting the above requirements of phase conservation and boundedness.

In order to proceed towards this expedient form, which eventually shall enable to numerically solve for the transport of α_φ as conserved property, in a first step it is of use to consider free-surface flows ($\overline{\mu}^\varphi \gg \overline{\mu}^\phi$ or vice versa), in the limiting case of which one of the conditional volume-averaged continuity equations in the form of 2.84 are expected to fully govern the transport of the respective volumetric phase fraction. Rearranging by use of the mixture velocity $\mathbf{U} \equiv \alpha_\varphi \overline{\mathbf{U}}^\varphi + \alpha_\phi \overline{\mathbf{U}}^\phi$ and the phase slip velocity $\mathbf{U}_r \equiv \overline{\mathbf{U}}^\varphi - \overline{\mathbf{U}}^\phi$, yields

$$\frac{\partial \alpha_\varphi}{\partial t} + \nabla_\bullet \left(\alpha_\varphi \, \overline{\mathbf{U}}^\varphi \right) = 0 \tag{4.53}$$

$$\Leftrightarrow \quad \frac{\partial \alpha_\varphi}{\partial t} + \nabla_\bullet \left(\alpha_\varphi \mathbf{U} \right) + \nabla_\bullet \left(\alpha_\varphi \alpha_\phi \mathbf{U}_r \right) = 0, \tag{4.54}$$

and similarly for phase ϕ,

$$\frac{\partial \alpha_\phi}{\partial t} + \nabla_\bullet \left(\alpha_\phi \, \overline{\mathbf{U}}^\phi \right) = 0 \tag{4.55}$$

$$\Leftrightarrow \quad \frac{\partial \alpha_\phi}{\partial t} + \nabla_\bullet \left(\alpha_\phi \mathbf{U} \right) - \nabla_\bullet \left(\alpha_\phi \alpha_\varphi \mathbf{U}_r \right) = 0. \tag{4.56}$$

Note that the two above transport terms on the l.h.s. of equations 4.54 and 4.56 are conservative – i.e., conservativeness can be guaranteed by discretization employing the Finite Volume Method as set out before. Furthermore, boundedness is ensured for the first term, since $\nabla_\bullet \mathbf{U} \overset{!}{=} 0$ (cf. equation 3.76) as well as for the second term, since it becomes zero as $\alpha_\varphi \to 0$ or $\alpha_\varphi \to 1$. I.e., the natural bounds of the differential forms according to equations 4.54 and 4.56 are preserved by its discretized counter-parts.

For these reasons and now turning to the general case of a segregated flow (i.e., for $\overline{\mu}^\varphi \not\gg \overline{\mu}^\phi$ and $\overline{\mu}^\varphi \not\ll \overline{\mu}^\phi$), it appears desirable to first rearrange the corresponding closed form of equation 3.77 (cf. equation 3.73), aiming at a form as close as possible to 4.54 for free-surface flows. Then, reassessment of the remaining (non-conservative)

terms shall be discussed against the background of phase conservation and boundedness with the arising additional terms being assigned to the departure from the limiting case of a segregated free-surface flow governed by equation 4.54. Analogously, the same procedure might be performed for phase ϕ aiming at a form close to equation 4.56.

Using equation 3.72 (closure model for $\widetilde{\overline{\mathbf{U}}}^{\varphi}$) and with the volumetric mean (or mixture) velocity being defined as $\mathbf{U} \equiv \alpha_\varphi \overline{\mathbf{U}}^{\varphi} + \alpha_\phi \overline{\mathbf{U}}^{\phi}$ and the phase-slip velocity as $\mathbf{U}_r \equiv \overline{\mathbf{U}}^{\varphi} - \overline{\mathbf{U}}^{\phi}$, the volume-averaged interfacial transport equation becomes (see corollary note 4.2):

$$\frac{\partial \alpha_\varphi}{\partial t} + \mathbf{U}\bullet\nabla\alpha_\varphi + \frac{\alpha_\phi\,\overline{\mu}^{\varphi} - \alpha_\varphi\,\overline{\mu}^{\phi}}{\overline{\mu}^{\varphi} + \overline{\mu}^{\phi}}\mathbf{U}_r\bullet\nabla\alpha_\varphi = 0. \tag{4.57}$$

Corollary Note 4.2

$$\frac{\partial \alpha_\varphi}{\partial t} + \widetilde{\overline{\mathbf{U}}}^{\varphi}\bullet\nabla\alpha_\varphi = 0$$

$$\Leftrightarrow \frac{\partial \alpha_\varphi}{\partial t} + \frac{\overline{\mu}^{\varphi}}{\overline{\mu}^{\varphi} + \overline{\mu}^{\phi}}\,\overline{\mathbf{U}}^{\varphi}\bullet\nabla\alpha_\varphi + \frac{\overline{\mu}^{\phi}}{\overline{\mu}^{\varphi} + \overline{\mu}^{\phi}}\,\overline{\mathbf{U}}^{\phi}\bullet\nabla\alpha_\varphi = 0.$$

Moreover, it is

$$\overline{\mathbf{U}}^{\varphi} = \mathbf{U} + \alpha_\phi\mathbf{U}_r \;\text{ and }\; \overline{\mathbf{U}}^{\phi} = \mathbf{U} - \alpha_\varphi\mathbf{U}_r.$$

Then,

$$\frac{\partial \alpha_\varphi}{\partial t} + \frac{\overline{\mu}^{\varphi}}{\overline{\mu}^{\varphi} + \overline{\mu}^{\phi}}\mathbf{U}\bullet\nabla\alpha_\varphi + \frac{\overline{\mu}^{\phi}}{\overline{\mu}^{\varphi} + \overline{\mu}^{\phi}}\mathbf{U}\bullet\nabla\alpha_\varphi + \frac{\overline{\mu}^{\varphi}}{\overline{\mu}^{\varphi} + \overline{\mu}^{\phi}}\,\alpha_\phi\mathbf{U}_r\bullet\nabla\alpha_\varphi - \frac{\overline{\mu}^{\phi}}{\overline{\mu}^{\varphi} + \overline{\mu}^{\phi}}\,\alpha_\varphi\mathbf{U}_r\bullet\nabla\alpha_\varphi = 0$$

$$\Rightarrow \frac{\partial \alpha_\varphi}{\partial t} + \mathbf{U}\bullet\nabla\alpha_\varphi + \frac{\alpha_\phi\,\overline{\mu}^{\varphi} - \alpha_\varphi\,\overline{\mu}^{\phi}}{\overline{\mu}^{\varphi} + \overline{\mu}^{\phi}}\mathbf{U}_r\bullet\nabla\alpha_\varphi = 0.$$

Equation 4.57 can be rewritten using equation 3.76 ($\nabla\bullet\mathbf{U} \overset{!}{=} 0$):

$$\frac{\partial \alpha_\varphi}{\partial t} + \nabla\bullet\left(\alpha_\varphi\mathbf{U}\right) + \frac{\alpha_\phi\,\overline{\mu}^{\varphi} - \alpha_\varphi\,\overline{\mu}^{\phi}}{\overline{\mu}^{\varphi} + \overline{\mu}^{\phi}}\mathbf{U}_r\bullet\nabla\alpha_\varphi = 0. \tag{4.58}$$

While the first transport term on the l.h.s. ensures both phase conservation and boundedness of the volumetric phase fraction α_φ, the second transport term requires further examination:

$$\begin{aligned}
&\frac{\alpha_\phi\,\overline{\mu}^{\varphi} - \alpha_\varphi\,\overline{\mu}^{\phi}}{\overline{\mu}^{\varphi} + \overline{\mu}^{\phi}}\mathbf{U}_r{\bullet}\nabla\alpha_\varphi \\
&\qquad \overset{\alpha_\varphi=1-\alpha_\phi}{=} \left[\alpha_\phi - \frac{\overline{\mu}^{\phi}}{\overline{\mu}^{\varphi} + \overline{\mu}^{\phi}}\right]\mathbf{U}_r{\bullet}\nabla\alpha_\varphi \qquad (4.59)\\
&\qquad \overset{\alpha_\phi=1-\alpha_\varphi}{=} \left[\alpha_\varphi - \frac{\overline{\mu}^{\varphi}}{\overline{\mu}^{\varphi} + \overline{\mu}^{\phi}}\right]\mathbf{U}_r{\bullet}\nabla\alpha_\phi. \qquad (4.60)
\end{aligned}$$

Consequently, the interface transport equations read

$$\frac{\partial\alpha_\varphi}{\partial t} + \nabla{\bullet}\left(\alpha_\varphi\mathbf{U}\right) + \alpha_\phi\mathbf{U}_r{\bullet}\nabla\alpha_\varphi - \frac{\overline{\mu}^{\phi}}{\overline{\mu}^{\varphi} + \overline{\mu}^{\phi}}\mathbf{U}_r{\bullet}\nabla\alpha_\varphi = 0, \qquad (4.61)$$

and similarly for phase ϕ,

$$\frac{\partial\alpha_\phi}{\partial t} + \nabla{\bullet}\left(\alpha_\phi\mathbf{U}\right) - \alpha_\varphi\mathbf{U}_r{\bullet}\nabla\alpha_\phi - \frac{\overline{\mu}^{\varphi}}{\overline{\mu}^{\varphi} + \overline{\mu}^{\phi}}\mathbf{U}_r{\bullet}\nabla\alpha_\phi = 0. \qquad (4.62)$$

Using the identities $\overline{\mathbf{U}}^{\varphi} = \mathbf{U} + \alpha_\phi\mathbf{U}_r$ and $\overline{\mathbf{U}}^{\phi} = \mathbf{U} - \alpha_\varphi\mathbf{U}_r$, this eventually expands to the desired form:

$$\frac{\partial\alpha_\varphi}{\partial t} + \nabla{\bullet}\left(\alpha_\varphi\mathbf{U}\right) + \nabla{\bullet}\left(\alpha_\varphi\alpha_\phi\mathbf{U}_r\right) - \alpha_\varphi\nabla{\bullet}\,\overline{\mathbf{U}}^{\varphi} - \frac{\overline{\mu}^{\phi}}{\overline{\mu}^{\varphi} + \overline{\mu}^{\phi}}\mathbf{U}_r{\bullet}\nabla\alpha_\varphi = 0, \qquad (4.63)$$

and for phase ϕ,

$$\frac{\partial\alpha_\phi}{\partial t} + \nabla{\bullet}\left(\alpha_\phi\mathbf{U}\right) - \nabla{\bullet}\left(\alpha_\phi\alpha_\varphi\mathbf{U}_r\right) - \alpha_\phi\nabla{\bullet}\,\overline{\mathbf{U}}^{\phi} - \frac{\overline{\mu}^{\varphi}}{\overline{\mu}^{\varphi} + \overline{\mu}^{\phi}}\mathbf{U}_r{\bullet}\nabla\alpha_\phi = 0. \qquad (4.64)$$

As can be seen, the form of the equations 4.54 and 4.56 is recovered – with additional terms being in non-conservative form. However, recognizing α_φ and α_ϕ as conserved properties, it is clear that corresponding transport equations should be devoid of any non-conservative terms. Against this background, we shall disregard these terms for now, which should be a good approximation at least for free-surface scenarios where $\overline{\mu}^{\varphi} \ll \overline{\mu}^{\phi}$ (or vice versa).

Discretization Practice

The discretization practice of the interface transport equations 4.63 and 4.63 is set out in the following according to the Finite Volume Notation as described on pg. xiii ff.:

$$\begin{aligned}&\left[\!\!\left[\frac{\partial[\alpha_\varphi]}{\partial t}\right]\!\!\right] + \left[\!\!\left[\nabla\bullet\Big(F[\alpha_\varphi]_{f(F,\Gamma,0.5)}\Big)\right]\!\!\right]\\ &+\left[\!\!\left[\nabla\bullet\Big(F_{r,\varphi}[\alpha_\varphi]_{f(F_{r,\varphi},\Gamma,0.5)}\Big)\right]\!\!\right] + \left[\!\!\left[\nabla\bullet\Big(F_{c,\varphi}[\alpha_\varphi]_{f(F_{c,\varphi},\Gamma,0.5)}\Big)\right]\!\!\right] = 0 \qquad (4.65)\\ &\left[\!\!\left[\frac{\partial[\alpha_\phi]}{\partial t}\right]\!\!\right] + \left[\!\!\left[\nabla\bullet\Big(F[\alpha_\phi]_{f(F,\Gamma,0.5)}\Big)\right]\!\!\right]\\ &+\left[\!\!\left[\nabla\bullet\Big(F_{r,\phi}[\alpha_\phi]_{f(F_{r,\phi},\Gamma,0.5)}\Big)\right]\!\!\right] + \left[\!\!\left[\nabla\bullet\Big(F_{c,\phi}[\alpha_\phi]_{f(F_{c,\phi},\Gamma,0.5)}\Big)\right]\!\!\right] = 0, \qquad (4.66)\end{aligned}$$

where the phase-relative fluxes read

$$\begin{aligned}&F_{r,\varphi} \equiv \alpha_{\phi_{f(-F_r,\Gamma,0.5)}} F_r \;\text{ and }\; F_{r,\phi} \equiv -\alpha_{\varphi_{f(F_r,\Gamma,0.5)}} F_r \qquad (4.67)\\ &\text{with }\; F_r \equiv F_\varphi - F_\phi,\end{aligned}$$

and the phase compression fluxes have been defined [14] as

$$\begin{aligned}&F_{c,\varphi} \equiv \alpha_{\phi_{f(-F_c,\Gamma,0.5)}} F_c \;\text{ and }\; F_{c,\phi} \equiv -\alpha_{\varphi_{f(F_c,\Gamma,0.5)}} F_c \qquad (4.68)\\ &\text{with }\; F_c \equiv \min\Big(\mathrm{c}_\alpha|F|, \max(|F|)\Big)\left(\frac{(\nabla\alpha_\varphi)_f}{|(\nabla\alpha_\varphi)_f|}\right)\bullet\frac{\mathbf{S}_f}{|\mathbf{S}_f|}.\end{aligned}$$

Solving for one volumetric phase fraction, i.e., for one of the above (equivalent) equations, enables to calculate the complementary phase fraction using the trivial identity $\alpha_\varphi = 1 - \alpha_\phi$.

4.4.2. Discretized Momentum Equation

Equation Formulation

One major difficulty is encountered with numerical two-phase flow simulations, when solving for equation 3.78 in the $\alpha \to 0$ limit (i.e., $\alpha_\varphi \to 0$ resp. $\alpha_\phi \to 0$), where this equation reduces to the identity $\mathbf{0} = \mathbf{0}$. In turn, this renders the evaluation of the phase velocity $\overline{\mathbf{U}}^\varphi$ (or $\overline{\mathbf{U}}^\phi$ for equation 3.79), which certainly takes finite values, rather troublesome.

In general, the issue breaks down to the challenge of specifying the value of a property which pertains to one phase in regions where it is non-existent and where it is of no physical significance [15]. This is of no problem for extensive properties as they will

evaluate to zero anyway. However, intensive flow properties cause problems in the $\alpha \to 0$ limit.

One way to alleviate this problem is to rearrange the governing equation at question in order to achieve a more expedient form. Generally, there are different possibilities to accomplish this for the momentum equations:

1.) solving for the superficial velocities $\mathbf{U}_s \equiv \alpha_\varphi \, \overline{\mathbf{U}}^\varphi$ and $\mathbf{V}_s \equiv \alpha_\phi \, \overline{\mathbf{U}}^\phi$

These velocities are well-defined in the entire domain, approaching zero where $\alpha \to 0$. However, as the face flux would be defined as $\mathbf{S}_f \bullet (\mathbf{U}_s / \alpha_\varphi)_f$, a model would become necessary in order to evaluate the face flux in this limit.

2.) solving for the volumetric mixture velocity $\mathbf{U} \equiv \alpha_\varphi \, \overline{\mathbf{U}}^\varphi + \alpha_\phi \, \overline{\mathbf{U}}^\phi$ and a relative or slip velocity $\mathbf{U}_r \equiv \overline{\mathbf{U}}^\phi - \overline{\mathbf{U}}^\varphi$

This approach is advantageous, since the mixture velocity $\mathbf{U}$ is well-defined in the entire domain and, moreover, clearly related to the mean pressure in the system. Moreover, interfacial momentum exchange, being significantly governed by interfacial slip, could be treated implicit in crucial parts. However, this approach has not yet been developed to a more evolved state.

3.) solving for phase-intensive forms of the momentum equations

In contrast to the two approaches above, this route is based upon the elimination of α_φ resp. α_ϕ from the momentum equations as much as possible. Thus, this represents a significant departure from the previous methodologies. The merit of this route mainly lies in the concentration of the dependency from the volumetric phase fraction α_φ into a few terms that can be dealt with in an appropriate manner.

The third approach has proven advantageous [12, 15] and thus shall be set out in more detail in the remainder.

Derivation of the phase-intensive momentum equations We might start from the known non-intensive form as given by equation 3.78 and repeated here for convenience:

$$\frac{\partial \alpha_\varphi \, \overline{\mathbf{U}}^\varphi}{\partial t} + \nabla \bullet \left(\alpha_\varphi \, \overline{\mathbf{U}}^\varphi \, \overline{\mathbf{U}}^\varphi \right) = - \frac{\alpha_\varphi \nabla \, \overline{p}^\varphi}{\overline{\rho}^\varphi} - \frac{\nabla \bullet \left(\alpha_\varphi \, \overline{\boldsymbol{\tau}}^\varphi \right)}{\overline{\rho}^\varphi} + \alpha_\varphi \mathbf{g} + \frac{\mathbf{M}_\varphi}{\overline{\rho}^\varphi}, \tag{4.69}$$

Considering the l.h.s. of this equation, factoring out α_φ yields:

$$\begin{aligned} \frac{\partial \alpha_\varphi \, \overline{\mathbf{U}}^\varphi}{\partial t} + \nabla \bullet \left(\alpha_\varphi \, \overline{\mathbf{U}}^\varphi \, \overline{\mathbf{U}}^\varphi \right) = & \alpha_\varphi \left[\frac{\partial \, \overline{\mathbf{U}}^\varphi}{\partial t} + \overline{\mathbf{U}}^\varphi \bullet \nabla \, \overline{\mathbf{U}}^\varphi \right] \\ & + \overline{\mathbf{U}}^\varphi \frac{\partial \alpha_\varphi}{\partial t} + \overline{\mathbf{U}}^\varphi \, \overline{\mathbf{U}}^\varphi \bullet \nabla \alpha_\varphi . \end{aligned} \tag{4.70}$$

From this, it is

$$\frac{\partial \alpha_\varphi \overline{\mathbf{U}}^\varphi}{\partial t} + \nabla\bullet\left(\alpha_\varphi \overline{\mathbf{U}}^\varphi \overline{\mathbf{U}}^\varphi\right) = \alpha_\varphi \left[\frac{\partial \overline{\mathbf{U}}^\varphi}{\partial t} + \overline{\mathbf{U}}^\varphi \bullet \nabla \overline{\mathbf{U}}^\varphi\right] + \overline{\mathbf{U}}^\varphi \underbrace{\left[\frac{\partial \alpha_\varphi}{\partial t} + \overline{\mathbf{U}}^\varphi \bullet \nabla \alpha_\varphi\right]}_{=0}, \tag{4.71}$$

where the last term on the r.h.s. can be set to zero, as can be seen from equation 3.75 (which is inherently presumed to be valid here).

Hence, the phase-intensive momentum equation reads in its final form

$$\frac{\partial \overline{\mathbf{U}}^\varphi}{\partial t} + \overline{\mathbf{U}}^\varphi \bullet \nabla \overline{\mathbf{U}}^\varphi = -\frac{1}{\overline{\rho}^\varphi}\nabla \overline{p}^\varphi - \frac{1}{\alpha_\varphi}\left[\frac{1}{\overline{\rho}^\varphi}\nabla\bullet\left(\alpha_\varphi \overline{\boldsymbol{\tau}}^\varphi\right)\right] + \mathbf{g} + \frac{\mathbf{M}_\varphi}{\alpha_\varphi \overline{\rho}^\varphi}. \tag{4.72}$$

Decomposition of the shear stress tensor The term in the squared brackets on the r.h.s. of equation 4.72 potentially causes trouble in the $\alpha \to 0$ limit and therefore needs further examination. This shall be described in the following first for the bulk and then for the interfacial contribution (cf. equation 3.66):

$$\frac{\nabla\bullet\left(\alpha_\varphi \overline{\boldsymbol{\tau}}^\varphi\right)}{\alpha_\varphi \overline{\rho}^\varphi} = \left.\frac{\nabla\bullet\left(\alpha_\varphi \overline{\boldsymbol{\tau}}^\varphi\right)}{\alpha_\varphi \overline{\rho}^\varphi}\right|_{\mathit{eff},b} + \left.\frac{\nabla\bullet\left(\alpha_\varphi \overline{\boldsymbol{\tau}}^\varphi\right)}{\alpha_\varphi \overline{\rho}^\varphi}\right|_{\mathit{eff},i}. \tag{4.73}$$

bulk part of shear stress tensor For the numerical implementation of the bulk part of the shear stress tensor in the phase-intensive momentum equations it is advantageous to consider a decomposition of the shear stress tensor into a diffusive component (implicit treatment) and a correction (explicit treatment). In doing so, the dependency from the volumetric phase fraction α_φ, can be grouped, which in effect produces two terms:

$$\left.\frac{\nabla\bullet\left(\alpha_\varphi \overline{\boldsymbol{\tau}}^\varphi\right)}{\alpha_\varphi \overline{\rho}^\varphi}\right|_{\mathit{eff},b} = \frac{1}{\overline{\rho}^\varphi}\nabla\bullet\overline{\boldsymbol{\tau}}^\varphi + \frac{\overline{\boldsymbol{\tau}}^\varphi}{\overline{\rho}^\varphi}\bullet\frac{\nabla\alpha_\varphi}{\alpha_\varphi}. \tag{4.74}$$

Then, considering the decomposition for the bulks of Newtonian fluids

$$\overline{\boldsymbol{\tau}}^\varphi = \overline{\boldsymbol{\tau}}^{\varphi,\mathrm{D}} + \overline{\boldsymbol{\tau}}^{\varphi,\mathrm{C}}$$
$$\text{with}\quad \overline{\boldsymbol{\tau}}^{\varphi,\mathrm{D}} \equiv -\overline{\mu}^\varphi \nabla \overline{\mathbf{U}}^\varphi \quad\text{and}\quad \overline{\boldsymbol{\tau}}^{\varphi,\mathrm{C}} \equiv -\overline{\mu}^\varphi \left(\nabla \overline{\mathbf{U}}^\varphi\right)^{\mathrm{T}}, \tag{4.75}$$

it follows with the effective bulk viscosity $\nu_\varphi^{\mathit{eff},b} \equiv \frac{\overline{\mu}^\varphi}{\overline{\rho}^\varphi}$ for the first addend on the r.h.s. of equation 4.74

$$\nabla\bullet\frac{\overline{\boldsymbol{\tau}}^{\varphi,\mathrm{D}}}{\overline{\rho}^\varphi} = -\nabla\bullet\left(\nu_\varphi^{\mathit{eff},b}\nabla \overline{\mathbf{U}}^\varphi\right) \tag{4.76}$$

and

$$\nabla\bullet\frac{\overline{\boldsymbol{\tau}}^{\varphi,\mathrm{C}}}{\overline{\rho}^{\varphi}}=\nabla\bullet\left(-\nu_{\varphi}^{\mathit{eff},b}\left(\nabla\,\overline{\mathbf{U}}^{\varphi}\right)^{\mathrm{T}}\right). \tag{4.77}$$

Furthermore, after the above decomposition the second addend on the r.h.s. of equation 4.74 can be written as

$$\frac{\overline{\boldsymbol{\tau}}^{\varphi,\mathrm{D}}}{\overline{\rho}^{\varphi}}\bullet\frac{\nabla\alpha_{\varphi}}{\alpha_{\varphi}}=\nabla\bullet\left(-\nu_{\varphi}^{\mathit{eff},b}\frac{\nabla\alpha_{\varphi}}{\alpha_{\varphi}}\,\overline{\mathbf{U}}^{\varphi}\right)-\overline{\mathbf{U}}^{\varphi}\left(\nabla\bullet\left(-\nu_{\varphi}^{\mathit{eff},b}\frac{\nabla\alpha_{\varphi}}{\alpha_{\varphi}}\right)\right) \tag{4.78}$$

and a rest

$$\frac{\overline{\boldsymbol{\tau}}^{\varphi,\mathrm{C}}}{\overline{\rho}^{\varphi}}\bullet\frac{\nabla\alpha_{\varphi}}{\alpha_{\varphi}}. \tag{4.79}$$

interfacial part of shear stress tensor It is clear from inspection that α_{φ} in the interfacial part of shear stress tensor, i.e., in

$$\left.\frac{\nabla\bullet\left(\alpha_{\varphi}\,\overline{\boldsymbol{\tau}}^{\varphi}\right)}{\alpha_{\varphi}\,\overline{\rho}^{\varphi}}\right|_{\mathit{eff},i}=\frac{1}{\alpha_{\varphi}\,\overline{\rho}^{\varphi}}\nabla\bullet\left[-\frac{\overline{\mu}^{\varphi}\,\overline{\mu}^{\phi}}{\overline{\mu}^{\varphi}+\overline{\mu}^{\phi}}\left(\left(\overline{\mathbf{U}}^{\varphi}-\overline{\mathbf{U}}^{\phi}\right)\nabla\alpha_{\varphi}\right.\right.$$
$$\left.\left.+\nabla\alpha_{\varphi}\left(\overline{\mathbf{U}}^{\varphi}-\overline{\mathbf{U}}^{\phi}\right)\right)\right], \tag{4.80}$$

can not be easily isolated as for its bulk counter-part. Due to non-commutativity the first addend needs to be handled 'as-is' (explicit treatment):

$$\frac{1}{\alpha_{\varphi}}\nabla\bullet\left(-\nu_{\varphi}^{\mathit{eff},i}\left(\overline{\mathbf{U}}^{\varphi}-\overline{\mathbf{U}}^{\phi}\right)\nabla\alpha_{\varphi}\right), \tag{4.81}$$

where the effective interfacial viscosity has been defined as $\nu_{\varphi}^{\mathit{eff},i}\equiv\frac{1}{\overline{\rho}^{\varphi}}\frac{\overline{\mu}^{\varphi}\,\overline{\mu}^{\phi}}{\overline{\mu}^{\varphi}+\overline{\mu}^{\phi}}$. However, the second addend in equation 4.80 might be split up for semi-implicit treatment:

$$\frac{1}{\alpha_{\varphi}}\nabla\bullet\left(-\nu_{\varphi}^{\mathit{eff},i}\nabla\alpha_{\varphi}\,\overline{\mathbf{U}}^{\varphi}\right)-\frac{1}{\alpha_{\varphi}}\nabla\bullet\left(-\nu_{\varphi}^{\mathit{eff},i}\nabla\alpha_{\varphi}\,\overline{\mathbf{U}}^{\phi}\right). \tag{4.82}$$

Eventually, the implemented momentum conservation equation becomes in its final phase-intensive form:

$$\frac{\partial\,\overline{\mathbf{U}}^{\varphi}}{\partial t}+\overline{\mathbf{U}}^{\varphi}\bullet\nabla\,\overline{\mathbf{U}}^{\varphi}+\nabla\bullet\left.\frac{\overline{\boldsymbol{\tau}}^{\varphi}}{\overline{\rho}^{\varphi}}\right|_{\mathit{eff},b}+\left.\frac{\overline{\boldsymbol{\tau}}^{\varphi}}{\overline{\rho}^{\varphi}}\bullet\frac{\nabla\alpha_{\varphi}}{\alpha_{\varphi}}\right|_{\mathit{eff},b}+\left.\frac{\nabla\bullet\left(\alpha_{\varphi}\,\overline{\boldsymbol{\tau}}^{\varphi}\right)}{\alpha_{\varphi}\,\overline{\rho}^{\varphi}}\right|_{\mathit{eff},i}$$
$$=-\frac{1}{\overline{\rho}^{\varphi}}\nabla\,\overline{p}+\mathbf{g}+\frac{\mathbf{M}_{\varphi}}{\alpha_{\varphi}\,\overline{\rho}^{\varphi}}, \tag{4.83}$$

where additionally the single-field assumption has been adopted. Consequently, the (mixture) pressure $\overline{p}=\overline{p}^{\varphi}=\overline{p}^{\phi}$, being shared by both phases, is utilized.

The adoption of a single-field pressure is a useful assumption being made by most researchers in the field. Alternatively, the coupled solution of two pressure equations (one for each phase), which are elliptic in nature, would become necessary. On the other side, the solution of a system with a mixture pressure driving both phases is potentially violating continuity, because a single pressure could force both the phases to leave a cell [15]. However, since for incompressible flows the overall continuity is to be ensured for the *mixture* (cp. equation 3.76), the mixture pressure has to be determined in such a way that the *continuity of the volumetric mixture flux* is guaranteed (cf. section 4.5), in which case its use is justified. Moreover, for a sharp interface representation there is also evidence of a physical substantiation of a mixture pressure (cf. section 3.5, p. 88). In effect however, the number of variables has been reduced by one by adopting this mixture assumption. In consequence, one governing equation – usually the interface transport equation – is obsolete and can be disregarded [12]. Hence, the volumetric phase distribution is commonly obtained from the mass conservation according to equation 2.84. The justification of this practice has been issued in section 4.4.1.

Discretization Practice

The second term on the l.h.s. of equation 4.83 has rendered the phase-intensive form of the momentum equation non-conservative. However, the dependency from the volumetric phase fraction α_φ advantageously has been grouped in two kind of terms – shear stress contributions on the l.h.s. and momenta exchange terms on the r.h.s. – which needs to be examined further in the $\alpha \to 0$ limit:

- shear stress terms on the l.h.s. being $\sim \nabla\alpha_\varphi/\alpha_\varphi$
  Terms containing $\nabla\alpha_\varphi/\alpha_\varphi$ do not necessarily become infinite in the limit where the volumetric phase fraction approaches zero, $\alpha_\varphi \to 0$ [12, p. 12]. However, the numerical evaluation of such terms proves demanding: the central issue can be addressed considering the situation where the cell-centered value of α_φ is zero, while adjacent values in neighboring cells are not. Obviously, in such cases $\nabla\alpha_\varphi/\alpha_\varphi$ can not be evaluated by simply dividing by the cell-centered values of α_φ, but the evaluation needs stabilization. This can be accomplished by first averaging the denominator over the computational molecule of the ∇ operator, and secondly by adding a small stabilizing factor δ to it resulting in

  $$\frac{\nabla\alpha_\varphi}{\alpha_\varphi} \quad \to \quad \frac{\nabla\alpha_\varphi}{\langle\alpha_\varphi\rangle_\nabla + \delta}, \tag{4.84}$$

  which can be treated explicitly in a stable manner.

- momentum exchange terms on the r.h.s. containing α_φ
  Momenta exchange terms $\mathbf{M}_\varphi$ on the r.h.s. , i.e., interfacial pressure and

unbalanced shear stress contributions, are found to contain either α_φ or $\nabla\alpha_\varphi$ (resp. $|\nabla\alpha_\varphi|$), or both. In the first and last case a division by the volumetric phase fraction α_φ in the $\alpha_\varphi \to 0$ limit is not particularly worrisome, whereas in the middle case again stabilization is required, i.e., any $1/\alpha_\varphi$ is stabilized using δ:

$$\frac{1}{\alpha_\varphi} \quad \to \quad \frac{1}{\alpha_\varphi + \delta}. \tag{4.85}$$

Moreover, it is important for two-phase systems to recognize these momenta exchange terms and additionally all body force terms (as the buoyancy term, for instance) as quite sensitive and possibly troublesome, since they might contribute to discontinuities in both the pressure and the pressure gradient field. In such cases, when using a pseudo-staggered, i.e., collocated cell-centered variable arrangement and associated interpolation practice for pressure-velocity coupling (cf. section 4.5), continuity errors occur and consequently cause an unphysical behavior of the solution [16]. This is always the case if the pressure field is not ensured to be sufficiently smooth, for instance, if the pressure gradient needs to balance strongly varying force densities. Hence, as a remedy, these terms will be treated appropriately along with the pressure-velocity coupling in the algorithm (cf. section 4.5) – in the spirit of Rhie-Chow.

Summarizing, all stress terms, the pressure gradient and buoyancy terms are treated explicitly. Convection and diffusion terms as well as the time derivative are handled implicitly according to the discretization practice that has been set out in the previous sections.

Consequently, the discretization of the momentum equation 4.83 can be presented according to the Finite Volume Notation as described on pg. xiii ff., stating a semi-implicit decoupled discretization practice:

$$\begin{aligned}
&\left[\!\!\left[\frac{\partial[\,\overline{\mathbf{U}}^{\varphi}]}{\partial t} \right]\!\!\right] + \left[\!\!\left[\nabla\!\bullet\!\left(F_\varphi^{\mathrm{T}}[\,\overline{\mathbf{U}}^{\varphi}]_{f(F_\varphi^{\mathrm{T}},S,\gamma)} \right) \right]\!\!\right] - \left[\!\!\left[\nabla\!\bullet\!\left(F_\varphi^{\mathrm{T}} \right)[\,\overline{\mathbf{U}}^{\varphi}] \right]\!\!\right] - \left[\!\!\left[\nabla\!\bullet\!\left(\nu_\varphi^{\mathit{eff},b} \nabla[\,\overline{\mathbf{U}}^{\varphi}] \right) \right]\!\!\right] \\
&+ \frac{\nabla\!\bullet\,\overline{\boldsymbol{\tau}}^{\varphi,\mathrm{C}}}{\overline{\rho}^{\varphi}} + \frac{\nabla\alpha_\varphi}{\langle\alpha_\varphi\rangle_\nabla + \delta}\bullet\frac{\overline{\boldsymbol{\tau}}^{\varphi,\mathrm{C}}}{\overline{\rho}^{\varphi}} + \frac{1}{\langle\alpha_\varphi\rangle_\nabla + \delta}\Big(- \nu_\varphi^{\mathit{eff},i}\Big(\left(\overline{\mathbf{U}}^{\varphi} - \overline{\mathbf{U}}^{\phi} \right)\nabla\alpha_\varphi - \nabla\alpha_\varphi\,\overline{\mathbf{U}}^{\phi} \Big) \Big) \\
&+ \left[\!\!\left[\nabla\!\bullet\!\left(-\nu_\varphi^{\mathit{eff},i} S_f \nabla_f^{\perp}\alpha_\varphi \right)[\,\overline{\mathbf{U}}^{\varphi}] \right]\!\!\right] = -\frac{\nabla\,\overline{p}}{\overline{\rho}^{\varphi}} + \mathbf{g} - \left[\!\!\left[\frac{\alpha_\phi}{\overline{\rho}^{\varphi}} A_d \left[\,\overline{\mathbf{U}}^{\varphi}\right] \right]\!\!\right] + \frac{\alpha_\phi}{\overline{\rho}^{\varphi}}\left(A_d\,\overline{\mathbf{U}}^{\phi} \right)
\end{aligned} \tag{4.86}$$

and

$$\left[\!\left[\frac{\partial[\,\overline{\mathbf{U}}^{\phi}]}{\partial t} \right]\!\right] + \left[\!\left[\nabla\!\bullet\!\left(F_{\phi}^{\mathrm{T}}[\,\overline{\mathbf{U}}^{\phi}]_{f(F_{\phi}^{\mathrm{T}},S,\gamma)} \right) \right]\!\right] - \left[\!\left[\nabla\!\bullet\!\left(F_{\phi}^{\mathrm{T}} \right)[\,\overline{\mathbf{U}}^{\phi}] \right]\!\right] - \left[\!\left[\nabla\!\bullet\!\left(\nu_{\phi}^{\mathit{eff},b} \nabla[\,\overline{\mathbf{U}}^{\phi}] \right) \right]\!\right]$$
$$+ \frac{\nabla\!\bullet\,\overline{\boldsymbol{\tau}}^{\phi,\mathrm{C}}}{\overline{\rho}^{\phi}} + \frac{\nabla\alpha_{\phi}}{\langle\alpha_{\phi}\rangle_{\nabla}+\delta}\!\bullet\!\frac{\overline{\boldsymbol{\tau}}^{\phi,\mathrm{C}}}{\overline{\rho}^{\phi}} + \frac{1}{\langle\alpha_{\phi}\rangle_{\nabla}+\delta}\Big(-\nu_{\phi}^{\mathit{eff},i}\Big(\left(\overline{\mathbf{U}}^{\phi} - \overline{\mathbf{U}}^{\varphi}\right)\nabla\alpha_{\phi} - \nabla\alpha_{\phi}\,\overline{\mathbf{U}}^{\varphi}\Big)\Big)$$
$$+ \left[\!\left[\nabla\!\bullet\!\left(-\nu_{\phi}^{\mathit{eff},i} S_f \nabla_f^{\perp}\alpha_{\phi} \right)[\,\overline{\mathbf{U}}^{\phi}] \right]\!\right] = -\frac{\nabla\,\overline{p}}{\overline{\rho}^{\phi}} + \mathbf{g} - \left[\!\left[\frac{\alpha_{\varphi}}{\overline{\rho}^{\phi}} A_d \left[\,\overline{\mathbf{U}}^{\phi}\right] \right]\!\right] + \frac{\alpha_{\varphi}}{\overline{\rho}^{\phi}}\left(A_d\,\overline{\mathbf{U}}^{\varphi}\right). \tag{4.87}$$

4.5. Solution Method and Algorithm

4.5.1. Solution Method – Linear Algebraic Equation System

Assembling the terms from the finite volume discretization method yields one algebraic equation for each computational cell and each quantity ϕ under consideration:

$$a_P\phi_P + \sum_N a_N\phi_N = r_P, \tag{4.88}$$

where r denotes the source term.

Note that the equations might be linear or non-linear dependent on the nature of the physical problem stating the subject of interest. However, the latter group needs first to be linearized in some manner before treating it as *linear algebraic equation system*.

According to the underlying methods, that have been chosen for time integration, the solution procedure for the algebraic equations is either explicit or implicit:

1.) explicit method
If ${\phi_P}^n$, i.e., the new value of ϕ_P, solely depends on the old neighbor values ${\phi_N}^o$, ${\phi_P}^n$ can be evaluated directly by 'visiting' each cell and using the available value ${\phi_N}^o$ to calculate

$${\phi_P}^n = \frac{r_P - \sum_N a_N {\phi_N}^o}{a_P}, \tag{4.89}$$

without any additional information needed. As intimated before, despite being fast and efficient, this method poses the Courant number limitation to the solution method, that is the information about the boundary conditions is only allowed to propagate slowly imposing a limit on the time-step size.

2.) implicit method
If the new value ${\phi_P}^n$ depends on the new neighbor values ${\phi_N}^n$, it is

$${\phi_P}^n = \frac{r_P - \sum\limits_N a_N {\phi_N}^n}{a_P}. \tag{4.90}$$

As can be seen, each new value of ${\phi_P}^n$ depends on the new values ${\phi_N}^n$ in the neighboring cells – resulting in a *system of linear algebraic equations.*

This system of linear algebraic equations can be rewritten in a generic matrix form as

$$\{A\}\,[\phi] = [r]\,, \tag{4.91}$$

where $\{A\}$ is a square matrix holding the coefficient a_P on its diagonal and a_N off its diagonal. Thus, $\{A\}$ is said to be a spare matrix, i.e., most of its matrix coefficients equal zero. $[\phi]$ and $[r]$ are column vectors holding the dependent variable and source terms, respectively. Thus every row represents one algebraic equation for each control volume of the spatial solution domain.

In the following, we shall further examine the implicit method on a term-by-term basis. Beforehand, it is advisable to introduce two important measures in matrix analysis and linear algebra; that is the *diagonal equality* and *diagonal dominance* of matrix $\{A\}$, being governed by the discretized terms as set out in the previous sections. These measures are closely linked to the issue of boundedness and convergence, when solving for the corresponding system of linear algebraic equations using iterative solvers.

- The matrix $\{A\}$ is said to be *diagonal equal* if the magnitude of the diagonal coefficient for each row equals the sum of magnitudes of off-diagonal coefficients:

$$|a_{ii}| = \sum_{j=1}^{N} |a_{ij}|;\ j \neq i \qquad \Rightarrow \qquad |a_P| = \sum_N |a_N|. \tag{4.92}$$

- The matrix $\{A\}$ is *diagonal dominant* if the sum of magnitudes of off-diagonal coefficients in each row is equal or smaller than the magnitude of the diagonal coefficient:

$$|a_{ii}| \geq \sum_{j=1}^{N} |a_{ij}|;\ j \neq i \qquad \Rightarrow \qquad |a_P| \geq \sum_N |a_N|, \tag{4.93}$$

and at least for one row:

$$|a_{ii}| > \sum_{j=1}^{N} |a_{ij}|;\ j \neq i \qquad \Rightarrow \qquad |a_P| > \sum_N |a_N|, \tag{4.94}$$

Table 4.1: Matrix contributions of discretized terms (exemplary).

type of term	**contribution to matrix**		
	diagonal	off-diagonal	source
temporal	$a_P = \frac{{\rho_P}^n}{\Delta t} V_P$	—	$r_P = \frac{{\rho_P}^o {\phi_P}^o}{\Delta t} V_P$
convective	$a_P = f_x F$	$a_N = (1 - f_x) F$	—
diffusive	$a_P = -\left(\Gamma_{\phi,d}\right)_f \frac{\lvert\mathbf{S}_f\rvert}{\lvert\mathbf{d}\rvert}$	$a_N = -\left(\Gamma_{\phi,d}\right)_f \frac{\lvert\mathbf{S}_f\rvert}{\lvert\mathbf{d}\rvert}$	—
source	$a_P = \begin{cases} S_p V_P & \text{if } S_P < 0 \\ 0 & \text{if } S_P \geq 0 \end{cases}$ (implicit treatment)	—	$r_P = S_u V_P + \begin{cases} 0 & \text{if } S_P < 0 \\ S_p V_P {\phi_P}^o & \text{if } S_P \geq 0 \end{cases}$ (explicit treatment)

The convergence of iterative solvers is significantly promoted with increasing diagonal dominance of the matrix $\{A\}$.

Generally, every discretized term constituting the discretized form of a governing equation under consideration contributes to the matrix coefficients of $\{A\}$ and/or the source vector $[r]$, and thus will bias the system's properties:

temporal term The discretization of the temporal term solely produces a contribution to the diagonal coefficient and the source term, since $\frac{\partial \phi}{\partial t}$ in a cell P only depends on ϕ_P – see table 4.1. As can be seen, the diagonal dominance is strengthened with an decrease in the time step size Δt.

convection term Within the discretized convection term, ϕ_f depends on the values in both P and N. In general this creates an asymmetric matrix contribution with off-diagonal coefficients. E.g., the case of central differencing creates the matrix contributions as provided in table 4.1. Note that this does not generally guarantee boundedness. A diagonally equal matrix contribution is only produced by use of upwind differencing. For some other schemes a source contribution (due to gradient-based correction terms) needs to be added.

diffusion term The discretized diffusion term causes a diagonally equal and symmetric matrix contribution – ensuring boundedness on orthogonal meshes. For an orthogonal mesh the corresponding matrix contributions read as provided in table 4.1. On non-orthogonal meshes this only holds for explicit non-orthogonal correction (whose contribution is going into the source). Implicit treatment of

the non-orthogonal correction would introduce negative matrix coefficients from the 'second neighbors' violating diagonal equality.

source term Source and sink terms do not depend on values from neighboring cells. Thus, they solely contribute to the diagonal coefficients of the matrix and the source: The coefficient $S_u V_P$ is added directly to the source, while handling of the linear part of the source term is case-dependent (implicit vs. explicit treatment) – see table 4.1. By this practice the diagonal dominance of the matrix is purposively increased.

In order to solve for the system of linear algebraic equations within the framework of this study, the Conjugate Gradient (CG) method, originally proposed by Henstens and Steifel [17] is utilized. The convergence rate is further enhanced by use of preconditioning: for symmetric matrices the Incomplete Cholesky Conjugate Gradient (ICCG) method is employed [18], while the Bi-Conjugate Gradient STABilized (Bi-CGSTAB) method is adopted for assymmetric matrices [19]. Moreover, beside CG solvers, also the Algebraic Multi-Grid (AMG) method according to [20] is utilized in this study.

4.5.2. Algorithm

As has been already set out, the 'core-level' procedure comprises of an implicit iterative solution method being based upon an arbitrary finite volume discretization technique. However, the 'top-level', i.e., the algorithm, is supposed to treat the system$s$[1] of linear equations adopting the segregated approach, that is to solve each system separately – generally handling potential coupling between the equations explicitly.

Hence, the purpose of the algorithm is to appropriately maintain the coupling between all governing equations and to impose any continuity and boundedness constraints on the system as a whole [21]. For two-phase systems – stating the subject of the present work – the algorithm structure is determined by two aspects requiring special attention concerning coupling between

1.) the phase momenta and the pressure (pressure-velocity coupling),

2.) the phase momenta themselves (interfacial momentum exchange).

The first issue shall be approached employing the *Pressure Implicit with Splitting of Operators* (PISO) algorithm by Issa [22], whereas for the second issue a semi-implicit approach has been adopted. Both aspects govern the final algorithm structure and shall be set out in detail in the remainder of this section.

[1] for several dependent variables

Pressure-velocity Coupling – PISO algorithm

PISO is a segregated approach that allows to solve for the Navier-Stokes equations in which pressure and velocity are treated sequentially using a predictor-corrector procedure. In doing so, this method couples the pressure with the velocity through flux conservation[2].

Hence, conservative fluxes are related to the pressure gradient using an interpolation practice *in the spirit of Rhie-Chow* [23]. The Rhie-Chow interpolation is absolutely necessary when dealing with pressure-velocity coupling along with a colocated variable arrangement on an arbitrary polyhedral mesh – as it is a common requirement in nowadays CFD codes. This interpolation practice has removed the issue of pressure-velocity decoupling (so-called checkerboarding), which arises if the pressure gradient does not exhibit a compact support and thus does not depend on the pressure in adjacent cells allowing for a jigsaw pressure pattern ('checkerboard').

However, the original concept of Rhie-Chow, that is the explicit correction of the cell face velocities,

$$\mathbf{U}_f = f_x \mathbf{U}_P + (1 - f_x)\,\mathbf{U}_N + \left(\frac{1}{\mathcal{A}}\right)_f \left[\hat{\mathbf{n}}_\bullet \left(\nabla p\right)_f - \frac{p_N - p_P}{|\mathbf{d}|}\right] \qquad (4.95)$$

$$\text{with} \qquad \mathbf{d} \parallel \hat{\mathbf{n}},$$

is adapted herein to an interpolation practice best described to be *in the spririt of Rhie-Chow*, which is set out in detail below.

Before expatiating on a more detailed description of the PISO algorithm, it is important to recognize the underlying assumptions for which its adoption is justified. The coupling characteristics of a incompressible flow system encompasses

- linear pressure-velocity coupling and
- non-linear **U**-**U** coupling in the convection term of the momentum equation.

It is well known that the PISO algorithm relies on the crucial assumption that the pressure-velocity coupling is much stronger than the non-linear coupling in the momentum convection term. However, this is only valid if the non-linearity can be assumed to vary slowly, which is given for a time-accurate solution employing small time-steps. Throughout this work, this assumption is considered to be valid. Thus, the lagged velocity $\mathbf{U}^o$ (within the linearized momentum convection term $\nabla_\bullet \left(\mathbf{U}^n \mathbf{U}^o\right)$) remains frozen and without any update during the pressure corrections performed within the PISO algorithm.

[2] A flux is said to be conservative, if it obeys continuity, i.e., for incompressible flows $\nabla_\bullet \mathbf{U} \stackrel{!}{=} 0 \Rightarrow \sum_f F \stackrel{!}{=} 0$.

Derivation of the Pressure Equation For the purpose of derivation, the discretization of the momentum equation has to be considered (adopting the techniques as they were described before). By preserving the pressure gradient term in its differential form, this results in the semi-discretized form of the momentum equation:

$$a_P^{\mathrm{U}}\mathbf{U}_P + \sum_N a_N^{\mathrm{U}}\mathbf{U}_N = \mathbf{r} - \nabla p. \tag{4.96}$$

For simplicity, we might now introduce the $\boldsymbol{\mathcal{H}}[\mathbf{U}]$ and the $\mathcal{A}[\mathbf{U}]$ operator. The $\boldsymbol{\mathcal{H}}[\mathbf{U}]$ operator holds the off-diagonal part of the momentum matrix and the source part, except the pressure gradient, while the $\mathcal{A}[\mathbf{U}]$ operator issues the diagonal coefficients of the momentum matrix:

$$\boldsymbol{\mathcal{H}}[\mathbf{U}] \equiv \mathbf{r} - \sum_N a_N^{\mathrm{U}}\mathbf{U}_N \qquad \text{and} \tag{4.97}$$

$$\mathcal{A}[\mathbf{U}] \equiv a_P^{\mathrm{U}}, \tag{4.98}$$

For readability, $[\mathbf{U}]$ shall be dropped henceforth. If not stated otherwise, both the $\boldsymbol{\mathcal{H}}$ and $\mathcal{A}$ operator are applied on the momentum equation. With 4.97 and 4.98, equation 4.96 can be rewritten as

$$\mathcal{A}\mathbf{U}_P = \boldsymbol{\mathcal{H}} - \nabla p, \tag{4.99}$$

which can be used to express the velocity $\mathbf{U}_P$:

$$\mathbf{U}_P = \frac{\boldsymbol{\mathcal{H}}}{\mathcal{A}} - \frac{\nabla p}{\mathcal{A}}. \tag{4.100}$$

Substituting into the continuity equation for incompressible flow ($\nabla\bullet\mathbf{U} \stackrel{!}{=} 0$), yields

$$\nabla\bullet\left(\frac{\nabla p}{\mathcal{A}}\right) \stackrel{!}{=} \nabla\bullet\left(\frac{\boldsymbol{\mathcal{H}}}{\mathcal{A}}\right) \qquad \text{or} \tag{4.101}$$

$$\int_{V_P} \nabla\bullet\mathbf{U}\, dV \approx \sum_f \mathbf{S}_f\bullet\mathbf{U}_f \stackrel{!}{=} 0 \;\Rightarrow\; \sum_f \mathbf{S}_f\bullet\left[\left(\frac{1}{\mathcal{A}}\right)_f (\nabla p)_f\right] \stackrel{!}{=} \sum_f \mathbf{S}_f\bullet\left(\frac{\boldsymbol{\mathcal{H}}}{\mathcal{A}}\right)_f. \tag{4.102}$$

Steps of the PISO Algorithm (single-phase system) Bearing in mind the pressure equation 4.102, it is now possible to summarize the particular steps of the PISO algorithm. The following description corresponds to the steps performed at each time-step:

momentum predictor step The first step of the PISO algorithm is the momentum predictor step. This comprises the discretization and solution of the momentum equation using the available pressure field and conservative fluxes from

the previous corrector step (p^* and F^*) or the old time step (p^o and F^o), respectively.

$$\mathcal{A}^* \mathbf{U}_P{}^* = \boldsymbol{\mathcal{H}}^* - \nabla p^*. \tag{4.103}$$

Next, the off-diagonal components $\boldsymbol{\mathcal{H}}$ are assembled. On this basis, the velocity field is updated to yield an approximative velocity field – neglecting the influence of the pressure:

$$\mathbf{U}_P{}^* = \frac{\boldsymbol{\mathcal{H}}^*}{\mathcal{A}^*} \tag{4.104}$$

By underlying the guessed pressure p^*, the new velocity field in general does not satisfy the continuity condition – i.e., the velocity field $\mathbf{U}_P{}^*$ is not divergence-free.

pressure correction step Calculating the interpolated face fluxes (flux predictor) from the approximative velocity field according to equation 4.104,

$$F^* = \mathbf{S}_f \bullet \left(\mathbf{U}_P{}^*\right)_f, \tag{4.105}$$

enables to calculate the pressure equation (compare to equation 4.102):

$$\sum_f \mathbf{S}_f \bullet \left[\left(\frac{1}{\mathcal{A}^*}\right)_f (\nabla p)_f\right] \stackrel{!}{=} \sum_f F^*. \tag{4.106}$$

Note that the r.h.s. of equation 4.106 is treated explicitly, when the pressure equation is formed and solved. This results in a new pressure field p^{**}.

assembly of conservative fluxes This step comprises the creation of the flux from the solution of the pressure equation:

$$F^{**} = F^* - \frac{1}{\left(\mathcal{A}^*\right)_f} \nabla_f^{\perp} p^{**} \tag{4.107}$$

Note that in order to arrive at conservative fluxes the assembly of the flux *must be completely consistent* with that of the pressure equation[3]. E.g., the last term of the r.h.s. of equation 4.107 for the flux appears when discretizing the l.h.s. of the pressure equation 4.106 and reads for othogonal meshes:

$$\left(\frac{1}{\mathcal{A}^*}\right)_f \mathbf{S}_f \bullet (\nabla p)_f = \left(\frac{1}{\mathcal{A}^*}\right)_f \frac{|\mathbf{S}_f|}{|\mathbf{d}|} (p_N - p_P). \tag{4.108}$$

Note that the pressure laplacian-term is calculated by use of Gauss' theorem. Thus, the calculation comprises the evaluation of the face-normal pressure gradient in terms of cell-centered pressure values.

[3] including non-orthogonal correction when discretizing the pressure laplacian, i.e., the l.h.s. of the pressure equation 4.106

explicit velocity correction Next an *explicit velocity correction* is performed, in which the new velocities are obtained from the approximative velocity field $\mathbf{U}_P{}^*$ using the corrected pressure gradient ∇p^{**}:

$$\mathbf{U}_P{}^{**} = \mathbf{U}_P{}^* - \frac{\nabla p^{**}}{\mathcal{A}^*}. \tag{4.109}$$

Note that the gradient calculation is accomplished using Gauss' theorem. Thus, only face-interpolated pressure values are necessary.

Comparing the r.h.s. 's of the equations 4.100 and 4.104 reveals, that up to now it has been inherently assumed that the entire velocity error stems from the pressure term. However, as the r.h.s. of equation 4.104 (as it is assembled) yields the approximative velocity field $\mathbf{U}_P{}^*$, which does not obey continuity, this assumption is not true and another iteration is to be established beginning from the pressure correction step until a pre-set tolerance is met.

Summarizing, the PISO algorithm along with the interpolation practice according to Rhie and Chow is characterized by:

1.) an approximative velocity field $\mathbf{U}_P{}^*$, which does not obey continuity and does not involve any pressure contribution. This approximative velocity field is considered constant during the pressure calculation.

2.) the conservative fluxes and the pressure gradient, being related to each other. In doing so, the continuity equation has effectively been transformed into a Poisson equation for pressure. The solution of this elliptic equation results in a new pressure field, that can be used as initial guess for subsequent steps.

Steps of the PISO Algorithm (two-phase system) Essentially, the PISO solution procedure follows the above steps also for the two-fluid methodology. However, special attention needs to be paid to the so-called Rhie-Chow error, that manifests itself in a continuity error due to the Rhie-Chow interpolation practice, which imperatively needs to be minimized in order to ensure stability of the numerical solution procedure. Otherwise this error causes unphysical behavior of the solution, i.e., oscillations of the pressure field, spurious currents etc. It can be shown [16] that the Rhie-Chow error is small provided that the pressure field is sufficiently smooth – i.e., in the absence of discontinuities in both the pressure and the pressure gradient.

Hence, an enhanced Rhie-Chow treatment becomes necessary. E.g., we might want to exclude those force densities already from the momentum predictor, that strongly vary or are subject to abrupt changes, as these body forces necessarily would have to be balanced by the pressure gradient. Thus, discontinuous body forces are to be treated on the cell faces and reintroduced again when explicitly reconstructing the cell-centered velocities. In doing so, the pressure gradient ∇p is effectively replaced

by a smooth substitute $\widetilde{\nabla p}$ in the pressure equation. This practice can be described best exemplary examining the buoyancy force, which for buoyant two-phase scenarios of segregated type would have to be balanced by the pressure gradient in the absence of flow and interfacial curvature:

$$\frac{\nabla \overline{p}}{\overline{\rho}^{\varphi}} = \mathbf{g}. \tag{4.110}$$

Eliminating the hydrostatic pressure $\rho \mathbf{g}_{\bullet}\mathbf{x}$ from the mixture pressure $\overline{p}$ yields a modified pressure p_d, which exhibits a smooth gradient across the interface. Hence, the l.h.s. of equation 4.110 can be re-formulated as

$$\frac{\nabla \overline{p}}{\overline{\rho}^{\varphi}} = \frac{\nabla p_d}{\overline{\rho}^{\varphi}} + \frac{1}{\overline{\rho}^{\varphi}} \underbrace{\left(\rho \mathbf{g} + \mathbf{g}_{\bullet}\mathbf{x} \nabla \rho\right)}_{=\nabla(\rho \mathbf{g}_{\bullet}\mathbf{x})}. \tag{4.111}$$

Substituting equation 4.111 into the momentum equation results in the following pressure and buoyancy terms on its r.h.s. :

$$-\frac{\nabla p_d}{\overline{\rho}^{\varphi}} + \left(1 - \frac{\rho}{\overline{\rho}^{\varphi}}\right) \mathbf{g} - \frac{\mathbf{g}_{\bullet}\mathbf{x}}{\overline{\rho}^{\varphi}} \nabla \rho. \tag{4.112}$$

Summarizing, the steps of the PISO algorithm for the two-fluid methodology read:

momentum predictor step The phase momentum predictor step comprises the decomposition of the equation system into $\mathcal{A}$- and $\boldsymbol{\mathcal{H}}$-parts, respectively. However, the buoyancy term, the explicit part of the drag term and force densities being proportional to the gradient of the volumetric phase fraction have been excluded.

The approximative phase velocities read[4]

$$\overline{\mathbf{U}}^{\varphi *} = \frac{\boldsymbol{\mathcal{H}}_{\varphi}{}^{*}}{\mathcal{A}_{\varphi}{}^{*}} \qquad \text{and} \qquad \overline{\mathbf{U}}^{\phi *} = \frac{\boldsymbol{\mathcal{H}}_{\phi}{}^{*}}{\mathcal{A}_{\phi}{}^{*}} \tag{4.113}$$

pressure correction step The approximative fluxes (flux predictor) are obtained from the approximative velocities using central differencing:

$$\begin{aligned} F_{\varphi}{}^{*} = \mathbf{S}_f \bullet \left(\overline{\mathbf{U}}^{\varphi *}\right)_f &+ \left(\frac{A_{\varphi,h}}{\alpha_{\varphi}\, \overline{\rho}^{\varphi} \mathcal{A}_{\varphi}}\right)_f F_{\phi} \\ &+ \left(\frac{1 - \rho/\,\overline{\rho}^{\varphi}}{\mathcal{A}_{\varphi}}\right)_f \mathbf{S}_f \bullet \mathbf{g} - \left(\frac{1}{\mathcal{A}_{\varphi}}\right)_f (\mathbf{g}_{\bullet}\mathbf{x})_f \, |\mathbf{S}_f| \nabla_f^{\perp} \rho \\ &+ \left(\frac{1}{\overline{\rho}^{\varphi} \mathcal{A}_{\varphi}}\right)_f \left(\frac{A_{\varphi,p}}{\alpha_{\varphi}}\right)_f |\mathbf{S}_f| \nabla_f^{\perp} \alpha_{\varphi} + \left(\frac{1}{\overline{\rho}^{\varphi} \mathcal{A}_{\varphi}}\right)_f \left(\frac{A_{\varphi,\sigma}}{\alpha_{\varphi}}\right)_f |\mathbf{S}_f| \nabla_f^{\perp} \alpha_{\varphi}, \end{aligned} \tag{4.114}$$

[4] Note that P as a subscript has been dropped for readability.

where $A_{\varphi,h}$, $A_{\varphi,p}$ and $A_{\varphi,\sigma}$ are multipliers being defined as provided by table 3.2. Consequently, it is for phase ϕ:

$$\begin{aligned} {F_\phi}^* = \mathbf{S}_f \bullet \left(\overline{\mathbf{U}}^{\phi\,*} \right)_f + \left(\frac{A_{\phi,h}}{\alpha_\phi \, \overline{\rho}^\phi \mathcal{A}_\phi} \right)_f F_\varphi \\ + \left(\frac{1 - \rho / \, \overline{\rho}^\phi}{\mathcal{A}_\phi} \right)_f \mathbf{S}_f \bullet \mathbf{g} - \left(\frac{1}{\mathcal{A}_\phi} \right)_f (\mathbf{g} \bullet \mathbf{x})_f \, |\mathbf{S}_f| \nabla_f^\perp \rho \\ + \left(\frac{1}{\overline{\rho}^\phi \mathcal{A}_\phi} \right)_f \left(\frac{A_{\phi,p}}{\alpha_\phi} \right)_f |\mathbf{S}_f| \nabla_f^\perp \alpha_\phi + \left(\frac{1}{\overline{\rho}^\phi \mathcal{A}_\phi} \right)_f \left(\frac{A_{\phi,\sigma}}{\alpha_\phi} \right)_f |\mathbf{S}_f| \nabla_f^\perp \alpha_\phi. \end{aligned} \tag{4.115}$$

The total volumetric face flux is expressed straightforward as

$$F^* = \sum_{k=\varphi,\phi} \alpha_{k,f} \, {F_k}^* \tag{4.116}$$

Since the single-field assumption has been adopted, we solve for one (mixture) pressure that is shared by both phases. Thus, the pressure equation as a recast of the continuity equation reads

$$\sum_f \mathbf{S}_f \bullet \left[\left(\sum_{k=\varphi,\phi} \alpha_{k,f} \left(\frac{1}{\overline{\rho}^k \mathcal{A}_k} \right)_f \right) (\nabla p)_f \right] = \sum_f F^*. \tag{4.117}$$

assembly of conservative fluxes The volumetric face fluxes are updated underlying the solution of the pressure equation:

$$\begin{aligned} {F_\varphi}^{**} &= {F_\varphi}^* - \frac{\frac{1}{\overline{\rho}^\varphi (\mathcal{A}_\varphi)_f}}{\sum_{k=\varphi,\phi} \frac{\alpha_{k,f}}{\overline{\rho}^k (\mathcal{A}_k)_f}} |\mathbf{S}_f| \nabla_f^\perp p^{**} \\ {F_\phi}^{**} &= {F_\phi}^* - \frac{\frac{1}{\overline{\rho}^\phi (\mathcal{A}_\phi)_f}}{\sum_{k=\varphi,\phi} \frac{\alpha_{k,f}}{\overline{\rho}^k (\mathcal{A}_k)_f}} |\mathbf{S}_f| \nabla_f^\perp p^{**}. \end{aligned} \tag{4.118}$$

Next, the conservative total volumetric face flux is calculated as

$$F^{**} = \sum_{k=\varphi,\phi} \alpha_{k,f} \, {F_k}^{**}. \tag{4.119}$$

explicit velocity correction The phase velocities $\overline{\mathbf{U}}^\varphi$ and $\overline{\mathbf{U}}^\phi$ are obtained from the conservative volumetric phase fluxes using an explicit reconstruction procedure that is based on least-square evaluation. For consistency, all contributions that

have been considered critical and thus have been excluded from the Rhie-Chow formula are taken into account in this step.

Eventually, the volumetric mixture velocity is evaluated:

$$\mathbf{U} = \alpha_\varphi \, \overline{\mathbf{U}}^{\varphi} + \alpha_\phi \, \overline{\mathbf{U}}^{\phi}. \tag{4.120}$$

References

[1] H. G. Weller, G. Tabor, H. Jasak, and C. Fureby. A tensorial approach to computational continuum mechanics using object orientated techniques. *Comput. Phys.*, 12(6):620–631, 1998. 97

[2] H. Jasak, A. Jemcov, and Ž Tuković. OpenFOAM: A C++ library for complex physics simulations. In *International Workshop on Coupled Methods in Numerical Dynamics IUC*, Dubrovnik, Croatia, September, 19-21 2007. 97

[3] H. Jasak. *Error Analysis and Estimation in the Finite Volume Method with Applications to Fluid Flows*. PhD thesis, Imperial College of Science, Technology & Medicine, 1996. 101, 103, 108

[4] B. P. Leonard. Simple high-accuracy resolution program for convective modelling of discontinuities. *Int. J. Num. Meth. Fluids*, 8:1291–1318, 1988. 103

[5] P. H. Gaskell and A. K. C. Lau. Curvature-compensated convective transport: SMART, a new boundedness-preserving transport algorithm. *Int. J. Num. Meth. Fluids*, 8:617–641, 1988. 103

[6] H. Jasak, H. G. Weller, and A. D. Gosman. High resolution NVD differencing scheme for arbitrarily unstructured meshes. *Int. J. Numer. Meth. Fluids*, 31:431–449, 1999. 104, 105

[7] H. Jasak and H. G. Weller. Interface-Tracking Capabilities of the InterGamma Differencing Scheme. Internal Report, CFD research group, Imperial College, London, February 1995. 104, 105

[8] S. V. Patankar. *Numerical Heat Transfer And Fluid Flow*. Series in computational methods in mechanics and thermal sciences. Taylor & Francis, Bristol, PA, 1980. 106

[9] D. B. Kothe. Perspective on Eulerian Finite-Volume Methods for incompressible interfacial flows. In *Free Surface Flows*, volume 88 of *CISM courses and lectures*, pages 267–331. Kuhlmann and Rath, H., 1999. 106

[10] E. de Villiers. *The Potential of Large Eddy Simulation for the Modeling of Wall Bounded Flows*. PhD thesis, Imperial College of Science, Technology & Medicine, 2006. 108

[11] F. Juretic. *Error Analysis in Finite Volume CFD*. PhD thesis, Imperial College of Science, Technology & Medicine, 2004. 112

[12] H. G. Weller. Derivation, Modeling and Solution of the Conditionally Averaged Two-Phase Flow Equations. Technical report, OpenCFD Limited, 2005. 114, 119, 122

[13] H. Rusche. *Computational Fluid Dynamics of Dispersed Two-Phase Flows at High Phase Fractions*. PhD thesis, Imperial College of Science, Technology & Medicine, 2002. 114

[14] H. G. Weller. A New Approach to VOF-based Interface Capturing Methods for Incompressible and Compressible Flow. Technical report, OpenCFD Limited, 2006. 118

[15] G. Tabor and H. Rusche. Algorithm Development – Multiphase Flow. Technical Report III-3 (Draft), BRITE/EuRam Project, 1998. 118, 119, 122

[16] S. Zhang and X. Zhao. General formulation for Rhie-Chow interpolation. In *Proceedings of HT-FED04*, 2004. 2004 ASME Heat Transfer/Fluids Engineering Summer Conf. 123, 131

[17] M. R. Hestens and E. L. Steifel. Method of conjugate gradients for solving linear systems. *J. Research*, 19:409–436, 1952. 127

[18] D. A. H. Jacobs. Preconditioned Conjugate Gradient Methods for Solving Systems of Algebraic Equations. Technical Report RD/L/N193/80, Central Electricity Research Laboratories, 1980. 127

[19] H. A. van der Vorst. Bi-CGSTAB: A fast and smoothly converging variant of Bi-CG for the solution of nonsymmetric linear systems. *SIAM J. Sci. Comput.*, 13(2):631–644, 1992. 127

[20] J. M. Weiss, J. P. Maruszewski, and W. A. Smith. Implicit solution of preconditioned Navier-Stokes equations using algebraic multigrid. *AIAA Journal*, 37(1):29–36, 1999. 127

[21] D. P. Hill. *The Computer Simulation of Dispersed Two-Phase Flows*. PhD thesis, Imperial College of Science, Technology & Medicine, 1998. 127

[22] R. I. Issa. Solution of the implicitly discretized fluid flow equations by operator-splitting. *J. Comp. Phys.*, 62:40–65, 1986. 127

[23] C. M. Rhie and W. L. Chow. A numerical study of the turbulent flow past an isolated airfoil with trailing edge separation. *AIAA J.*, 21(11):1525–1532, 1983. 128

Results & Publications

5

Numerical Simulation of dispersed Gas-Liquid Flows in Bubble Columns at high Gas Phase Fractions using OpenFOAM® – Part I: Modeling Basics

Abstract

Various chemical products are synthesized in processes using gas/liquid reactors with bubbly flows. Hence, there is a significant interest in a more efficient process design as well as in process intensification with a strong focus on this reactor class. However, the design of industrial gas/liquid reactors requires more detailed information about the flow structures and characteristics of two- or multiphase systems. The basic models for two-fluid model simulations of dispersed gas/liquid flows in bubble columns at high gas fractions are presented.

5.1. Introduction

Computational Fluid Dynamics (CFD) provides an efficient way to examine fluid dynamic phenomena within the interior of chemical reactors on the basis of numerical simulations. This *virtual prototyping* (virtual numerical experiments) aims at both the clarification of physical interrelations and the reliable and efficient prediction of complex flow phenomena in multiphase systems, as they are found in process and chemical engineering apparatus.

Crucial parameters for process design – concerning both fluid dynamics and reaction engineering aspects of bubble column operation – are found to be the interfacial area density as well as the velocities, flow patterns and mixing characteristics evolving in the interior of the reactor [1–3].

Considering its basic cylindrical geometry, the design of a bubble column reactor is certainly a simple one. For the ease of phase separation, the design of the column features a widened cross-section in the upper part. However, albeit the design appears to be simple, the two-phase flow within the interior of bubble columns turns out to be very complex: the phase velocities, volumetric phase fractions, turbulence properties and the flow structure (topology) are characterized by both spatial and temporal scales that inherently differ by orders of magnitude. This depends on the particular operation mode (co-current vs. counter-current flow and superficial gas velocity) and design (gas sparger and aspect ratio) of the column.

5.1.1. State-of-the-Art

Flow Regimes in Bubble Columns

For a fixed geometry (aspect ratio), the flow regime in bubble columns is basically determined by the superficial gas velocity. In general, there are three regimes to be distinguished [4]:

homogeneous flow regime At low superficial gas velocities the flow within bubble columns is characterized by an approximately uniform bubble distribution. The bubble swarm moves upwards through the liquid with a constant rising velocity. The bubble size distribution is found to be narrow and monomodal. It solely depends on the choice of the gas sparger. Any interactions between bubbles such as coalescence and break-up are negligible.

heterogeneous flow regime Transition into the heterogeneous flow regime occurs when increasing the superficial gas velocity [5]. This regime is characterized by

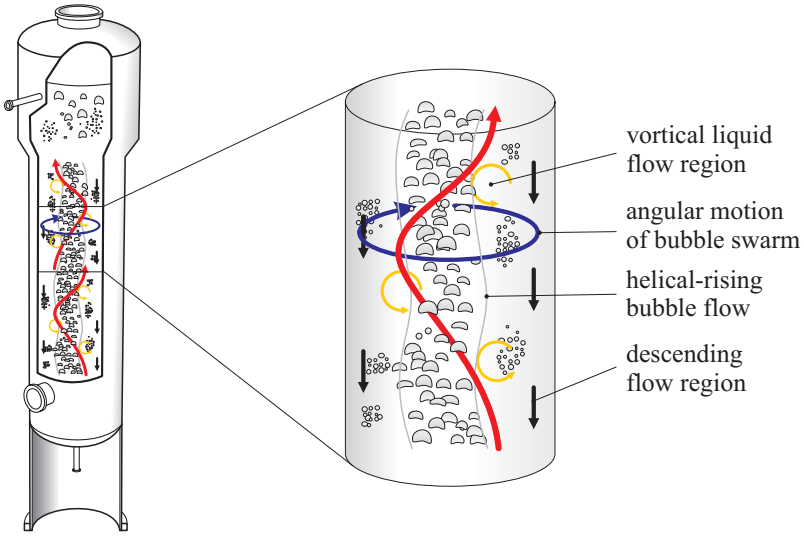

Figure 5.1: Characteristic flow pattern in a bubble column.

bubbles of quite different size and form, high gas-fractions and interactions between bubbles and vortical liquid flow regions [6].

slug flow regime At high superficial gas velocities and for high column aspect ratios the slug flow regime is observed. This regime possesses large gas compartments, i.e., large bubbles rising intermittently through the column while spanning its entire cross-section. For this reason, the slug flow regime is an undesired operation mode, being usually omitted in practice. The liquid-rich regions in between large bubbles, which are commonly entitled liquid slugs, are rising through the column at high velocities as well.

Figure 5.1 shows a typical flow pattern in bubble columns during operation within the heterogeneous flow regime [3, 7, 8]: a swarm of large bubbles rises along helical trajectories around the center line of the column. Vortical flow structures are observed in regions between the centrally rising swarm and the wall of the column. These vortical structures are found to entrain small bubbles, hindering their rise to some extent. On the other side, the liquid phase flows downwards near the wall. This is owed to continuity, as large bubbles generally entrain parts of the liquid phase near the center line of the column; these parts in turn need to be passed downwards again. Hence, a large-scale flow pattern within the liquid phase is observed which is owed to the requirement of continuity, while the dispersed gas phase largely rises along helical trajectories within a central bubble plume [9, 10].

Important aspects of process design are the interfacial area density available for species and mass transfer and the mixing of the liquid phase.

Usually *dispersion* is defined as a stochastic mixing process, which causes gradients of intensive quantities (such as concentration and temperature) to decrease [9]. In general, the dispersion within one phase is inherently influenced by the presence of the second phase within a two-phase bubbly flow. Moreover, both macroscopic (channel formations, dead zones, large flow patterns) and microscopic (turbulent fluctuation within the liquid phase) effects affect dispersion [3]. However, despite of this complex interplay in bubble columns, that is already observed for only two phases, the axial back-mixing as a prevalent design parameter can be characterized by the axial dispersion coefficient for the liquid phase. This coefficient can even be correlated with basic data of operation: the diameter of the column, the gas hold-up, the superficial gas velocity and the mean rise velocity of the gaseous phase [11].

Numerical Simulation of the Flow in Bubble Columns

There are various CFD approaches to describe two-phase flows. However, these differ as to both their spatial resolution and their applicability when facing cases of practical interest.

Basically, one can distinguish between two CFD approaches that adequately capture the flow in bubble columns [12–14]: the two-fluid model [15] (often also called Eulerian-Eulerian method) and particle-based methods (often called Eulerian-Lagrangian methods). Both approaches yield the same result – given that a sufficient discretization and adequate modeling has been adopted [12]. However, considering high gas fractions, particle-based methods suffer from high computational costs caused by likewise increasing inter-phase interactions, which need to be captured at these gas fractions [16,17]. For this reason, we shall restrict ourselves to the two-fluid model, which omits this disadvantage and thus is to be favored over particle-based methods. Two-fluid models are widely used and are among the most important approaches in the group of so-called *averaging methods*. These methods are certainly of significance for industry due to their ability to deal even with large-scale industrial flow domains and dispersed two-phase flows.

Early work has been devoted to the simulation of bubbly flows in bubble columns focusing on the problem of sufficiently modeling interfacial forces and turbulence. Further focus has been set upon appropriately capturing polydispersity in bubble swarms. Subsequent simulative studies have been performed in order to examine regime transition. An overview of these topics and corresponding correlations can be found in [18–26]. In the following a review covering two-fluid model based studies of two-phase flows in bubble columns is given.

Interfacial forces Sokolichin and Eigenberger [27] and Becker et al. [28] have employed a simplified momentum balance for the gaseous phase, solely accounting for the drag force along with a constant drag coefficient. However, both other bubble forces and bubble-bubble interactions have been neglected. Mudde and Simonin [29] have additionally modeled turbulence effects, causing the dispersion of a bubble swarm. In other studies this is considered by an explicit dispersion force [30].

Subsequent studies consider the relevance and modeling of another crucial bubble force as central topic of research: the so-called lateral lift force plays a central role for correctly describing the bubbly flow perpendicular to the main rising direction of the gas phase [31–33].

Turbulence For turbulence modeling, the standard $k-\epsilon$ model has initially been applied. This approach has been originally developed for turbulence modeling in single-phase flows and thus solely accounts for turbulence within the continuous liquid phase [28, 29, 34]. However, an excessive dampening of flow characteristics has been observed, which certainly is caused by the over-evaluation of the eddy viscosity in such approaches.

Recent studies employ enhanced $k-\epsilon$ models, in which either additional model terms account for the bubble-induced turbulence when calculating the eddy viscosity [35], or additional source terms are directly introduced into the governing equations of the $k-\epsilon$ model [1, 36]. Other methods are based upon a $k-\epsilon$ mixture model [37] or a two-phase $k-\epsilon$ model [38, 39]. Both methodologies consistently take the form of the single-phase $k-\epsilon$ model when approaching the limiting case of pure phases (i.e., gas *or* liquid flow).

More sophisticated approaches are subject of ongoing scientific research. For instance, one of these approaches, which aims at turbulence modeling of bubbly flow within the framework of a two-fluid model, comprises the adaption of the Large Eddy Simulation (LES) concept [40, 41].

Polydispersity Similar progress has been achieved capturing the polydispersity, as it is typically found in bubble swarms. Initially, either one equivalent bubble diameter has been applied to all bubbles assuming monodispersity [1] or, alternatively, the bubble phase has been split up into two fractions providing two characteristic diameters [42] – a priori at the beginning of a simulation.

Recent approaches encompass the solution of additional transport equations: on the basis of mean bubble volumes, this enables to calculate a local characteristic mean diameter from the volumetric gas (bubble) fraction [43]. Taking into account different mechanisms for coalescence and break-up, this consideration leads to a small and large bubble fraction. Similarly, other studies adopt additional transport equations

for a mean bubble number density or interfacial area density in order to calculate the respective equivalent diameter [44–49].

In contrast to the aforementioned simplistic approaches, the full or simplified solution of population balance models remains to be mentioned as another modeling approach. One has to distinguish among class methods [40, 50–52], MUSIG (MUltiple SIze Group) models [53–56], the method of moments [57–60] and the Monte-Carlo method [52, 61].

Flow Regime Transition Each of the aforementioned studies cover partial aspects of modeling for the simulation of bubbly flows in bubble columns. However, they have been restricted to mostly one single flow regime. The scope of subsequent studies has been set upon the simulation of regime transition occurring in bubble columns. Regime transition criteria have been deduced from either the drift-flux approach [62, 63] or linear stability analysis [64–69] – focusing on the influence of the specific model choice and formulation.

5.1.2. Scope and Objectives

Since the two-fluid model is based on averaging, models are required taking into ac-count the following aspects:

- interfacial forces,
- turbulence at high gas fractions (incl. bubble induced turbulence),
- swarm effects in dense bubble swarms,
- polydispersity due to bubble coalescence and break-up in dense bubble swarms and
- mixing within the continuous liquid phase

Appropriate models to encounter these points have to be considered [70]: it is important to determine the underlying model parameters in a physically sound manner. In doing so, attention must be paid to the efficiency and stability of the numerical simulation procedure. Furthermore, realizability and reliability needs to be examined; thus, a validation study has to be performed.

This work [71] aims at the comprehensive simulation of both the fluid dynamics and liquid mixing characteristics in bubble column reactors at high gas phase fractions using CFD. In particular, solely models obeying the aforementioned requirements will be ultimately applied. This covers both the stability and efficiency as well as a conceptual proximity to the underlying two-fluid model.

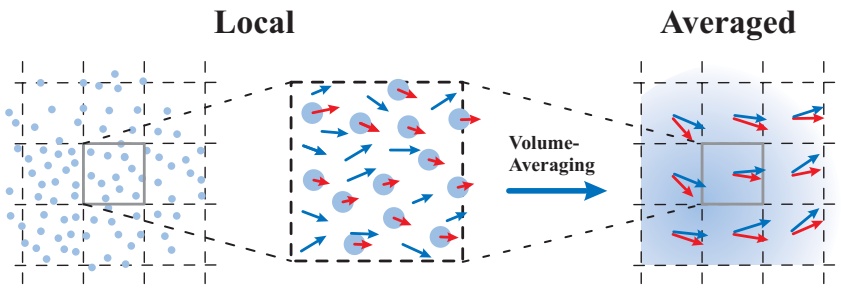

Figure 5.2: Concept of interpenetrating continua and principle of volume-averaging.

5.2. Modeling

One pivotal benefit of the two-fluid model is its use for the numerical simulation of flows in even large industrial-scale reactors at eligible computational costs. The reason for this is the model's capability to apply a quite rough spatial resolution of the flow domain. With the framework of a two-fluid model the present phases are considered as interacting and interpenetrating continua [15]. This principle is schematically illustrated in figure 5.2 [72]. However, as a consequence of the underlying averaging procedure, the flow structure and topology is not explicitly resolved. Therefore, additional modeling of so-called closure terms is required in order to fully describe a two-phase flow and subsequently solve a corresponding two-fluid model. These closure terms characterize the intensive interplay of both phases and thus their flow.

Closure modeling is commonly based upon empirical data, that depend on flow properties and parameters. Thus, in turn, the quality and the performance of a two-fluid CFD study significantly depend on the underlying closure models.

Presuming incompressible two-phase flow without phase change (i.e., evaporation or condensation), the following conservation equations have to be solved [27, 73]:

$$\frac{\partial \alpha_\varphi}{\partial t} + \nabla\bullet\left(\alpha_\varphi\,\overline{\mathbf{U}}^\varphi\right) = 0, \tag{5.1}$$

$$\begin{aligned}\frac{\partial \alpha_\varphi\,\overline{\mathbf{U}}^\varphi}{\partial t} &+ \nabla\bullet\left(\alpha_\varphi\,\overline{\mathbf{U}}^\varphi\,\overline{\mathbf{U}}^\varphi\right) + \nabla\bullet\left(\alpha_\varphi \mathbf{R}^\varphi_{\mathit{eff}}\right)\\ &= -\frac{\alpha_\varphi}{\overline{\rho}^\varphi}\nabla\,\overline{p}^\varphi + \alpha_\varphi \mathbf{g} + \frac{\sum \mathbf{F}_\varphi}{\overline{\rho}^\varphi}.\end{aligned} \tag{5.2}$$

Herein, α_φ and $\overline{\mathbf{U}}^\varphi$ denote the volumetric phase fraction and velocity of a phase φ with density $\overline{\rho}^\varphi$. $\mathbf{R}^\varphi_{\mathit{eff}}$ is the effective Reynolds stress tensor. The term $\sum \mathbf{F}_\varphi$

represents the sum of all interfacial forces and thus states the pivotal closure term taking into account the interfacial momentum transfer.

Generally, it is of no relevance within a two-fluid model framework, which phase actually takes the part of the continuous phase and which phase takes the one of the dispersed phase. However, since the term $\sum \mathbf{F}_\varphi$ in equation 5.2 depends on the particular structure of the interacting phases, it is necessary to distinguish the dispersed from the continuous phase for further modeling purposes.

Since this study focuses on bubbly flows, the gas (bubble) phase shall be denoted as $\varphi = a$ being consequently modeled as dispersed phase, whereas the continuous liquid phase is identified by $\varphi = b$.

5.2.1. Interfacial Interactions

The closure term $\sum \mathbf{F}_\varphi$ represents the sum of all interfacial forces and thus comprises the momentum transfer between both phases to be treated within the two-fluid model framework. In general two distinct categories are of interest:

- drag force and
- non-drag forces.

For bubbly flows the non-drag forces basically encompass the lateral lift force $\mathbf{F}_l$, the turbulent dispersion force $\mathbf{F}_{td}$ and the virtual mass force $\mathbf{F}_{vm}$. Consequently, the closure term results in

$$\sum \mathbf{F}_\varphi = \mathbf{F}_d + \mathbf{F}_l + \mathbf{F}_{vm} + \mathbf{F}_{td}. \tag{5.3}$$

The fluid dynamical origins of these forces are provided in table 5.1.

Figure 5.3 schematically summarizes the respective effects of interfacial forces within a bubbly flow scenario [74]. In the remainder the corresponding interfacial force models are described in detail, as they have been implemented and employed in the present study.

Drag force Within a two-fluid model the drag-force reads

$$\mathbf{F}_d = \frac{3}{4}\alpha_a C_d \frac{\overline{\rho}^b}{d_a} |\,\overline{\mathbf{U}}^b - \overline{\mathbf{U}}^a|\left(\overline{\mathbf{U}}^b - \overline{\mathbf{U}}^a\right). \tag{5.4}$$

The drag coefficient C_d herein is a function of the bubble Reynolds number:

$$Re \equiv \frac{d_a|\mathbf{U}_r|}{\nu_b}. \tag{5.5}$$

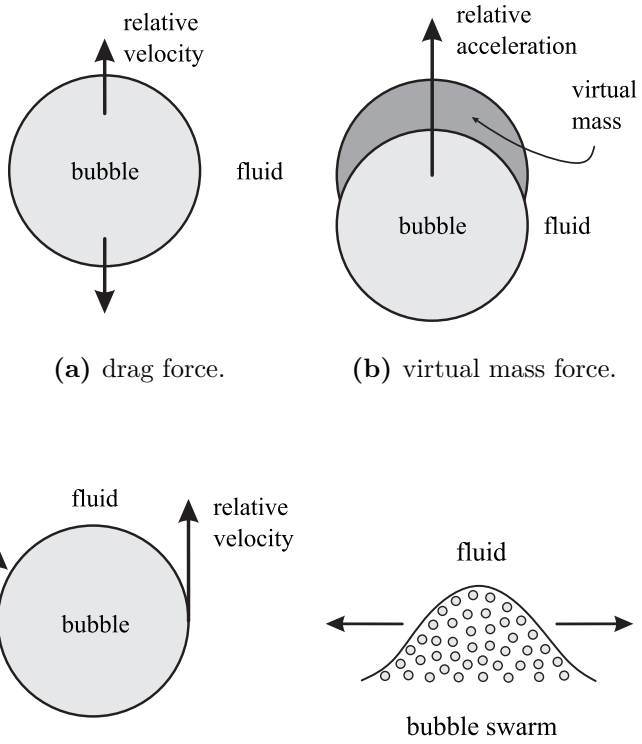

(a) drag force.

(b) virtual mass force.

(c) lateral lift force.

(d) turbulent dispersion force.

Figure 5.3: Interfacial forces in bubbly flows.

Table 5.1: Forces exerted on a fluid particle.

$\mathbf{F}_d$	The drag force acts on particles in case they move with a relative (slip) velocity $\mathbf{U}_r$ with respect to an underlying flow. Consequently a fluid particle is exerted to a resisting force which is opposed to the direction of its movement.
$\mathbf{F}_l$	The lateral lift force is a shear-induced force on the fluid particle due to a non-uniform incident flow of the continuous phase. For bubbly flows this is the most important non-drag force, since the lateral lift force acts perpendicular to the drag force. It crucially affects the evolution of typical bubbly flow characteristics.
$\mathbf{F}_{vm}$	The virtual mass force accounts for the effect that accelerating particles always entrain a certain amount of surrounding fluid.
$\mathbf{F}_{td}$	The turbulent dispersion force accounts for turbulent fluctuations in the flow field acting on the fluid particles. These turbulent eddies in the continuous phase usually tend to scatter the dispersed phase particles.

There are various models present in literature, aiming at the modeling of the drag co-efficient. Exemplary the correlations according to Schiller and Naumann [75] and Tomiyama [19] are provided below, as they were implemented as drag force models:

- Schiller and Naumann [75]
  Considering small spherical bubbles at low bubble Reynolds numbers, the drag coefficient C_d can be modeled by underlying the correlation according to Schiller and Naumann:

$$C_d = \begin{cases} \frac{24}{Re}\left(1 + 0.15Re^{0.687}\right) & Re \leq 1000 \\ 0.44 & Re > 1000. \end{cases} \tag{5.6}$$

  The deviation from the experimental standard drag curve is ±5% for bubble Reynolds numbers below 1000 [76].

- Tomiyama [19]
  In 1998 Tomiyama has published a correlation for the drag coefficient covering the effect of the bubble shapes as well as the contamination of the liquid phase.

$$C_d = \max\left[\min\left(\frac{A}{Re}\left(1 + 0.15Re^{0.687}\right), \frac{3A}{Re}\right), \frac{3}{8}\frac{Eo}{Eo+4}\right]. \tag{5.7}$$

Another dimensionless number, the Eötvös number Eo, is used in this correlation in order to account for the altering shape of large non-spherical bubbles, which affects the drag coefficient. The Eötvös number represents the ratio between buoyancy and surface tension force:

$$Eo \equiv \frac{\Delta\rho g d_a^2}{\sigma}. \tag{5.8}$$

The additional parameter A can be thought of a model parameter taking into account the effect of contamination in the continuous phase – and thus the contamination of the phase interface – on the drag coefficient of a single bubble. Tomiyama determined this parameter to be between $A = 16$ for a pure gas/liquid system (e.g., pure water and air bubbles) and $A = 24$ for a slightly contaminated system (air bubbles in tab water) [19, 77].

Non-drag forces

lateral lift force There are various model formulations, aiming at the description of the lateral lift force. The following is found to be widely used:

$$\mathbf{F}_l = \alpha_a \, \overline{\rho}^b C_l \left(\overline{\mathbf{U}}^b - \overline{\mathbf{U}}^a \right) \times \bar{\boldsymbol{\omega}}_b \qquad \text{with } \bar{\boldsymbol{\omega}}_b = \nabla \times \overline{\mathbf{U}}^b. \tag{5.9}$$

For the corresponding coefficient C_l again a multitude of models are available. Exemplary, the models according to Tomiyama [19] and [19] and Legendre & Magnaudet [78] are set out below.

- Tomiyama [19]

$$C_l = \begin{cases} \min \begin{cases} 0.288 tanh(0.121 Re) \\ 0.00105 Eo^3 - 0.0159 Eo^2 - 0.0204 Eo + 0.474 \end{cases} & Eo < 4 \\ 0.00105 Eo^3 - 0.0159 Eo^2 - 0.0204 Eo + 0.474 & 4 \leq Eo \leq 10 \\ -0.29 & Eo > 10. \end{cases} \tag{5.10}$$

This correlation has been published in 1998 for large bubbles in pipe flows. Currently it is one of the most used correlations – beside the use of a constant lift coefficient using $C_l = 0.5$. It is based upon experiments where trajectories of gas bubbles in shear flow have been evaluated. These measurement were persued in water/glycerine mixtures at various concentrations.

Evidently, the particular model correlation to evaluate the lift coefficient holds the Eötvös number as given by equation 5.8. Thus, the correlation

according to Tomiyama results in lift coefficients of $0 < C_l \leq 0.288$ for small bubbles and a negative value for large ones. From the above correlation a limiting diameter of 5.6 mm can be extracted for an air/water system, at which the lift coefficient changes its sign. In consequence, bubbles larger than 5.6 mm are moving towards the center line, while smaller bubbles move towards the wall of a bubble column.

However, it has to be noted, that this correlation should be applied with care when considering systems different from air/water. Tomiyama's experiments have been pursued using a glycerine/water mixture, the viscosity of which has exceeded the viscosity of pure water by far. Thus, the transfer of results to an air/water system has to be done by means of extrapolation.

- Legendre and Magnaudet [78]

$$C_l = \sqrt{\left(C_l^{\mathrm{low}Re}\right)^2 + \left(C_l^{\mathrm{high}Re}\right)^2} \tag{5.11}$$

$$\text{with} \qquad C_l^{\mathrm{low}Re} = \frac{6}{\pi^2}\left(ReSr\right)^{1/2} J(\epsilon)$$

$$C_l^{\mathrm{high}Re} = \frac{1}{2}\frac{1+16Re^{-1}}{1+29Re^{-1}}$$

$$Sr \equiv \frac{Re_\Delta}{Re},\ Re_\Delta \equiv \frac{\bar{\boldsymbol{\omega}}_b d_a^2}{\nu_b}$$

$$\epsilon \equiv \sqrt{\frac{Sr}{Re}} \text{ and } J(\epsilon) \equiv \frac{2.255}{\left(1+0.2\epsilon^{-2}\right)^{3/2}}.$$

In 1998 Legendre and Magnaudet have derived this correlation for a uniformly moving bubble in linear shear flow. This has been done by numerically solving the Navier-Stokes equations assuming a smooth and pure bubble surface, such that no particle rotation was induced.

The model has been found to be valid for $0.1 \leq Re \leq 500$ and for $0 \leq Sr \leq 1$.

turbulent dispersion force The turbulent dispersion force is usually introduced into the momentum balance by a term that is proportional to the gradient of the dispersed phase volume fraction. Examining the concrete model formulation, however, particularly the turbulent dispersion force models exhibit various forms. The following is found to be widely used [79]:

$$\mathbf{F}_{td} = C_{td}\,\overline{\rho}^b\,\overline{k}\,\nabla\alpha_a. \tag{5.12}$$

In the following, the dispersion coefficient C_{td} is assumed to be constant, taking a value between 0.1 and 1.0 [80]. Thus, the turbulent dispersion force is assumed

to be proportional to the product of the mean kinetic energy and the gradient of the volumetric gas phase fraction. In this work, the dispersion coefficient C_{td} is 0.1.

virtual mass force The virtual mass force is written in the form:

$$\mathbf{F}_{vm} = C_{vm}\alpha_a\,\overline{\rho}^b\left(\frac{D_a\,\overline{\mathbf{U}}^a}{Dt} - \frac{D_b\,\overline{\mathbf{U}}^b}{Dt}\right) \tag{5.13}$$

$$\text{with} \qquad \frac{D_i}{Dt} \equiv \frac{\partial}{\partial t} + \overline{\mathbf{U}}^i \bullet \nabla.$$

For spherical single bubbles the virtual mass force coefficient reads $C_{vm} = 0.5$ [81, 82]. For bubbles with altering shapes this value is usually found to be smaller. However, there are not many reliable correlations, which mostly have been stated to be the reason for neglecting the virtual mass force so far. Sokolichin and Eigenberger [83] propose a constant virtual mass force coefficient of $C_{vm} = 0.25$ for these bubbles with variable shapes.

However, Zhang [84] states that the effective influence of the virtual mass force coefficient in bubbly flows is rather small.

wall lubrication force At this point, the so-called wall lubrication force should be mentioned as well for completeness. This force has first been introduced by Antal et al. [85] in order to account for the repulsive effect, which bubbles are exerted to in the vicinity of the wall of the column as a consequence of an asymmetric incident flow near the wall boundary layer.

However, since models for the wall lubrication force are subject to various restrictions and constraints, it is neglected in the further course of this study. Instead of the wall lubrication force, its tantamount effect can be mimicked: in suspending the lateral lift force near walls, we achieve the expected increase of the gas phase fraction in vicinity of walls (wall peak).

5.2.2. Turbulence

For turbulent two-phase flows in bubble columns the governing equations 5.1 and 5.2 require further closure due to the turbulent contribution to the stress tensor.

The standard $k-\epsilon$ model approach – even though it is commonly applied and widely used – fails, since it solely considers the turbulence (turbulence fluctuations) within the liquid phase: the standard model is usually extended by a simple additional term, aiming to incorporate the turbulence induced by bubbles in their wake. The model failure can be assigned to the fact, that with increasing gas phase fractions

the turbulent fluctuations can no longer be assumed to be dominated by the liquid phase.

For this reason, we adopted the so-called 'basic-mixture turbulence model' according to Rusche [37,86] in the present study. The turbulent kinetic energy $\overline{k}$ and dissipation $\overline{\epsilon}$ are considered as mixture quantities:

$$\frac{\partial \overline{k}}{\partial t} + \nabla\bullet\left(\mathbf{U}\,\overline{k}\right) - \nabla\bullet\left(\frac{\nu_t}{\sigma_k}\nabla\,\overline{k}\right) = P - \overline{\epsilon}\,, \tag{5.14}$$

$$\frac{\partial \overline{\epsilon}}{\partial t} + \nabla\bullet\left(\mathbf{U}\,\overline{\epsilon}\right) - \nabla\bullet\left(\frac{\nu_t}{\sigma_\epsilon}\nabla\,\overline{\epsilon}\right) = \frac{\overline{\epsilon}}{\overline{k}}\left(C_1 P - C_2\,\overline{\epsilon}\right), \tag{5.15}$$

where the turbulent viscosity can be evaluated according to equation 5.16.

$$\nu_t = C_\mu \frac{\overline{k}^{\,2}}{\overline{\epsilon}}. \tag{5.16}$$

The model parameters are given in table 5.2.

Table 5.2: Coefficients of the basic-mixture turbulence model.

C_μ	C_1	C_2	σ_k	σ_ϵ
0.09	1.44	1.92	1.00	1.30

5.2.3. Swarm Effects

The issue of 'swarm effects' has to be addressed for cases, where correlations are generally valid for single bubbles, but fail for bubble swarms. This becomes more significant for high volumetric phase fractions of the dispersed phase. In this case single bubble correlations have to be corrected.

Throughout this work we corrected the coefficients pertaining to the drag force [87–93], the lateral lift force [94] and the virtual mass force [95]. This is accomplished by use of a pre-factor being a function of the volumetric phase fraction α_a. Illustratively, this approach can be demonstrated for the drag force coefficient, for instance, in which the well known swarm correction according to Richardson and Zaki [87] applies:

$$C_{d,s} = C_d\, f\left(\alpha_a\right) \qquad \text{with } f\left(\alpha_a\right) = \frac{1}{\left(1-\alpha_a\right)^m}, \tag{5.17}$$

where m denotes the so-called swarm exponent, which depends on the flow conditions based on the bubble Reynolds number provided in equation 5.5. For laminar

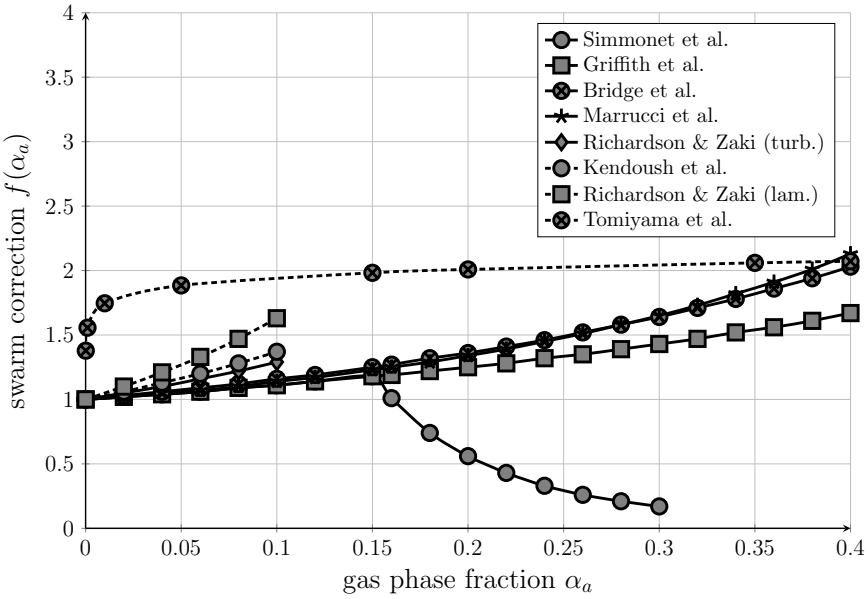

Figure 5.4: Swarm correction for the drag force coefficient.

conditions $m = 4.65$, whereas for a developed turbulent flow $m = 2.39$ is found to be valid. Generally,

$$m = \begin{cases} 4.65 & Re \leq 0.2 \\ \frac{4.35}{Re^{0.03}} & 0.2 < Re \leq 1 \\ \frac{4.45}{Re^{0.1}} & 1 < Re \leq 500 \\ 2.39 & 500 < Re \end{cases}. \tag{5.18}$$

Admittedly there is usually a significant uncertainty of the applicability of swarm corrections – especially for the numerical simulation of dense bubbly flows employing the two-fluid model [96]. In figure 5.4 results for various correlations are depicted, all of which are claiming to account for the swarm effect on the drag force coefficient by use of a pre-factor. However, employing these correlation is in the strict sense only justified for cases, where both the (usually different) ranges of validity and the under-lying model assumptions are found to be fulfilled. For instance, the correlation according to Richardson and Zaki is solely valid for a system comprising rigid particles. Evidently, this assumption is no longer valid for bubble flows at high local gas phase fractions.

5.2.4. Polydispersity

Capturing polydispersity within gas/liquid flows at high gas phase fraction (heterogeneous flow regime) in bubble columns plays another crucial role within a numerical

solution procedure: at high bubble densities the phase contact is typically very intensive. In consequence, bubble coalescence and break-up are observed, which leads to a polydisperse bubble size distribution.

In general, different approaches can be chosen for modeling. In general, bubble population balances are widely used. The disperse system is split up into bubble size classes, for each of which one transport equation needs to be solved.

In the framework of the present study, we applied both the concept of a mean interfacial area density (IATE[1]) according to Kocamustafaogullari, Ishii and Hibiki [44–46] and Mewes, Lehr and Millies [47, 48], as well as Reyes' concept of a mean bubble number density [49] ([2], according to [97, 98]). The major advantage of these concepts is based on the fact, that only one additional transport equation – either for the interfacial area density a_i or the bubble number density n – needs to be solved:

$$\frac{\partial a_i}{\partial t} + \nabla_\bullet \left(a_i \, \overline{\mathbf{U}}_{a_i} \right) = \overline{\Phi}_{a_i}, \tag{5.19}$$

$$\frac{\partial n}{\partial t} + \nabla_\bullet \left(n_i \, \overline{\mathbf{U}}_{n} \right) = \overline{\Phi}_{n}. \tag{5.20}$$

Within a two-fluid model the convection of the interfacial area density and the bubble number density is accomplished in terms of their corresponding transport velocities, $\overline{\mathbf{U}}_{a_i}$ and $\overline{\mathbf{U}}_{n}$ respectively. Advantageously, these are usually modeled as $\overline{\mathbf{U}}_{a_i} = \overline{\mathbf{U}}_{n} = \overline{\mathbf{U}}^{a}$. The source terms $\overline{\Phi}_{a_i}$ and $\overline{\Phi}_{n}$ account for the change in the mean interfacial area density resp. bubble number density due to the mean of coalescence and break-up events being observable. As depicted in figure 5.5, there are basically three mechanisms to be considered. Hence, the source terms take the final form: $\overline{\Phi} = \overline{\Phi}_{TI} + \overline{\Phi}_{RC} + \overline{\Phi}_{WE}$ [99].

In particular the effects as given in table 5.3 are considered.

The interfacial area density and the bubble number density are related to each other according to equation 5.21, which relies on a known shape factor Ψ (assuming solely spherical bubbles, for instance):

$$n = \Psi \left(\frac{a_i^3}{\alpha_a^2} \right), \qquad \text{where} \qquad \Psi \equiv \frac{1}{36\pi}. \tag{5.21}$$

Furthermore, a local equivalent diameter d_a can be evaluated from the local volumetric gas fraction α_a. This diameter *representatively* accounts for the bubble size distribution (local polydispersity) by means of *a single* diameter (global polydispersity) [100]:

[1] IATE: Interfacial Area Transport Equation
[2] ABND: Averaged Bubble Number Density

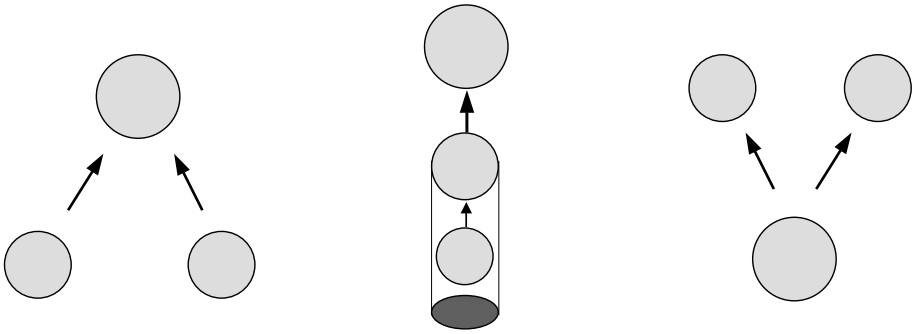

(a) random collision.

(b) wake entrainment.

(c) turbulent impact.

Figure 5.5: Basic bubble coalescence and break-up mechanisms.

Table 5.3: Bubble coalescence and break-up sources.

$\overline{\Phi}_{RC}$	mean effect of random collisions (RC) due to fluctuating bubbles
$\overline{\Phi}_{WE}$	mean effect of wake entrainment (WE), accounting for small bubbles being entrained and accelerated in the wake of larger bubbles. In consequence, these small bubbles might catch up leading to coalescence with larger ones
$\overline{\Phi}_{TI}$	mean effect of turbulence induced bubble break-up due to turbulent impact (TI) of bubbles with eddies in the turbulent liquid phase

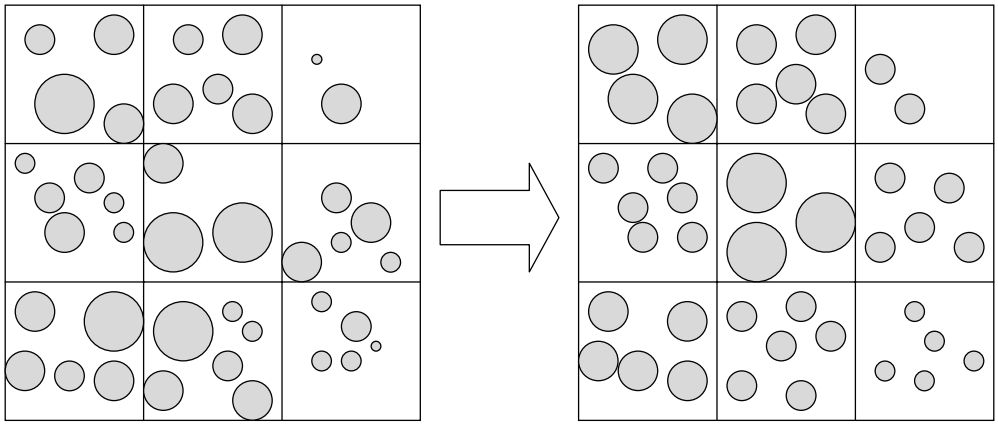

Figure 5.6: Principle of local vs. global polydispersity.

$$d_a \equiv d_{30,a} = \sqrt[3]{\frac{6\alpha_a}{n\pi}}. \tag{5.22}$$

This (paradigm) shift from local to global polydispersity is illustrated in figure 5.6.

5.2.5. Mixing

In order to capture the phenomenon of macro-mixing within the continuous phase, virtual tracer experiments are considered. For this purpose, we introduce and solve another scalar transport equation for a tracer concentration c in the liquid phase:

$$\frac{\partial \phi_c}{\partial t} + \nabla\bullet\left(\phi_c\,\overline{\mathbf{U}}^b\right) - \nabla\bullet\left(\alpha_b\left(D_c + D_c^t\right)\nabla c\right) = \Phi_c. \tag{5.23}$$

Herein $\phi_c = \alpha_b c$ denotes the total amount of tracer in the continuous phase. D_c and D_c^t represent the transport coefficients for molecular and turbulent diffusion, respectively. The latter is modeled as $D_c^t = \nu_t / Sc_t$, which can be deduced from the analogy of momentum and mass (chemical species) transfer. Herein the turbulence Schmidt number is assumed to be $Sc_t = 0.3$.

In this simulative study the source term Φ_c is used to accomplish a tracer unit step-injection. This imposes a unit or Heaviside step, which is well-known in Residence-Time-Distribution (RTD) studies. Subsequently – after the tracer has been injected near the liquid surface – we examine the tracer distribution and its temporal evolution of the tracer concentration field.

5.3. Summary

For the simulation of gas/liquid flows in large industrial-scale bubble columns, the two-fluid model has proven to be an appropriate and notable tool due to its beneficial assumptions. However, prior to its adoption, various effects in dense bubble swarms need to be considered first. This has to be done by means of appropriate and physically sound modeling.

In order to capture the two-phase flow correctly, it is important to examine interfacial forces, turbulence, swarm effects and polydispersity (inter alia). The first part of this contribution sets out the detailed modeling of dense bubble swarms in bubble columns by use of the two-fluid model. The subsequent second part – *Numerical Simulation and Results* – focuses on quality and performance of the CFD simulation when the introduced basic model approaches for bubbly flows in bubble columns are applied.

5.A. References

[1] J. Sanyal, S. Vásquez, S. Roy, and M. P. Dudukovic. Numerical simulation of gas-liquid dynamics in cylindrical bubble column reactors. *Chem. Eng. Sci.*, 54(21):5071–5083, 1999. 138, 141

[2] J. B. Joshi. Computational flow modelling and design of bubble column reactors. *Chem. Eng. Sci.*, 56(21-22):5893–5933, 2001. 138

[3] D. Wiemann. *Numerisches Berechnen der Strömungs- und Konzentrationsfelder in zwei- und dreiphasig betriebenen Blasensäulen*. PhD thesis, Universität Hannover, 2005. 138, 139, 140

[4] J. Zahradník, M. Fialová, M. Ruzicka, J. Drahos, F. Kastánek, and N. H. Thomas. Duality of the gas-liquid flow regimes in bubble column reactors. *Chem. Eng. Sci.*, 52(21-22):3811–3826, 1997. Gas-Liquid-Solid Reactor Engineering. 138

[5] Y. Shah and W. D. Deckwer. Hydrodynamics of bubble columns. In N. P. Cheremisinoff and R. Gupta, editors, *Handbook of Fluids in Motion*, pages 583–620. Ann Arbor Science, Ann Arbor, Mich., 1983. 138

[6] R. C. Chen, J. Reese, and L.-S. Fan. Flow structure in a three-dimensional bubble column and three-phase fluidized bed. *AIChE J.*, 40(7):1093–1104, 1994. 139

[7] H. Marschall. Numerical Simulation of Bubble Column Reactors using a Hybrid Multiphase-CFD Approach. Posterpräsentation anlässlich der Konferenz Computational Fluid Dynamics in Chemical Reaction Engineering V, Whistler BC Kanada, 15.-20. Juni 2008. 139

[8] H. Marschall. Numerical Simulation of Bubble Column Reactors using a Hybrid Multiphase-CFD Approach. Vortrag anlässlich der Konferenz Computational Fluid Dynamics in Chemical Reaction Engineering V, Whistler BC Kanada, 15.-20. Juni 2008. 139

[9] W. D. Deckwer. *Reaktionstechnik in Blasensäulen*. Otto Salle, 1985. 139, 140

[10] G. Wild, S. Poncin, H.-Z. Li, and E. Olmos. Some aspects of the hydrodynamics of bubble columns. *Int. J. Chem. Reactor Eng.*, 1:1–36, 2003. 139

[11] J. B. Joshi. Axial mixing in multiphase contactors – An unified correlation. *Trans. I. Chem. Eng.*, 58:155–165, 1980. 140

[12] A. Sokolichin, G. Eigenberger, A. Lapin, and A. Lübert. Dynamic numerical simulation of gas-liquid two-phase flows Euler/Euler versus Euler/Lagrange. *Chem. Eng. Sci.*, 52(4):611–626, 1997. 140

[13] B. G. M. van Wachem and A. E. Almstedt. Methods for multiphase computational fluid dynamics. *Chem. Eng. J.*, 96(1-3):81–98, 2003. Festschrift Prof. Cor M. van den Bleek. 140

[14] V. V. Buwa, D. S. Deo, and V. V. Ranade. Modeling of gas-liquid flows in bubble columns: Experiments vs. Eulerian-Eulerian vs. Eulerian-Lagrangian simulations. *Int.*

J. Multiphase Flow, 32:864–885, 2006. 140

[15] M. Ishii. Two-fluid model for two-phase flow. *Multiphase. Sci. Tech.*, 5(1-4):1–63, 1990. 140, 143

[16] J. Schallenberg. *Modellierung von zwei- und dreiphasigen Strömungen in Blasensäulenreaktoren*. PhD thesis, Technische Universität Braunschweig, 2006. 140

[17] D. Zhang. *Eulerian Modeling of Reactive Gas-Liquid Flow in a Bubble Column*. PhD thesis, University Twente, 2007. 140

[18] H. A. Jakobsen, S. Grevskott, and H. F. Svendsen. Modeling of vertical bubble-driven flows. *Ind. Eng. Chem. Res.*, 36(10):4052–4074, October 1997. 140

[19] A. Tomiyama. Struggle with computional bubble dynamics. In *3rd Int. Conf. Multiphase Flow (1998), Lyon, France*, volume 1, pages 1–18, 1998. 140, 146, 147

[20] T. Frank. Entwicklung von CFD-Software zur Simulation mehrdimensionaler Strömungen im Reaktorkühlsystem. Abschlussbericht: Reaktorsicherheitsforschung Vorhaben-Nr.: 150 1271, ANSYS Germany GmbH, Staudenfeldweg 12 ,D-83624 Otterfing, January 2006. 140

[21] M. V. Tabib, S. A. Roy, and J. B. Joshi. CFD simulation of bubble column – An analysis of interphase forces and turbulence models. *Chem. Eng. J.*, 139(3):589–614, 2008. 140

[22] J. Sanyal, D. L. Marchisio, R. O. Fox, and K. Dhanasekharan. On the comparison between population balance models for CFD simulation of bubble columns. *Ind. Eng. Chem. Res.*, 44(14):5063–5072, July 2005. 140

[23] E. Loth. Numerical approaches for motion of dispersed particles, droplets and bubbles. *Prog. Energy Comb.*, 26(3):161–223, 2000. 140

[24] J. B. Joshi and V. V. Ranade. Computational fluid dynamics for designing process equipment: Expectations, current status and path forward. *Ind. Eng. Chem. Res.*, 42(6):1115–1128, March 2003. 140

[25] A. R. Paschedag. *CFD in der Verfahrenstechnik*. Wiley-VCH, Weinheim, 2004. 140

[26] M. Sommerfeld, editor. *Bubbly flows*, Heat and mass transfer, Berlin [u.a.], 2004. Springer. 140

[27] A. Sokolichin and G. Eigenberger. Gas-liquid flows in bubble column reactors and loop reactors – Part I: detailed modeling and numerical simulation. *Chem. Eng. Sci.*, 49:5747–5762, 1994. 141, 143

[28] S. Becker, A. Sokolichin, and G. Eigenberger. Gas-liquid flow in bubble columns and loop reactors – Part II. Comparison of detailed experiments and flow simulations. *Chem. Eng. Sci.*, 49(24 B):5747–5762, 1995. 141

[29] R. F. Mudde and O. Simonin. Two- and three-dimensional simulations of a bubble plume using a two-fluid model. *Chem. Eng. Sci.*, 54(21):5061–5069, 1999. 141

[30] A. D. Gosman, C. Lekakou, S. Politis, R. I. Issa, and M. K. Looney. Multidimensional

modeling of turbulent two-phase flows in stirred vessels. *AIChE J.*, 38(12):1946–1956, 1992. 141

[31] R. Krishna and J. M. van Baten. Eulerian simulations of bubble columns operating at elevated pressures in the churn turbulent flow regime. *Chem. Eng. Sci.*, 56(21-22):6249–6258, 2001. 141

[32] H. A. Jakobsen. Phase distribution phenomena in two-phase bubble column reactors. *Chem. Eng. Sci.*, 56(3):1049–1056, 2001. 141

[33] R. S. Oey, R. F. Mudde, and H. E. A. van den Akker. Sensitivity study on interfacial closure laws in two-fluid bubbly flow simulations. *AIChE J.*, 49(7):1621–1636, 2003. 141

[34] A. Sokolichin and G. Eigenberger. Applicability of the standard k-e turbulence model to the dynamic simulation of bubble columns: Part. I. Detailed numerical simulations. *Chem. Eng. Sci.*, 54:2273–2284, 1999. 141

[35] Y. Pan, M. P. Dudukovic, and M. Chang. Dynamic simulation of bubbly flow in bubble columns. *Chem. Eng. Sci.*, 54(13-14):2481–2489, 1999. 141

[36] D. Pfleger and S. Becker. Modelling and simulation of the dynamic flow behaviour in a bubble column. *Chem. Eng. Sci.*, 56(4):1737–1747, 2001. 141

[37] A. Behzadi, R. I. Issa, and H. Rusche. Modelling of dispersed bubble and droplet flow at high phase fractions. *Chem. Eng. Sci.*, 59(4):759–770, 2004. 141, 150

[38] G. Tabor. Turbulence in Two-Phase Systems. Technical report, Dept. of Mechanical Engineering, Imperial College of Science, Technology and Medicine, 1999. 141

[39] M. S. Politano, P. M. Carrica, and J. Converti. A model for turbulent polydisperse two-phase flow in vertical channels. *Int. J. Multiphase Flow*, 29(7):1153–1182, 2003. 141

[40] S. Bove. *Computational Fluid Dynamics of Gas-Liquid Flows including Bubble Population Balances*. PhD thesis, Aalborg University, 2005. 141, 142

[41] B. Ničeno, M. Boucker, and M. Smith. Euler-Euler Large Eddy Simulation of a square cross-sectional bubble column using the Neptune-CFD Code. *Sci. Techn. Nucl. Instrum.*, 2009:1–8, 2009. 141

[42] R. Krishna, M. I. Urseanu, J. M. van Baten, and J. Ellenberger. Influence of scale on the hydrodynamics of bubble columns operating in the churn-turbulent regime: Experiments vs. Eulerian simulations. *Chem. Eng. Sci.*, 54(21):4903–4911, 1999. 141

[43] F. Lehr, M. Millies, and D. Mewes. Numerical simulation of bubble size distributions and flow fields in bubble columns. *AIChE J.*, 48(11):2426–2443, 2002. 141

[44] G. Kocamustafaogullari and M. Ishii. Foundation of the interfacial area transport equation and its closure relations. *Int. J. Heat Mass Transfer*, 38:481–493, 1994. 142, 152

[45] T. Hibiki and M. Ishii. One-group interfacial area transport of bubbly flows in vertical round tubes. *Int. J. Heat Mass Transfer*, 43:2711–2726, 2000. 142, 152

[46] T. Hibiki and M. Ishii. Two-group interfacial area transport equations at bubbly-to-slug flow transition. *Nucl. Eng. Des.*, 202:39–76, 2000. 142, 152

[47] F. Lehr and M. Mewes. A transport equation for the interfacial area density applied to bubble columns. *Chem. Eng. Sci.*, 56:1159, 2001. 142, 152

[48] M. Millies and D. Mewes. Interfacial area density in bubbly flow. *Chem. Eng. Process.*, 38:307–319, 1999. 142, 152

[49] J. N. Reyes. Statistically derived conservation equtions for fluid particle flows. *Proc. ANS-THD*, 5:12–19, 1989. 142, 152

[50] S. Kumar and D. Ramkrishna. On the solution of population balance equations by discretization–I. A fixed pivot technique. *Chem. Eng. Sci.*, 51(8):1311–1332, 1996. 142

[51] S. Kumar and D. Ramkrishna. On the solution of population balance equations by discretization–II. A moving pivot technique. *Chem. Eng. Sci.*, 51(8):1333–1342, 1996. 142

[52] D. Ramkrishna. *Population Balances: Theory and Applications to Particulate Systems in Engineering*. Academic Press, 1st edition, July 2000. 142

[53] S. Lo. Application of the MUSIG Model to Bubbly Flows. Technical Report AEAT-1096, AEA Technology, June 1996. 142

[54] E. Olmos, C. Gentric, C. Vial, G. Wild, and N. Midoux. Numerical simulation of multiphase flow in bubble column reactors. Influence of bubble coalescence and break-up. *Chem. Eng. Sci.*, 56(21-22):6359–6365, 2001. 142

[55] P. Zwart, A. Burns, and C. Montavon. Multiple Size Group Models. Technical report, AEA Technology plc, Oxfordshire, UK, November 2003. 142

[56] E. Krepper, D. Lucas, T. Frank, H.-M. Prasser, and P. J. Zwart. The inhomogeneous MUSIG model for the simulation of polydispersed flows. *Nucl. Eng. Des.*, 238(7):1690–1702, 2008. 142

[57] D. L. Marchisio, J. T. Pikturna, R. O. Fox, R. D. Vigil, and A. A. Barresi. Quadrature method of moments for population-balance equations. *AIChE J.*, 49(5):1266–1276, 2003. 142

[58] D. L. Marchisio and R. O. Fox. Solution of population balance equations using the direct quadrature method of moments. *J. Aerosol Sci.*, 36(1):43–73, 2005. 142

[59] E. Gharaibah. *Entwicklung und Validierung eines Modells polydisperser Zweiphasenströmungen unter Berücksichtigung von Koaleszenz und Dispersion*. PhD thesis, Technische Universität München, 2008. 142

[60] J. N. E. Carneiro, V. Kaufmann, and W. Polifke. Numerical simulation of droplet dispersion and evaporation with a moments-based CFD model. In *COBEM 2009 - 20th Int. Congr. Mechanical Engineering*, November 15-20 2009. 142

[61] M. Smith and T. Matsoukas. Constant-number Monte Carlo simulation of population balances. *Chem. Eng. Sci.*, 53(9):1777–1786, 1998. 142

[62] G. B. Wallis. *One-Dimensional Two-Phase Flow*. McGraw-Hill, New York [u.a.], 1969. 142

[63] M. C. Ruzicka, J. Zahradnik, J. Drahos, and N. H. Thomas. Homogeneous-heterogeneous regime transition in bubble columns. *Chem. Eng. Sci.*, 56(15):4609–4626, 2001. 142

[64] S. M. Monahan, V. S. Vitankar, and R. O. Fox. CFD predictions for flow-regime transitions in bubble columns. *AIChE J.*, 51(7):1897–1923, 2005. 142

[65] S. M. Monahan and R. O. Fox. Linear stability analysis of a two-fluid model for air-water bubble columns. *Chem. Eng. Sci.*, 62(12):3159–3177, 2007. 142

[66] S. M. Monahan and R. O. Fox. Effect of model formulation on flow-regime predictions for bubble columns. *AIChE J.*, 53(1):9–18, 2007. 142

[67] D. Lucas, H.-M. Prasser, and A. Manera. Influence of the lift force on the stability of a bubble column. *Chem. Eng. Sci.*, 60(13):3609–3619, 2005. 142

[68] D. Lucas, E. Krepper, H.-M. Prasser, and A. Manera. Investigations on the stability of the flow characteristics in a bubble column. *Chem. Eng. Technol.*, 29(9):1066–1072, 2006. 142

[69] M. R. Bhole and J. B. Joshi. Stability analysis of bubble columns: Predictions for regime transition. *Chem. Eng. Sci.*, 60(16):4493–4507, 2005. 142

[70] S. Monahan. *Computational Fluid Dynamics Analysis of Air-Water Bubble Columns*. PhD thesis, Iowa State University, 2007. 142

[71] H. Marschall. Numerical Simulation of dispersed Gas-Liquid-Flows in Bubble Columns at high Phase Fractions. Vortrag anlässlich des Jahrestreffens der ProcessNet Fachausschüsse Computational Fluid Dynamics, Mischvorgänge und Extraktion, Fulda, 30.-31. März 2009. 142

[72] H. Marschall. Numerical Simulation of Bubble Column Reactors using a Hybrid Multiphase-CFD Approach. Vortrag anlässlich des ProcessNet Jahrestreffens der Reaktionstechnik, Würzburg, 8.-10. Juni 2009. 143

[73] H. G. Weller. Derivation, Modeling and Solution of the Conditionally Averaged Two-Phase Flow Equations. Technical report, OpenCFD Limited, 2005. 143

[74] C. G. Mendez, N. Nigro, and A. Cardona. Drag and non-drag force influences in numerical simulations of metallurgical ladles. *J. Mater. Process. Technol.*, 160(3):296–305, 2005. 144

[75] L. Schiller and A. Naumann. Über die grundlegenden Berechnungen bei der Schwerkraftaufbereitung. *Z. Ver. Dtsch. Ing.*, 77(12):318–320, 1933. 146

[76] R. Clift, J. R. Grace, and M. E. Weber. *Bubbles, Drops and Particles*. Academic Press, 1978. 146

[77] T. Frank. A Review on Advanced Eulerian Multiphase Flow Modelling for Gas-Liquid Flows. Technical report, AEA Technology GmbH / ANSYS CFX, 2003. 147

[78] D. Legendre and J. Magnaudet. The lift force on a spherical bubble in a viscous linear shear flow. *J. Fluid. Mech.*, 368:81–126, 1998. 147, 148

[79] F. J. Moraga, A. E. Larreteguy, D. A. Drew, and R. T. Lahey. Assessment of turbulent dispersion models for bubbly flows in the low Stokes number limit. *Int. J. Multiphase Flow*, 29(4):655–673, 2003. 148

[80] R. T. Lahey Jr. and D. A. Lahey. An analysis of two-phase flow and heat transfer using a multidimensional, multi-field, two-fluid computational fluid dynamics (CFD) model. In *Japan/US Sem. Two-Phase Flow Dynamics, Santa Barbara, Kalifornien*, 2000. 148

[81] D. A. Drew and S. L. Passman. *Theory of Multicomponent Fluids*. Springer, New York, 1998. 149

[82] O. Kramer. Forces Acting on Bubbles. Technical report, University of Twente, Faculty of Chemical Technology, 2000. 149

[83] A. Sokolichin, G. Eigenberger, and A. Lapin. Simulation of buoyancy driven bubbly flow: Established simplifications and open questions. *AIChE J.*, 50:24–45, 2004. 149

[84] D. Zhang, N. G. Deen, and J. A. M. Kuipers. Numerical simulation of the dynamic flow behavior in a bubble column: A study of closures for turbulence and interface forces. *Chem. Eng. Sci.*, 61:7593–7608, 2006. 149

[85] S. P. Antal, R. T. Lahey Jr., and J. E. Flaherty. Analysis of phase distribution in fully developd laminar bubbly two-phase flow. *Int. J. Multiphase Flow*, 17:635–652, 1991. 149

[86] H. Rusche. *Computational Fluid Dynamics of Dispersed Two-Phase Flows at High Phase Fractions*. PhD thesis, Imperial College of Science, Technology & Medicine London, 2002. 150

[87] J. F. Richardson and W. N. Zaki. Sedimentationand fluidsation: Part I. *Trans. Inst. Chem. Eng.*, 32:35–53, 1954. 150

[88] A. Bridge, L. Lapidus, and J. Elgin. The mechanics of vertical gas-liquid fluidized system. Part I: Countercurrent flow. *AIChE J.*, 10:810–826, 1964. 150

[89] P. Griffith and G. B. Wallis. Two-phase slug flow. *J. Heat Transfer*, 83:307–320, 1961. 150

[90] A. A. Kendoush. Hydrodynamic model for bubbles in a swarm. *Chem. Eng. Sci.*, 56:235–238, 2001. 150

[91] M. Maekawa, N. Shimada, A. Sou, and A. Tomiyama. Numerical simulation of poly dispersed flow using a multi-fluid model. *J. Fluid Sci. Technol.*, 2:502–512, 2007. 150

[92] G. Marrucci. Rising velocity of a swarm of spherical bubbles. *Ind. Eng. Chem. Fundam.*, 4:224–225, 1965. 150

[93] M. Simonnet, C. Gentric, E. Olmos, and N. Midoux. CFD formulation of the flow flied of a bubble column reactor: Importance of the drag force formulation to describe regime transitions. *Chem. Eng. Process.*, 47:1726–1737, 2007. 150

[94] S. Beyerlein, R. Cossmann, and H. Richter. Prediction of bubble concentration profiles in vertical turbulent two-phase flow. *Int. J. Multiphase Flow*, 11:629–641, 1985. 150

[95] E. Laurien and J. Niemann. Determination of the virtual mass coefficient for dense bubbly flows by direct numerical simulation. In *5th Int. Conf. Multiphase Flow, ICMF 2004, Yokohama, Japan*, 2004. 150

[96] K. Langbein. Simulation und Modellierung der Fluiddynamik in Blasenschwärmen auf Basis des Zwei-Fluid-Modells mittels CFD - Modellierung der Strömungswiderstandskraft. Master's thesis, Technische Universität München, 2008. 151

[97] W. Yao and C. Morel. Volumetric interfacial area prediction in upward bubbly two-phase flow. *Int. J. Heat Mass Transfer*, 47:307–328, 2004. 152

[98] S. C. P. Cheung, G. H. Yeoh, and J. Y. Tu. On the numerical study of isothermal vertical bubbly flow using two population balance approaches. *Chem. Eng. Sci.*, 62:4659–4674, 2007. 152

[99] M. Ishii, Q. Wu, and S. Kim. One-group interfacial area transport in vertical bubbly flow. *Int. J. Heat Mass Transfer*, 41:1103–1112, 1998. 152

[100] S. Oberhauser. Numerical Simulation of Polydisperse Bubbly Flows with Averaged Bubble Number Density and Interfacial Area Concentration Concepts. Master's thesis, Technische Universität München, 2008. 152

6

Numerical Simulation of dispersed Gas-Liquid Flows in Bubble Columns at high Gas Phase Fractions using OpenFOAM® – Part II: Numerical Simulation and Results

Abstract

The design of industrial gas/liquid reactors such as bubble columns requires detailed information with respect to the flow structure and characteristics of two- or multiphase systems in the reactor. The contribution is focused on the evaluation of the simulation results obtained by a selection of models. The results are further compared with those reported in literature. The simulation have been performed with the CFD software OpenFOAM®. The main focus of the numerical simulation was set on capturing the characteristic process and design parameters of bubble columns.

6.1. Introduction

As a platform for model implementation the Open Source CFD software OpenFOAM® (*Open Field Operation And Manipulation*) is used [1–3]. OpenFOAM is a flexible and efficient C++ library, providing numerous numerical algorithms, methods and solvers for solving continuum mechanics problems in the field of chemical and process engineering. For this purpose, OpenFOAM employs a syntax – even when programing on a user level (top-level) – being as close as possible to the conventional mathematical notation for tensors and partial differential equations. Various Object Oriented Programing (OOP) techniques allow to mimic common data types and basic operators [1]. Hence, OpenFOAM might be seen as a flexible and efficient development platform for a variety of continuum models in the field of reactor design.

In OpenFOAM v.1.4.1, which was used at the beginning of code development, the top-level solver *bubbleFoam* has already been provided. However, bubbleFoam only exhibits a limited capability for simulating bubble swarms in bubble columns at high superficial gas velocities. Thus, the code was extended towards *bubbleFoamExt*. The present study particularly focusses on capturing the interfacial forces, turbulence, swarm effects, polydispersity and the mixing characteristics adopting basic models - as they were described in detail in part I *Basics and Modeling* of this contribution.

6.1.1. Flow Domain Discrimination

In general, there exist two two-phase flow regions in a bubble column. These flow regions differ from each other in the phases taking either the continuous or the disperse part and interchanging their role when crossing the liquid surface. Thus, flow domain discrimination states another pivotal modeling aspect - beside capturing of characteristic two-phase flow phenomena. This discrimination is necessary since the used model correlations are commonly restricted to either bubbly or droplet flows and hence rarely encompasses both cases in their applicability. Within the framework of this work the flow domain discrimination is accomplished using a simple scalar field Γ_i.

The underlying principle is illustrated schematically in figure 6.1: the evaluation is based upon the gradient of the volumetric phase fraction field. Interpolating the volumetric gas-phase fraction linearly between two cell centers, the formal 'owner' of the gas/liquid interface can be identified. This is accomplished using the cell-face interpolated value of the volumetric gas-phase fraction and the slope of the straight line educing from its linear interpolation, where the conditions $\alpha_a > 0.5$ in one cell and $\alpha_a < 0.5$ in the respective neighboring cell is found to be fulfilled. Consequently, the resulting scalar field Γ_i enables to distinguish between the two flow regions, taking the value $\Gamma_i = 1$ below and $\Gamma_i = 0$ above the surface of the liquid.

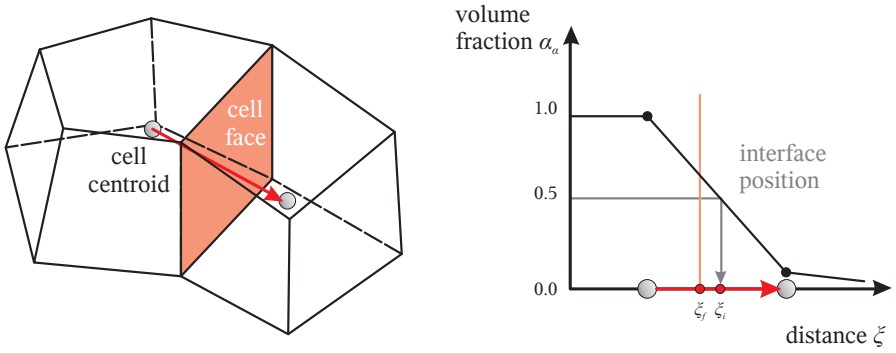

Figure 6.1: Principle of flow domain discrimination.

6.2. Numerical Simulation

For a substantial simulation-based analysis of both the fluid dynamics and liquid-phase mixing characteristics in bubble columns at high superficial gas velocities, a rectangular bubble column (Pseudo-2D) and a cylindrical bubble column (3D) have been examined. The following underlying phenomena are of paramount interest in the present study:

- transient dynamics of the dispersed gas phase,
- integral gas hold-up and
- distribution of a tracer within the continuous phase.

The results are compared with own reference data based upon experiments. Then, conclusions are drawn with respect to the performance, the quality and the applicability of the models as they were introduced for the purpose of capturing the various flow phenomena in bubble columns.

Since experimental reference cases *and* models are mostly based on the air/water system, the present simulations of two-phase flows in bubble columns have been restricted to this system as well.

Furthermore, all numerical simulations are subject to the same initial and boundary conditions for the domain interior (*a priori*) as well as for the domain boundaries (*ab initio*): a non-slip boundary condition is imposed on the liquid-phase velocity at the wall of the column, while for the gas-phase velocity a free-slip condition is applied. For all other scalar fields the Neumann (or second-type) boundary condition dictates a zero gradient at the domain boundaries. The conditions at the gas inlet are specified in terms of the phase velocities (i.e. the respective superficial phase velocities), the volumetric gas-phase fraction and bubble number density (Dirichlet

boundary conditions). Furthermore, a Neumann boundary condition is imposed on the inlet pressure. Inverse conditions can be found at the top of the bubble column, where the gas having entered the bottom of the column leaves the flow domain.

Additionally, mesh sensitivity and convergence analyses have been performed in order to minimize discretization and convergence errors. Thus, the results can be regarded as independent from both the underlying mesh resolution and the applied residuum.

6.2.1. Rectangular Bubble Column (Pseudo-2D)

Scope and Objectives The simulations are performed for a rectangular bubble column in order to clarify the contribution of the lateral lift force to the transient behavior of an evolving bubble plume.

The reason for the choice of a pseudo-2D bubble column lies in its fundamental suitability for videometric analysis: at low integral gas hold-up bubble-bubble overlapping can be neglected to a good approximation. Thus, the local volumetric gas fraction might be determined using a high-speed camera system along with an automatic image processing. This enables to assess both the performance and the quality of a simulation through a detailed validation study.

Reference cases There are numerous reference cases for rectangular bubble columns. In the present work, we focus on the horizontal liquid-phase velocity and the local volumetric gas phase fraction. Hence, the following reference studies for a pseudo-2D bubble column (100 cm x 20 cm x 5 cm) have been considered:

- Gomes et al. have pursued experiments, aiming at the horizontal velocities of the continuous phase [4]. The measurements were performed in a rectangular bubble column with the above dimensions. This bubble column was operated at a filling level of 45 cm with a air/water system. The measurements were taken at half the filling level.

- Additionally, own videometric measurements in such a pseudo-2D bubble column have been accomplished in order to evaluate the local volumetric gas-phase fraction [5].

Geometry modeling and mesh generation Figure 6.2 shows a schematic illustration of the flow domain for the pseudo-2D bubble column. The size of the area is given by 20 cm x 5 cm in width and depth. Herein, the gas inlet is centered with an area of 5 cm x 2.5 cm. For all simulation runs the initial filling level was chosen to be 50% being equivalent to a filling height of 50 cm.

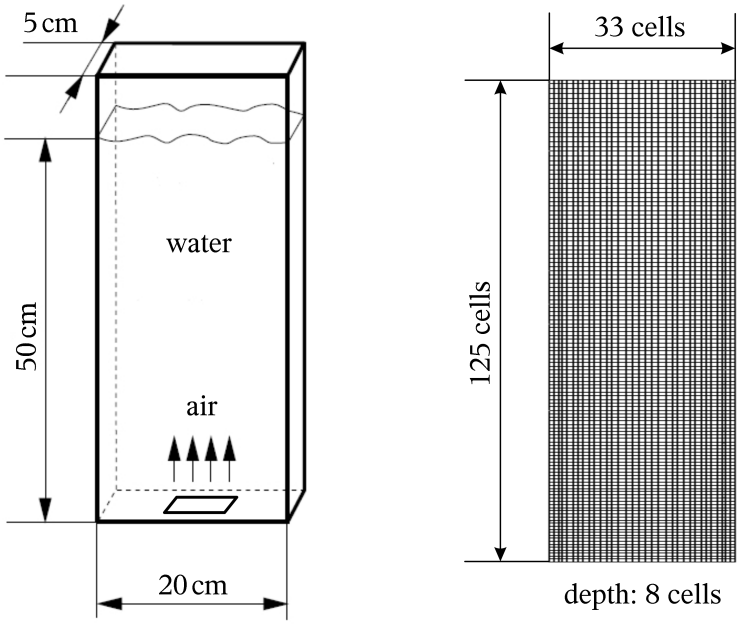

Figure 6.2: Domain and computational mesh for the pseudo-2D bubble column.

Owing to the rectangular geometry of the column, a structured cartesian mesh might be applied advantageously. As depicted in figure 6.2, the mesh exhibits a higher spatial resolution near the inlet and walls in order to capture gradients sufficiently. The mesh consists of 33 000 computational cells in total.

6.2.2. Cylindrical Bubble Column (3D)

Scope and Objectives For the simulations of the cylindrical bubble column the objective was to capture both the dynamics of the dispersed phase and the continuous phase mixing characteristics in a most detailed and realistic manner. Contrary to the aforementioned simulation of the pseudo-2D bubble column, conditions for the 3D case now correspond to a higher gas hold-up.

Reference cases For the validation of the fluid dynamics, we first consider the integral gas hold-up in the cylindrical bubble column of 20 cm in diameter. Furthermore, the mixing characteristics within the continuous liquid phase will be examined by following the distribution of a tracer subsequent to a step-injection at a height of 1.5 m near the liquid surface. The detection of the tracer concentration is performed 2 cm above the gas inlet.

The validation study is based on the following reference cases:

- Deckwer [6] has examined the integral gas hold-up for an air/water system in a bubble column of 20 cm in diameter operating at various superficial gas velocities.

- Deckwer [6] has published a correlation for the axial dispersion coefficient in the continuous liquid phase in terms of the Bodenstein number Bo_L and the Froude number Fr_G,

$$Bo_L = 2.83 Fr_G^{0.34}, \tag{6.1}$$

which is based upon experimental data from the work of various groups. In particular, the Bo_L and the Froude number Fr_G are defined as

$$Bo_L \equiv \frac{\mathbf{U}_{S,0} d_{BC}}{D_{ax}} \tag{6.2}$$

$$Fr_G \equiv \frac{\mathbf{U}_{S,0}^2}{g d_{BC}}, \tag{6.3}$$

where $\mathbf{U}_{S,0}$ and d_{BC} denote the superficial gas velocity and bubble column diameter, respectively.

Geometry modeling and mesh generation Figure 6.3 depicts a schematic of the flow domain representing the cylindrical bubble column. The flow domain comprises of a cylinder of 20 cm in diameter. The bubble column is 2 m in height and has been initialized up to a filling level of 75% equivalent to 1.5 m in filling height. Based upon this geometry, a structured hexahedral mesh has been generated as depicted in figure 6.3. The domain is sub-divided into 150 computational cells in the axial direction and into 217 cells used for the cross sectional area, forming a so-called butterfly-grid. For the latter, a square with an edge length of 8 cm is resolved by 7x7 cells. The remainder of the cross sectional area is sub-divided into four segments of equal size, each of that spatially discretized by 6x7 cells. In total, the computational mesh comprises of 32 550 cells.

6.3. Results

6.3.1. Rectangular Bubble Column (Pseudo-2D)

Illustration of Results Figure 6.4 shows a sectional view of the bubble column at different times after its start-up [7]. The lower part is completely filled with water, while the upper part is filled with air.

At $t = 0.0$ s, the lower part is completely filled with water. Initially, when air enters the bubble column a symmetric bubble plume evolves. However, an asymmetric distribution within the bubble plume (indicated by the change in the color in the

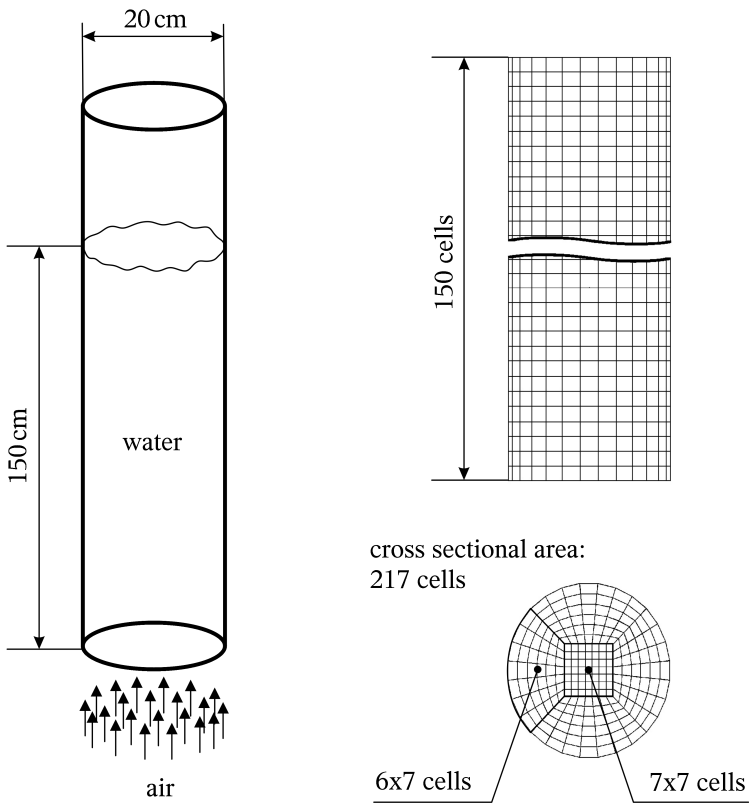

Figure 6.3: Domain and computational mesh for the pseudo-2D bubble column.

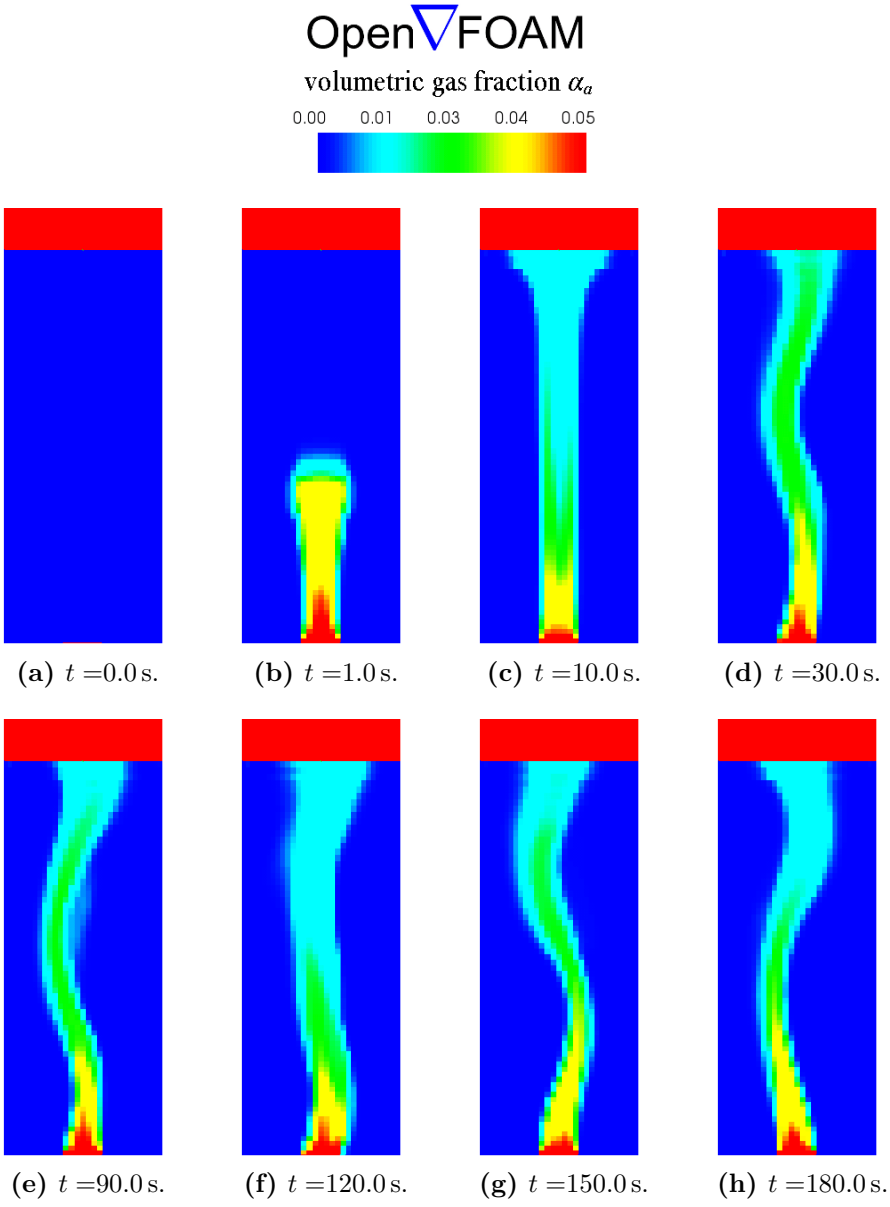

(a) t =0.0 s. **(b)** t =1.0 s. **(c)** t =10.0 s. **(d)** t =30.0 s.

(e) t =90.0 s. **(f)** t =120.0 s. **(g)** t =150.0 s. **(h)** t =180.0 s.

Figure 6.4: Simulation results for the pseudo-2D bubble column: volumetric gas-phase fraction.

gas-phase fraction) can already be observed for the next time step. Subsequently, a notable asymmetric bubble plume develops. Finally, the bubble plume begins to oscillate periodically significantly deviating from its central position.

Evaluation of Results For a quantitative evaluation, three distinct model approaches have been adopted to determine the lateral lift force coefficient, namely the models according to Tomiyama [8] and Legendre & Magnaudet [9] as well as a model employing a constant lateral lift force coefficient, which was chosen to take the value $C_l = 0.25$.

The horizontal liquid velocity has been taken in the center of the column with respect to its initial filling level. Figures 6.5a to 6.5c depict the results of the simulation runs with respect to the three models mentioned before.

Discussion of Results A similar trend can be observed in all three cases: after about 40 s the maximum amplitude of the horizontal liquid velocity is reached at approximately $0.2\,\frac{\mathrm{m}}{\mathrm{s}}$. Hence, only marginal deviations are recognized during the start-up phase of the column. The amplitudes obtained from numerical simulations are found to be in very good agreement with the ones determined by Gomes et al. in their experiments [4].

Regarding the maximum gas-phase fraction, a comparison with results from videometry (including subsequent image processing) reveals a very good agreement: the maximum volumetric gas-phase fraction was found to be below 5% both in simulations and in experiments.

At this point, we should emphasize, that this low value is the reason for the slight differences in the results, even though different lateral lift force models have been employed: at this low gas-phase fractions bubble coalescence and break-up phenomena have not yet notably taken place. Thus, the lateral lift force has not yet started to set notable effect on the transient movement of the bubble swarm. However, even these marginal differences surely show the pivotal relevance of model selection considering the lateral lift force. This inherently involves the issue of correctly capturing the corresponding transient movement of the bubble plume.

6.3.2. Cylindrical Bubble Column (3D)

Illustration of Results Figures 6.6 and 6.7 show the vertical cross section, illustrating the gas-phase velocity (vectors) and volumetric gas-phase fraction (contours) at a superficial gas velocity of $6\,\frac{\mathrm{cm}}{\mathrm{s}}$ [10]. The time interval between two subsequent cross sectional views was chosen to be $\Delta t = 2\,\mathrm{s}$.

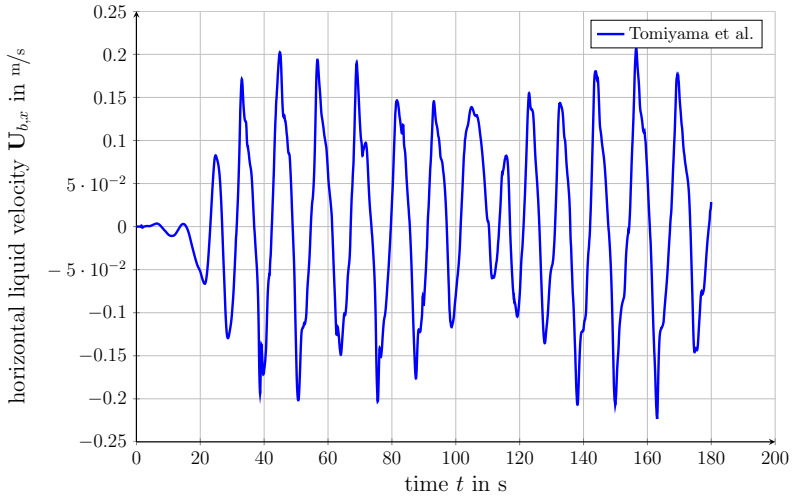

(a) Tomiyama et al..

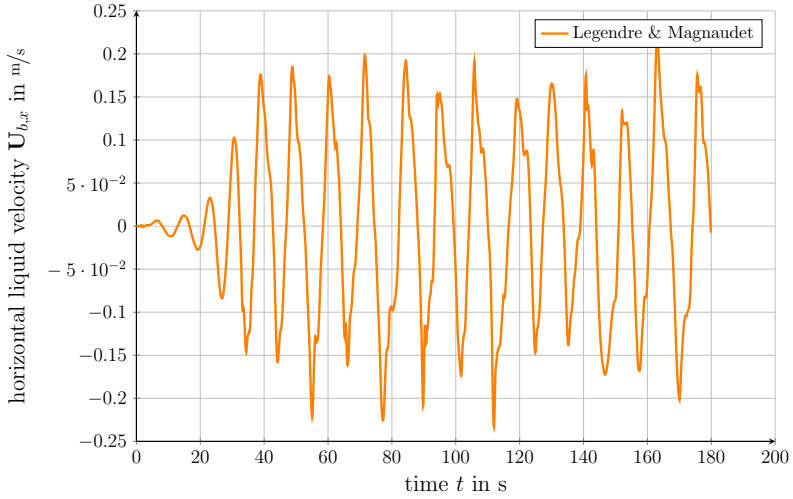

(b) Legendre & Magnaudet.

Figure 6.5: Evaluation of Results: change of the horizontal liquid velocity obtained in the center of the pseudo-2D bubble column.

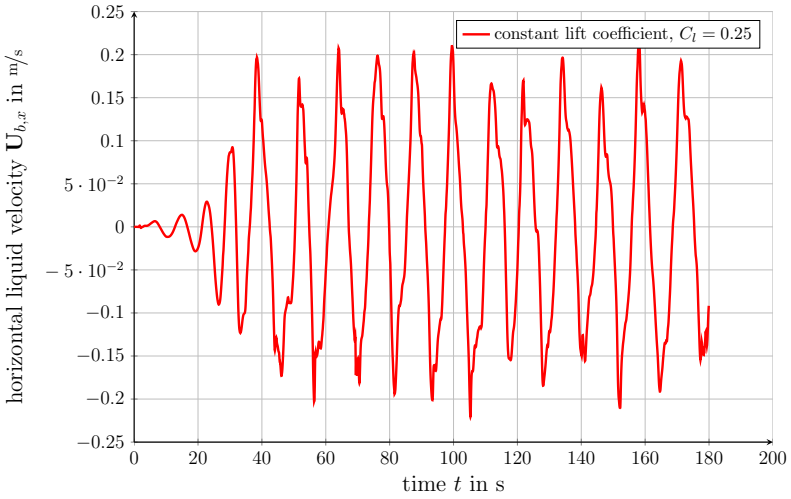

(c) constant lift coefficient.

Figure 6.5: Evaluation of Results: change of the horizontal liquid velocity obtained in the center of the pseudo-2D bubble column.

As shown in figure 6.6, the bubble swarm rises near the center line of the bubble column and exhibits a high rising velocity. The reason for this certainly rests on the radial separation of small and large bubbles due to lateral lift, resulting in a central bubble swarm of mostly large bubbles.

Figure 6.7 illustratively depicts the significant differences which can be observed for the radial distribution of the local gas-phase fraction. Taking quite low values near the column wall, the gas fraction increases towards the center line. A closer look further reveals that at these high gas velocities the movement of the dense bubble swarm is clearly transient. Moreover, a notable wall effect can be observed hindering the central bubble plume in its lateral movement.

Figure 6.8 shows the corresponding concentration field of a distributed tracer. The tracer has been introduced step-wise into the liquid close to its surface. Again, the time intervals between respective cross sectional views have been chosen to be $\Delta t = 2\,\mathrm{s}$ at a superficial gas velocity of $6\,\frac{\mathrm{cm}}{\mathrm{s}}$. Evidently, an asymmetric dispersion can be ascertained, which does not exhibit a homogeneous distribution even after $15\,\mathrm{s}$.

Evaluation of Results For the purpose of a quantitative analysis and evaluation of both the simulation quality and performance – with respect to the comprehensive capturing of the fluid dynamics in bubble columns – a comparison is drawn between

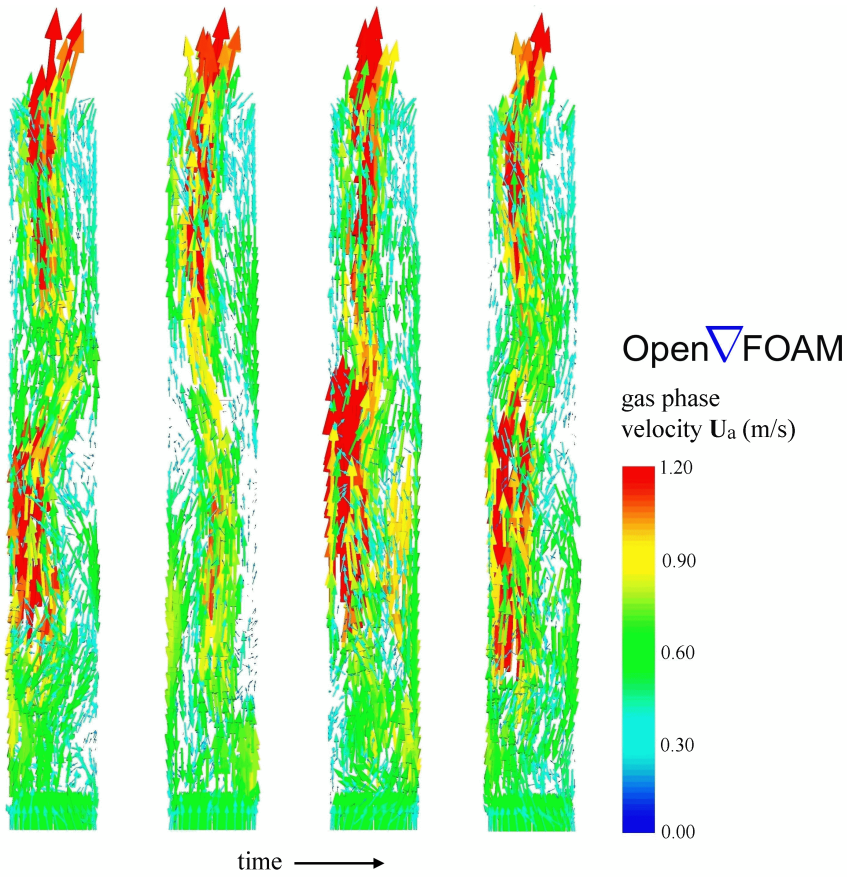

Figure 6.6: Simulation results for the 3D bubble column: gas phase velocity.

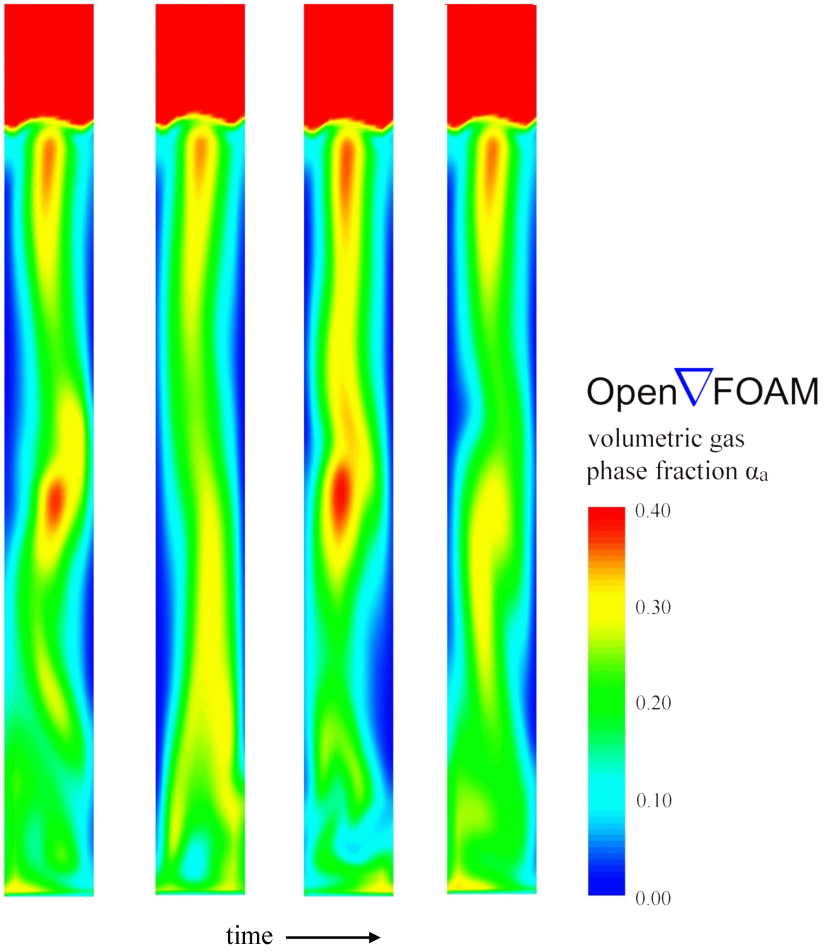

Figure 6.7: Simulation results for the 3D bubble column: volumetric gas-phase fraction.

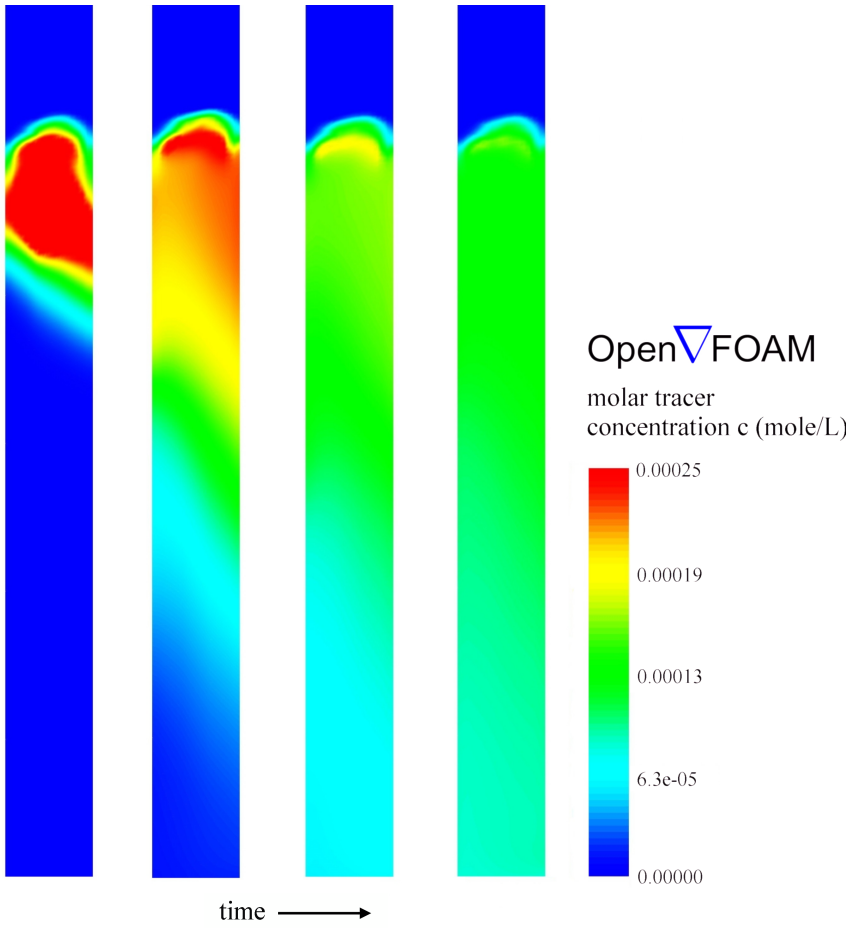

Figure 6.8: Simulation results for the 3D bubble column: tracer distribution.

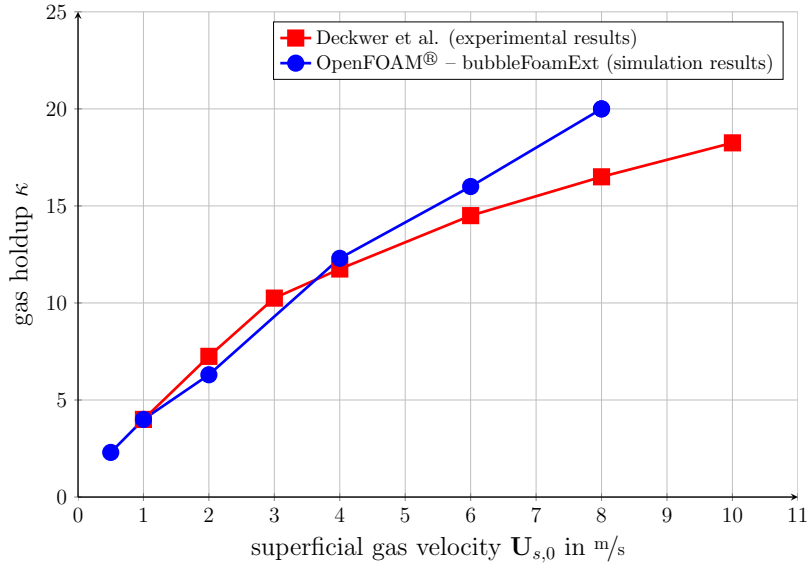

Figure 6.9: Evaluation of Results: gas hold-up vs. superficial gas velocity obtained in a cylindrical bubble column.

measurements performed by Deckwer [6] and the simulation results – figure 6.9. For this, we examine the integral gas hold-up for different superficial gas velocities.

Figure 6.10 depicts the resulting course of the tracer concentration subsequent to step-wise introduction near the surface of the liquid. For a quantitative comparison, the 1D-axial dispersion model [11] is adopted in order to evaluate the axial dispersion coefficient D_{ax} as a model parameter by means of least-square fitting. The resulting dispersion coefficient of $D_{ax} = 353.9\,\frac{\mathrm{cm}^2}{\mathrm{s}}$ is in good agreement with $D_{ax} = 361.2\,\frac{\mathrm{cm}^2}{\mathrm{s}}$ obtained from the correlation according to equation 6.1.

Discussion of Results A comparison of the experimental results with the simulation results for the integral gas hold-up yields a good agreement as indicated in figure 6.9. However, it should be noted that the gas hold-up represents an integral (overall) quantity and thus taking the gas hold-up as a measure clearly does not assure the local gas-phase fractions to be equivalent at different operation conditions. Nevertheless, it is the conformity over a broad range of the superficial gas velocity including the sharp bend (indicating the regime transition from homogeneous to heterogeneous flow regime) at a superficial gas velocity of about $3 - 4\,\frac{\mathrm{cm}}{\mathrm{s}}$, indicating a decent involvement of crucial phenomena by the respective models. This surely includes the physically sound modeling of interfacial forces (drag force, lateral lift force, turbulent dispersion force) as well as associated correction terms accounting for swarm effects. Further, the consideration of polydispersity in the gas phase found for high superficial gas velocities plays a pivotal role. This directly affects the different

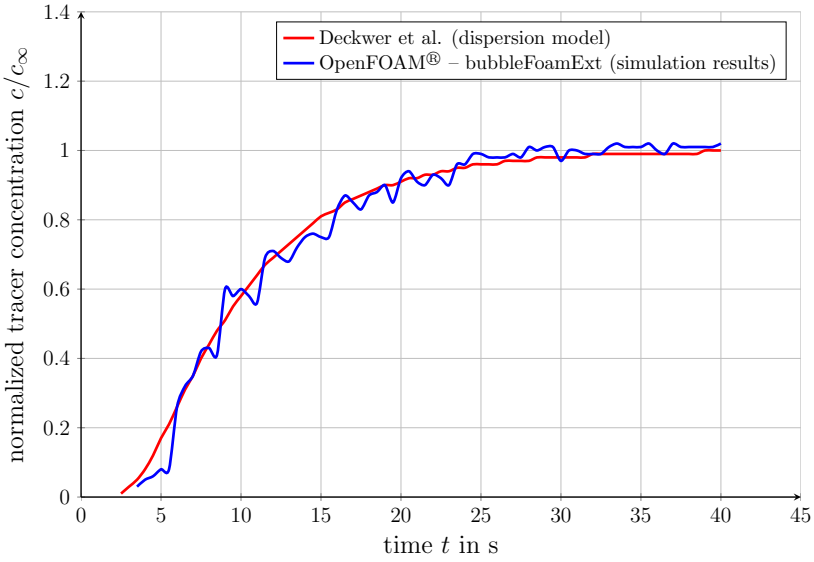

Figure 6.10: Evaluation of Results: tracer distribution subsequent to a stepwise dosing in a cylindrical bubble column.

bubble rising velocities and thus different bubble residence times within the bubble column.

However, at a higher superficial gas velocity discrepancies can be observed. The reason for this can be found in approaching the limits of validity of the underlying two-fluid model regarding its constraints to the local mesh resolution: for modeling the inter-phase interactions within the two-fluid model framework (based on the concept of interpenetrating continua), the gas phase was chosen to take the part of the dispersed phase. Due to the high superficial gas velocities, subsequent coalescence causes the emergence of large bubbles. The size of these bubbles locally approaches the size of the computational mesh cells, which, in turn, causes the corresponding underlying assumption to be invalid.

A comparison of the tracer concentration obtained by the 1D-axial dispersion model and by the CFD simulation clearly reveals that both approaches take into account both the convective and the dispersive transport. However, the CFD approach includes the three-dimensional case and (which is more important) is independent from any geometry constraints. Thus, the non-uniform transport of the tracer within the liquid phase is caused by the transient flow of the dispersed phase. Figure 6.10 shows the relevant simulation results. The strong coupling being inherent to the transient two-phase flows within a bubble column is taken into account. As the superposition of convective and dispersive transport surely looses relevance when increasing the superficial gas velocity, the observed concentration fluctuations are

reasonable. Thus, it is CFD offering a new avenue towards the local analysis of transient transport phenomena within bubble columns.

6.4. Summary and Outlook

Numerical simulations of both fluid dynamics and mixing characteristics in bubble columns show, that a good qualitative and quantitative agreement between experimental and simulative results can be achieved when a physically sound modeling base is provided. This approach encompasses inter-phase interactions (including swarm effects), two-phase turbulence and polydispersity, taking into account basic bubble coalescence and break-up mechanism.

Furthermore, the extent of validity of the models along with the underlying assumptions seems to be critical. For the simulation of dense bubble flows the following considerations can be pointed out as possible directions for model enhancements:

- Currently, the use of swarm corrections is associated with significant uncertainties. Although numerous correlations for the swarm correction of the drag coefficient can be found, additional correlations are required, taking into account the swarm effect biasing non-drag forces (i.e. lateral lift and turbulent dispersion force). More validation studies based on experimental reference cases have still to be performed.

- The development of turbulence models is still a crucial point. The *basic mixture turbulence model* presented in this work is based upon mixture quantities and thus can only be seen as a simple (numerically stable) basis for continuing studies. As turbulence models typically couple with models for bubble coalescence and break-up or with bubble forces models, turbulence modeling has to be considered crucial for correctly capturing both mixing characteristics within a phase and among phases.

- When selecting a particular model for the description of bubbly flows, one needs to bear in mind that most of these models rely upon experiments with the air/water system. Hence, capturing the effects of contamination (surfactants) and of other material properties different from the air/water system is crucial. The latter surely has to be altered towards more relevant systems in reaction engineering applications.

6.A. References

[1] H. G. Weller, G. Tabor, H. Jasak, and C. Fureby. A tensorial approach to computational continuum mechanics using object orientated techniques. *Comp. Phys.*, 12(6):620–631, 1998. 164

[2] OpenCFD Limited. *OpenFOAM User Guide*, 1.5 edition, 2008. 164

[3] OpenCFD Limited. *OpenFOAM Programmer's Guide*, 1.5 edition, 2008. 164

[4] S. Gomes, N. Gilbert, D. Pfleger, and H.-G. Wagner. Experimental Investigations of Two-Phase Gas-Liquid Flows in Bubble Column Reactors. Technical report, BASF AG, Fluid Dynamics Group, Engineering Research and Development, 1999. 166, 171

[5] F. Kraus. Entwicklung und Implementierung eines videometrischen Messsystems zur Erfassung transienter, polydisperser Mehrphasenströmungen in Blasensäulen mittels High-Speed-Kamera. Master's thesis, Technische Universität München, 2008. 166

[6] W. D. Deckwer. *Reaktionstechnik in Blasensäulen.* Otto Salle, 1985. 168, 177

[7] A. Kossmann. Simulation und Modellierung der Fluiddynamik in Blasenschwärmen auf Basis des Zwei-Fluid-Modells mittels CFD - Modellierung der lateralen Auftriebskraft. Semesterarbeit, 2008. Technische Universität München. 168

[8] A. Tomiyama. Struggle with computional bubble dynamics. In *3rd Int. Conf. Multiphase Flow (1998), Lyon, France*, volume 1, pages 1–18, 1998. 171

[9] D. Legendre and J. Magnaudet. The lift force on a spherical bubble in a viscous linear shear flow. *J. Fluid. Mech.*, 368:81–126, 1998. 171

[10] R. Mornhinweg. Numerische Simulation disperser Gas-Flüssig-Strömungen in Blasensäulen bei hohen Gasphasenanteilen. Master's thesis, Technische Universität München, 2008. 171

[11] O. Levenspiel. *Chemical Reaction Engineering.* Wiley, Hoboken, NJ, 3. ed edition, 1999. 177

7

Numerical Simulation of Species Transfer across Fluid Interfaces in Free-Surface Flows using OpenFOAM®

Abstract

This paper presents the Continuous-Species-Transfer (CST) method, which enables interface capturing techniques – a group among Computational Multi-Fluid Dynamics (CMFD) methods that rely upon a smooth interface representation – to deal with species transfer. In this study we examine realistic species transfer across fluid interfaces, taking into account both the steep interfacial concentration gradients (at high Schmidt numbers) and the sharp interfacial concentration jump (at high Henry coefficients due to different species solubilities). Thus, the main objective is to establish the CST method for species transfer across fluid interfaces of arbitrary morphology in free-surface flows at high viscosity and density ratios.

Detailed numerical simulations of single rising bubbles have been performed at high resolutions. Results were compared to experimental data and correlations derived thereof.

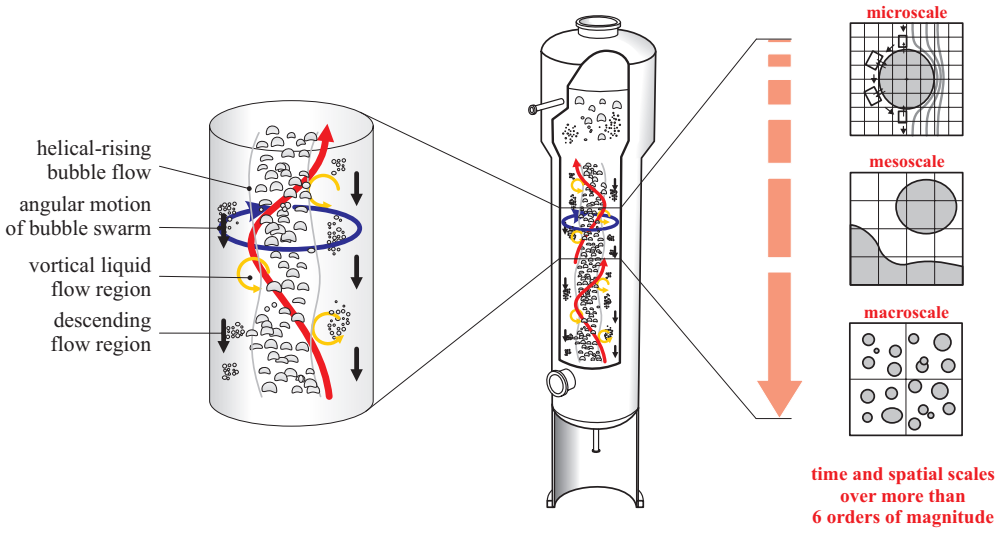

Figure 7.1: Flow structures and physico-chemical phenomena in bubble column reactors.

7.1. Introduction

Chemical reactors with bubbly flows are widely used in chemical reaction engineering for a variety of processes, e.g., bubble columns in the chemical, petroleum, metallurgical and energy industries. Common examples for the applications of bubble columns are liquid-phase oxidations, hydrogenations, chlorination, gas scrubbing, waste water treatment and various biotechnological applications.

One pivotal point of interest concerns the flow regimes in bubble columns, as this significantly influences the reactor's performance – its conversion, site time yield and selectivity. Though it is well known, that different flow regimes can be obtained by variation of the bubble column's operating parameters (such as superficial gas velocity, pressure, etc.) or design parameters (aspect ratio, sparger, internals, etc.), there is still a pivotal lack of detailed knowledge concerning the inherently complex nature of the underlying fluid dynamics in bubble columns: flow structures are intrinsically transient and characterized by very different spatial and temporal scales as depicted in figure 7.1.

It is therefore of major importance to develop both understanding and predictive simulation tools in order to obtain better and economically viable (efficient) technologies for process intensification and optimisation of bubble column reactors.

For this purpose, a detailed understanding of the influence of mixing characteristics within the continuous liquid phase as well as of the dynamics of the dispersed gaseous phase upon *species transport within a phase* and *species transfer across phase interfaces* is crucial. This clearly becomes even more important for fast chemical reactions, where conversions take place in close vincinity to the bubble surface, greatly influenced by its surrounding local mixing pattern and corresponding diffusive and convective transport of the chemical species involved with these reactions.

In this work we perform detailed three-dimensional simulations covering the fluid dynamics and species transfer in single bubble systems. Emphasis is put upon the underlying physical background as well as the mathematical model and governing equations derived thereof (sections 7.2 and 7.3), the basic framework of the employed solution methodology (section 7.4), and detailed validation of both bubble dynamics and species transfer across its interface (section 7.5).

7.2. Physical Background

7.2.1. Bubble Dynamics

In the past considerable research effort has been devoted to fluid dynamics in bubbly flows (bubble dynamics) focusing on the bubble's shape, wakes and velocities in various liquids [1–9].

From the wide base of experiments examining the rising of single bubbles in a quiescent liquid Clift et al. [5] presented a diagram as shown in figure 7.2. This illustratively allows to distinguish among different bubble shape regimes dependending on characteristic dimensionless numbers. These are the bubble Reynolds number $Re_b \equiv U_\infty d_b/\nu_l$ representing the ratio of inertia to viscous forces, the Eötvös number $Eo \equiv g(\rho_l - \rho_b)d_b^2/\sigma$ representing the ratio of buoyancy to surface tension forces and the Morton number $Mo \equiv g(\rho_l - \rho_b)\eta_l^4/\rho_l^2\sigma^3$, which is defined by the ratio of viscous to surface tension forces. Note that this is not a complete set describing single bubble dynamics in a quiescent liquid. Dimensional analysis reveals two more dimensionless numbers, the density ratio $\Pi_\rho \equiv \rho_l/\rho_b$ and viscosity ratio $\Pi_\nu \equiv \nu_l/\nu_b$. Moreover, the system purity plays a major role. Furthermore, other dimensionless groups might be used in a complementary manner, i.e., $We = Re^2\sqrt{Mo/Eo}$ or $Fr = \sqrt{We/Eo}$. However, it is common practice to base parametric studies upon this set of non-dimensional numbers, when examining the bubbles' shapes, rising velocities and/or trajectories and wake phenomena.

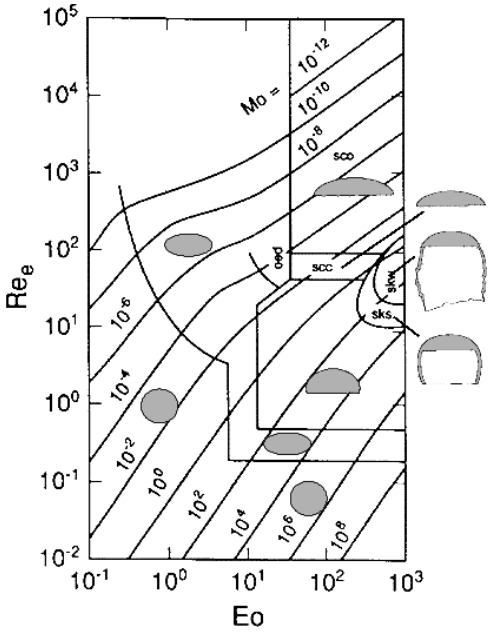

Figure 7.2: Bubble shape depending on Reynolds, Eötvös and Morton number [10].

It seems evident that the interplay of these characteristics of bubbly flows and their underlying physical phenomena is utmost complex and cannot be considered decoupled. However, the above characteristics are useful for comparison with the bubble dynamics and the species transfer across the bubble's surface, and consequently serve as a validation base in this study.

bubble shape According to figure 7.2 bubble shapes can be generally categorised into three types, namely (1) spherical/ellipsoidal, (2) cap/skirted and (3) irregular/wobbling. As the bubble interfacial area (or its specific area defined as bubble interfacial area per bubble volume) characteristically varies among these shape regimes – which as a consequence has a significant influence on the overall species transfer across the bubble surface – it is advisable to examine bubbles that pertain to different regimes. Thus bubbles of different size and shapes were subject to this study.

bubble rising velocity Mainly depending on material properties and the purity of the system under consideration the terminal rising velocity of bubbles provides another feature to be considered. The terminal rising velocity significantly influences the overall contact time and mean residence time available for the species transfer. Thus, it must be captured correctly by the numerical simulations.

Figure 7.3 shows the terminal rising velocities of bubbles within different shape regimes for the air/water system. This velocity mainly depends on the surface tension, the liquid phase viscosity and surfactants present in the system, each

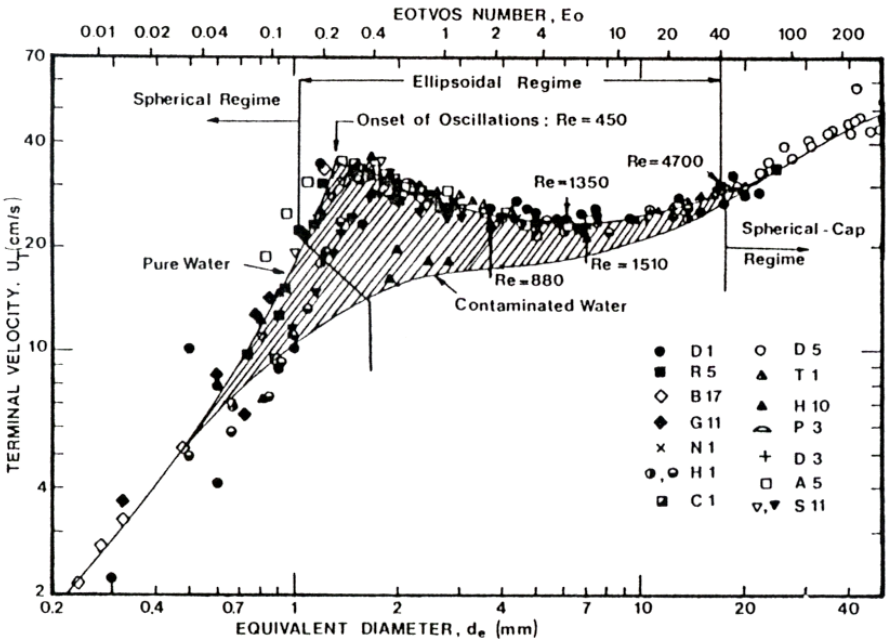

Figure 7.3: Bubble terminal rising velocity at different bubble (equivalent) diameters in air/water system [5].

of which is influencing the bubbles' inner circulation, shape deformation and oscillation – in return impairing, e.g., the drag a rising bubble is exerted to.

bubble trajectory Probably the most important characteristics to be examined are bubble wake phenomena. These greatly influence both the rising path and mixing pattern in the proximity of the bubble, which in turn will influence the chemical conversion of a component in the liquid phase after having undergone the interfacial species transfer.

In order to provide an avenue for quantitative validation of our numerical simulations, it is useful to have a more detailed look on the bubble's trajectory, as this depends on the wake behind a rising bubble. Figure 7.4a depicts typical wake types that are found to exhibit completely different flow and mixing patterns: (1) steady wake without circulation (2) steady wake with circulation (3) unsteady wake with vortex structures and vortex shedding. Figure 7.4b illustrates the different bubble trajectories associated to the different wake types that are observed while bubbles rise. Accordingly, bubble trajectories can be categorised into (1) straight (2) zigzag and (3) spiral/helical. It is worth noting that the second type – zigzag trajectories – are instable for bubbles larger than 2 mm. Thus they are often found to switch to a spiral/helical type, as it is shown in figure 7.4b.

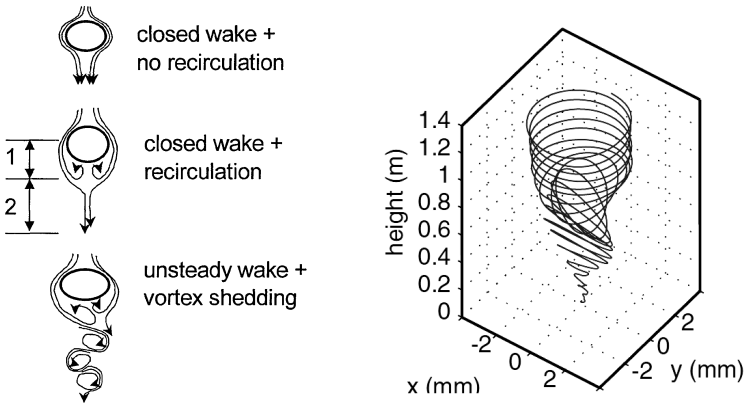

(a) bubble wake patterns [8].

(b) bubble rising trajectory [11].

Figure 7.4: Bubble wake and rise trajectories at different bubble (equivalent) diameters.

7.2.2. Species Transfer

Extensive research aiming at the associated species transfer across the interfaces in bubbly flows dates back to the early 60ies of the last century [12–19].

Herein, species transfer is commonly examined using several characteristic dimensionless groups, out of which the bubble Reynolds number is a pivotal one. Furthermore, the Schmidt number $Sc \equiv \nu_l / D_l$ and the Sherwood number $Sh \equiv \beta_l d_b / D_l$ are utilized in order to describe the ratio of momentum to species diffusivity and overall species transfer to pure diffusive species transfer, respectively. Additionally, the interfacial concentration jump of a transferred species i must be taken into account. It is common practice to do so by means of a simple distribution relation known as Henry's law, which reads $c_{i;I,\phi} = He \cdot c_{i;I,\varphi}$, where He denotes a (constant) distribution coefficient that mostly differs from unity due to different solubilities of species i within the phases φ compared to phase ϕ. This situation is depicted schematically in figure 7.5 for a spherical bubble.

It is emphasized that the interplay of species transfer and bubble (fluid) dynamics is still a topic of ongoing research and not fully understood. However, as in many fields of engineering, dimensionless correlations have proven to be reliable in most cases of practical interest. For the bubbles considered within this study two Sherwood correlations are found to be applicable for further quantitative validation of species transfer at high Schmidt numbers, namely

$$Sh_l = 2 + 9.45 \cdot 10^{-4} \cdot Re_b^{1.07} Sc_l^{0.888} \tag{7.1}$$

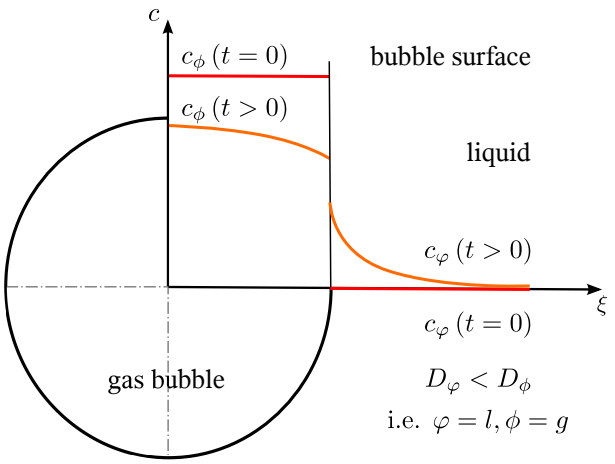

Figure 7.5: Schematic illustration of a characteristic concentration profile across a bubble surface for a transfer species.

according to Brauer [20] and

$$Sh_l = 2 + 1.5 \cdot 10^{-2} \cdot Re_b^{0.89} Sc_l^{0.7} \tag{7.2}$$

according to Hong and Brauer [21]. For correlation 7.1 the validity range of $1 \leq Re_b \leq 5000$ is rather broad, while correlation 7.2 is only valid for bubbles of dynamic shape and thus depends on the material properties of the system. The validity range can only be stated approximately: $3.73\,Mo^{-0.209} \lesssim Re_b \lesssim 3.1\,Mo^{-0.25}$ according to Brauer [20], which means a range of $610 \lesssim Re_b \lesssim 1390$ for the air/water system ($Mo \approx 2.5 \cdot 10^{-11}$). However, it has to be mentioned, that there is some scope of uncertainty: both the quantities involved within the dimensionless groups and the parameters within the dimensionless correlations constituted thereof are subject to this uncertainty. Their evaluation significantly depends on experimental conditions, which must ensure reproducibility, e.g., a constant temperature and constant bubble sizes, for instance. In effect, the results must be considered as an expected estimate rather than an exact prediction.

7.3. Mathematical Model and Governing Equations

Free-surface flows are incompressible flows possessing multiple distinct, immiscible fluids separated by interfaces of arbitrary complex morphology, across which fluid properties vary by orders of magnitude [22]. These characteristics generally make it challenging to follow the interface within a free-surface flow using Computational Multi-Fluid Dynamics (CMFD) methods.

Many approaches have evolved aiming at both a flexible and an accurate detailed simulation of bubbly flows. Methods cover front or interface tracking and interface

capturing methodologies, such as Front-Tracking, Level-Set and Volume-Of-Fluid methods as well known and widely employed approaches [22–24]. However, the Volume-Of-Fluid (VOF) methods have turned out to be an appropriate choice for the simulation of free-surface flows due to their robustness and flexibility, their simplicity and straightforward implementation along with inherent mass conservation when simulating morphological changes (coalescence and breakup) in two-phase systems. However, there are some disadvantages of the VOF approach as well: since the original VOF methods approximate the interface employing a geometrical reconstruction algorithm that ensures a sharp interface that is captured within one computational cell, it makes them not easily applicable on arbitrary polyhedral meshes where geometric reconstruction procedures turn out as very demanding. Therefore, so-called pseudo-VOF methods have emerged in both proprietary and Open Source CFD software (i.e., the *Free-Surface Model* in ANSYS CFX® or *interFoam* in OpenFOAM®). They rely upon continuum advection schemes which compress the interface in order to remain it as sharp as possible either using compressive discretisation schemes (as HRIC, CICSAM, inter-Gamma [25–29]) or employing a counter-gradient convective term [30–35] both of which are counter-acting the numerical diffusion that evolves from the algebraic treatment of the interface [22]. A main difficulty when dealing with pseudo-VOF methods is their accuracy and reliability of the underlying numerical schemes to ensure the constraint of a *sharp* interface: in contrast to a sharp interface representation, the interface is often blurred towards a more diffuse one, which is then inherently assigned a certain width of several cells thickness. More generally, the choice of an appropriate VOF approach is mainly about the balance of its simplicity and robustness and its accuracy.

This work employs a pseudo-VOF approach based on interFoam (OpenFOAM-1.5-dev), which, however, was considerably modified to meet the requirements as set out in section 7.4.

Addressing the numerical simulation of species transfer across fluid bubble interfaces, again considerable efforts have been devoted to gather insights both experimentally [12–19] and theoretically [5,20,36–47]. However, the majority of theoretical work was based upon approximate solutions for either simplified flow conditions (e.g., Stokes regime) or simplifying assumptions concerning the bubble's shape (e.g., spherical or ellipsoidal). Later more sophisticated approaches have evolved focusing both on purely physical [48–55] and reactive species transfer [56–62]. Conceptual approaches cover front-tracking [10,56,57,59,63–73], level-set [54,58,74,75] and Volume-Of-Fluid methods [53,60,61,76–81]. However, they mainly suffer from numerical difficulties due to both the steep interfacial concentration gradient at high Schmidt numbers (that needs to be resolved down to the Batchelor length scale) and a sharp concentration jump at high Henry coefficients occurring at the interface due to different species solubilities.

In this work a continuum modeling approach for solubility and species transfer is employed, in order to overcome these problems for interface capturing methods. This approach enables both VOF and pseudo-VOF approaches to deal with species transfer across fluid interfaces. This is accomplished by converting Henry's law into a solubility flux over the fluid interface, i.e., by conveying the concentration jump into a continuous effect being spread over interfacial cells. Note in passing, that this is a well-established practice in VOF methods for the interfacial momentum jump due to the surface tension force at free-surfaces known as Continuous-Surface-Force (CSF) Method [82]. We developed an analogous continuous approach for species transfer across fluid interfaces being treated by interface capturing approaches. The resulting model is entitled *Continuous-Species-Transfer (CST)* Method. The CST method is capable of reproducing the species flux across fluid interfaces evolving in a free-surface flow, where chemical species is transferred across a fluid interface of arbitrary morphology.

In the remainder, we will consider the mathematical model and the governing equations derived thereof that enables the three-dimensional numerical simulation of both the bubble dynamics (VOF method, subsection 7.3.3) and the interfacial species transfer (CST method, subsection 7.3.4) occurring in bubbly flows as they are found in bubble columns, for instance.

7.3.1. Conceptual Approach and Methodology

In the following a mathematical model framework for the fluid dynamics of free-surface flows comprising two incompressible Newtonian fluids is presented.

The concept of both the solver dealing with the free-surface and the CST method capturing the species transfer across it, is based on the so called *immersed interface concept* [83]. In this concept the interfaces between the two immiscible fluids are considered immersed or embedded into the computational domain. Hence, the resulting set of governing equations is valid throughout the entire domain including the two phases present in the system (i.e., the gas/bubble and liquid phase) and the interface separating them from each other.

In order to arrive at such a set of equations we start from first principles – that are the local instantaneous conservation equations valid within one phase. We apply the *conditional volume-averaging technique* [84–86]: the equations are first 'conditioned' for phase discrimination by multiplication with the phase-indicator or existence function for each phase φ

$$I_\varphi(\mathbf{x}, t) \equiv \begin{cases} 1 & \text{phase } \varphi \text{ present at } (\mathbf{x}, t) \\ 0 & \text{otherwise,} \end{cases} \tag{7.3}$$

and secondly volume-averaged. This reads for an arbitrary general flow quantity $\mathbf{\Phi}$, that might represent any physical property, scalar or tensor of any rank:

$$\overline{I_\varphi \mathbf{\Phi}} \equiv \frac{1}{V} \int_V I_\varphi \left(\mathbf{x} + \boldsymbol{\eta}, t\right) \mathbf{\Phi} \left(\mathbf{x} + \boldsymbol{\eta}, t\right) d\mathbf{x}_\eta. \tag{7.4}$$

The averaging is done over a spatially and temporally invariant control volume $V \in \Omega$, the centroid of which is located at $\mathbf{x}$. The relative position vector $\boldsymbol{\eta}$ is used to locate any point within V. Henceforth, the conditioned flow quantity $I_\varphi \mathbf{\Phi}$ might also be denoted as $\mathbf{\Phi}_\varphi$.

Subsequently summing up the conditional volume-averaged conservation equations for both phases yields the desired set of governing equations that suffices the immersed interface concept and is valid in the entire domain possessing the two phases – including the (embedded) interfacial structures separating them from each other.

Note, that this approach has been successfully applied to various two-phase systems, i.e., by Weller [85] for modeling turbulent flames or by Jasak [86] for modeling sea ice dynamics. In its essence this approach is a simple extension of that one applied by Dopazo [84] for turbulent single-phase flows. The analytical methods developed therefore can now be applied in a very general manner for two- or multiphase systems, if the phase-indicator function is introduced for phase discrimination and the interfaces separating the system's phases are allowed to propagate.

By use of this technique the volume-averaged indicator function itself can be interpreted most intuitively as the volumetric phase fraction within the control volume. In the case of $\mathbf{\Phi} = 1$ it follows from equation 7.4:

$$\overline{I_\varphi \left(\mathbf{x},\, t\right)} \equiv \alpha_\varphi \begin{cases} = 1 & \text{within phase } \varphi, \\ \in]0, 1[& \text{within the interfacial region,} \\ = 0 & \text{within phase } \phi. \end{cases} \tag{7.5}$$

As can be seen, by volume-averaging the interface as an intermittent entity (i.e., represented by a surface separating the two phases φ and ϕ) has become an interfacial transition zone within the computational domain, representing the immersed interface. Basically this is an interfacial region of finite width, over which material and transport properties are found to vary smoothly but rapidly towards the values pertaining to the pure phases. This conceptual transfer is depicted in figure 7.6 for both the local-instantaneous (7.6a) and the conditional volume-averaged (7.6b) situation.

As will be seen in the remainder, the local instantaneous conservation equations hold spatial and temporal derivatives of their dependent variables. Hence, let us have a detailed look at these derivatives in the same manner. For generality, this is

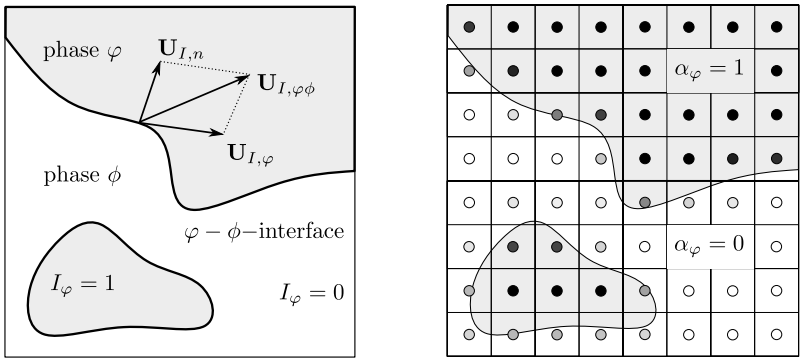

(a) physical domain Ω (local-instantaneous).

(b) computational domain (volume-averaged).

Figure 7.6: Conceptual approach of the conditional volume-averaging procedure and the immersed interface concept.

again done for an arbitrary general quantity $\mathbf{\Phi}$ being conditioned and subsequently averaged.

$$\overline{\nabla I_\varphi \mathbf{\Phi}} = \nabla\left(\overline{I_\varphi \mathbf{\Phi}}\right) = \nabla\,\overline{\mathbf{\Phi}_\varphi} = \nabla\Big(\alpha_\varphi\,\overline{\mathbf{\Phi}}^{\varphi}\Big). \tag{7.6}$$

Similarly, for a temporal derivative of a conditioned quantity $\mathbf{\Phi}_\varphi$, it is

$$\overline{\frac{\partial I_\varphi \mathbf{\Phi}}{\partial t}} = \frac{\partial\,\overline{I_\varphi \mathbf{\Phi}}}{\partial t} = \frac{\partial\,\overline{\mathbf{\Phi}_\varphi}}{\partial t} = \frac{\partial \alpha_\varphi\,\overline{\mathbf{\Phi}}^{\varphi}}{\partial t}. \tag{7.7}$$

By introducing a short-hand notation for the φ-sided surface average $\widetilde{\overline{\mathbf{\Phi}}}^{\varphi}$ of the property $\mathbf{\Phi}$ as the surface integral per unit volume divided by the surface area per unit volume,

$$\widetilde{\overline{\mathbf{\Phi}}}^{\varphi} \equiv \frac{1}{\Sigma} \lim_{\delta V_\varphi \to 0} \overline{\frac{1}{\delta V_\varphi} \int\limits_{S_I(\mathbf{x},\,t)} \mathbf{\Phi}(\mathbf{x},\,t) dS}\,, \tag{7.8}$$

where

$$\Sigma \equiv \lim_{\delta V \to 0} \overline{\frac{1}{\delta V} \int\limits_{S_I(\mathbf{x},\,t)} dS}\,, \tag{7.9}$$

we are able to consider conditioned derivatives of the arbitrary quantity $\mathbf{\Phi}$ rather than derivatives of the conditioned quantity $\mathbf{\Phi}_\varphi$. It follows expediently:

$$\overline{I_\varphi \nabla \mathbf{\Phi}} = \nabla\Big(\alpha_\varphi\,\overline{\mathbf{\Phi}}^{\varphi}\Big) - \widetilde{\overline{\mathbf{\Phi}\mathbf{n}_I}}^{\varphi} \Sigma, \tag{7.10}$$

$$\overline{I_\varphi \nabla\bullet\boldsymbol{\Phi}} = \nabla\bullet\Big(\alpha_\varphi \, \overline{\boldsymbol{\Phi}}^{\varphi}\Big) - \widetilde{\boldsymbol{\Phi}\bullet\mathbf{n}_I}^{\varphi} \Sigma, \tag{7.11}$$

and

$$\overline{I_\varphi \frac{\partial \boldsymbol{\Phi}}{\partial t}} = \frac{\partial \alpha_\varphi \, \overline{\boldsymbol{\Phi}}^{\varphi}}{\partial t} + \widetilde{\boldsymbol{\Phi}_{I,\varphi}\mathbf{n}_I\bullet\mathbf{U}_{I,\varphi\phi}}\Sigma, \tag{7.12}$$

where $\mathbf{U}_{I,\varphi\phi} = \mathbf{U}_{I,\varphi}$ denotes the interfacial velocity, in the absence of mass transfer due to condensation or evaporation ($\mathbf{U}_{I,n} = \mathbf{0}$), and $\mathbf{n}_I$ (short-hand notation for $\mathbf{n}_{I,\varphi\phi}$) represents the interfacial unit normal vector pointing from phase φ into phase ϕ (and vice versa for $\mathbf{n}_{I,\phi\varphi}$, since $\mathbf{n}_{I,\varphi\phi} = -\mathbf{n}_{I,\phi\varphi}$).

7.3.2. Assumptions

The so-called *one-field assumption* (mixture model) is utilized, where each phase moves with the centre-of-mass velocity $\mathbf{U}$ sharing one pressure field p, such that

$$\mathbf{U} \equiv \overline{\mathbf{U}}^{\varphi} = \overline{\mathbf{U}}^{\phi} = \widetilde{\mathbf{U}}^{\varphi} \qquad \text{and} \qquad p \equiv \overline{p}^{\varphi} = \overline{p}^{\phi}. \tag{7.13}$$

Of course, validity and fidelity of such kind of modeling approach will highly depend on an

1.) appropriate local resolution of the interface morphology, that is the local interface normal $\mathbf{n}_I$ and its curvature κ_I and an

2.) appropriate local resolution of the boundary layer at the interface.

Otherwise, either the constraint of an adequate interface representation characterized by a rapid (but still smooth) change of phase properties as density and viscosity is violated, or the one-field assumption becomes inappropriate since the phase velocities will differ from the centre-of-mass velocity giving rise to some interfacial drift or phase-slip velocity.

7.3.3. Bubble Dynamics – Volume-of-Fluid Method

Governing Equations

The governing equations covering the fluid dynamics of the two-phase system under consideration comprise the conditional volume-averaged conservation equations of mass (continuity), momentum and the volumetric phase fraction. The technique of conditional volume-averaging is pointed out in detail in 7.A and will be utilized as well for the conservation equation of chemical species for the derivation of the CST

method. Hence, the conditional volume-averaged governing equations covering the fluid dynamics are just stated here. The continuity equation reads

$$\nabla\bullet\mathbf{U} = 0 \tag{7.14}$$

ensuring mass conservation. Further, the momentum equation can be written as

$$\frac{\partial\rho\mathbf{U}}{\partial t} + \nabla\bullet\left(\rho\mathbf{U}\mathbf{U}\right) = -\nabla p + \nabla\bullet\boldsymbol{\tau} + \mathbf{f}_g + \mathbf{f}_\sigma, \tag{7.15}$$

and the volumetric phase fraction equation as

$$\frac{\partial\alpha_\varphi}{\partial t} + \nabla\bullet\left(\mathbf{U}\alpha_\varphi\right) + \nabla\bullet\left(\mathbf{U}_r\alpha_\varphi(1-\alpha_\varphi)\right) = 0. \tag{7.16}$$

Note in passing, that the relative velocity $\mathbf{U}_r \equiv \overline{\mathbf{U}}^{\varphi} - \overline{\mathbf{U}}^{\phi}$ clearly is zero for the adopted mixture model. However, as set out in the remainder (cf. pg. 195) $\mathbf{U}_r$ is modelled as compressive velocity $\mathbf{U}_c$ in order to maintain a sharp interface representation while loosing its physical significance.

$\boldsymbol{\tau}$ represents the viscous stress tensor, which reads for an incompressible Newtonian fluid $\boldsymbol{\tau} = -\mu\left(\nabla\mathbf{U} + \nabla\mathbf{U}^T\right)$. $\mathbf{f}$ denotes volumentric momentum sources due to gravity (subscript g) and interfacial surface tension (subscript σ). α_φ is the volumetric phase fraction pertaining to one phase while the second can be evaluated to $(1-\alpha_\varphi)$, since the sum needs to be equal to unity in a two-phase system.

For comprehension it is important to note, that equation 7.16 is the conditional volume-averaged equivalent of the so-called topological equation: $\frac{\partial I_\varphi}{\partial t} + \mathbf{U}_I\bullet\nabla I_\varphi = 0$, since I_φ as a genuine phase characteristics can be considered as a Lagrangian invariant and thus suffices this transport equation. Physically this simply states the fact that the interface travels with the local interfacial velocity $\mathbf{U}_I$, thus representing the temporal evolution of the interfacial structure (morphology) in a free-surface flow. Assuming $\widetilde{\overline{\mathbf{U}}}^{\varphi} = \mathbf{U}$ then leads to the volumetric phase fraction equation according to equation 7.16.

Furthermore, note that the governing equations 7.14 to 7.16 are commonly found to constitute a VOF model and are well-established. However, though they are commonly claimed valid, they are indeed the result of a consistent derivation starting from local instantaneous conservation equations for mass and momentum and the so-called topological equation, by means of which interfacial propagation is taken into account.

Models

The methodology of conditional volume-averaging employed for derivation causes terms stemming from averaging that are a priori unknown and cause the system of

governing equations to be unclosed. Hence, modeling of these terms is necessary in order to arrive at a closed set of governing equations.

Buoyancy Force and Viscous Stress Model The density ρ and viscosity μ in the momentum equation 7.15 must be considered as mixture quantities within the interfacial region, that generally need appropriate modeling. As the mixture density ρ might be seen as a *volumetric mass concentration*, modeling is simply accomplished using the *volumetric* phase fractions:

$$\rho = \sum_{k=\varphi,\phi} \alpha_k \, \overline{\rho}^k. \tag{7.17}$$

However, the issue of correct viscous stress modeling at fluid interfaces – e.g., correct capturing of the viscosity term within $\boldsymbol{\tau} = -\mu \left(\nabla \mathbf{U} + \nabla \mathbf{U}^T \right)$ at the free-surface – is a quite important one, though not being adressed often in the literature dealing with the VOF approach: it is common practice to use a arithmetic mean as $\mu = \sum_\varphi \alpha_\varphi \, \overline{\mu}^\varphi$ for the mixture viscosity – as being done for the mixture density. However, being confronted with free-surface flows possessing gross and abrupt changes of the viscosity across the interface the correct evaluation of μ at the interface (i.e., the interfacial viscosity) is crucial for reproducing the correct free-surface dynamics in numerical simulations. Simply using a arithmetic mean actually causes an artificial (increased) acceleration of fluid elements in the lighter phase which yields too high velocities due to an unphysical viscous term $\nabla\bullet(\mu \left(\nabla \mathbf{U} + \nabla \mathbf{U}^{\mathrm{T}} \right))$ [22].

In order to employ the correct mixture viscosity, μ must be evaluated consistent with its discretization in $\nabla\bullet \left(\mu \left(\nabla \mathbf{U} + \nabla \mathbf{U}^T \right) \right)$ as μ_f (meaning at the cell faces rather than at the cell centres). Moreover, according to Kothe [22], one must account for the relative interface/cell-face orientation:

$$\mu_f = \eta_f \mu^s + (1 - \eta_f) \, \mu^p, \tag{7.18}$$

$$\text{where} \quad \eta_f \equiv |\hat{\mathbf{n}}_{\varphi,f} \bullet \hat{\mathbf{n}}_{S,f}| \quad \text{with} \quad \hat{\mathbf{n}}_{\varphi,f} = \left(\frac{\nabla \alpha_\varphi}{|\nabla \alpha_\varphi|} \right)_f, \quad \hat{\mathbf{n}}_{S,f} = \frac{\mathbf{S}_f}{|\mathbf{S}_f|},$$

$$\text{and} \quad \mu^s = \sum_{k=\varphi,\phi} \alpha_{k,f} \, \overline{\mu}^k, \quad \mu^p = \left(\sum_{k=\varphi,\phi} \frac{\alpha_{k,f}}{\overline{\mu}^k} \right)^{-1}. \tag{7.19}$$

As can be seen, η_f represents an interpolation factor accounting for the interface/cell-face orientation, and evaluating μ_f in the limits of a harmonic mean μ^s ($\eta_f \to 1$, serial connection of viscous resistances [22]) and a arithmetic mean μ^p ($\eta_f \to 0$, parallel connection of viscous resistances [22]).

Interfacial Surface Tension Model The influence of surface tension to the momentum needs further attention, as the interface is represented by an interfacial transition region of a finite width. However, the nature of the surface tension force is that of a surface force imposing a momentum jump at the interface *surface*.

Thus, in order to be consistent, the so-called Continuous-Surface-Force (CSF) method according to Brackbill et al. [82] is adopted. This approach reads:

$$\mathbf{f}_\sigma = \sigma \widehat{\kappa} \nabla \alpha_\varphi, \quad \text{with} \quad \widehat{\kappa} = -\nabla\bullet \left(\frac{\nabla \alpha_\varphi}{|\nabla \alpha_\varphi|} \right), \tag{7.20}$$

where σ denotes the surface tension which is assumed to be constant. I.e., phenomena rendering the surface tension variable (e.g. Marangoni effects) are neglected.

Phase Relative Velocity Model Another issue to be addressed when considering pseudo-VOF methods, is that both accuracy and reliability heavily rely upon the numerical approach employed to ensure a sharp interface representation – counteracting numerical diffusion.

Note that the third term in the volumetric phase fraction equation 7.16 does represent a convective transport term being different from zero only in the interfacial transition region due to $\alpha_\varphi (1 - \alpha_\varphi)$. However, the phase relative velocity $\mathbf{U}_r$ needs to be modeled as the VOF model has been derived under the one-field assumption and thus its governing equation only holds *one* mixture momentum.

According to Weller [30] and Olsson [33–35] this modeling can be accomplished appropriately[1] (in a conservative and bounded manner) by modeling this term such that it ensures a sharp interface. For this the phase relative velocity $\mathbf{U}_r$ is considered as compressive velocity $\mathbf{U}_c$ being oriented normal to the interface:

$$\mathbf{U}_c \equiv \min\left[c_\alpha |\mathbf{U}|, \max(|\mathbf{U}|)\right] \frac{\nabla \alpha_\varphi}{|\nabla \alpha_\varphi|} \quad \text{, where usually } 1 \leq c_\alpha \leq 4. \tag{7.21}$$

By this approach the third term in the volumetric phase fraction equation 7.16 becomes a compressive term acting counter-gradient with respect to the volumetric phase fraction – that is perpendicular to the interface without biasing the free-surface flow at all but ensuring a sharp interface representation.

[1] Indeed the relative velocity $\mathbf{U}_r$ approaches zero when increasing the mesh resolution sufficiently. However, modeling $\mathbf{U}_r$ in an other way provides an avenue to ensure a sharp interface. It shall be emphasized that doing so results in a model approach that is motivated purely numerically.

7.3.4. Species Transfer – Continuous-Species-Transfer (CST) Method

In order to derive a species transport equation that is valid throughout the entire domain and accounts for species transfer across the interface(s) in a free-surface flow scenario, we start from first principles: the local instantaneous conservation equation of an arbitrary chemical species i being valid within a phase φ (bulk) reads

$$\frac{\partial c_i}{\partial t} + \nabla\bullet\left(c_i\mathbf{U}\right) = \nabla\bullet\left(D_i\nabla c_i\right) + R_i \qquad \text{within } \Omega_\varphi(t). \tag{7.22}$$

Its corresponding jump conditions are

$$\left\|\left(-D_i\nabla c_i\right)\bullet\mathbf{n}_I\right\| = 0 \qquad \text{and} \qquad \left\|c_i\right\| = c_{i;I,\varphi}\cdot\left(1-He\right) \Leftrightarrow He = \frac{c_{i;I,\phi}}{c_{i;I,\varphi}}, \tag{7.23}$$

where $\|\cdot\|$ denotes an interfacial jump as $\|f\| = f_{I,\varphi} - f_{I,\phi}$. Hence, the latter equation represents Henry's law.

Conditioning and volume-averaging of equation 7.22, eventually yields[2]:

$$\overline{I_\varphi\frac{\partial c_i}{\partial t}} + \overline{I_\varphi\nabla\bullet\left(c_i\mathbf{U}\right)} = \overline{I_\varphi\nabla\bullet\left(D_i\nabla c_i\right)} + \overline{I_\varphi R_i} \tag{7.24}$$

$$\Leftrightarrow \frac{\partial\alpha_\varphi\,\overline{c_i}^\varphi}{\partial t} + \nabla\bullet\left(\alpha_\varphi\,\overline{c_i}^\varphi\,\overline{\mathbf{U}}^\varphi\right) = \nabla\bullet\left(\alpha_\varphi\,\overline{D_i}^\varphi\nabla\,\overline{c_i}^\varphi\right) + \alpha_\varphi\,\overline{R_i}^\varphi - \overbrace{\overline{D_i\nabla c_i\bullet\mathbf{n}_{I,\varphi\phi}}}^{\varphi}\,\Sigma. \tag{7.25}$$

In the remainder, we will neglect chemical reactions: thus, $\overline{R_i}^\varphi = \overline{R_i}^\phi = 0$.

Now, in order to employ the immersed interface concept we sum up for both phases φ and ϕ present in the system. Note that the surface integral in the resulting governing equation, i.e., the sum over the phases of the last term on the r.h.s. of equation 7.25, equals zero due to the continuity of species fluxes across the interface.

In order to arrive at the desired governing equation solely in terms of mixture quantities, we define a volumetric mixture concentration as

$$C_i \equiv \alpha_\varphi\,\overline{c_i}^\varphi + \alpha_\phi\,\overline{c_i}^\phi. \tag{7.26}$$

However, when summing up for both phases φ and ϕ, this only works for the terms on the l.h.s. of equation 7.25, while the first term on the r.h.s. of equation 7.25 needs further analysis in order to finally formulate solely in terms of the mixture

[2] For details on the conceptual approach of conditional volume-averaging see 7.A

concentration. This term might be split up more conveniently into (a) bulk and (b) interfacial contributions according to

$$\sum_{k=\varphi,\phi} \nabla\bullet\left(\alpha_k\,\overline{D_i}^{k}\nabla\,\overline{c_i}^{k}\right) = \underbrace{\sum_{k=\varphi,\phi} \nabla\bullet\left(\nabla\left(\overline{D_i}^{k}\alpha_k\,\overline{c_i}^{k}\right)\right)}_{\text{(a)}} - \underbrace{\sum_{k=\varphi,\phi} \nabla\bullet\left(\overline{D_i}^{k}\,\overline{c_i}^{k}\nabla\alpha_k\right)}_{\text{(b)}}. \tag{7.27}$$

(a) Without loss of generality, the molar mixture concentration C_i might be defined expediently as well as

$$C_i \equiv \frac{\overline{D_i}^{\varphi}\alpha_\varphi\,\overline{c_i}^{\varphi} + \overline{D_i}^{\phi}\alpha_\phi\,\overline{c_i}^{\phi}}{\alpha_\varphi\,\overline{D_i}^{\varphi} + \alpha_\phi\,\overline{D_i}^{\phi}}, \tag{7.28}$$

where the denominator could be denoted shorter as molecular diffusivity $D_i \equiv \alpha_\varphi\,\overline{D_i}^{\varphi} + \alpha_\phi\,\overline{D_i}^{\phi}$ – similar to μ, the momentum diffusivity.

This variant enables us to rewrite the bulk term (a) in equation 7.27 solely in terms of the mixture quantities C_i and D_i:

$$\sum_{k=\varphi,\phi} \nabla\bullet\left(\nabla\left(\overline{D_i}^{k}\alpha_k\,\overline{c_i}^{k}\right)\right) = \nabla\bullet\left(D_i\nabla C_i\right) + \nabla\bullet\left(C_i\nabla D_i\right). \tag{7.29}$$

However, while the above procedure leads to the known diffusive terms being valid for species transport within the bulk, equation 7.28 in a strict sense can only be regarded as a model, which requires validation in order to assess its accuracy (cf. 7.B).

(b) Noting that $\nabla\alpha_\varphi = -\nabla\alpha_\phi$ the interfacial term (b) reads

$$\nabla\bullet\left[\left(\overline{D_i}^{\varphi}\,\overline{c_i}^{\varphi} - \overline{D_i}^{\phi}\,\overline{c_i}^{\phi}\right)\nabla\alpha_\varphi\right].$$

Making use of Henry's law (consistently as an averaged jump condition: $\overline{c_i}^{\varphi} = He\cdot\overline{c_i}^{\phi}$) at the interface, this becomes

$$\nabla\bullet\left[\left(\overline{D_i}^{\varphi} - \frac{\overline{D_i}^{\phi}}{He}\right)\overline{c_i}^{\varphi}\nabla\alpha_\varphi\right],$$

which may be rewritten in terms of $C_i \equiv \alpha_\varphi\,\overline{c_i}^{\varphi} + (1-\alpha_\varphi)\,\overline{c_i}^{\phi}$ by using Henry's law again, which yields $\overline{c_i}^{\varphi} = \frac{C_i}{\alpha_\varphi + (1-\alpha_\varphi)/He}$. Hence, it is

$$\sum_{k=\varphi,\phi} \nabla\bullet\left(\overline{D_i}^{k}\,\overline{c_i}^{k}\nabla\alpha_k\right) = \nabla\bullet\left[\left(\frac{\overline{D_i}^{\varphi} - \overline{D_i}^{\phi}/He}{\alpha_\varphi + (1-\alpha_\varphi)/He}\right)C_i\nabla\alpha_\varphi\right]. \tag{7.30}$$

Thus, the conditional volume-averaged transport equation for an arbitrary species i reads in its final form

$$\frac{\partial C_i}{\partial t} + \nabla_\bullet \left(C_i \mathbf{U}\right) = \nabla_\bullet \left(D_i \nabla C_i\right) + \nabla_\bullet \left(C_i \nabla D_i\right) - \nabla_\bullet \left[\left(\frac{\overline{D_i}^{\varphi} - \overline{D_i}^{\phi}/He}{\alpha_\varphi + (1-\alpha_\varphi)/He} \right) C_i \nabla \alpha_\varphi \right]. \tag{7.31}$$

Note that this governing equation 7.31 is – as initially claimed – valid throughout the entire computational domain (including the interface) accounting for both convective and diffusive species *transport* and interfacial species *transfer* for diffusivities and solubilities that are allowed to severly differ within the phases under consideration.

7.4. Implementation

For this study OpenFOAM® (Open Field Operation And Manipulation) has been employed. OpenFOAM is a flexible and efficient C++ library for the customization and extension of applications (solvers and utilities) and models manipulating and operating on scalar, vectorial and tensorial fields [87–89]. Thus, OpenFOAM is suitable to handle all kind of continuum problems.

OpenFOAM is based on an unstructured mesh formulation with an collocated cell-centered variable arrangement featuring unstructured boundary-fitted meshes (including topological mesh changes) for arbitrary complex geometries. In its essence, OpenFOAM provides numerical methods for the discretization of partial differential equations along with solvers for the corresponding numerical solution of the resulting system of algebraic equations. I.e., differential operators as $\nabla_\bullet$, ∇^2, $\frac{\partial}{\partial t}$ can be invoked using *two main tensor-derivative namespaces*: the `fvm` (finiteVolumeMethod) namespace and the `fvc` (finiteVolumeCalculus) namespace. E.g., the above differential operators correspond to `fvm::div()`, `fvm::laplacian()`, `fvm::ddt()` or alternatively `fvc::div()`, `fvc::laplacian()`, `fvc::ddt()` in OpenFOAM. The `fvc` functions perform an explicit evaluation of predetermined data by mapping from one field to another, while the `fvm` functions construct appropriate matrices using the finite-volume discretization, which, in turn, enables to create entire matrix representations of differential equations and their implicit numerical solution. For this purpose, equation objects have been defined: `fvMatrixScalar`, `fvMatrixVector`. These hold the matrices that represent the equations and handle the numerical solution.

Moreover, to represent fields, there exist both *basic tensor field classes* and *geometric tensor field classes*: e.g., `scalarField`, `vectorField`, `tensorField` and `volScalarField`, `volVectorField`, `volTensorField`. Note, that the latter three classes are referred to as geometric tensor field classes as they contain a reference to the mesh – corresponding to the control volumes constituting the computational

domain. Furthermore, they comprise boundary information, previous time steps necessary for the temporal discretization, and SI dimension set information. Additionally, `surfaceScalarField`, `surfaceVectorField` and `surfaceTensorField` hold data associated to fields at the surfaces of control volumes.

Now addressing multiple chemical species, we extended the present OpenFOAM solver *interFoam* using a `PtrList<T>` C++ template: `PtrList<volScalarField>` declares a list of pointers to a number of volumetric scalar fields in memory. This enables to create and initialize all required fields and quantities as provided in Source Code 7.1. Note that the number of created fields conveniently corresponds to the number of field data files provided in the initialization directory for each species.

```
// Determine number of species concentration fields
scalar n = 0;

// Search for list of objects at startTime
IOobjectList objects(mesh, "0");

// Search list of objects for volScalarFields
IOobjectList scalarFields
(
    objects.lookupClass("volScalarField")
);

for
(
    IOobjectList::iterator scalarFieldIter
      = scalarFields.begin();
    scalarFieldIter != scalarFields.end();
    ++scalarFieldIter
)
{
    // Read field
    volScalarField field
    (
        *scalarFieldIter(),
        mesh
    );
    word fieldname = field.name();
    if( fieldname.find("C") == 0)
    {
        n++;
    }
}
Info<< "Number of Species = " << n << endl;

// Create species concentration fields
```

```
PtrList<volScalarField> C(n);
for(label i=0; i<C.size(); i++)
{
    word fieldName = "C" + Foam::name(i);
    Info<< "Reading field " << fieldName << endl;

    C.set //—HM 'set or hook' (OF—version dependent)
    (
    i,
    new volScalarField
        (
        IOobject
            (
            fieldName,
            runTime.timeName(),
            mesh,
            IOobject::MUST_READ,
            IOobject::AUTO_WRITE
            ),
            mesh
        )
    );
}

// Read Henry coefficients associated to Species
PtrList<dimensionedScalar> He(n);
for(label i=0; i<He.size(); i++)
{
    Info<< "Reading He"<<Foam::name(i)
        << " coefficient for species " << i
        << endl;
    He.set
    (
        i,
        new dimensionedScalar
        (
            twoPhaseProperties.lookup ("He" + Foam::name(i))
        )
    );
}
```

Source Code 7.1: createFields.H.

The solution of the conditional volume-averaged species conservation equation 7.31 is then invoked at the end of the algorithm of *interFoam* as presented in Source Code 7.2.

```
for(label i=0; i<C.size(); i++)
{
    volScalarField& Ci = C[i];
    dimensionedScalar& Hei = He[i];

    surfaceScalarField phiCi =
    (
       fvc::interpolate((Dl - Dg/Hei)/(gamma + (1 - gamma)/Hei))
       * fvc::snGrad(gamma)
    ) * mesh.magSf();

    surfaceScalarField phiD =
    (
        fvc::snGrad(Dmolar)
    )*mesh.magSf();

    solve
    (
        fvm::ddt(Ci)
      + fvm::div(phi, Ci, scheme)
      - fvm::laplacian(fvc::interpolate(Dmolar),Ci)
      - fvm::div(phiD, Ci, CScheme)
      + fvm::div(phiCi, Ci, CScheme),
      mesh.solver("Ci")
    );

    Info<< "  Min(C" << Foam::name(i) << ") = " << min(Ci).value()
        << "  Max(C" << Foam::name(i) << ") = " << max(Ci).value()
        << endl;
}
```

Source Code 7.2: cEqn.H.

Furthermore, we have adopted the adaptive mesh refinement (AMR) technique [90,91] and a moving frame of reference (MFR) method [92]. The MFR technique ensures a significant decrease of computational costs, since the computational domain can be thought of moving along with the rising bubbles through the quiescent liquid. Beside that, the numerical requirement of a sufficiently resolved mesh in the proximity of the bubble surface is taken care of by AMR. This allows for capturing the details of species transport and interfacial species transfer adequately. In order to fulfill the requirement of a sufficient spatial resolution, we consider the Batchelor length scale l_B as a first measure for the required resolution. This length scale can be expressed in terms of the Kolmogorov length scale l_K: $l_B = l_K/\sqrt{Sc_l}$ with $l_K \equiv \left(\nu_l^3/\epsilon\right)^{0.25}$. Assuming the specific energy dissipation ϵ, i.e., the work that is done by a bubble while rising through a quiescent liquid, can be estimated according to $\epsilon \approx U_\infty g$,

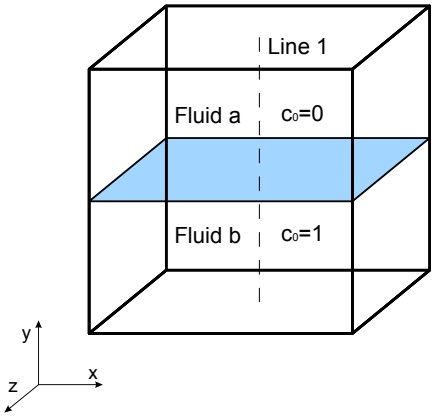

Figure 7.7: Schematic illustration of the test case for species transfer across a planar interface in a cube.

eventually the Batchelor length scale takes values of $l_B \approx 1.5\,\mu\text{m}$ for bubbles with rising velocities of about $0.2\,\frac{\text{m}}{\text{s}}$.

7.5. Validation Studies

7.5.1. Species Transfer across a Planar Interface in a Cube – Test Case I

For the purpose of proof-of-concept and preliminary validation, the first test case to be considered simply comprises a cube with 1 cm edge length, the lower half of which is filled with water, that is initially loaded with a transfer component. As such, the lower phase serves as the phase to be stripped off a transfer component, while the upper half is filled with air, that initially is pure – i.e., devoid of the transfer component. The test case configuration is shown in figure 7.7.

The material properties are provided in table 7.1. As a preliminary study, transport properties (i.e., the diffusion coefficients) have been depicted such that the transient process of species transfer within the cube can be observed within an endurable time-frame of about 1.2 s. The Henry coefficient has been set to $He = 3$. The Morton number is $Mo = 2.52 \cdot 10^{-11}$.

In order to assess solely the quality of the CST method – that is governed by the species transfer and solubility terms of the CST method (i.e., the r.h.s of equation 7.31) – the fluids are to be considered at rest. Therefore, no-slip boundary conditions are imposed upon the walls of the cube. Wetting phenomena have been neglected, e.g., the contact angle was assumed to be 90°. Consequently, the Neumann boundary condition has been chosen for the species concentration equation. The mesh comprises

Table 7.1: Material and transport properties.

air	
density	$1.122\ \frac{\mathrm{kg}}{\mathrm{m}^3}$
dynamic viscosity	$18.24 \cdot 10^{-3}$ mPa s
diffusion coefficient	$1\ \frac{\mathrm{cm}^2}{\mathrm{s}}$ (a)
	$0.1916\ \frac{\mathrm{cm}^2}{\mathrm{s}}$ (b)
water	
density	$998.2\ \frac{\mathrm{kg}}{\mathrm{m}^3}$
dynamic viscosity	1 mPa s
diffusion coefficient	$0.2\ \frac{\mathrm{cm}^2}{\mathrm{s}}$ (a)
	$2.01 \cdot 10^{-5}\ \frac{\mathrm{cm}^2}{\mathrm{s}}$ (b)

(a) test case I – species transfer across a planar interface in a cube, $Sh_l = 0.05$

(b) test case II – species transfer across a deforming bubble surface while rising through a quiescent liquid, $Sh_l = 498.4$

102 400 hexahedral cells, with 256 cells being used for the spatial discretization over the cube's height and 20 cells for each other direction.

Figure 7.8 shows the normalized species concentration profiles across the planar interface within the cube. For comparison and in order to gather quantitative insights, the results of the numerical solution using the CST method in OpenFOAM were compared to the results gained from a one-dimensional model, the solution of which can be considered exact due to the high temporal and spatial resolution which has been adopted. These reference simulations were performed using Matlab® v. 7.9 (R2009). A decent agreement is observed between the CST method and the exact solution gathered by the one-dimensional reference model. Of course, a further validation has been accomplished, through the course of which the model parameters have been varied to more demanding extremes as well – appendix 7.B. However, the results are still found to be in very good agreement.

7.5.2. Species Transfer across a Deforming Bubble Surface – Test Case II

Figure 7.9 illustrates the corresponding configuration for the simulation of a single bubble rising in a quiescent liquid. In this work the computational domain is 'moved'

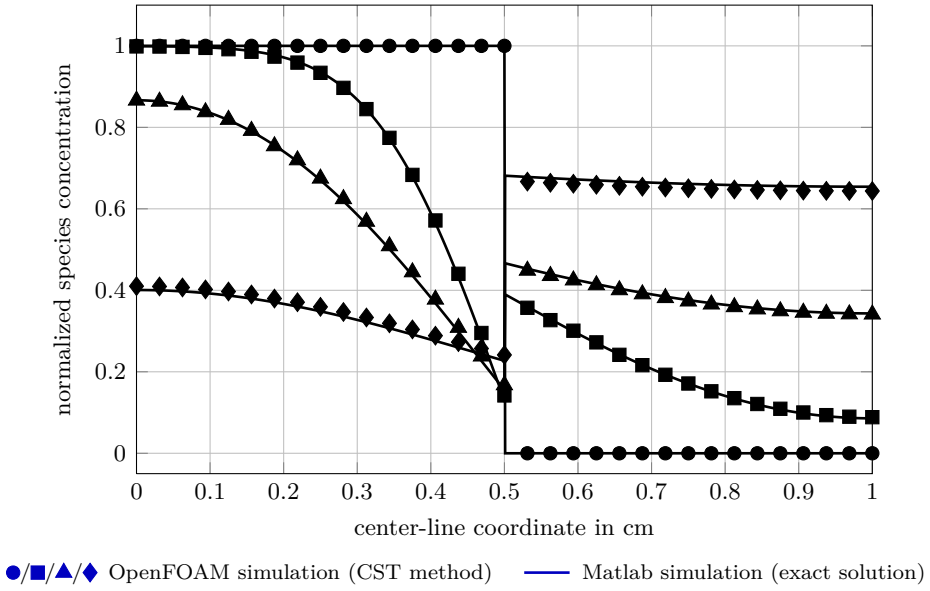

Figure 7.8: Quantitative comparison of normalized species concentration profiles across a planar interface in a cube – Exact reference solution (1D model) and numerical solution (CST method). Measures taken along the center-line for 0.0 s (●), 0.05 s (■), 0.2 s (▲) and 0.8 s (♦), respectively..

along with a rising bubble using a MFR technique. For this reason, the size of the computational domain is only in the range of several bubble diameters.

The material and transport properties are listed in table 7.1. Note that these values refer to an air-water system, i.e., an air bubble in water and oxygen being the dilute species transferred from the air-bubble into pure water. The Henry coefficient has been set appropriately to $He = 33$. The validation study has been performed for bubbles of different sizes. Three simulations for bubbles of 2-6 mm diameter, which is in the industrial relevant range, are performed.

For a qualitative consideration, we have extracted the iso-surfaces of the oxygen concentration around an air bubble while rising through a quiescent water – as shown in figure 7.10 for the concentration wakes of a 6 mm bubble. Results were compared with experimental results exposing the concentration wake by laser-induced fluorescence (LIF). In doing so, a reasonable good agreement regarding both bubble shape and wake shape has been observed. In order to assess quantitative measures, two basic features of reactive bubbly flow are subject to validation: (1) bubble dynamics and (2) bubble species transfer. The figures include experimental results of Duineveld and Schlüter et al. [93, 94] as well as numerical results of Bothe et al. [95, 96].

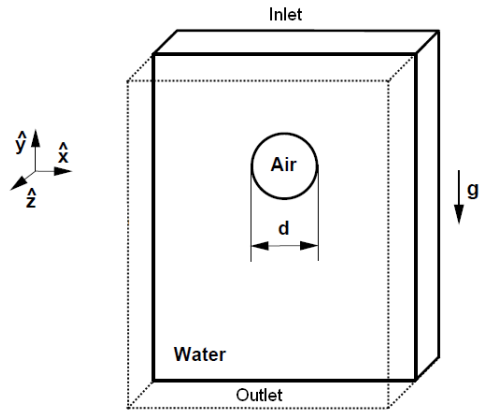

Figure 7.9: Schematic illustration of the test case for species transfer across a deforming bubble surface while rising through a quiescent liquid; cubic domain with edge length $l = 7\,d$.

(1) Figure 7.11 shows the terminal rising velocity taken from the simulation results. The rising velocity is around 20 $\frac{\text{cm}}{\text{s}}$ as one would expect for these systems. The rising velocities were found to coincide over different bubble diameters with the same undulating characteristics as exposed by the underlying experimental velocity data. Figure 7.12 depicts the trajectory of a 4 mm bubble in top view. The trajectory expands over $0.6 \cdot 10^{-2}$ m in both directions perpendicular to the bubble's rising direction. Moreover, different bubble trajectory types (i.e., straight, zigzag and spiral/helical) and shape regimes (spherical and ellipsoidal) have been observed. This indicates (at least) that the major features of the bubbly flow dynamics – form/shape oscillation and wake phenomena – are captured correctly. Hence, the conclusion might be drawn that both results are in very good agreement with experimental data.

(2) Extracting the integral overall mass transfer coefficient from the numerical data enables us to compare the numerical results with the vast variety of correlations available in literature. This is accomplished by examining the temporal evolution of the normalized bubble mean concentration. Taking into account Henry's law, the integral overall mass transfer coefficient k_l is determined. Consequently, this yields the desired Sherwood number $Sh = \beta_l d_b / D_l$ by using the so-called 'overall concept', that is the overall mass transfer resistance is presumably laid into the liquid phase. Hence, it is $\beta_l \approx k_l$. Two Sherwood correlations (cf. equations 7.1 and 7.2) have been used for quantitative comparison. The bubble Reynolds numbers are $Re_b = 461.8$, $Re_b = 881.0$ and $Re_b = 1239.5$ for the 2, 4 and 6 mm bubbles under consideration within this study. The results are listed table 7.2.

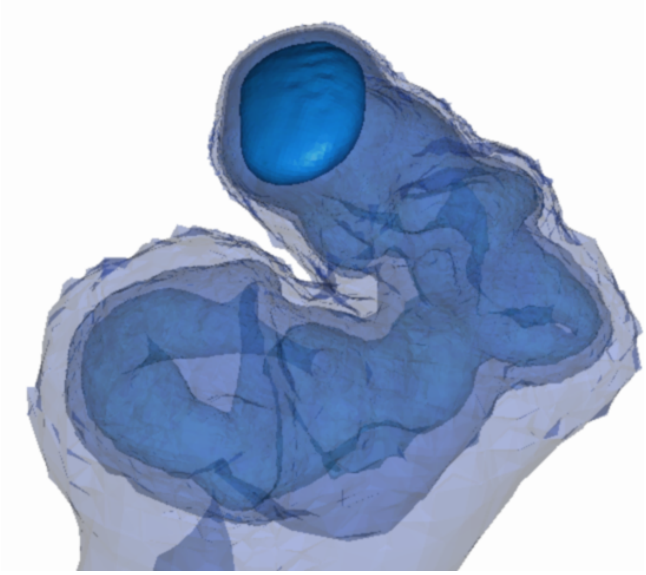

(a) Iso-surfaces $(0.005, 0.01, 0.025)$ of normalized oxygen concentration in the wake of a 6 mm air bubble while rising through a quiescent water.

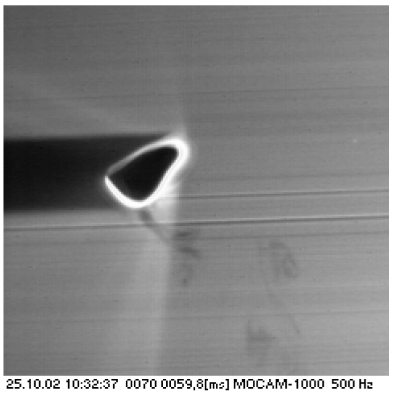

(b) Oxygen concentration wake exposed by laser-induced fluorescence (LIF) measurements – decreasing brightness indicates an increasing oxygen concentration [18]..

Figure 7.10: Oxygen concentration wake behind a rising 6 mm bubble.

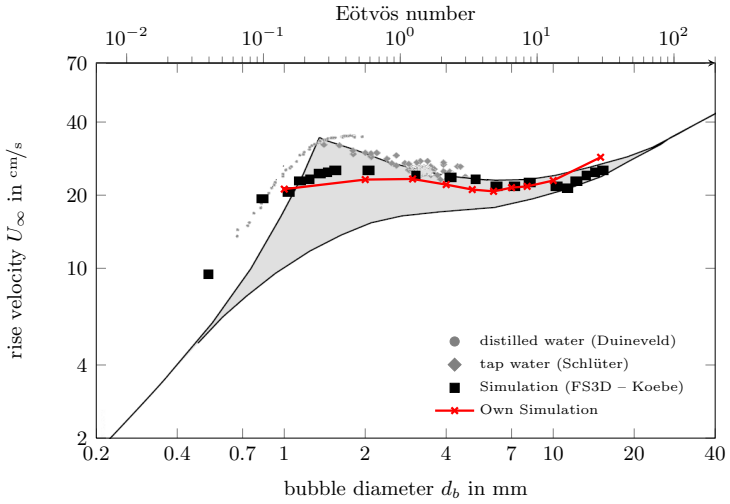

Figure 7.11: Quantitative comparison of terminal rising velocities of single bubbles at different (equivalent) diameters rising in a quiescent liquid – results of numerical simulation and experimental data.

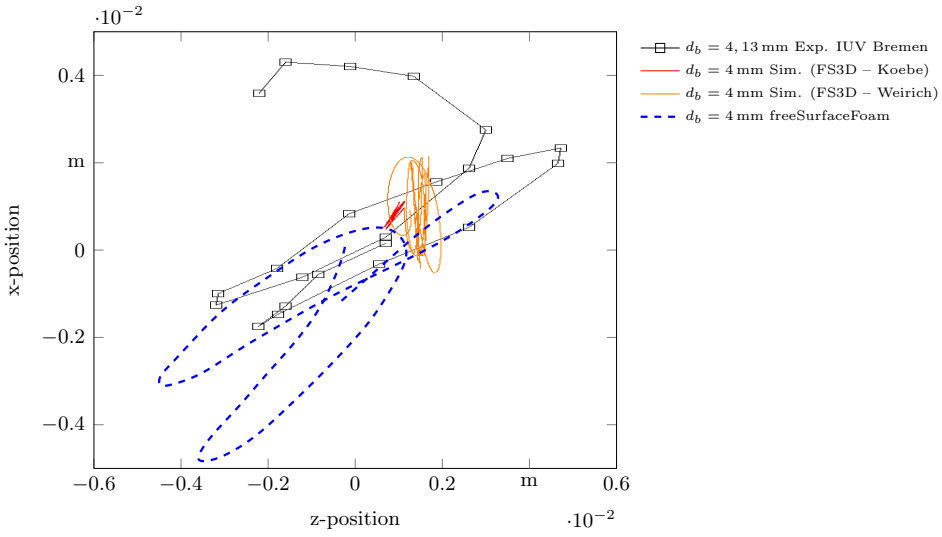

Figure 7.12: Quantitative comparison of the trajectory (top view) of a 4 mm bubble rising in a quiescent liquid – results of numerical simulation and experimental data.

Table 7.2: Quantitative comparison of Sherwood numbers – experiments (Sherwood correlations) and numerical simulations (CST method).

Sherwood numbers acc. to	**bubble diameter**		
	2 mm (Eo=0.54)	4 mm (Eo=2.14)	6 mm (Eo=4.82)
CST method	221.3	514.2	792.0
Brauer [20]	169.0	335.3	482.3
Hong & Brauer [21]	275.2	487.4	659.7

Evidently, table 7.2 indicates again a good agreement with reference values, allowing the conclusion to be drawn that the CST method is capable of capturing species transfer in (gas-liquid) free-surface flows – as proved by means of bubbly flows as example. However, there is some scope of uncertainty regarding the values of the Sherwood numbers: these clearly show some deviation even when underlying established Sherwood correlations. However, the CST method is found to deliver values within the same confines as the Sherwood correlations. Thus, the CST method might be justifiably considered to be applicable for the range of transport and material properties that are typically found in the chemical and process industries, where species transfer plays a major role.

7.6. Summary

A new numerical approach – entitled Continuous-Species-Transfer (CST) Method – is presented in this paper. The CST method is capable of simulating species transfer across fluid interfaces of arbitrary morphology as they are typically dealt with in interface capturing (volume tracking) methods as the VOF method.

The derivation starts from first principles, that is the conservation equation for an arbitrary chemical species. By use of conditional volume-averaging and the immersed interface concept, we arrive at a final form which comprises terms accounting for both species *transport* within the phases and species *transfer* between the phases at different diffusivities and solubilities. The resulting governing equation is valid throughout the entire computational domain holding the volumetric molar species concentration as a mixture quantity.

Validation studies show a decent agreement of the obtained results compared to both analytical and exact numerical reference solutions as well as to experimental results. By examining the oxygen transfer of a single (air) bubble rising in a quiescent liquid, the CST method was found to be applicable to a wide range of material and transport properties.

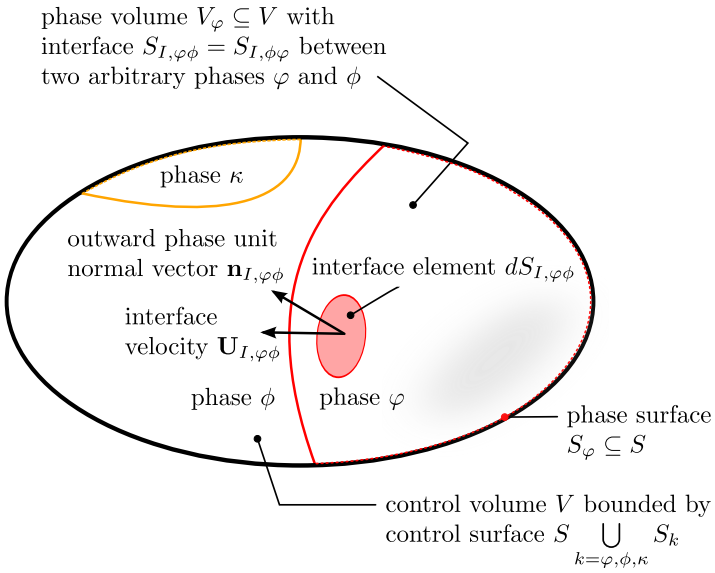

Figure 7.13: Control volume – Two-phase flow.

7.A. Conceptual Approach of Conditional Volume-Averaging

Local Instantaneous Conservation Equation and Interfacial Jump Condition

To start from the first principles, we consider an arbitrary control volume V, that is spatially fixed within an Eulerian framework and arbitrary in its shape. Over this control volume balances shall be formulated in the following. In order to extend the consideration towards a two- or multiphase case, it is instructive to immerse an assemblage of interfaces separating the phases of the system from each other within the control volume V (*immersed interface concept*) as illustrated in figure 7.13. Thus, the system comprises several phase volumes $V_k \subseteq V \bigcup_{k=\varphi,\phi,\ldots} V_k$, each possessing an interface S_I separating it from its neighboring phase. In consequence, the control surface S is composed of phase surfaces $S_k \subseteq S \bigcup_{k=\varphi,\phi,\ldots} S_k$ that arise where the control volume V cuts the phase volumes V_k.

In general, more phases – i.e., a third phase κ – might be present within the control volume. However, without loss of generality[3] these will be dropped in the remainder of this work when discussing the interaction of two arbitrary phases φ and ϕ. In the

[3] One or more additional phases would be treated analogously without imposing additional complexity.

following, the first phase, i.e., phase φ, shall be examined, whereas the latter phase ϕ is considered as neighboring phase.

For generality, we further use a generic arbitrary transport quantity $\mathbf{\Phi}$ in the following, which will be substituted by the molar species concentration at the end of our derivation. Let $\mathbf{\Phi}(\mathbf{x}, t)$ be an arbitrary general intensive physical quantitity, e.g. a fluid property (scalar or tensor of any rank) being transported and thus distributed within a spatio-temporal domain. Note that the transport quantity $\mathbf{\Phi}$ represents the intensive equivalent of extensive balance quantities, e.g., mass, momentum, energy or chemical species, on the basis of which balance equations are stated commonly. Owed to the presence of two or more phases within the control volume V, it is necessary to distinguish among the respective contributions of each of the phases to the transport quantity $\mathbf{\Phi}$. For this purpose all balances have to be considered over the *phase* surfaces S_k and the *phase* volumes V_k – with $k \in [\varphi, \phi]$. Consequently, the overall balance equation for $\mathbf{\Phi}$ within the control volume V reads:

$$\begin{aligned}\sum_{k=\varphi,\phi}\left(\frac{d}{dt}\int_{V_k(t)}\rho\mathbf{\Phi}dV\right) = &-\sum_{k=\varphi,\phi}\int_{S_k(t)}\mathbf{n}_k\bullet\left(\rho\mathbf{\Phi}\mathbf{U}\right)dS\\ &-\sum_{k=\varphi,\phi}\int_{S_k(t)}\mathbf{n}_k\bullet\left(-\Gamma_{\mathbf{\Phi},d}\nabla\mathbf{\Phi}\right)dS\\ &+\sum_{k=\varphi,\phi}\int_{V_k(t)}S_{\mathbf{\Phi}}\left(\mathbf{\Phi}\right)dV\\ &+\frac{1}{2}\sum_{k=\varphi,\phi}\sum_{j=\varphi,\phi}\left(1-\delta_{jk}\right)\int_{S_{I,jk}(t)}S_{\mathbf{\Phi},I}\left(\mathbf{\Phi}\right)dS, \qquad (7.32)\end{aligned}$$

with the last term on the r.h.s. of equation 7.32 representing a generic coupling interfacial source term, and the first three terms holding the already introduced bulk (phase interior) contributions *within* the phases φ and ϕ, respectively.

Next, Leibniz' and Gauss' theorem are utilized for the temporal and spatial term, respectively. This enables to interchange the volume integral with the temporal derivative in the temporal term and to transform the surface integrals into volume integrals in the spatial terms. E.g., for phase φ, it is:

$$\begin{aligned}\frac{d}{dt}\int_{V_\varphi(t)}\rho\mathbf{\Phi}dV = &\int_{V_\varphi(t)}\frac{\partial}{\partial t}\left(\rho\mathbf{\Phi}\right)dV\\ &+\int_{S_{I,\varphi\phi}(t)}\mathbf{n}_{I,\varphi\phi}\bullet\mathbf{U}_{I,\varphi\phi}\left(\rho\mathbf{\Phi}\right)dS, \qquad (7.33)\end{aligned}$$

and

$$\int_{S_\varphi(t)} \mathbf{n}_\varphi \bullet (\rho \boldsymbol{\Phi} \mathbf{U})\, dS = \int_{V_\varphi(t)} \nabla \bullet (\rho \boldsymbol{\Phi} \mathbf{U})\, dV - \int_{S_{I,\varphi\phi}(t)} \mathbf{n}_{I,\varphi\phi} \bullet (\rho \boldsymbol{\Phi} \mathbf{U})\, dS \qquad \text{and} \tag{7.34}$$

$$\int_{S_\varphi(t)} \mathbf{n}_\varphi \bullet (-\Gamma_{\boldsymbol{\Phi},d} \nabla \boldsymbol{\Phi})\, dS = \int_{V_\varphi(t)} \nabla \bullet (-\Gamma_{\boldsymbol{\Phi},d} \nabla \boldsymbol{\Phi})\, dV - \int_{S_{I,\varphi\phi}(t)} \mathbf{n}_{I,\varphi\phi} \bullet (-\Gamma_{\boldsymbol{\Phi},d} \nabla \boldsymbol{\Phi})\, dS. \tag{7.35}$$

Hence, the balance equation 7.32 can be compacted as

$$0 = \sum_{k=\varphi,\phi} \int_{V_k(t)} \left[\frac{\partial}{\partial t} (\rho \boldsymbol{\Phi}) + \nabla \bullet (\rho \boldsymbol{\Phi} \mathbf{U}) - \nabla \bullet (\Gamma_{\boldsymbol{\Phi},d} \nabla \boldsymbol{\Phi}) - S_{\boldsymbol{\Phi}} (\boldsymbol{\Phi}) \right] dV - \frac{1}{2} \sum_{k=\varphi,\phi} \sum_{j=\varphi,\phi} (1 - \delta_{jk}) \int_{S_{I,kj}(t)} \left[\rho \boldsymbol{\Phi} (\mathbf{U} - \mathbf{U}_{I,kj}) \bullet \mathbf{n}_{I,kj} - (\Gamma_{\boldsymbol{\Phi},d} \nabla \boldsymbol{\Phi}) \bullet \mathbf{n}_{I,kj} + S_{\boldsymbol{\Phi},I} \right] dS \tag{7.36}$$

As equation 7.36 is valid for arbitrary phase volumes V_k and arbitrary configurations of phase interfaces $S_{I,\varphi\phi}$ within V, the two addends and therein the integrands can be set to zero interchangeably. Thus the *local instantaneous generic transport equation* can be deduced from the first integrand (representing the bulk phase contributions). I.e., for phase φ it is stated

$$\frac{\partial \rho \boldsymbol{\Phi}}{\partial t} + \nabla \bullet (\rho \boldsymbol{\Phi} \mathbf{U}) - \nabla \bullet (\Gamma_{\boldsymbol{\Phi},d} \nabla \boldsymbol{\Phi}) - S_{\boldsymbol{\Phi}} (\boldsymbol{\Phi}) = 0, \tag{7.37}$$

as it is the well-known outcome for the single phase case. However, there is always a coupling with (at least) another transport equation of the same type due to the presence of a neighboring phase ϕ. Hence interfacial jump conditions have to be specified from the second addend of equation 7.36 in order to close the system. Note that the generic condition as set out in the second addend of equation 7.36 is independent of the particular choice of the phases φ and ϕ, respectively. φ and ϕ are interchangeable, i.e., $\mathbf{n}_{I,\varphi\phi} = -\mathbf{n}_{I,\phi\varphi}$. Hence, this symmetry can be utilized to simplify. Introducing a jump notation, where $\| \cdot \|$ shall denote a jump across the interface S_I as $\|f\| \equiv f_{I,\varphi} - f_{I,\phi}$, the second addend in equation 7.36 reveals the generic jump condition as

$$\| \rho \boldsymbol{\Phi} (\mathbf{U} - \mathbf{U}_I) \bullet \mathbf{n}_I - (\Gamma_{\boldsymbol{\Phi},d} \nabla \boldsymbol{\Phi}) \bullet \mathbf{n}_I \| = -S_{\boldsymbol{\Phi},I}. \tag{7.38}$$

Conditional Volume-averaged Conservation Equation and Interfacial Jump Condition

Terminology

Volume-Averaging Let $\mathcal{R}$ be a space domain with $\mathbf{x} \in \mathcal{R}$ being a position vector. Then, volume-averaging is defined as

$$\overline{\mathbf{\Phi}}^{V} \equiv \frac{1}{V} \int_{V} \mathbf{\Phi}\left(\mathbf{x}+\boldsymbol{\eta}, t\right) d\mathbf{x}_{\boldsymbol{\eta}} \quad \text{with} \quad V \subset \mathcal{R}, \tag{7.39}$$

where V denotes the averaging volume based on an averaging length scale, which is invariant in time and space. The location vector $\mathbf{x}$ points to the centroid of V, whereas $\boldsymbol{\eta}$ is used as a relative position vector to locate any position within V relative to its centroid. For the sake of brevity and ease of reading, the volume-averaging operator shall further be denoted with a simple overbar, i.e., without the 'V'.

Conditioning Conditioning of the arbitrary general local instantaneous quantity $\mathbf{\Phi}$ is provided by multiplication with the so-called *phase indicator function* I_{φ} that takes the value one within phase φ and zero elsewhere.

$$I_{\varphi}\left(\mathbf{x},\, t\right) = \begin{cases} 1 & \text{if } \mathbf{x} \in \varphi \text{ at time } t \\ 0 & \text{otherwise.} \end{cases} \tag{7.40}$$

The product $I_{\varphi}\mathbf{\Phi}$ is generally entitled *conditioned quantity* and is denoted $\mathbf{\Phi}_{\varphi}$ in the remainder of this thesis, $\mathbf{\Phi}_{\varphi} \equiv I_{\varphi}\mathbf{\Phi}$.

Conditional Volume-averaged Quantities and Derivatives

The above definitions enable to examine the generic arbitrary transport quantity $\mathbf{\Phi}$ after conditioning and volume-averaging:

$$\begin{aligned} \overline{I_{\varphi}\mathbf{\Phi}} \;=\; \overline{\mathbf{\Phi}_{\varphi}} &= \frac{1}{V} \int_{V} I_{\varphi}\left(\mathbf{x}+\boldsymbol{\eta},\, t\right) \mathbf{\Phi}\left(\mathbf{x}+\boldsymbol{\eta},\, t\right) d\mathbf{x}_{\boldsymbol{\eta}} \\ &= \frac{1}{V} \int_{V_{\varphi}} \mathbf{\Phi}\left(\mathbf{x}+\boldsymbol{\eta},\, t\right) d\mathbf{x}_{\boldsymbol{\eta}} \\ &= \frac{V_{\varphi}}{V} \frac{1}{V_{\varphi}} \int_{V_{\varphi}} \mathbf{\Phi}\left(\mathbf{x}+\boldsymbol{\eta},\, t\right) d\mathbf{x}_{\boldsymbol{\eta}} \\ &= \alpha_{\varphi}\, \overline{\mathbf{\Phi}}^{\varphi}, \end{aligned} \tag{7.41}$$

where $\alpha_{\varphi} \equiv V_{\varphi}/V$ denotes the *volumetric phase fraction* and $\overline{\mathbf{\Phi}}^{\varphi}$ represents the *phasic or intrinsic average* which has been defined according to

$$\overline{\mathbf{\Phi}}^{\varphi} \equiv \frac{1}{V_{\varphi}} \int_{V_{\varphi}} \mathbf{\Phi}\left(\mathbf{x}+\boldsymbol{\eta},\, t\right) d\mathbf{x}_{\boldsymbol{\eta}}. \tag{7.42}$$

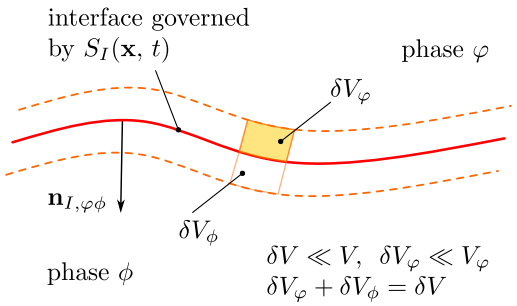

Figure 7.14: Illustration of the interfacial surface averaging procedure.

However, in order to arrive at the *conditional volume-averaged generic transport equation*, we additionally need to consider conditional volume averaging of spatial and temporal derivatives:

$$\begin{aligned}
\overline{I_\varphi \nabla \boldsymbol{\Phi}} &= \overline{\nabla I_\varphi \boldsymbol{\Phi}} - \overline{\boldsymbol{\Phi} \nabla I_\varphi} \\
&= \nabla \left(\alpha_\varphi \overline{\boldsymbol{\Phi}}^\varphi \right) + \widetilde{\boldsymbol{\Phi} \mathbf{n}_I}^\varphi \Sigma, && (7.43) \\
\overline{I_\varphi \nabla \boldsymbol{\cdot} \boldsymbol{\Phi}} &= \nabla \boldsymbol{\cdot} \overline{I_\varphi \boldsymbol{\Phi}} - \overline{\boldsymbol{\Phi} \boldsymbol{\cdot} \nabla I_\varphi} \\
&= \nabla \boldsymbol{\cdot} \left(\alpha_\varphi \overline{\boldsymbol{\Phi}}^\varphi \right) + \widetilde{\boldsymbol{\Phi} \boldsymbol{\cdot} \mathbf{n}_I}^\varphi \Sigma \qquad \text{and} && (7.44) \\
\overline{I_\varphi \frac{\partial \boldsymbol{\Phi}}{\partial t}} &= \frac{\partial \overline{I_\varphi \boldsymbol{\Phi}}}{\partial t} - \overline{\boldsymbol{\Phi} \frac{\partial I_\varphi}{\partial t}} = \frac{\partial \overline{I_\varphi \boldsymbol{\Phi}}}{\partial t} + \overline{\boldsymbol{\Phi} \left(\mathbf{U}_{I,\varphi\phi} \boldsymbol{\cdot} \nabla I_\varphi \right)} \\
&= \frac{\partial \alpha_\varphi \overline{\boldsymbol{\Phi}}^\varphi}{\partial t} + \widetilde{\boldsymbol{\Phi}_{I,\varphi} \mathbf{n}_{I,\varphi\phi} \boldsymbol{\cdot} \mathbf{U}_{I,\varphi\phi}} \Sigma, && (7.45)
\end{aligned}$$

where $\widetilde{\boldsymbol{\Phi}}^\varphi$ denotes a conditioned interface-average of a quantity $\boldsymbol{\Phi}$. According to [85, 97], who follows [84], this can be understood from a further analysis, when integrating each term in equation 7.43 and 7.44 over an infinitesimal volume element δV.

Conditioned Interface-averages

Consider the volume element $\delta V = \delta V_\varphi + \delta V_\phi$ as illustrated in figure 7.14 being composed of two infinitesimal volume elements adjacent to the interface – δV_φ on the φ-side and δV_ϕ on the ϕ-side. Then, integrating over δV_φ, when examining $\overline{I_\varphi \nabla \boldsymbol{\Phi}}$ and $\overline{I_\varphi \nabla \boldsymbol{\cdot} \boldsymbol{\Phi}}$, has no net effect on the first terms on the r.h.s. of equations 7.43 and 7.44, respectively, since the bulk (phase interior) contributions can be regarded constant

over δV_φ. However, the second terms can be transferred into surface integrals (as they contain the Dirac delta function), and then read:

$$\begin{aligned}\overline{\boldsymbol{\Phi}\nabla I_\varphi} &= -\overline{\delta_I \boldsymbol{\Phi}\mathbf{n}_{I,\varphi\phi}} = -\overline{\boldsymbol{\Phi}_I \mathbf{n}_{I,\varphi\phi}} \\ &= -\lim_{\delta V_\varphi \to 0} \overline{\frac{1}{\delta V_\varphi}\int_{\delta V_\varphi(\mathbf{x},t)} \boldsymbol{\Phi}_I \mathbf{n}_{I,\varphi\phi}\, dV} \\ &= -\lim_{\delta V_\varphi \to 0} \overline{\frac{1}{\delta V_\varphi}\int_{S_I(\mathbf{x},t)} \boldsymbol{\Phi}\mathbf{n}_{I,\varphi\phi}\; dS}, \end{aligned} \tag{7.46}$$

where $S_I(\mathbf{x}, t)$ is the equation for the interface. Note further that the two volume-average operations have been interchanged since they commute. Similarly, one obtains

$$\begin{aligned}\overline{\boldsymbol{\Phi}\bullet\nabla I_\varphi} &= -\overline{\delta_I \boldsymbol{\Phi}\bullet\mathbf{n}_{I,\varphi\phi}} = -\overline{\boldsymbol{\Phi}_I\bullet\mathbf{n}_{I,\varphi\phi}} \\ &= -\lim_{\delta V_\varphi \to 0} \overline{\frac{1}{\delta V_\varphi}\int_{\delta V_\varphi(\mathbf{x},t)} \boldsymbol{\Phi}_I\bullet\mathbf{n}_{I,\varphi\phi}\, dV} \\ &= -\lim_{\delta V_\varphi \to 0} \overline{\frac{1}{\delta V_\varphi}\int_{S_I(\mathbf{x},t)} \boldsymbol{\Phi}\bullet\mathbf{n}_{I,\varphi\phi}\; dS}. \end{aligned} \tag{7.47}$$

To omit this rather ponderous (yet illustrative) presentation, it is useful to introduce the definition of a conditioned interface-average $\widetilde{\boldsymbol{\Phi}}^\varphi$:

$$\widetilde{\boldsymbol{\Phi}}^\varphi \equiv \frac{1}{\Sigma}\lim_{\delta V_\varphi \to 0} \overline{\frac{1}{\delta V_\varphi}\int_{\delta V_\varphi} \boldsymbol{\Phi}_I dV} = \frac{1}{\Sigma}\lim_{\delta V_\varphi \to 0} \overline{\frac{1}{\delta V_\varphi}\int_{S_I(\mathbf{x},t)} \boldsymbol{\Phi}\, dS}, \tag{7.48}$$

$$\text{with} \qquad \Sigma \equiv \lim_{\delta V \to 0} \overline{\frac{1}{\delta V}\int_{S_I(\mathbf{x},t)} dS}, \tag{7.49}$$

where Σ denotes the interfacial area density, i.e., the interfacial surface area per unit volume. Similarly, we define an interface average $\widetilde{\boldsymbol{\Phi}}$ according to [85], being the surface integral per unit volume divided by the interfacial area density,

$$\widetilde{\boldsymbol{\Phi}} \equiv \frac{1}{\Sigma}\lim_{\delta V \to 0} \overline{\frac{1}{\delta V}\int_{S_I(\mathbf{x},t)} \boldsymbol{\Phi}\,(\mathbf{x},\, t)\; dS}, \tag{7.50}$$

which can be transferred into $\widetilde{\boldsymbol{\Phi}}^\varphi$ considering the limiting value of $\boldsymbol{\Phi}$ after conditioning and approaching the interface from the φ-side:

$$\widetilde{\boldsymbol{\Phi}}^\varphi = \widetilde{\boldsymbol{\Phi}_{I,\varphi}} \tag{7.51}$$

$$\text{with} \qquad \boldsymbol{\Phi}_{I,\varphi} = \delta_I \boldsymbol{\Phi}_\varphi.$$

In doing so, *interfacial quantities*, i.e., quantities that are inherently defined on the interface, can be written as

$$\widetilde{\boldsymbol{\Phi}_{I,\varphi\phi}}^\varphi = \widetilde{\boldsymbol{\Phi}_{I,\varphi\phi}}, \tag{7.52}$$

whereas the limiting values of *bulk quantities*, when the interface is approached from one side – either the φ- or the ϕ-side – still needs to be distinguished according to equation 7.51.

Conditional Volume-averaged Conservation Equation and Interfacial Jump Condition

In order to obtain the averaged arbitrary generic transport equation its local instantaneous counter-part (7.37) is conditional volume-averaged, which reads

$$\overline{I_\varphi \frac{\partial \rho \mathbf{\Phi}}{\partial t}} + \overline{I_\varphi \nabla\bullet \left(\rho \mathbf{\Phi} \mathbf{U}\right)} - \overline{I_\varphi \nabla\bullet \left(\Gamma_{\mathbf{\Phi},d} \nabla \mathbf{\Phi}\right)} - \overline{I_\varphi S_{\mathbf{\Phi}}} = \mathbf{0}. \tag{7.53}$$

Now recalling equations 7.41, 7.43, 7.44 and 7.45 yields, when neglecting mass transfer:

$$\frac{\partial \alpha_\varphi \overline{\rho \mathbf{\Phi}}^\varphi}{\partial t} + \nabla\bullet \left(\alpha_\varphi \overline{\rho \mathbf{\Phi} \mathbf{U}}^\varphi\right) - \nabla\bullet \left(\alpha_\varphi \overline{\Gamma_{\mathbf{\Phi},d} \nabla \mathbf{\Phi}}^\varphi\right) = \overline{I_\varphi S_{\mathbf{\Phi}}} + \overbrace{\left(\Gamma_{\mathbf{\Phi},d} \nabla \mathbf{\Phi}\right) \bullet \mathbf{n}_I}^\varphi \Sigma. \tag{7.54}$$

Equation 7.38 represents the local-instantaneous jump condition for a generic transport quantity $\mathbf{\Phi}$. Therefore, we arrive at the corresponding volume-averaged interface balance by conditioning and subsequently volume-averaging. Conditioning is accomplished by multiplication with $\delta_I\left(\mathbf{x} - \mathbf{x}_I, t\right)$, which represents the interface delta function. Taking into account the symmetry, $\mathbf{n}_{I,\varphi\phi} = -\mathbf{n}_{I,\phi\varphi}$, and neglecting mass transfer, it is:

$$\begin{aligned}
& \overline{\| \left(\Gamma_{\mathbf{\Phi},d} \nabla \mathbf{\Phi}\right) \bullet \mathbf{n}_I \| \delta_I} = - \overline{S_{\mathbf{\Phi},I} \delta_I} \\
\Leftrightarrow \quad & \overline{\left(\Gamma_{\mathbf{\Phi},d} \nabla \mathbf{\Phi}\right)_{I,\varphi} \bullet \nabla I_\varphi} + \overline{\left(\Gamma_{\mathbf{\Phi},d} \nabla \mathbf{\Phi}\right)_{I,\phi} \bullet \nabla I_\phi} = - \overline{S_{\mathbf{\Phi},I} \delta_I} \\
\Leftrightarrow \quad & \overbrace{\left(\Gamma_{\mathbf{\Phi},d} \nabla \mathbf{\Phi}\right) \bullet \mathbf{n}_{I,\varphi\phi}}^\varphi \Sigma + \overbrace{\left(\Gamma_{\mathbf{\Phi},d} \nabla \mathbf{\Phi}\right) \bullet \mathbf{n}_{I,\phi\varphi}}^\phi \Sigma = \overline{S_{\mathbf{\Phi},I} \delta_I}\,.
\end{aligned} \tag{7.55}$$

By replacing the generic transport quantity $\mathbf{\Phi}$ as well as corresponding coefficients and source terms according to table 7.3 we arrive at the conditional volume-averaged conservation equation of an arbitrary chemical species i

$$\frac{\partial \alpha_\varphi \overline{\rho x_i}^\varphi}{\partial t} + \nabla\bullet \left(\alpha_\varphi \overline{\rho x_i \mathbf{U}}^\varphi\right) - \nabla\bullet \left(\alpha_\varphi \overline{\rho D_i \nabla x_i}^\varphi\right) - \alpha_\varphi \overline{\hat{R}_i}^\varphi = \overbrace{\left(\rho D_i \nabla x_i\right) \bullet \mathbf{n}_{I,\varphi\phi}}^\varphi \Sigma, \tag{7.56}$$

and its corresponding jump condition,

$$\overbrace{\left(\rho D_i \nabla x_i\right) \bullet \mathbf{n}_{I,\varphi\phi}}^\varphi \Sigma + \overbrace{\left(\rho D_i \nabla x_i\right) \bullet \mathbf{n}_{I,\phi\varphi}}^\phi \Sigma = 0. \tag{7.57}$$

By substituting $c_i = x_i \cdot c = x_i \cdot \rho / M$ – where c, ρ and M denote the mean mixture concentration, density and molar mass, respectively – it follows for a diluted species i ($c = \text{const}$, $\rho = \text{const}$ and $M = \text{const}$, even for varying c_i) from equation 7.56:

$$\frac{\partial \alpha_\varphi \overline{c_i}^\varphi}{\partial t} + \nabla\bullet \left(\alpha_\varphi \overline{c_i \mathbf{U}}^\varphi\right) - \nabla\bullet \alpha_\varphi \overline{D_i \nabla c_i}^\varphi - \alpha_\varphi \overline{R_i}^\varphi = \overbrace{D_i \nabla c_i}^\varphi \Sigma. \tag{7.58}$$

Table 7.3: Coefficients for the generic transport equation – species conservation.

balance	$\boldsymbol{\Phi}$	$\Gamma_{\boldsymbol{\Phi},d}$	$S_{\boldsymbol{\Phi}}$	$S_{\boldsymbol{\Phi},I}$
species	x_i	ρD_i	$\hat{R}_i$	0
	$M/\rho\, c_i$	$M\, D_i$	$M\, R_i$	0

and from equation 7.57 for the corresponding jump condition:

$$\overbrace{(D_i \nabla c_i) \bullet \mathbf{n}_{I,\varphi\phi}}^{\varphi} \Sigma + \overbrace{(D_i \nabla c_i) \bullet \mathbf{n}_{I,\phi\varphi}}^{\phi} \Sigma = 0. \tag{7.59}$$

Neglecting fluctuations, i.e., assuming $\overline{c_i'^{\varphi} \mathbf{U}'^{\varphi}}^{\varphi} = \mathbf{0}$, and recognizing $D_i'^{\varphi} = 0$, equation 7.58 reads finally

$$\begin{aligned} \frac{\partial \alpha_\varphi \overline{c_i}^{\varphi}}{\partial t} + \nabla\bullet \left(\alpha_\varphi \overline{c_i}^{\varphi} \overline{\mathbf{U}}^{\varphi} \right) = \nabla\bullet \left(\alpha_\varphi \overline{D_i}^{\varphi} \nabla \overline{c_i}^{\varphi} \right) + \alpha_\varphi \overline{R_i}^{\varphi} \\ - \overbrace{D_i \nabla c_i \bullet \mathbf{n}_{I,\varphi\phi}}^{\varphi} \Sigma. \end{aligned} \tag{7.60}$$

7.B. Validation Study

The derivation procedure for the CST model reveals one basic prerequisite which needs to be fulfilled for an accurate and reliable solution. This is related to the split of the diffusive term into (a) bulk and (b) interfacial contributions (cf. equation 7.27):

ad b) In the derivation for the *interfacial contribution* we employ $\overline{c_i}^{\varphi} = He \cdot \overline{c_i}^{\phi}$ as the conditional volume-averaged counter-part of the local-instantaneous jump condition according to Henry's law. However, this clearly implicates the requirement to resolve *all scales* (DNS) such that the volume-averaged concentration values in cells adjacent to the interface approach their corresponding phase-sided limits at the interface.

ad a) As for the *bulk contribution*, the same requirement follows: while we get the known outcome for the diffusive bulk term, we expect the derivation to be reasonable. However, by redefining the molar mixture concentration C_i, a model error might have been introduced, since the expressions for C_i are only the same for equivalent diffusivities. However, if we exploit the analogy of volume-averaging and spatial filtering using a box filter kernel, a simple study of the one-dimensional species transfer problem indicates only a minor impact:

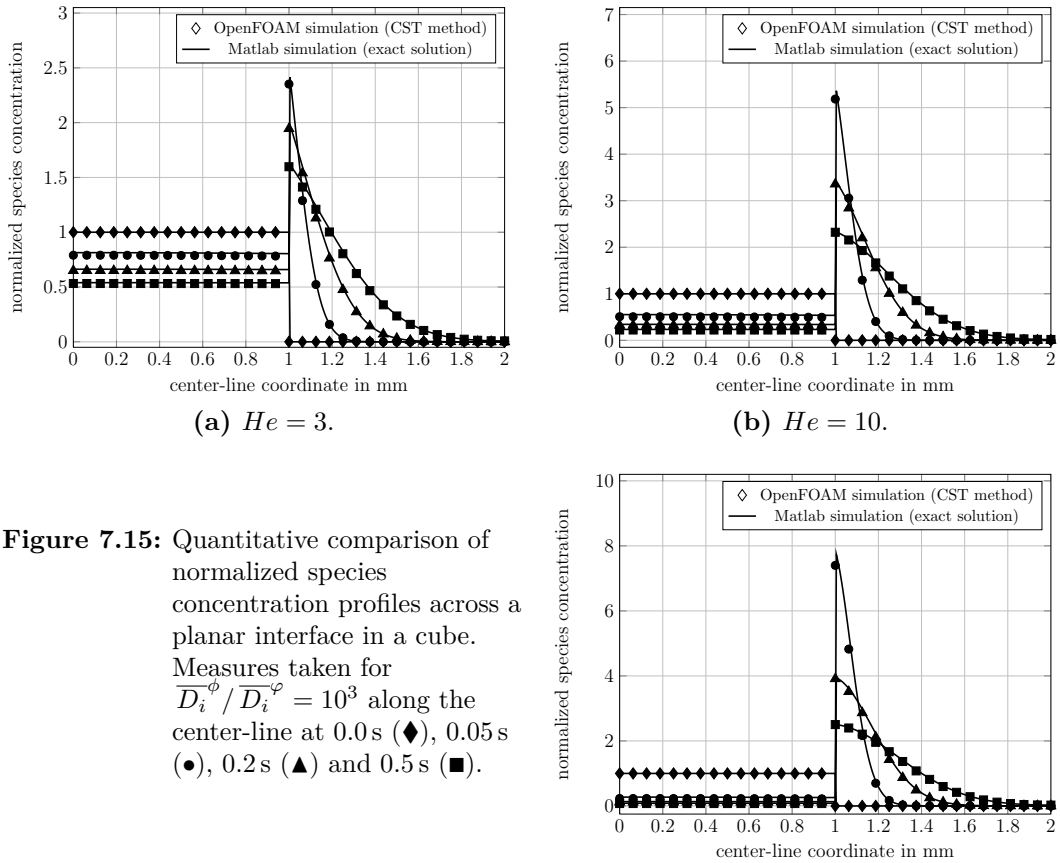

(a) $He = 3$.

(b) $He = 10$.

(c) $He = 30$.

Figure 7.15: Quantitative comparison of normalized species concentration profiles across a planar interface in a cube. Measures taken for $\overline{D_i}^{\phi} / \overline{D_i}^{\varphi} = 10^3$ along the center-line at 0.0 s (♦), 0.05 s (●), 0.2 s (▲) and 0.5 s (■).

the local instantaneous profiles of both concentration [98, pg. 38 ff.] and the phase indicator across the interface within an averaging length are known. Hence, the phasic concentrations $\overline{c_i}^{\varphi}$ and $\overline{c_i}^{\phi}$ (from employing conditional volume-averaging) as well as the volumetric phase fractions α_{φ} and α_{ϕ} (from convolution of phase indicator I_{φ} and the box filter kernel) can be used to explicitly calculate the mixture concentration C_i within an averaging length scale. We then state that a model error is only introduced, if the molar mixture concentrations C_i are found to vary when applying different formulations for C_i. However, the deviation of C_i within the averaging length is below 2% for sufficient spatial resolution and scales linearly with the averaging length provided to resolve the species concentration profiles.

In order to assess the range of validity of the CST model, within which an accurate and reliable solution can be expected, we have accomplished a validation study. For this purpose, the test case for *species transfer across a planar interface in a cube* (cf. section 7.5) can be adapted towards more demanding Henry coefficients and

more realistic diffusivities: the Henry coefficients have been varied from $He = 3$ over $He = 10$ to $He = 30$; with $\overline{D_i}^{\varphi} = 10^{-7}\,\frac{\mathrm{m}^2}{\mathrm{s}}$ and $\overline{D_i}^{\phi} = 10^{-4}\,\frac{\mathrm{m}^2}{\mathrm{s}}$, diffusion coefficients have been chosen such that their ratio is 10^3 [4]. The results as depicted in figure 7.15 are in very good agreement with the exact solution obtained using Matlab® v. 7.9 (R2009) at high temporal and spatial resolutions. Thus, the CST method is applicable to a wide and realistic range of material and transport properties.

[4] Further increase of the diffusivity ratio only results in the requirement of an increased spatial resolution but per se does not impair the accuracy of the CST model.

7.C. References

[1] W. L. Habermann and R. K. Morton. An experimental investigation of the drag and shape of bubbles rising in various liquids. In *David Taylor Model Basin Report No. 802*, 1953. 183

[2] J. T. Lindt. Note on the wake behind a two-dimensional bubble. *Chem. Eng. Sci.*, 26(10):1776–1777, 1971. 183

[3] J. T. Lindt. On the periodic nature of the drag on a rising bubble. *Chem. Eng. Sci.*, 27(10):1775–1781, 1972. 183

[4] J. R. Grace, T. Wairegi, and T. H. Nguyen. Shapes and sizes of bubbles rising in infinite liquids. *Trans. Inst. Chem. Eng.*, 54:167–173, 1976. 183

[5] R. Clift, J. R. Grace, and M. E. Weber. *Bubbles, Drops and Particles*. Acad. Press, New York [u.a.], 1978. 183, 185, 188

[6] H. Brauer. Turbulenz in mehrphasigen Strömungen. *Chem. Ing. Tech.*, 51(10):934–948, 1979. 183

[7] D. Bhaga and M. E. Weber. Bubbles in viscous liquids: Shapes, wakes and velocities. *J. Fluid Mech.*, 105(1):61–85, 1981. 183

[8] L.-S. Fan and K. Tsuchiya. *Bubble Wake Dynamics in Liquids and Liquid-Solid Suspensions*. Butterworth-Heinemann Series in Chemical Engineering. Butterworth-Heinemann, Boston, Mass. [u.a.], 1990. 183, 186

[9] K. L. Tse. *Bubble Coalescence in a Range of Fluids: Surface and Viscous Effects*. PhD thesis, University of Birmingham, 2000. 183

[10] A. A. Koynov and J. G. Khinast. Micromixing in reactive, deformable bubble and droplet swarms. *Chem. Eng. Technol.*, 29(1):13–23, 2006. 184, 188

[11] W. L. Shew and J.-F. Pinton. Dynamical model of bubble path instability. *Phys. Rev. Lett.*, 97(14):144508, 2006. 186

[12] M. H. I. Baird and J. F. Davidson. Gas absorption by large bubbles. *Chem. Eng. Sci.*, 17:87–93, 1962. 186, 188

[13] P. H. Calderbank, D. S. L. Johnson, and J. London. Mechanics and mass transfer of single bubbles in free rise through some Newtonian and non-Newtonian liquids. *Chem. Eng. Sci.*, 25:235–256, 1970. 186, 188

[14] J. H. C. Coppus. *The Structure of the Wake behind Spherical Cap Bubbles and its Relation to the Mass Transfer Mechanism*. PhD thesis, Technische Hogeschool Eindhoven, 1977. 186, 188

[15] G.-H. Song and L.-S. Fan. Gas-liquid mass transfer from a single bubble in liquid-solid fluidized beds. *AIChE J.*, 36(3):439–449, 1990. 186, 188

[16] O. Bork, M. Schlüter, S. Scheid, and N. Räbiger. New phenomena of mass transfer in gas/liquid flows. In *ASME HTD, Fluid-Physics and Heat Transfer for Macro- and*

Micro-Scale Gas-Liquid and Phase-Change Flows, pages 1 – 6, New York, 2001. 186, 188

[17] O. Bork, M. Schlüter, and N. Räbiger. Influence of wake mixing on mass transfer in gas-liquid reactors. In *15th Int. Congr. Chem. Proc. Eng., CHISA*, Prag, Czech Republic, 2002. 186, 188

[18] O. Bork, M. Schlüter, S. Scheid, and N. Räbiger. Analysis of the effect of local hydrodynamics on mass transfer from bubbles using laser induced fluorescence. In *4th ASME Joint U.S.-European Fluids Eng. Conf.*, Honolulu, USA, 2003. ASME. FEDSM2003-45569. 186, 188, 206

[19] O. Bork, M. Schlüter, and N. Räbiger. The impact of local phenomena on mass transfer in gas-liquid systems. *Can. J. Chem. Eng.*, 83(4):658–666, 2005. 186, 188

[20] H. Brauer. *Stoffaustausch einschließlich chemischer Reaktionen.* Grundlagen der chemischen Technik. Sauerländer, Aarau [u.a.], 1971. 187, 188, 208

[21] Hong and Brauer. Stoffaustausch zwischen Gas und Flüssigkeit in Blasensäulen. VDI-Forschungsheft, Nr. 624, 1984. 187, 208

[22] D. B. Kothe. Perspective on Eulerian Finite-Volume Methods for incompressible interfacial flows. In *Free Surface Flows*, volume 88 of *CISM courses and lectures*, pages 267–331. Kuhlmann and Rath, H., 1999. 187, 188, 194

[23] R. Scardovelli and S. Zaleski. Direct numerical simulation of free-surface and interfacial flow. *Annu. Rev. Fluid. Mech.*, 31(1):567–603, 1999. 188

[24] A. Caboussat. Numerical simulation of two-phase free surface flows. *Arch. Comput. Meth. Eng.*, 12(2):165–224, 2005. 188

[25] M. Darwish and F. Moukalled. Convective schemes for capturing interfaces of free-surface flows on unstructured grids. *Num. Heat Transfer, Part B: Fundamentals*, 49:19–42, 2006. 188

[26] V. R. Gopala and B. G. M. van Wachem. Volume of fluid methods for immiscible-fluid and free-surface flows. *Chem. Eng. J.*, 141(1-3):204–221, 2008. 188

[27] O. Ubbink. *Numerical Prediction of Two Fluid Systems with Sharp Interfaces.* PhD thesis, Imperial College of Science, Technology & Medicine (Department of Mechanical Engineering), 1997. 188

[28] O. Ubbink and R. I. Issa. A method for capturing sharp fluid interfaces on arbitrary meshes. *J. Comput. Phys.*, 153(1):26–50, 1999. 188

[29] H. Jasak and H. G. Weller. Interface-Tracking Capabilities of the InterGamma Differencing Scheme. Internal Report, CFD research group, Imperial College, London, February 1995. 188

[30] H. G. Weller. A New Approach to VOF-based Interface Capturing Methods for Incompressible and Compressible Flow. Technical report, OpenCFD Limited, 2006. 188, 195

[31] L. Štrubelj. *Numerical Simulations of Stratified Two-Phase Flows with Two-Fluid Model*

and Interface Sharpening. PhD thesis, University of Ljubljana, Faculty of Mathematics and Physics (Department of Physics), 2009. 188

[32] L. Štrubelj, I. Tiselj, and B. Mavko. Simulations of free surface flows with implementation of surface tension and interface sharpening in the two-fluid model. *Int. J. Heat Fluid Flow*, 30(4):741–750, 2009. 188

[33] E. Olsson and G. Kreiss. A conservative level set method for two phase flow. *J. Comput. Phys.*, 210(1):225–246, 2005. 188, 195

[34] E. Olsson. *Mass Conserving Simulations of Two Phase Flow*. PhD thesis, KTH School of Computer Science and Communication, Stockholm, Sweden, 2006. 188, 195

[35] E. Olsson, G. Kreiss, and S. Zahedi. A conservative level set method for two phase flow II. *J. Comput. Phys.*, 225(1):785–807, 2007. 188, 195

[36] R. Aris. Mass transfer from small ascending bubbles. *Chem. Eng. Sci.*, 52(24):4439–4446, 1997. Festschrift for Prof. M. M. Sharma. 188

[37] D. Legendre and J. Magnaudet. Effect of flow acceleration on mass or heat transfer at the surface of a spherical bubble. *Comptes Rendus de l'Academie des Sciences Series IIB Mechanics Physics Astronomy*, 327:63–70, 1999. 188

[38] Z.-S. Mao, T. Li, and J. Chen. Numerical simulation of steady and transient mass transfer to a single drop dominated by external resistance. *Int. J. Heat Mass Transfer*, 44(6):1235–1247, 2001. 188

[39] A. R. Paschedag, W. H. Piarah, and M. Kraume. Sensitivity study for the mass transfer at a single droplet. *Int. J. Heat Mass Transfer*, 48(16):3402–3410, 2005. 188

[40] A. Pfennig. Modelling mass transfer and equilibria at liquid-liquid interfaces. In F.-P. Schindler, editor, *Fortschritt-Berichte VDI, Reihe 3 Verfahrenstechnik 738*, pages 13 – 23. VDI, 2002. 188

[41] W. H. Piarah, A. Paschedag, and M. Kraume. Numerical simulation of mass transfer between a single drop and ambient flow. *AIChE J.*, 47:1701–1704, 2001. 188

[42] K. Schulze and M. Kraume. Influence of mass transfer on drop rise velocity. In F.-P. Schindler, editor, *Fortschritt-Berichte VDI, Reihe 3 Verfahrenstechnik 738*, pages 97 – 106. VDI, 2002. 188

[43] M. A. Waheed, M. Henschke, and A. Pfennig. Mass transfer by free and forced convection from single spherical liquid drops. *Int. J. Heat Mass Transfer*, 45(22):4507–4514, 2002. 188

[44] A. S. Brignell. Mass transfer from a spherical cap bubble in laminar flow. *Chem. Eng. Sci.*, 29(1):135–147, 1974. 188

[45] M. E. Weber. The effect of surface active agents on mass transfer from spherical cap bubbles. *Chem. Eng. Sci.*, 30(12):1507–1510, 1975. 188

[46] S. S. Sadhal, P. S. Ayyaswamy, and J. N.-C. Chung. *Transport Phenomena with Drops and Bubbles*. Mechanical engineering series. Springer, New York, NY [u.a.], 1997. 188

[47] J. M. van Baten and R. Krishna. CFD simulations of mass transfer from Taylor bubbles rising in circular capillaries. *Chem. Eng. Sci.*, 59(12):2535–2545, 2004. 188

[48] M. Ohta and M. Suzuki. Numerical analysis of mass transfer from a free motion drop in a solvent extraction process. *Solvent Extr. Res. Dev.*, 3:138–149, 1996. 188

[49] S. S. Ponoth and J. B. McLaughlin. Numerical simulation of mass transfer for bubbles in water. *Chem. Eng. Sci.*, 55(7):1237–1255, 2000. 188

[50] T. Sato, R.-T. Jung, and S. Abe. Direct simulation of droplet flow with mass transfer at interface. *J. Fluid Eng.*, 122(3):510–516, 2000. 188

[51] R.-T. Jung and T. Sato. Direct numerical simulation on single-droplet flow with mass transfer. *Chem. Eng. Technol.*, 24(10):1071–1075, 2001. 188

[52] M. R. Davidson and M. Rudman. Volume-of-fluid calculation of heat or mass transfer across deforming interfaces in two-fluid flow. *Num. Heat Transfer, Part B: Fundamentals*, 41(3):291–308, 2002. Taylor & Francis. 188

[53] D. Bothe, M. Koebe, K. Wielage, J. Prüss, and H.-J. Warnecke. Direct numerical simulation of mass transfer between rising gas bubbles and water. In M. Sommerfeld, editor, *Bubble Flows: Analysis, Modelling, and Calculation*, pages 159 – 174. Springer, Berlin, 2004. 188

[54] K. B. Deshpande and W. B. Zimmerman. Simulation of interfacial mass transfer by droplet dynamics using the level set method. *Chem. Eng. Sci.*, 61(19):6486–6498, 2006. 188

[55] A. Onea, M. Wörner, and D. G. Cacuci. A qualitative computational study of mass transfer in upward bubble train flow through square and rectangular mini-channels. *Chem. Eng. Sci.*, 64(7):1416–1435, 2009. 188

[56] J. Wang, A. Bindal, T. M. Leib, and J. G. Khinast. Analysis of the complex nonlinear behavior of reacting bubble flows: Steady-state multiplicity. *Chem. Eng. Sci.*, 59(22–23):5575–5585, 2004. ISCRE18. 188

[57] A. Koynov, J. G. Khinast, and G. Tryggvason. Mass transfer and chemical reactions in bubble swarms with dynamic interfaces. *AIChE J.*, 51(10):2786–2800, 2005. 188

[58] K. B. Deshpande and W. B. Zimmerman. Simulations of mass transfer limited reaction in a moving droplet to study transport limited characteristics. *Chem. Eng. Sci.*, 61(19):6424–6441, 2006. 188

[59] S. Radl, A. Koynov, G. Tryggvason, and J. G. Khinast. DNS-based prediction of the selectivity of fast multiphase reactions: Hydrogenation of nitroarenes. *Chem. Eng. Sci.*, 63(12):3279–3291, 2008. 188

[60] A. Alke, D. Bothe, M. Kröger, and H.-J.Warnecke. Vof-based simulation of conjugate mass transfer from freely moving fluid particles. In *Computational Methods in Multiphase Flow, Transactions on Engineering Sciences*, pages 157 – 168. A.A. Mammoli and C.A. Brebbia, 2009. 188

[61] D. Bothe, A. Alke, M. Kröger, and H.-J. Warnecke. VOF-based simulation of reactive

mass transfer across deformable interfaces. *Prog. Comput. Fluid Dyn.*, 9(6–7):325–331, 2009. 188

[62] Y. Haroun, D. Legendre, and L. Raynal. Direct numerical simulation of reactive absorption in gas-liquid flow on structured packing using interface capturing method. *Chem. Eng. Sci.*, 65(1):351–356, 2010. 20th International Symposium in Chemical Reaction Engineering–Green Chemical Reaction Engineering for a Sustainable Future. 188

[63] C. Brücker. Structure and dynamics of the wake of bubbles and its relevance for bubble interaction. *Phys. Fluids*, 11(7):1781, 1999. 188

[64] J. G. Khinast. Impact of 2-D bubble dynamics on the selectivity of fast gas-liquid reactions. *AIChE J.*, 47(10):2304–2319, 2001. 188

[65] M. F. Göz, B. Bunner, M. Sommerfeld, and G. Tryggvason. Direct numerical simulation of bubble swarms with a parallel front tracking method. In M. Breuer, F. Durst, and C. Zenger, editors, *High Performance Scientific and Engineering Computing*, pages 97 – 106, Erlangen, 2002. Springer Verlag. Proc. 3rd Int. FORTWIHR Conf. on HPSEC. 188

[66] R.-T. Jung, S. Toru, H. G. Sung, and C. G. Kang. Numerical study of a droplet behavior with mass transfer. http://dbpia.co.kr/view/ar_view.asp?arid=851914, 2003. 188

[67] J. G. Khinast, A. A. Koynov, and T. M. Leib. Reactive mass transfer at gas-liquid interfaces: Impact of micro-scale fluid dynamics on yield and selectivity of liquid-phase cyclohexane oxidation. *Chem. Eng. Sci.*, 58(17):3961–3971, 2003. 188

[68] A. A. Koynov and J. G. Khinast. Effects of hydrodynamics and Lagrangian transport on chemically reacting bubble flows. *Chem. Eng. Sci.*, 59(18):3907–3927, 2004. 188

[69] J. G. Khinast. Mikrovermischung in reaktiven deformierbaren Blasen- und Tropfenschwärmen. *Chem. Ing. Tech.*, 77(11):1723–1736, 2005. 188

[70] D. Darmana, N. G. Deen, and J. A. M. Kuipers. Detailed 3d modeling of mass transfer processes in two-phase flows with dynamic interfaces. *Chem. Eng. Technol.*, 29(9):1027–1033, 2006. 188

[71] A. A. Koynov, G. Tryggvason, M. Schlüter, and J. G. Khinast. Mass transfer and chemical reactions in reactive deformable bubble swarms. *Appl. Phys. Lett.*, 88(13):134102, 2006. 188

[72] S. Radl, G. Tryggvason, and J. G. Khinast. Flow and mass transfer of fully resolved bubbles in non-Newtonian fluids. *AIChE J.*, 53(7):1861–1878, 2007. 188

[73] Ž Tuković and H. Jasak. Simulation of free-rising bubble with soluble surfactant using moving mesh finite volume/area method. In *6th Int. Conf. on CFD in Oil & Gas, Metallurgical and Process Industries*, SINTEF/NTNU, Trondheim, Norway, 10-12 June 2008. 188

[74] C. Yang and Z.-S. Mao. Numerical simulation of interphase mass transfer with the level set approach. *Chem. Eng. Sci.*, 60(10):2643–2660, 2005. 188

[75] J. Wang, P. Lu, Z. Wang, C. Yang, and Z.-S. Mao. Numerical simulation of unsteady mass transfer by the level set method. *Chem. Eng. Sci.*, 63(12):3141–3151, 2008. 188

[76] D. Bothe, M. Koebe, and H.-J. Warnecke. VOF-simulation of the rise behavior of single air bubbles with oxygen transfer to the ambient liquid. In *Conf. on Transport Phenomena with Moving Boundaries*, 2003. 188

[77] D. Bothe, M. Koebe, K. Wielage, and H.-J. Warnecke. VOF-simulations of mass transfer from single bubbles and bubble chains rising in aqueous solutions. In *Proc. of FEDSM'03: 4th ASME-JSME Joint Fluids Eng. Conf.*, Honolulu, Hawaii, USA, July 6-11 2003. 188

[78] D. Bothe and H.-J. Warnecke. VOF-simulation of rising air bubbles with mass transfer to the ambient liquid. In C. Boyadjiev and J. Hristov, editors, *Proc. of 10th Workshop on Transport Phenomena in Two-Phase Flow*, pages 61 – 72, Slanchev Bryag, Bulgaria, 2005. 188

[79] M. Kröger, A. Alke, D. Bothe, and H.-J. Warnecke. A VOF-based approach for the simulation of reactive mass transfer from rising bubbles. In F.-P. Schindler, editor, *4th Int. Berlin Workshop - IBW4 on Transport Phenomena with Moving Boundaries*, pages 290 – 301, TU Berlin, 2007. 188

[80] D. Bothe, M. Kröger, A. Alke, and H.-J. Warnecke. VOF-based simulation of reactive mass transfer across deformable interfaces. In *Proc. 6th Int. Conf. on Computational Fluid Dynamics in the Oil & Gas, Metallurgical and Process Industries*, Trondheim, Norway, 2008. 188

[81] A. Alke, D. Bothe, M. Kröger, and H.-J. Warnecke. VOF-Based simulation of conjugate mass transfer from freely moving fluid particles. In A. A. Mammoli and C. A. Brebbia, editors, *Computational Methods in Multiphase Flow V*, pages 157–168. WIT Press, Southampton, 2009. 188

[82] J. U. Brackbill, D. B. Kothe, and C. Zemach. A continuum method for modeling surface tension. *J. Comput. Phys.*, 100(2):335–354, 1992. 189, 195

[83] C. S. Peskin. Numerical analysis of blood flow in the heart. *J. Comput. Phys.*, 25(3):220–252, 1977. 189

[84] C. Dopazo. On conditional averages for intermittent turbulent flow. *J. Fluid Mech.*, 81(3):433–438, 1977. 189, 190, 213

[85] H. G. Weller. The Development of a New Flame Area Combustion Model Using Conditional Averaging. Technical report, Thermo-Fluids Section Report TF 9307, Imperial College of Science, Technology and Medicine, 1993. 189, 190, 213, 214

[86] H. Jasak. A consistent derivation of the sea-ice model using conditional averaging. `http://powerlab.fsb.hr/ped/kturbo/OpenFOAM/docs/conditionalIceModel.pdf`, 2003. 189, 190

[87] H. G. Weller, G. Tabor, H. Jasak, and C. Fureby. A tensorial approach to computational continuum mechanics using object orientated techniques. *Comp. Phys.*, 12(6):620–631, 1998. 198

[88] H. Jasak. Multi-physics simulations in continuum mechanics. In *5th Int. Congr. Croatian*

Society of Mechanics, Trogir/Split, Croatia, September, 21-23 2006. 198

[89] H. Jasak, A. Jemcov, and Ž Tuković. OpenFOAM: A C++ library for complex physics simulations. In *International Workshop on Coupled Methods in Numerical Dynamics IUC*, Dubrovnik, Croatia, September, 19-21 2007. 198

[90] H. Jasak and A. D. Gosman. Automatic resolution control for the Finite-Volume Method, Part 2: Adaptive mesh refinement and coarsening. *Numer. Heat Tran. B*, 38:257–271, 2000. 201

[91] A.-V. Vuong, B. Simeon, and S. Boschert. Adaptive finite volume methods for interfacial flows. available at `http://www-m2.ma.tum.de/homepages/simeon/publica.html`, February 2010. 201

[92] H. Rusche. *Computational Fluid Dynamics of Dispersed Two-Phase Flows at High Phase Fractions*. PhD thesis, Imperial College of Science, Technology & Medicine London, 2002. 201

[93] P. C. Duineveld. The rise velocity and shape of bubbles in pure water at high Reynolds number. *J. Fluid Mech.*, 292:325–332, 1995. 204

[94] M. Schlüter. Blasenbewegung in praxisrelevanten Zweiphasenströmungen. In F.-P. Schindler, editor, *Fortschritt-Berichte VDI, Reihe 7 Strömungstechnik 432*, pages 13 – 23. VDI, 2002. 204

[95] M. Koebe, D. Bothe, J. Prüss, and H.-J. Warnecke. 3D direct numerical simulation of air bubbles in water at high Reynolds numbers. In *Proc. ASME*, Montreal, 2002. 204

[96] D. Bothe. Current status of capturing the trajectory of a single bubble rising through quiescent liquid using FS3D. private communication, March 2010. 204

[97] H. G. Weller. Derivation, Modelling and Solution of the Conditionally Averaged Two-Phase Flow Equations. Technical report, OpenCFD Limited, 2005. 213

[98] J. Crank. *The Mathematics of Diffusion*. Clarendon Press, Oxford, 1975. 217

8

Numerical Simulation of Multi-scale Two-Phase Flows using a Hybrid Interface-Resolving Two-Fluid Model (HIRES-TFM)

Abstract

The main challenge in Computational Multi-Fluid Dynamics (CMFD) is the description of phenomena that occur over a wide range of scale, ranging from micro- over meso- to macroscale (multi-scale CMFD). We present the coherent and mathematical rigorous derivation of a generalized multi-scale model framework, that is based on the Eulerian-Eulerian two-fluid methodology. For this purpose, we start from first principles that are the local instantaneous conservation equations for mass and momentum. By conditional volume-averaging (based on the immersed interface concept) and closure modeling, the two-phase flow features are first divided into an unresolved portion (on average or sub-grid scale) *and a* resolved portion *and subsequently interpreted on a physical basis leading to constitutive relations for closure.*

Our resulting two-fluid model framework HIRES-TFM (Hybrid Interface-Resolving Two-Fluid Model) exhibits the same basic structure as found for single-phase flow, which results in an inherently stable method and enables us to reuse numerical methodologies that have been developed for single-phase problems. Moreover, the conceptual approach is compatible with the LES framework for turbulence modeling, and can be used for multi-scale flow scenarios, i.e., dispersed and segregated two-phase flows.

8.1. Introduction

Many applications in chemical and process engineering involve two-phase flows. Examples of industrial two-phase flow applications are found in chemical, petroleum, metallurgical and energy industries and span over various processes from liquid-phase oxidations, hydrogenations, chlorination, gas scrubbing, waste water treatment to various bio-technological applications.

The types of flows above often involve both a *continuous cascade of temporal and spatial scales* usually varying over orders of magnitude (multi-scale) and *multiple coupled phenomena* (multiphysics). Their numerical treatment proves to be extremely complex. Thus, no general methodology or technique has evolved.

Throughout the last two decades different approaches have been developed establishing the field of Computational Multi-Fluid Dynamics (CMFD). These CMFD approaches were motivated by a scale separation that is presumed for two-phase flows: a given flow type (or flow regime) is regarded as invariant throughout the simulation. Consequently, a classification of CMFD approaches can be done according to their ability of capturing certain interfacial scales which characterize a two-phase flow at

- macroscopic scales, i.e., mean/main flow features on the scales of the flow domain,
- mesoscopic scales, i.e., major changes of the fluid dynamic phenomena on the scale of large eddies and recirculation regions,
- microscopic scales, i.e., flow features on the scale of bubble-bubble and bubble-turbulence interaction or in the range of the thickness of the interfacial boundary layer.

Several methodologies have been developed to take advantage of this presumed scale separation. A rough categorization might read as follows:

Interfacial scale averaging methods. For simulation of industrial two-phase flow applications the scale of interest is typically rather large – in the order of several meters. In contrast, the smallest scale one might have to consider is that of a characteristic "dispersed phase element" (DPE[1]), which predominantly determines the fluid dynamics in an industrial two-phase flow application.

The scales of DPEs typically vary from tens of microns to several millimeters dependent on underlying process and material parameters under consideration.

[1] generalized term for bubbles, drops or particles that will be used as general substitute in the following.

Compared to the scale of the flow domain, there exists a clear scale separation that enables interfacial scale averaging approaches to be used. Averaging techniques can be employed such that they efficiently decrease computational costs. Here, all interfacial scales under consideration are averaged – either spatially over an averaging volume[2], temporally over an averaging time interval, or ensemble-averaged over a set of realizations. The resulting two-phase flow model is called the two-fluid model or the Eulerian-Eulerian method. It is described by a concept of inter-penetrating continua: both phases are treated separately – each with an averaged velocity and pressure field[3].

As a consequence of averaging over all interfacial scales, *all* interfacial exchange phenomena are subject to modeling via closure models. Therefore, the choice of closure models is crucial for properly reproducing the desired interfacial physics. Moreover, this must be accomplished in a way that the closure restores the physical information that became unresolved (and hence lost) due to the applied averaging procedure. The challenge is to assemble models on a physically sound basis, rather than relying on empirical closures.

Interfacial scale resolving methods. For fundamental simulations aiming at the detailed resolution of physico-chemical phenomena at interfaces of two-phase flows, the scale of interest is typically rather small – of the order of several microns.

At the other end of scale range, an interfacial flow comprises the motion of molecules where the interface is represented by a transition region of a few tens of Ångströms. Over this region, collections of molecules belonging to one phase (out of the two phases) coexist at a certain probability, promoting a smooth but rapid transition between the phases.

As a common modeling hypothesis, the interface is approximated as a mathematical surface of discontinuity. This assumption is based on a clear scale separation between the molecular and interfacial scale (i.e. of a DPE) by orders of magnitude.

However, only a small number of studies have considered averaging based on this scale separation. Wörner et al. have found that volume-averaging of local instantaneous conservation equations for mass, momentum and energy yields the well-known governing equations of the Volume-of-Fluid (VoF) method, provided that the interfacial structures are sufficiently well resolved [1,2]. Sun and

[2] Due to its straightforward interpretability the volume-averaging technique is mostly employed in the context of two-phase flows.

[3] For numerical simulations, usually the so-called *one-field assumption* is applied to the pressures that is the phases share a single pressure field. We have adopted this assumption for our simulations as well.

Beckermann [3] have shown that ensemble-averaging of conservation equations with sharp interfaces results in a diffuse interface model, which can also be related to thermodynamically derived models. This is achieved by superimposing microscopic (atomic-scale) and macroscopic interface morphologies.

The majority of research has been based on the sharp interface formulation resulting in a multitude of methods, each of which treats the characteristic interfacial jump (in flow and material properties) in a specific manner. Typical examples are the ghost-fluid methods [4], interface tracking methods [5, 6] and interface capturing methods [7–9]. Special treatment of the interfacial jump conditions is needed since there is no natural or straightforward representation to handle these sharp discontinuities in an Eulerian framework.

In both averaged and sharp interface formulations of interfacial scale resolving methods some problems need to be addressed:

- flexibility and robustness (stability) for complex two-phase flow scenarios, e.g., changing interfacial morphology due to coalescence or break-up. This is a problem usually present in sharp interface models, as they become singular in extreme situations,e.g., in the moment of coalescence or breakup.

- capability to handle multi-scale two-phase flow scenarios, i.e., capturing mean interfacial evolution while using models for interfacial details such as microscale curvature or interfacial boundary layers.

Both interface scale averaging and interface scale resolving techniques are established methodologies and have been successfully applied to various two-phase flows. However, although two-phase flow systems and related interfacial transport phenomena commonly cover a wide range of physical scales, both CMFD approaches presume a distinct scale range in narrow confines. Consequently, they are usually restricted to one flow type. For DPEs larger than the characteristic resolution length scale (control or averaging volume) are dealt with via interfacial scale resolving methods, whereas DPEs smaller than the characteristic length scale are modeled, using interfacial scale averaging techniques. In general, different scales of interest involves using different CMFD approaches in a decoupled manner. Typically the choice is based on grounds of mesh resolution. Really, a more *general multi-scale modeling framework* is needed without constraints of mesh resolution.

It has been recently suggested to explicitly couple interfacial scale averaging and interfacial scale resolving methods in order to arrive at a more general two-phase flow model, capable of treating flow phenomena over a wider range of interfacial scales. Multi-scale models either explicitly couple the two-fluid model (TFM) with the Volume-of-Fluid (VoF) method [10–24] or they mimic the VoF method within the TFM framework [25–34]. Tomiyama et al. [18] recognize the issue by introducing

the dimensionless ratio $d^\star \equiv \frac{d_\mathrm{b}}{\Delta x}$: if $d^\star \gg 1$, i.e., the characteristic interfacial length scale is much larger than the computational cell size, the VoF method is adopted, while for $d^\star \ll 1$, a two-/multi-fluid approach is utilized. In consequence, there is a gap in the scales, rendering the above hybrid methods inconsistent. However, this introduces a level of uncertainty and doubts on the applicability of models.

This work is concerned with a general modeling framework, that *not only inherently* encompasses both interfacial scale resolving and interfacial scale averaging approaches, *but also consistently* involves *intermediate* scale situations. In this work we will present an approach based on a consistent model capturing under-resolved interfacial features. For this purpose, the Eulerian-Eulerian two-fluid approach is examined. The two-fluid model is rooted in fundamental local-instantaneous conservation equations, that are valid within each phase up to the interface separating the phases. Consequently, an appropriate conditional averaging procedure (based on the immersed interface concept) and closure modeling constitute the derivation for a generalized two-fluid approach.

In the remainder, we present a consistent derivation of a model framework, starting from first principles: local instantaneous conservation equations for mass and momentum and interfacial jump conditions. This leads to a closed set of governing equations suitable for numerical simulations of two-phase multi-scale flows. The framework will encompass both interfacial scale resolving and averaging approaches with a smooth transition between these. Section 8.2 gives the theoretical basis for the two-phase model framework: the conditional volume-averaging technique applied to both the local instantaneous conservation equations and to coupling interfacial jump conditions. In section 8.3 constitutive relations are given for closure regarding a *segregated two-phase flow*. This focus has been chosen, since conditional volume-averaging and closure modeling for the dispersed flow types lead to the Eulerian-Eulerian two-fluid model of Ishii [35]. The presented model framework for segregated flows is complementary to Ishii's two-fluid model for dispersed two-phase flows. This results in a flexible novel closure framework covering the intermediate interfacial scale range and allowing for partially (un)resolved scales within the flow domain. In section 8.4 the model is examined for simple two-phase test cases. A brief summary and an outlook is provided in section 8.5.

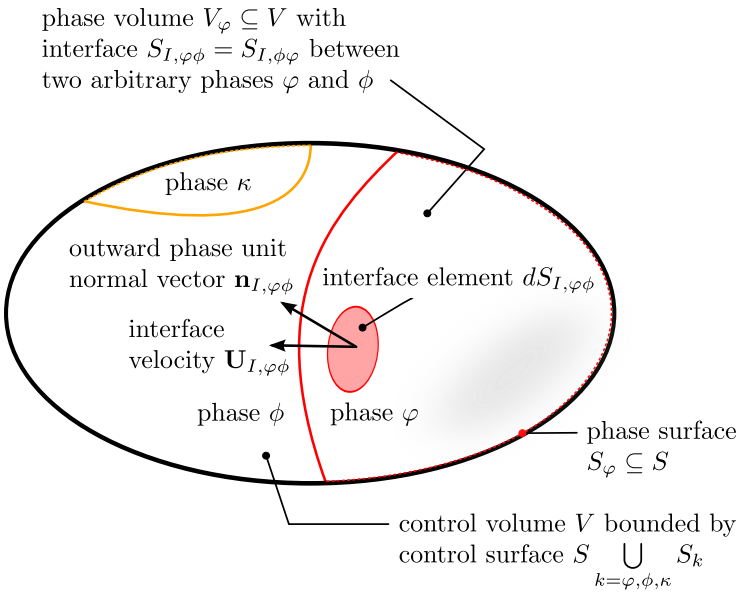

Figure 8.1: Control volume – Two-phase flow.

8.2. Conceptual Approach of Conditional Volume-Averaging

8.2.1. Local Instantaneous Conservation Equation and Interfacial Jump Condition

Starting from first principles, consider an arbitrary control volume V. In order to extend the consideration towards a two- or multiphase case, it is instructive to immerse an interface separating the phases of the system from each other within the control volume V (*immersed interface concept*), figure 8.1. Thus, the system comprises several phase volumes $V_k \subseteq V \bigcup_{k=\varphi,\phi,\ldots} V_k$, each possessing an interface S_I separating it from its neighboring phase. The control surface S is composed of phase surfaces $S_k \subseteq S \bigcup_{k=\varphi,\phi,\ldots} S_k$ that arise where the control volume V cuts the phase volumes V_k.

In general, more phases – i.e., a third phase κ – might be present within the control volume. Without loss of generality[4] these will be dropped, using two phases φ and ϕ. In the following, phase φ shall be examined, whereas phase ϕ is a phase neighbor.

[4] One or more additional phases would be treated analogously without imposing additional complexity.

Due to the presence of two or more phases within the control volume V, we will distinguish among the respective phase contributions to the transport quantity $\mathbf{\Phi}$. For this purpose, all balances have to be considered over the *phase* surfaces S_k and the *phase* volumes V_k – with $k \in [\varphi, \phi]$. The overall balance equation for $\mathbf{\Phi}$ within the control volume V reads:

$$\begin{aligned}\sum_{k=\varphi,\phi}\left(\frac{d}{dt}\int_{V_k(t)}\rho\mathbf{\Phi}dV\right) = &-\sum_{k=\varphi,\phi}\int_{S_k(t)}\mathbf{n}_{k\bullet}\left(\rho\mathbf{\Phi}\mathbf{U}\right)dS\\ &-\sum_{k=\varphi,\phi}\int_{S_k(t)}\mathbf{n}_{k\bullet}\left(-\Gamma_{\mathbf{\Phi},d}\nabla\mathbf{\Phi}\right)dS\\ &+\sum_{k=\varphi,\phi}\int_{V_k(t)}S_{\mathbf{\Phi}}\left(\mathbf{\Phi}\right)dV\\ &+\frac{1}{2}\sum_{k=\varphi,\phi}\sum_{j=\varphi,\phi}\left(1-\delta_{jk}\right)\int_{S_{I,jk}(t)}S_{\mathbf{\Phi},I}\left(\mathbf{\Phi}\right)dS, \qquad (8.1)\end{aligned}$$

with the last term on the r.h.s. of equation 8.1 representing a generic coupling interfacial source term, and the first three terms holding the bulk (phase interior) contributions *within* phases φ and ϕ, respectively.

Next, Leibniz' and Gauss' theorem are utilized for the temporal and spatial term, respectively. The balance equation 8.1 reads

$$\begin{aligned}0 = &\sum_{k=\varphi,\phi}\int_{V_k(t)}\left[\frac{\partial}{\partial t}\left(\rho\mathbf{\Phi}\right)+\nabla_{\bullet}\left(\rho\mathbf{\Phi}\mathbf{U}\right)-\nabla_{\bullet}\left(\Gamma_{\mathbf{\Phi},d}\nabla\mathbf{\Phi}\right)-S_{\mathbf{\Phi}}\left(\mathbf{\Phi}\right)\right]dV\\ &-\frac{1}{2}\sum_{k=\varphi,\phi}\sum_{j=\varphi,\phi}\left(1-\delta_{jk}\right)\int_{S_{I,kj}(t)}\Big[\rho\mathbf{\Phi}\left(\mathbf{U}-\mathbf{U}_{I,kj}\right)_{\bullet}\mathbf{n}_{I,kj}\\ &\qquad -\left(\Gamma_{\mathbf{\Phi},d}\nabla\mathbf{\Phi}\right)_{\bullet}\mathbf{n}_{I,kj}+S_{\mathbf{\Phi},I}\Big]dS. \qquad (8.2)\end{aligned}$$

Since equation 8.2 is valid for arbitrary phase volumes V_k and arbitrary configurations of phase interfaces $S_{I,\varphi\phi}$ within V, its r.h.s. terms can be set to zero independently. The *local instantaneous generic transport equation* for phase φ reads

$$\frac{\partial\rho\mathbf{\Phi}}{\partial t}+\nabla_{\bullet}\left(\rho\mathbf{\Phi}\mathbf{U}\right)-\nabla_{\bullet}\left(\Gamma_{\mathbf{\Phi},d}\nabla\mathbf{\Phi}\right)-S_{\mathbf{\Phi}}\left(\mathbf{\Phi}\right)=0. \qquad (8.3)$$

There always exists a coupling with (at least) another transport equation of the same type due to the presence of a neighboring phase ϕ. Interfacial jump conditions are specified from the second term of equation 8.2 in order to close the system. Note that the generic condition as set out in the second term of equation 8.2 is independent of the choice of phase, i.e., $\mathbf{n}_{I,\varphi\phi} = -\mathbf{n}_{I,\phi\varphi}$. Hence, symmetry can be utilized to simplify the derivation. Introducing a jump notation, $\|\cdot\|$ across the interface S_I as $\|f\| \equiv f_{I,\varphi} - f_{I,\phi}$, the second term in equation 8.2 yields the *generic jump condition*:

$$\left\|\rho\mathbf{\Phi}\left(\mathbf{U}-\mathbf{U}_I\right)_{\bullet}\mathbf{n}_I-\left(\Gamma_{\mathbf{\Phi},d}\nabla\mathbf{\Phi}\right)_{\bullet}\mathbf{n}_I\right\| = -S_{\mathbf{\Phi},I}. \qquad (8.4)$$

8.2.2. Conditional Volume-averaged Conservation Equation and Interfacial Jump Condition

Terminology

Volume-Averaging Let $\mathcal{R}$ be a space domain with $\mathbf{x} \in \mathcal{R}$ being a position vector. Then, volume-averaging is defined as

$$\overline{\mathbf{\Phi}}^{V} \equiv \frac{1}{V} \int_{V} \mathbf{\Phi}\left(\mathbf{x}+\boldsymbol{\eta}, t;\, \mu\right) d\mathbf{x}_{\boldsymbol{\eta}} \quad \text{with} \quad V \subset \mathcal{R}, \tag{8.5}$$

where V denotes the averaging volume based on an averaging length scale, invariant in time and space. The location vector $\mathbf{x}$ points to the centroid of V, whereas $\boldsymbol{\eta}$ is a relative position within V. The volume-averaging operator shall be denoted with an overbar.

Conditioning Conditioning of the local instantaneous quantity $\mathbf{\Phi}$ is done by multiplication with the *phase indicator function* I_{φ}:

$$I_{\varphi}\left(\mathbf{x},\, t\right) = \begin{cases} 1 & \text{if } \mathbf{x} \in \varphi \text{ at time } t \\ 0 & \text{otherwise.} \end{cases} \tag{8.6}$$

The product $I_{\varphi}\mathbf{\Phi}$ is entitled *conditioned quantity* and is denoted $\mathbf{\Phi}_{\varphi}$ in the remainder, $\mathbf{\Phi}_{\varphi} \equiv I_{\varphi}\mathbf{\Phi}$.

Conditional Volume-averaged Quantities and Derivatives

Let us examine the generic arbitrary transport quantity $\mathbf{\Phi}$ after conditioning and volume-averaging:

$$\begin{aligned} \overline{I_{\varphi}\mathbf{\Phi}} \;=\; \overline{\mathbf{\Phi}_{\varphi}} &= \frac{1}{V} \int_{V} I_{\varphi}\left(\mathbf{x}+\boldsymbol{\eta},\, t\right) \mathbf{\Phi}\left(\mathbf{x}+\boldsymbol{\eta},\, t\right) d\mathbf{x}_{\boldsymbol{\eta}} \\ &= \frac{1}{V} \int_{V_{\varphi}} \mathbf{\Phi}\left(\mathbf{x}+\boldsymbol{\eta},\, t\right) d\mathbf{x}_{\boldsymbol{\eta}} \\ &= \frac{V_{\varphi}}{V} \frac{1}{V_{\varphi}} \int_{V_{\varphi}} \mathbf{\Phi}\left(\mathbf{x}+\boldsymbol{\eta},\, t\right) d\mathbf{x}_{\boldsymbol{\eta}} \\ &= \alpha_{\varphi}\, \overline{\mathbf{\Phi}}^{\varphi}, \end{aligned} \tag{8.7}$$

where $\alpha_{\varphi} \equiv V_{\varphi}/V$ denotes the *volumetric phase fraction* and $\overline{\mathbf{\Phi}}^{\varphi}$ represents the *phasic or intrinsic average*:

$$\overline{\mathbf{\Phi}}^{\varphi} \equiv \frac{1}{V_{\varphi}} \int_{V_{\varphi}} \mathbf{\Phi}\left(\mathbf{x}+\boldsymbol{\eta},\, t\right) d\mathbf{x}_{\boldsymbol{\eta}}. \tag{8.8}$$

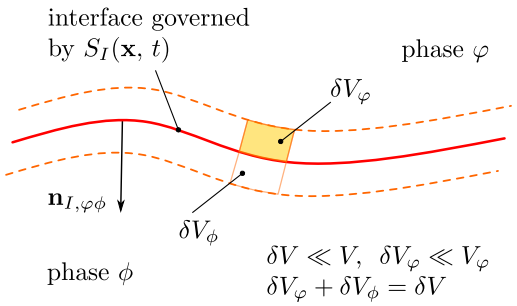

Figure 8.2: Illustration of the interfacial surface averaging procedure.

In order to arrive at the *conditional volume-averaged generic transport equation*, we additionally need to consider conditional volume-averaging of spatial and temporal derivatives of $\mathbf{\Phi}$:

$$\begin{aligned}
\overline{I_\varphi \nabla \mathbf{\Phi}} &= \overline{\nabla I_\varphi \mathbf{\Phi}} - \overline{\mathbf{\Phi} \nabla I_\varphi} \\
&= \nabla \left(\alpha_\varphi \, \overline{\mathbf{\Phi}}^{\varphi} \right) + \overbrace{\mathbf{\Phi} \mathbf{n}_I}^{\varphi} \Sigma, && (8.9) \\
\overline{I_\varphi \nabla \bullet \mathbf{\Phi}} &= \nabla \bullet \overline{I_\varphi \mathbf{\Phi}} - \overline{\mathbf{\Phi} \bullet \nabla I_\varphi} \\
&= \nabla \bullet \left(\alpha_\varphi \, \overline{\mathbf{\Phi}}^{\varphi} \right) + \overbrace{\mathbf{\Phi} \bullet \mathbf{n}_I}^{\varphi} \Sigma \qquad \text{and} && (8.10) \\
\overline{I_\varphi \frac{\partial \mathbf{\Phi}}{\partial t}} &= \frac{\partial \overline{I_\varphi \mathbf{\Phi}}}{\partial t} - \overline{\mathbf{\Phi} \frac{\partial I_\varphi}{\partial t}} = \frac{\partial \overline{I_\varphi \mathbf{\Phi}}}{\partial t} + \overline{\mathbf{\Phi} \left(\mathbf{U}_{I,\varphi\phi} \bullet \nabla I_\varphi \right)} \\
&= \frac{\partial \alpha_\varphi \, \overline{\mathbf{\Phi}}^{\varphi}}{\partial t} + \overbrace{\mathbf{\Phi}_{I,\varphi} \mathbf{n}_{I,\varphi\phi} \bullet \mathbf{U}_{I,\varphi\phi}}^{\varphi} \Sigma, && (8.11)
\end{aligned}$$

where $\overbrace{\mathbf{\Phi}}^{\varphi}$ denotes a conditioned interface-average of a quantity $\mathbf{\Phi}$. According to Weller [36,37], following Dopazo [38], this can be understood from a further analysis, when integrating each term in equation 8.9 and 8.10 over an infinitesimal volume element δV, which is considered below.

Conditioned Interface-averages

Consider the volume element $\delta V = \delta V_\varphi + \delta V_\phi$, figure 8.2, composed of two infinitesimal volume elements adjacent to the interface – δV_φ on the φ-side and δV_ϕ on the ϕ-side. Integrating over δV_φ, when examining $\overline{I_\varphi \nabla \mathbf{\Phi}}$ and $\overline{I_\varphi \nabla \bullet \mathbf{\Phi}}$, has no net effect on the first terms on the r.h.s. of equations 8.9 and 8.10, respectively, since the bulk

(phase interior) contributions are regarded constant over δV_φ. The second terms can be transfered into surface integrals:

$$\begin{aligned}\overline{\boldsymbol{\Phi}\nabla I_\varphi} &= -\overline{\delta_I \boldsymbol{\Phi}\mathbf{n}_{I,\varphi\phi}} = -\overline{\boldsymbol{\Phi}_I \mathbf{n}_{I,\varphi\phi}} \\ &= -\lim_{\delta V_\varphi \to 0} \overline{\frac{1}{\delta V_\varphi}\int_{\delta V_\varphi(\mathbf{x},t)} \boldsymbol{\Phi}_I \mathbf{n}_{I,\varphi\phi}\, dV} \\ &= -\lim_{\delta V_\varphi \to 0} \overline{\frac{1}{\delta V_\varphi}\int_{S_I(\mathbf{x},t)} \boldsymbol{\Phi}\mathbf{n}_{I,\varphi\phi}\; dS}, \end{aligned} \tag{8.12}$$

where $S_I(\mathbf{x}, t)$ is the equation for the interface. Note that the two volume-average operations have been interchanged since they commute. Similarly, one obtains

$$\begin{aligned}\overline{\boldsymbol{\Phi}\bullet\nabla I_\varphi} &= -\overline{\delta_I \boldsymbol{\Phi}\bullet\mathbf{n}_{I,\varphi\phi}} = -\overline{\boldsymbol{\Phi}_I\bullet\mathbf{n}_{I,\varphi\phi}} \\ &= -\lim_{\delta V_\varphi \to 0} \overline{\frac{1}{\delta V_\varphi}\int_{\delta V_\varphi(\mathbf{x},t)} \boldsymbol{\Phi}_I\bullet\mathbf{n}_{I,\varphi\phi}\, dV} \\ &= -\lim_{\delta V_\varphi \to 0} \overline{\frac{1}{\delta V_\varphi}\int_{S_I(\mathbf{x},t)} \boldsymbol{\Phi}\bullet\mathbf{n}_{I,\varphi\phi}\; dS}. \end{aligned} \tag{8.13}$$

It is useful to introduce the definition of a conditioned interface-average $\widetilde{\boldsymbol{\Phi}}^\varphi$:

$$\widetilde{\boldsymbol{\Phi}}^\varphi \equiv \frac{1}{\Sigma}\lim_{\delta V_\varphi \to 0} \overline{\frac{1}{\delta V_\varphi}\int_{\delta V_\varphi} \boldsymbol{\Phi}_I dV} = \frac{1}{\Sigma}\lim_{\delta V_\varphi \to 0} \overline{\frac{1}{\delta V_\varphi}\int_{S_I(\mathbf{x},t)} \boldsymbol{\Phi}\, dS}, \tag{8.14}$$

$$\text{with} \qquad \Sigma \equiv \lim_{\delta V \to 0} \overline{\frac{1}{\delta V}\int_{S_I(\mathbf{x},t)} dS}, \tag{8.15}$$

where Σ denotes the interfacial area density – the interfacial surface area per unit volume. Similarly, we define an interface average $\widetilde{\boldsymbol{\Phi}}$ according to Weller [36], as surface integral per unit volume divided by the interfacial area density,

$$\widetilde{\boldsymbol{\Phi}} \equiv \frac{1}{\Sigma}\lim_{\delta V \to 0} \overline{\frac{1}{\delta V}\int_{S_I(\mathbf{x},t)} \boldsymbol{\Phi}\,(\mathbf{x},\, t)\; dS}, \tag{8.16}$$

which can be transferred into $\widetilde{\boldsymbol{\Phi}}^\varphi$ – considering the limiting value of $\boldsymbol{\Phi}$ after conditioning and approaching the interface from the φ-side:

$$\widetilde{\boldsymbol{\Phi}}^\varphi = \widetilde{\boldsymbol{\Phi}_{I,\varphi}} \tag{8.17}$$

$$\text{with} \qquad \boldsymbol{\Phi}_{I,\varphi} = \delta_I \boldsymbol{\Phi}_\varphi.$$

In doing so, *interfacial quantities* can be written as

$$\widetilde{\boldsymbol{\Phi}_{I,\varphi\phi}}^\varphi = \widetilde{\boldsymbol{\Phi}_{I,\varphi\phi}}, \tag{8.18}$$

whereas the limiting values of *bulk quantities*, when approaching the interface from one side – either the φ- or the ϕ-side – still needs to be distinguished according to equation 8.17.

Table 8.1: Coefficients for the generic transport equation (two-phase flow) – mass and momentum balance.

balance	$\boldsymbol{\Phi}$	$\Gamma_{\boldsymbol{\Phi},d}$	$S_{\boldsymbol{\Phi}}$	$S_{\boldsymbol{\Phi},I}$
mass	1	0	0	0
momentum	$\mathbf{U}$	μ	$\rho\mathbf{g} - \nabla p$	$\|p\mathbf{n}_I\| - \sigma\kappa_{I,\varphi\phi}\,\mathbf{n}_{I,\varphi\phi} - \nabla_{I,\varphi\phi}\sigma$

Conditional Volume-averaged Conservation Equation and Interfacial Jump Condition

In order to obtain the averaged generic transport equation, its local instantaneous counter-part 8.3 is conditional volume-averaged,

$$\overline{I_\varphi \frac{\partial \rho\boldsymbol{\Phi}}{\partial t}} + \overline{I_\varphi \nabla\bullet\left(\rho\boldsymbol{\Phi}\mathbf{U}\right)} - \overline{I_\varphi \nabla\bullet\left(\Gamma_{\boldsymbol{\Phi},d}\nabla\boldsymbol{\Phi}\right)} - \overline{I_\varphi S_{\boldsymbol{\Phi}}} = \mathbf{0}. \tag{8.19}$$

Now recalling equations 8.7, 8.9, 8.10 and 8.11, and neglecting mass transfer $\mathbf{U}_I = \mathbf{U}_{I,\varphi}$ yields:

$$\frac{\partial \alpha_\varphi\, \overline{\rho\boldsymbol{\Phi}}^{\varphi}}{\partial t} + \nabla\bullet\left(\alpha_\varphi\, \overline{\rho\boldsymbol{\Phi}\mathbf{U}}^{\varphi}\right) - \nabla\bullet\left(\alpha_\varphi\, \overline{\Gamma_{\boldsymbol{\Phi},d}\nabla\boldsymbol{\Phi}}^{\varphi}\right) = \overline{I_\varphi S_{\boldsymbol{\Phi}}} + \overbrace{\left(\Gamma_{\boldsymbol{\Phi},d}\nabla\boldsymbol{\Phi}\right)\bullet\mathbf{n}_I}^{\varphi}\,\Sigma. \tag{8.20}$$

From equation 8.4, representing the local-instantaneous jump condition for a generic transport quantity $\boldsymbol{\Phi}$, we arrive at the corresponding volume-averaged interface balance by conditioning and subsequently volume-averaging. Conditioning is accomplished by multiplication with $\delta_I\left(\mathbf{x} - \mathbf{x}_I,\, t\right)$. Taking into account the symmetry, $\mathbf{n}_{I,\varphi\phi} = -\mathbf{n}_{I,\phi\varphi}$, and neglecting mass transfer, it is:

$$\begin{aligned}
& \overline{\|\left(\Gamma_{\boldsymbol{\Phi},d}\nabla\boldsymbol{\Phi}\right)\bullet\mathbf{n}_I\|\delta_I} = -\overline{S_{\boldsymbol{\Phi},I}\delta_I} \\
\Leftrightarrow\quad & \overline{\left(\Gamma_{\boldsymbol{\Phi},d}\nabla\boldsymbol{\Phi}\right)_{I,\varphi}\bullet\nabla I_\varphi} + \overline{\left(\Gamma_{\boldsymbol{\Phi},d}\nabla\boldsymbol{\Phi}\right)_{I,\phi}\bullet\nabla I_\phi} = -\overline{S_{\boldsymbol{\Phi},I}\delta_I} \\
\Leftrightarrow\quad & \overbrace{\left(\Gamma_{\boldsymbol{\Phi},d}\nabla\boldsymbol{\Phi}\right)\bullet\mathbf{n}_{I,\varphi\phi}}^{\varphi}\,\Sigma + \overbrace{\left(\Gamma_{\boldsymbol{\Phi},d}\nabla\boldsymbol{\Phi}\right)\bullet\mathbf{n}_{I,\phi\varphi}}^{\phi}\,\Sigma = \overline{S_{\boldsymbol{\Phi},I}\delta_I}\,.
\end{aligned} \tag{8.21}$$

By replacing the generic transport quantity $\boldsymbol{\Phi}$ as well as corresponding coefficients and source terms according to table 8.1 we arrive at the conditional volume-averaged conservation equation of mass and momentum, respectively.

- conditional volume-averaged continuity equation:

$$\frac{\partial \alpha_\varphi\, \overline{\rho}^{\varphi}}{\partial t} + \nabla\bullet\left(\alpha_\varphi\, \overline{\rho\mathbf{U}}^{\varphi}\right) = 0. \tag{8.22}$$

By use of an density-weighted decomposition[5], this yields:

$$\frac{\partial \alpha_\varphi \, \overline{\rho}^\varphi}{\partial t} + \nabla\bullet\left(\alpha_\varphi \, \overline{\rho}^\varphi \widetilde{\mathbf{U}}^\varphi\right) = 0. \tag{8.23}$$

Considering incompressible flows with constant densities $\overline{\rho}^\varphi$ and $\overline{\rho}^\phi$ in both phases φ and ϕ, it is $\widetilde{\mathbf{\Phi}}^\varphi \overset{!}{=} \overline{\mathbf{\Phi}}^\varphi$, since $I_\varphi \rho = \overline{\rho}^\varphi = \text{const}$. Then, the conditional volume-averaged continuity equation reads:

$$\frac{\partial \alpha_\varphi}{\partial t} + \nabla\bullet\left(\alpha_\varphi \, \overline{\mathbf{U}}^\varphi\right) = 0. \tag{8.24}$$

- conditional volume-averaged momentum equation:

$$\begin{aligned}\frac{\partial \alpha_\varphi \, \overline{\rho\mathbf{U}}^\varphi}{\partial t} + \nabla\bullet\left(\alpha_\varphi \, \overline{\rho\mathbf{U}\mathbf{U}}^\varphi\right) - \nabla\bullet\left(\alpha_\varphi \, \overline{\mu\nabla\mathbf{U}}^\varphi\right) = &- \nabla\left(\alpha_\varphi \, \overline{p}^\varphi\right) + \alpha_\varphi \, \overline{\rho}^\varphi \mathbf{g} \\ &- \widetilde{p\mathbf{n}_I}^\varphi \Sigma + \widetilde{(\mu\nabla\mathbf{U})\bullet\mathbf{n}_I}^\varphi \Sigma.\end{aligned} \tag{8.25}$$

The second term on the l.h.s. of equation 8.25, needs a density-weighted decomposition:

$$\begin{aligned}\overline{\rho\mathbf{U}\mathbf{U}}^\varphi &= \overline{\rho}^\varphi \widetilde{\widetilde{\mathbf{U}}^\varphi \widetilde{\mathbf{U}}^\varphi}^\varphi + \underbrace{2\,\overline{\rho}^\varphi \widetilde{\widetilde{\mathbf{U}}^\varphi \mathbf{U}''^\varphi}^\varphi}_{=\mathbf{0}} + \overline{\rho}^\varphi \underbrace{\widetilde{\mathbf{U}''^\varphi \mathbf{U}''^\varphi}^\varphi}_{\equiv \widetilde{\mathbf{R}}^\varphi} \\ &= \overline{\rho}^\varphi \widetilde{\mathbf{U}}^\varphi \widetilde{\mathbf{U}}^\varphi + \overline{\rho}^\varphi \widetilde{\mathbf{R}}^\varphi,\end{aligned} \tag{8.26}$$

with $\widetilde{\mathbf{R}}^\varphi$ representing the density-weighted Reynolds stress tensor, by means of which velocity fluctuations, which may be introduced by interface motion and turbulence, are accounted for.

Equation 8.25 can be rewritten into a more common form by reformulation of the diffusive term for incompressible Newtonian flows decomposing the velocity gradient tensor $\nabla\mathbf{U}$ into $\mathbf{D} \equiv -\frac{1}{2}(\nabla\mathbf{U} + (\nabla\mathbf{U})^T)$ and $\mathbf{S} \equiv -\frac{1}{2}(\nabla\mathbf{U} - (\nabla\mathbf{U})^T)$. The conditional volume-averaged momentum equation finally reads:

$$\begin{aligned}&\frac{\partial \alpha_\varphi \, \overline{\rho}^\varphi \widetilde{\mathbf{U}}^\varphi}{\partial t} + \nabla\bullet\left(\alpha_\varphi \, \overline{\rho}^\varphi \widetilde{\mathbf{U}}^\varphi \widetilde{\mathbf{U}}^\varphi\right) + \nabla\bullet\left(\alpha_\varphi \, \overline{\rho}^\varphi \widetilde{\mathbf{R}}^\varphi\right) \\ &= - \nabla\left(\alpha_\varphi \, \overline{p}^\varphi\right) - \nabla\bullet\left(\alpha_\varphi \, \overline{\boldsymbol{\tau}}^\varphi\right) + \alpha_\varphi \, \overline{\rho}^\varphi \mathbf{g} + \mathbf{M}_\varphi,\end{aligned} \tag{8.27}$$

[5] Generally, Reynolds decomposition of local-instantaneous quantities $\mathbf{\Phi}$ and $\mathbf{\Psi}$ into their average and corresponding fluctuating parts $\mathbf{\Phi} = \overline{\mathbf{\Phi}} + \mathbf{\Phi}'$ and $\mathbf{\Psi} = \overline{\mathbf{\Psi}} + \mathbf{\Psi}'$ is adopted. However, considering the average of the product $\overline{\mathbf{\Psi}\mathbf{\Phi}} = \overline{\mathbf{\Psi}}\,\overline{\mathbf{\Phi}} + \overline{\mathbf{\Psi}'\mathbf{\Phi}'}$ inherently results in the need for modeling the fluctuation term $\overline{\mathbf{\Psi}'\mathbf{\Phi}'}$. Hence, we adopt an appropriate (weighted) decomposition to avoid this a priori unclosed term: $\overline{\mathbf{\Phi}(\mathbf{x}, t)} = \frac{\overline{\mathbf{\Psi}\mathbf{\Phi}}}{\overline{\mathbf{\Psi}}} - \frac{\overline{\mathbf{\Psi}'\mathbf{\Phi}'}}{\overline{\mathbf{\Psi}}} \equiv \widetilde{\mathbf{\Phi}} + \mathbf{\Phi}''$, where $\mathbf{\Phi}''$ represents the fluctuation with respect to the weighted average. We introduce the so-called phase-weighted or density-weighted (Favre) average by choosing the weight $\mathbf{\Psi} = I_\varphi \rho = \rho_\varphi$, which results in $\widetilde{\mathbf{\Phi}}^\varphi \equiv \frac{\overline{I_\varphi \rho \mathbf{\Phi}}}{\alpha_\varphi \, \overline{\rho}^\varphi}$ and the corresponding fluctuation $\mathbf{\Phi}''^\varphi \equiv \mathbf{\Phi} - \widetilde{\mathbf{\Phi}}^\varphi$.

with the viscous shear stress tensor being defined as $\boldsymbol{\tau} \equiv 2\mu\mathbf{D}$, and the last term in the r.h.s. being

$$\begin{aligned}\mathbf{M}_\varphi &\equiv -\overbrace{(p\mathbf{I}+\boldsymbol{\tau})\bullet\mathbf{n}_I}^{\varphi}\Sigma = \overline{(p\mathbf{I}+\boldsymbol{\tau})_{I,\varphi}\bullet\nabla I_\varphi} \\ &= -\overbrace{\boldsymbol{\sigma}\bullet\mathbf{n}_I}^{\varphi}\Sigma = \overline{\boldsymbol{\sigma}_{I,\varphi}\bullet\nabla I_\varphi}\,, \end{aligned} \tag{8.28}$$

denoting the *interfacial momentum transfer* term.

For incompressible two-phase flows, i.e., $\widetilde{\boldsymbol{\Phi}}^\varphi \overset{!}{=} \overline{\boldsymbol{\Phi}}^\varphi$, the conditional volume-averaged momentum equation becomes

$$\begin{aligned}&\frac{\partial\alpha_\varphi\,\overline{\mathbf{U}}^\varphi}{\partial t} + \nabla\bullet\left(\alpha_\varphi\,\overline{\mathbf{U}}^\varphi\,\overline{\mathbf{U}}^\varphi\right) + \nabla\bullet\left(\alpha_\varphi\,\overline{\mathbf{R}}^\varphi\right) \\ &= -\frac{\nabla\left(\alpha_\varphi\,\overline{p}^\varphi\right)}{\overline{\rho}^\varphi} - \frac{\nabla\bullet\left(\alpha_\varphi\,\overline{\boldsymbol{\tau}}^\varphi\right)}{\overline{\rho}^\varphi} + \alpha_\varphi\mathbf{g} + \frac{\mathbf{M}_\varphi}{\overline{\rho}^\varphi}. \end{aligned} \tag{8.29}$$

Replacing the generic transport quantity $\boldsymbol{\Phi}$ and corresponding coefficients and source terms, one can state the following for the

- conditional volume-averaged interfacial mass jump condition:
  In the absence of mass transfer (e.g., due to phase change) the generic jump condition as provided in equation 8.21 degenerates to the trivial identity $0 = 0$, indicating that no additional condition has to be taken into account.

- condition volume-averaged interfacial momentum jump condition:

$$\begin{aligned}&\overline{(\mu\nabla\mathbf{U})_{I,\varphi}\bullet\nabla I_\varphi} + \overline{(\mu\nabla\mathbf{U})_{I,\phi}\bullet\nabla I_\phi} \\ &\quad= \overline{p_{I,\varphi}\mathbf{n}_{I,\varphi\phi}\,\delta_I - p_{I,\phi}\mathbf{n}_{I,\phi\varphi}\,\delta_I - \sigma\kappa_{I,\varphi\phi}\,\mathbf{n}_{I,\varphi\phi}\,\delta_I} \\ &\quad= \overline{p_{I,\varphi}\nabla I_\varphi} + \overline{p_{I,\phi}\nabla I_\phi} + \sigma\,\overline{\kappa_{I,\varphi\phi}\,\nabla I_\varphi} \end{aligned} \tag{8.30}$$

$$\Leftrightarrow \quad -\overbrace{(p\mathbf{I}+\boldsymbol{\tau})\bullet\mathbf{n}_I}^{\varphi}\Sigma - \overbrace{(p\mathbf{I}+\boldsymbol{\tau})\bullet\mathbf{n}_I}^{\phi}\Sigma = \sigma\,\overbrace{\kappa_I\mathbf{n}_I}^{\varphi}\Sigma$$

$$-\overbrace{\boldsymbol{\sigma}\bullet\mathbf{n}_I}^{\varphi}\Sigma - \overbrace{\boldsymbol{\sigma}\bullet\mathbf{n}_I}^{\phi}\Sigma = \sigma\,\overbrace{\kappa_I\mathbf{n}_I}^{\varphi}\Sigma. \tag{8.31}$$

Taking into account the definition of the interfacial momentum transfer term $\mathbf{M}_\varphi$ (and for $\mathbf{M}_\phi$) according to equation 8.28, we arrive at the shorthand notation for the conditional volume-averaged momentum jump condition. In the absence of mass transfer and neglecting any variations of the surface tension σ along the interface, it is:

$$\mathbf{M}_\varphi + \mathbf{M}_\phi = \mathbf{M}_\sigma, \tag{8.32}$$

where $\mathbf{M}_\sigma$ on the r.h.s. of equation 8.32 denotes the averaged interfacial momentum source due to surface tension:

$$\mathbf{M}_\sigma \equiv -\sigma\,\overline{\kappa_{I,\varphi\phi}\,\nabla I_\varphi} = \sigma\,\overbrace{\kappa_{I,\varphi\phi}\,\mathbf{n}_{I,\varphi\phi}}^{}\Sigma. \tag{8.33}$$

8.3. Multi-scale Two-Phase Methodology & Closure

Equations 8.24 and 8.29 constitute a two-phase flow model, which is applicable for different flow types that might occur in a two-phase system. In this form the two-phase flow model is not solvable.

The unclosed terms in the two-phase flow model equations might be categorized into three groups, that are

- phase-interaction terms: interfacial momenta transfer terms $\mathbf{M}_\varphi$ and $\mathbf{M}_\phi$ along with the interfacial momentum source term due to surface tension $\mathbf{M}_\sigma$
- self-interaction terms: averaged shear stress terms $\overline{\boldsymbol{\tau}}^\varphi$ and $\overline{\boldsymbol{\tau}}^\phi$
- turbulence terms: averaged Reynolds stress tensors $\overline{\mathbf{R}}^\varphi$ and $\overline{\mathbf{R}}^\phi$[6].

All of the above terms will differ when considering different flow types. The concrete form of closure might vary dependent upon the length scale down to which the two-phase flow under consideration is *resolved*. In the remainder of this section closure relations shall be examined. The emphasize is given to the 'information loss' due to averaging beyond the averaging scale.

In order to develop a consistent closure it is first advisable to have a closer look on the 'conceptual picture' that can be drawn from the applied averaging procedure and its physical interpretation. For this purpose it is of use to distinguish between two specific flow types as shown in figure 8.3, namely

1.) dispersed flows (figure 8.3a), e.g., bubbly or droplet flows, and

2.) segregated flows (figure 8.3b), e.g., stratified or wavy free-surface flows,

as limiting cases of a two-phase flow scenario of mixed type, where bubbles and droplets exist in the liquid and the gaseous phase.

Figure 8.3 shows that the conditional volume-averaging results in *one uniform 'physical picture'* for both two-phase flow types. It shows a clear separation into resolved mesoscale and unresolved microscale. We refer to the two-phase flow models as *interfacial scale averaging* or *interfacial scale resolving*.

[6] Turbulence modeling of two- and multiphase systems, is still an open research area on its own, that requires detailed knowledge of the interaction between turbulent and morphological interfacial structures. The interested reader is referred to the work of Toutant et al. [39–42], who examine the interplay of under-resolved discontinuous interfaces and turbulence structures, employing spatial filtering as central tool. We will disregard turbulence modeling in this study.

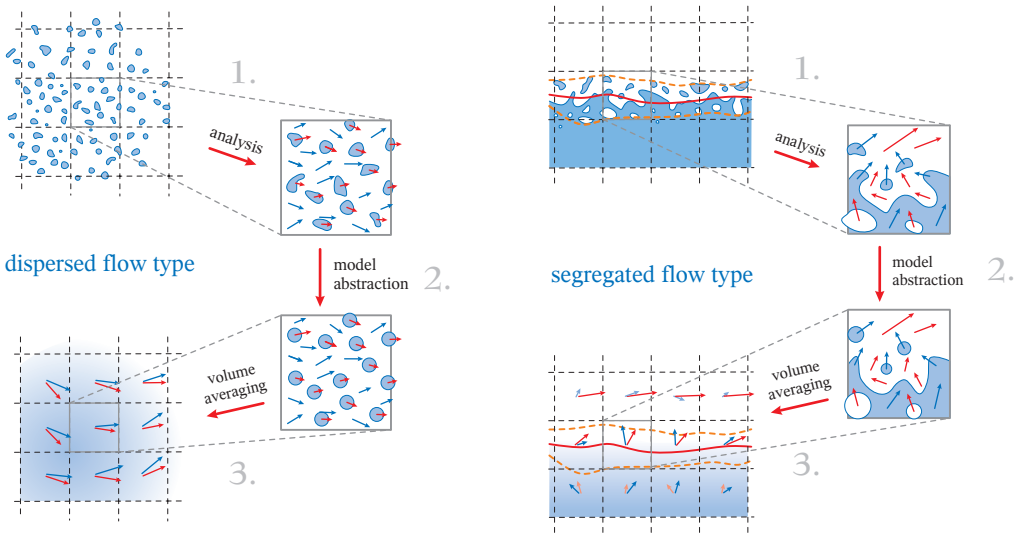

(a) Dispersed flow type. **(b)** Segregated flow type.

Figure 8.3: Principles of model closure.

In dispersed two-phase flows, the interfacial scale averaging models are well-known and established. These approaches model all (unresolved) interfacial scales [35] – that of DPEs (bubbles, droplets or particles) – employing *closure relations in the underlying averaging framework*, and resolve the other scales by means of *numerically solving for averaged conservation equations*. In segregated flows partially interfacial scale resolving models have not been considered yet, while the use of fully interfacial scale resolving models is again a well-known and established practise [7–9]. However, the latter does not allow for under-resolved interfacial details. Furthermore, since a volume-averaging procedure acts as spatial filtering, the partially interfacial scale resolving models appear to be fully compatible with the LES methodology as it is commonly adopted for modeling single-phase turbulence (using a box-filter). Consequently, for the purpose of a consistent and general closure, we shall focus on partially interfacial scale resolving methods. For this purpose a *scale similarity hypothesis* is proposed for two-phase flows:

> the smallest resolved scales of a two-phase flow are assumed to exhibit similar characteristics as the largest unresolved ones.

Consequently, conditional volume-averaging leads to two model approaches that are conceptually compatible. In both approaches each phase is treated separately and is assumed to coexist within the averaging volumes, possessing characteristic properties

and an own velocity and pressure field. Hence, separate sets of averaged conservation equations are solved for each phase present in the system (Eulerian-Eulerian two-fluid methodology). Depending on the two-phase flow type, two concepts emerge:

- Concept of Interpenetrating Continua and
- Concept of Partially Penetrating Continua,

where the former corresponds to the interfacial scale averaging closure framework, which is well-established for dispersed flows, and the latter concept corresponds to the partially interfacial scale resolving model framework. The terminology 'concept of partially penetrating continua' has been introduced in order to account for the conceptual proximity. The concept of partially penetrating continua shall be examined in detail in the following, while we only briefly consider the concept of interpenetrating continua.

8.3.1. Closure Strategy & Conceptual Approach

Concept of Interpenetrating Continua The dispersed two-phase flow is considered as a two-constituent pseudo-continuum, with each phase being treated separately. The concept of interpenetrating continua corresponds to the interfacial scale averaging model framework. Closure models for the dispersed two phase-flow type are well-established [43, 44]. The interfacial morphology is not resolved at all. One has to act on specific assumptions regarding the flow morphology when modeling phase interactions via closure relations within the averaging framework,e.g., fluid DPEs of spherical or ellipsoidal shape.

Concept of Partially Penetrating Continua A conceptual framework for segregated flows has to be formulated that is *(scale-)compatible and in the same spirit* as the concept of interpenetrating continua for dispersed flow types, called the *concept of partially penetrating continua* in the interfacial transition region.

The interfacial morphology is partially resolved, where unresolved interfacial morphologies and phase interactions again must be accounted for in the underlying averaging framework by appropriate closure. As a consequence, the interface becomes an interfacial transition region of certain characteristic width, determined by the averaging length scale.

A model representation of the interface is needed. This can be illustrated along several quantities representing pivotal features of two-phase flows, the interfacial averaged curvature $\widetilde{\kappa_I}$, the unit normal vector $\widetilde{\mathbf{n}_I}$, the interfacial area density Σ,

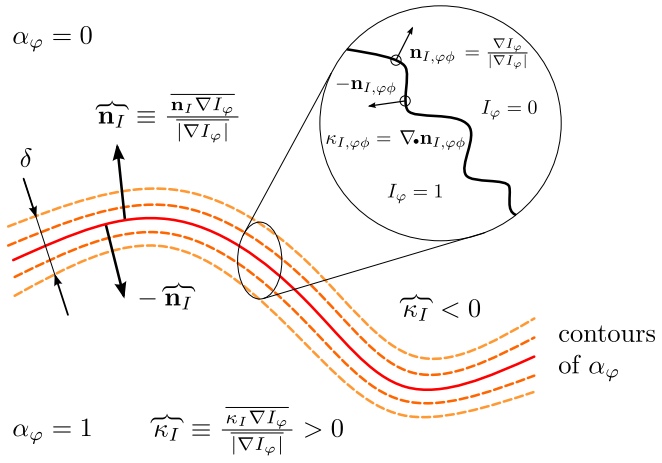

Figure 8.4: Closure model for the interfacial morphology.

the interfacial averaged velocity $\widetilde{\mathbf{U}}^\varphi$, and the interfacial width δ – characterizing either the interface morphology or its transport (interfacial dynamics).

interfacial morphology The *local* interface morphology is characterized by the *local* curvature $\kappa_{I,\varphi\phi}$, and the local unit vector normal to the microscale interface, $\mathbf{n}_{I,\varphi\phi}$. Using the phase indicator function I_φ, it is

$$\kappa_I = \kappa_{I,\varphi\phi} = \nabla\bullet\mathbf{n}_{I,\varphi\phi} \qquad \text{and} \qquad \mathbf{n}_I = \mathbf{n}_{I,\varphi\phi} = \frac{\nabla I_\varphi}{|\nabla I_\varphi|}. \tag{8.34}$$

Evaluation of the interfacial averaged counter-parts,

$$\widetilde{\kappa_I} \equiv \frac{\overline{\kappa_I \nabla I_\varphi}}{\overline{|\nabla I_\varphi|}} \qquad \text{and} \qquad \widetilde{\mathbf{n}_I} \equiv \frac{\overline{\mathbf{n}_I \nabla I_\varphi}}{\overline{|\nabla I_\varphi|}}, \tag{8.35}$$

requires detailed knowledge of the microscopic interfacial morphology, which is a priori unknown. The limit might be pushed somewhat further by taking advantage of equation 8.9 and substituting $\mathbf{\Phi} = 1$, which results in $\widetilde{\mathbf{n}_I}\Sigma = -\nabla\alpha_\varphi$. Thus, it is:

$$\widetilde{\mathbf{n}_I} = -\frac{\nabla\alpha_\varphi}{\Sigma} \qquad \text{and} \qquad \widetilde{\kappa_I} = \widetilde{\nabla\bullet\mathbf{n}_I} = \nabla\bullet\,\widetilde{\mathbf{n}_I} = -\nabla\bullet\left(\frac{\nabla\alpha_\varphi}{\Sigma}\right). \tag{8.36}$$

Here, Σ comprises two contributions: the averaged (mesoscale, resolved) curvature and the fluctuating (microscale, unresolved) curvature.

A closure model for the interfacial area density Σ is derived from equation 8.9:

$$
\begin{aligned}
& |\widetilde{\mathbf{n}_I}|\Sigma = |\nabla\alpha_\varphi| \\
\overset{|\widetilde{\mathbf{n}_I}|\approx 1}{\Longleftrightarrow} \quad & \Sigma \equiv \overline{|\nabla I_\varphi|} \approx |\nabla \overline{I_\varphi}| = |\nabla\alpha_\varphi|.
\end{aligned}
\tag{8.37}
$$

This model is justified under the assumption $|\widetilde{\mathbf{n}_{I,\varphi\phi}}| \approx 1$ stating that the interfacial area density is allowed to vary only across the interfacial transition region normal to $\widetilde{\mathbf{n}_{I,\varphi\phi}}$ – but not along contours of constant α_φ. Σ is assumed to be dominated by contributions from the unresolved interfacial morphology within the interfacial transition region, while macroscopic contributions (e.g., from the resolved mean curvature) play a much lesser role. Note that assuming such a local instantaneous *isotropic interfacial morphology* fully complies with the requirement of phase invariance, since $\nabla\alpha_\varphi = -\nabla\alpha_\phi$.

For the interfacial averaged interface morphology it follows:

$$
\widetilde{\mathbf{n}_I} = \frac{\nabla\alpha_\varphi}{|\nabla\alpha_\varphi|} \qquad \text{and} \qquad \widetilde{\kappa_I} = -\nabla\bullet\left(\frac{\nabla\alpha_\varphi}{|\nabla\alpha_\varphi|}\right), \tag{8.38}
$$

resulting in the desired separation of unresolved and resolved contributions:

$$
\begin{aligned}
\widetilde{\kappa_I} &= -\nabla\bullet\left(\frac{\nabla\alpha_\varphi}{|\nabla\alpha_\varphi|}\right) = -\frac{1}{|\nabla\alpha_\varphi|}\left[\nabla\bullet\nabla\alpha_\varphi + \nabla\left(\frac{1}{|\nabla\alpha_\varphi|}\right)\bullet\nabla\alpha_\varphi\right] \\
&= -\frac{1}{|\nabla\alpha_\varphi|}\Bigg[\nabla^2\alpha_\varphi - \underbrace{\frac{\nabla\alpha_\varphi}{|\nabla\alpha_\varphi|}\bullet\nabla|\nabla\alpha_\varphi|}_{=\widetilde{\mathbf{n}_I}\bullet\nabla\Sigma}\Bigg].
\end{aligned}
\tag{8.39}
$$

Since Σ only varies across the interfacial transition region normal to $\widetilde{\mathbf{n}_I}$, it is

$$
\widetilde{\kappa_I} = -\frac{\nabla^2\alpha_\varphi}{|\nabla\alpha_\varphi|} + \frac{d\Sigma}{d\alpha_\varphi}, \tag{8.40}
$$

with the latter contribution identified as contribution from the microscopic unresolved curvature to $\widetilde{\kappa_I}$ – stemming from local fluctuations *inside* the interfacial transition region.

interface transport Decomposition of the instantaneous velocity at the interface into an interfacial averaged velocity and local interfacial velocity fluctuation yields

$$
\mathbf{U}_{I,\varphi} = \widetilde{\mathbf{U}}^{\varphi} + \mathbf{U}^{\sharp}_{I,\varphi}. \tag{8.41}
$$

Stating that the unresolved velocity profile is continuous across the interface – interfacial no-slip condition – a closure model for the interfacial averaged

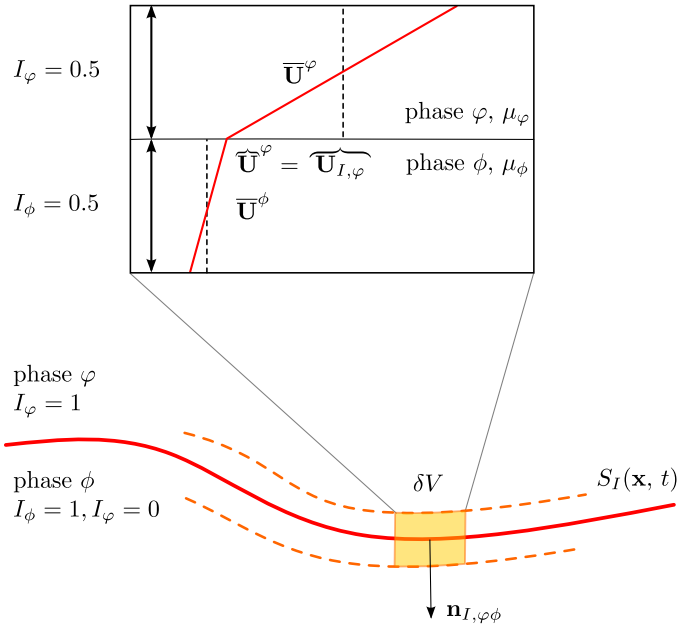

Figure 8.5: Closure model for the interfacial averaged velocity.

velocity $\widetilde{\mathbf{U}}^{\varphi}$ can be deduced, figure 8.5 for a shear flow scenario. From elementary geometry (intercept theorem) it can be seen, that for a simple case where $\overline{\mu}^{\varphi} = \overline{\mu}^{\phi}$:

$$\frac{\widetilde{\mathbf{U}}^{\varphi} - \overline{\mathbf{U}}^{\phi}}{\overline{\mathbf{U}}^{\varphi} - \widetilde{\mathbf{U}}^{\varphi}} = \frac{I_\phi}{I_\varphi} \quad \Leftrightarrow \quad \widetilde{\mathbf{U}}^{\varphi} = I_\phi \, \overline{\mathbf{U}}^{\varphi} + I_\varphi \, \overline{\mathbf{U}}^{\phi}, \tag{8.42}$$

and with a correction for the general case where $\overline{\mu}^{\varphi} \neq \overline{\mu}^{\phi}$:

$$\frac{\overline{\mu}^{\phi}}{\overline{\mu}^{\varphi}} \frac{\widetilde{\mathbf{U}}^{\varphi} - \overline{\mathbf{U}}^{\phi}}{\overline{\mathbf{U}}^{\varphi} - \widetilde{\mathbf{U}}^{\varphi}} = \frac{I_\phi}{I_\varphi} \quad \Leftrightarrow \quad \widetilde{\mathbf{U}}^{\varphi} = \frac{I_\phi \, \overline{\mu}^{\varphi} \, \overline{\mathbf{U}}^{\varphi} + I_\varphi \, \overline{\mu}^{\phi} \, \overline{\mathbf{U}}^{\phi}}{I_\varphi \, \overline{\mu}^{\phi} + I_\phi \, \overline{\mu}^{\varphi}}. \tag{8.43}$$

Consequently, equation 8.43 results in the closure relation for $\widetilde{\mathbf{U}}^{\varphi}$ (for $I_\varphi = I_\phi \overset{!}{=} 1/2$ at the interface):

$$\widetilde{\mathbf{U}}^{\varphi} = \widetilde{\mathbf{U}_{I,\varphi}} = \frac{\overline{\mu}^{\varphi} \, \overline{\mathbf{U}}^{\varphi} + \overline{\mu}^{\phi} \, \overline{\mathbf{U}}^{\phi}}{\overline{\mu}^{\varphi} + \overline{\mu}^{\phi}}. \tag{8.44}$$

Phase symmetry is preserved. Considering limiting cases, this closure yields physically reasonable results. If we choose phase φ as liquid phase and ϕ as gaseous phase, where $\overline{\mu}^{\phi} \ll \overline{\mu}^{\varphi}$, it follows $\widetilde{\mathbf{U}}^{\varphi} = \overline{\mathbf{U}}^{\varphi}$, which clearly is a physically plausible outcome.

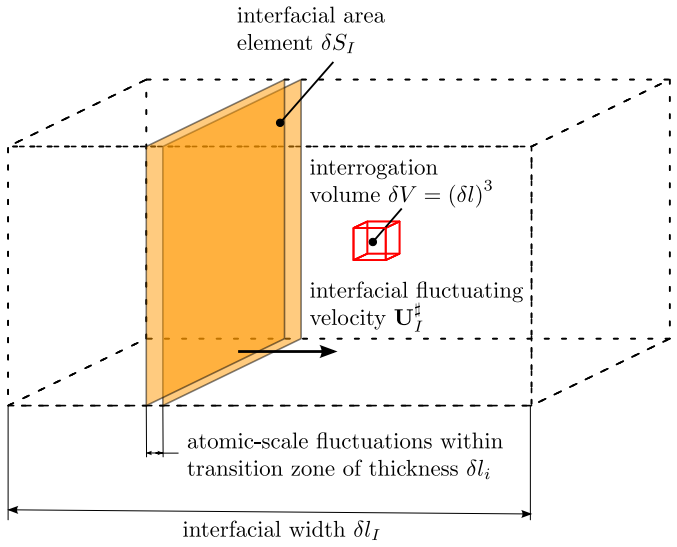

(a) fluctuating interface within the interfacial transition region.

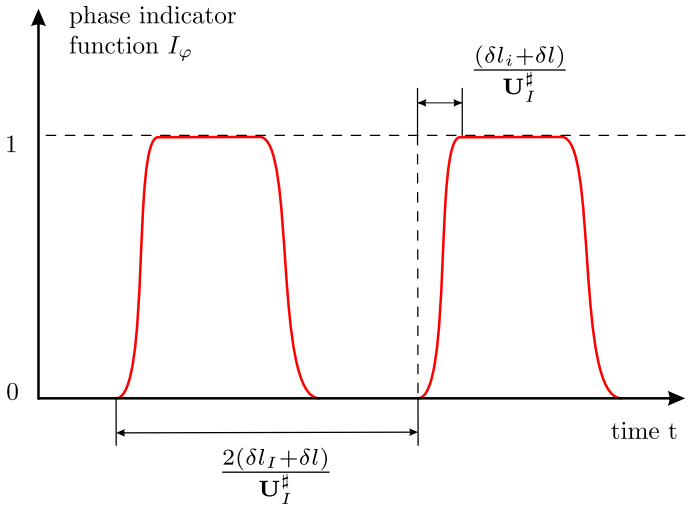

(b) time history of the phase indicator function.

Figure 8.6: Illustration of a fluctuating interface for an isotropic interfacial morphology.

The second term on the r.h.s. of equation 8.41, i.e., the interfacial velocity fluctuation $\mathbf{U}^{\sharp}_{I,\varphi}$, is related to the width δ of the interfacial transition region. Consider the simple case as illustrated in figure 8.6a, where a flat surface element of the gas-liquid interface is assumed to oscillate vertically within the interfacial transition region. Boundaries between which this happens are characterized by the root-mean-squared position deviation of interfacial fluctuations from the interface mean position. The resulting distance shall be entitled interfacial width δl_I.

This scenario is compatible with the model representation of an isotropic interfacial morphology illustrated in figure 8.4 and set out for the interfacial area density Σ. The interfacial surface element shall move with a (for now) constant interfacial fluctuation velocity $\mathbf{U}^{\sharp}_{I}$ – back and forth in the presumed horizontal direction. Furthermore, the phase indicator function I_φ shall vary smoothly between its limiting values of 0 and 1 within a thin transition zone, where on molecular-scale fluctuations occur governing the inner atomic-scale structure of the *diffuse interface* (as it is commonly described by diffuse interface or phase-field methods). The width δl_i of this thin transition zone is assumed to be of the order of several nanometers.

To approach a more exploitable expression for the interfacial area density Σ consider an infinitesimal 'interrogation' volume δV in the limiting case where $\delta V \to 0$. Then, the *local* interfacial area density reads:

$$\Sigma = \lim_{\delta V \to 0} \frac{\delta S_I}{\delta V} = \lim_{\delta l \to 0} \frac{\delta S_I}{(\delta l)^3}, \tag{8.45}$$

where δl represents the edge length of the 'interrogation' volume δV, and δS_I denotes the interfacial area density, in case the interface is found to be in the 'interrogation' volume $(\delta l)^2$ multiplied by the time fraction, that it is effectively present within δV considering the whole fluctuation in progress. With the help of figure 8.6b showing the time history of the phase indicator function averaged over δV, it follows

$$\Sigma = \lim_{\delta l \to 0} (\delta l)^2 \, \frac{2\,(\delta l_i + \delta l)\,/\mathbf{U}^{\sharp}_{I}}{2\,(\delta l_I + \delta l)\,/\mathbf{U}^{\sharp}_{I}} \frac{1}{(\delta l)^3}. \tag{8.46}$$

As a clear scale separation applies,

$$\delta l \ll \delta l_I \qquad \text{and} \qquad \delta l \gg \delta l_i, \tag{8.47}$$

which is considered fulfilled by orders of magnitude, equation 8.46 reduces to

$$\Sigma = \frac{1}{\delta l_I}, \tag{8.48}$$

and thus for the closure of the interfacial width, it follows from equation 8.37

$$\delta_I (= \delta) = \frac{1}{|\nabla \alpha_\varphi|}. \tag{8.49}$$

A first attempt for a closure model for δ, it is suggested that

$$\delta \approx \frac{1}{\Sigma} = \frac{1}{|\nabla \alpha_\varphi|}, \tag{8.50}$$

which inversely relates interfacial width δ and interfacial area density Σ, motivated from the closure for the *flame brush thickness* of an unwrinkled flamelet [45].

8.3.2. Momentum Closure

Phase-interaction Terms – $\mathbf{M}_\varphi$ and $\mathbf{M}_\phi$

The first phase-interaction term is the interfacial momentum transfer term $\mathbf{M}_\varphi$ as defined in equation 8.28. The momentum equations 8.29 for phase φ and ϕ are coupled through the conditional volume-averaged momentum jump condition set out in equation 8.32. Equation 8.28 shows that the integral of the instantaneous pressure and viscous stress distribution needs to be expressed as constitutive equation. It is useful to decompose the instantaneous pressure into a static (mean interfacial pressure) and a dynamic contribution (fluctuating pressure).

$$p_{I,\varphi} = \widetilde{p}^{\varphi} + p^{\sharp}_{I,\varphi}, \tag{8.51}$$

yielding

$$\begin{aligned} \mathbf{M}_\varphi &= \overline{\widetilde{p}^{\varphi} \mathbf{I} \bullet \nabla I_\varphi} + \overline{(p^{\sharp}\mathbf{I} + \boldsymbol{\tau})_{I,\varphi} \bullet \nabla I_\varphi} = \overline{\widetilde{p}^{\varphi} \mathbf{I} \bullet \nabla I_\varphi} - \overbrace{\left(p^{\sharp}\mathbf{I} + \boldsymbol{\tau}\right) \bullet \mathbf{n}_I}^{\varphi} \Sigma \\ &= \widetilde{p}^{\varphi} \nabla \alpha_\varphi + \mathbf{M}_{\varphi,h}, \end{aligned} \tag{8.52}$$

since

$$\overline{\widetilde{p}^{\varphi} \nabla I_\varphi} = -\overbrace{\delta_I \widetilde{p}^{\varphi} \mathbf{n}_I}^{\varphi} \Sigma = -\overbrace{\widetilde{p}^{\varphi}}^{\varphi} \widetilde{\mathbf{n}_I}^{\varphi} \Sigma = \widetilde{p}^{\varphi} \nabla \alpha_\varphi. \tag{8.53}$$

The second term on the r.h.s. of equation 8.52 is defined as

$$\mathbf{M}_{\varphi,h} \equiv \overline{(p^{\sharp}\mathbf{I} + \boldsymbol{\tau})_{I,\varphi} \bullet \nabla I_\varphi} = -\overbrace{\left(p^{\sharp}\mathbf{I} + \boldsymbol{\tau}\right) \bullet \mathbf{n}_I}^{\varphi} \Sigma. \tag{8.54}$$

The first term on the r.h.s. of equation 8.52 represents a net force contribution from the interfacial averaged pressure $\widetilde{p}^{\varphi}$ in case there is a gradient in the volumetric phase fraction of phase φ, $\nabla \alpha_\varphi$, and the second term holds the unbalanced interfacial pressure and shear (viscous) stress contribution $\overbrace{(p^{\sharp}\mathbf{I}+\boldsymbol{\tau})\bullet\mathbf{n}_I}^{\varphi} \Sigma$.

Mean interfacial pressure contributions. There are two constituents, that *generally* cause the 'mean interfacial' pressure $\widetilde{p}^{\varphi}$ to be different from the 'mean bulk' pressure $\overline{p}^{\varphi}$:

- phase slip,

  i.e., relative motion between the phases, reducing the mean pressure in vicinity to the interface (Bernoulli effect). For closure an expression would be of use, that clearly relates the pressure distribution over the interface to the bulk mean pressure. Subsequent averaging over the interface would result in a closure relation.

  For segregated flows it is suggested to relate the 'interfacial mean' and the 'bulk mean' pressure as

  $$\widetilde{p}^{\varphi} = \overline{p}^{\varphi} - \frac{\alpha_{\varphi}\alpha_{\phi}\,\overline{\rho}^{\varphi}\,\overline{\rho}^{\phi}}{\alpha_{\varphi}\,\overline{\rho}^{\phi} + \alpha_{\phi}\,\overline{\rho}^{\varphi}} |\,\overline{\mathbf{U}}^{\phi} - \overline{\mathbf{U}}^{\varphi}|^2 \tag{8.55}$$

  following Bestion [46], who introduced this term in the CATHARE CODE without physical argumentation, however, resulting in a form expected by Drew and Lahey [47]. This expression vanishes for stagnant fluids, while at the same time preserving hyperbolicity at least in presence of phase slip [48].

- surface tension,

  manifesting in an interfacial force balance with a force contribution due to interfacial averaged pressure (Young-Laplace effect).

  Since closure relations obviously are related to an interfacial force density due to surface tension, that is assumed to be dominated by unresolved (microscopic/local) curvature, i.e., the inner morphological structure of the interfacial transition region, it is advisable to revisit the underlying assumption of an *isotropic interfacial topology*. According to equation 8.40 the interfacial averaged curvature $\widetilde{\kappa_I}$ is decomposed into a resolved mesoscopic contribution and a dominant unresolved microscopic contribution $d\Sigma/d\alpha_{\varphi}$, where the interfacial area density Σ is only allowed to vary across the interfacial transition region, that is in the direction of $\widetilde{\mathbf{n}_I}$ – perpendicular to contours of constant α_{φ}.

  Closure models are needed for the terms $\mathbf{M}_{\varphi,\sigma}$ and $\mathbf{M}_{\phi,\sigma}$ as well as for $\mathbf{M}_{\sigma}$. Considering the adoption of this assumption in the context of interfacial surface tension modeling it is proposed that

  $$\mathbf{M}_{\varphi,\sigma} = \alpha_{\varphi} \cdot 4\alpha_{\varphi}\alpha_{\phi}\mathbf{M}_{\sigma} \qquad \text{and} \qquad \mathbf{M}_{\phi,\sigma} = \alpha_{\phi} \cdot 4\alpha_{\varphi}\alpha_{\phi}\mathbf{M}_{\sigma}, \tag{8.56}$$

where $4\alpha_\varphi\alpha_\phi$ represents a symmetric regularization term. The pre-factor is the contribution of the interfacial force density due to surface tension to the momentum equation of a particular phase *localized in a part of the interfacial transition region that features the inner curvature*: on the adjacent sites of the interface from the respective "phases' view point".

It remains to formulate a closure relation for $\mathbf{M}_\sigma$ defined as $\sigma\widetilde{\kappa_I\mathbf{n}_I}\Sigma$, equation 8.33: This will be decomposed into an interfacial average and an interfacial fluctuating contribution:

$$\mathbf{M}_\sigma = \sigma\widetilde{\kappa_I\mathbf{n}_I}\Sigma = \sigma\left(\widetilde{\kappa_I}\,\widetilde{\mathbf{n}_I} + \widetilde{\kappa_I^\sharp\mathbf{n}_I^\sharp}\right)\Sigma. \tag{8.57}$$

Using equation equation 8.9 (substituting $\mathbf{\Phi} = 1$) and 8.40, and underlying an isotropic interfacial morphology, equation 8.57 can be rewritten as

$$\Rightarrow \qquad \mathbf{M}_\sigma = -\sigma\left(-\frac{\nabla^2\alpha_\varphi}{|\nabla\alpha_\varphi|} + \frac{d\Sigma}{d\alpha_\varphi}\right)\nabla\alpha_\varphi + \sigma\widetilde{\kappa_I^\sharp\mathbf{n}_I^\sharp}\Sigma. \tag{8.58}$$

Equation 8.40, $d\Sigma/d\alpha_\varphi$ states the contribution of the microscopic unresolved curvature stemming from fluctuations inside the interfacial transition region. Thus, it seems rational to assume the same form for $\widetilde{\kappa_I^\sharp\mathbf{n}_I^\sharp}\Sigma$. Consequently, we propose:

$$\widetilde{\kappa_I^\sharp\mathbf{n}_I^\sharp}\Sigma \sim \frac{d\Sigma}{d\alpha_\varphi}\nabla\alpha_\varphi. \tag{8.59}$$

An algebraic expression for the interfacial area density Σ is needed. For this purpose, it is suggested to adopt the following phase-invariant algebraic model formulation for Σ:

$$\Sigma = 4\alpha_\varphi\alpha_\phi\,\Sigma_0, \tag{8.60}$$

where Σ_0 depends on the presumed unresolved interfacial morphology, assumed to be constant. Using the equations 8.38 and incorporating the proportionality factor (q.v. relation 8.59) into Σ_0 (equation 8.60), we can rewrite equation 8.57:

$$\begin{aligned}\mathbf{M}_\sigma &= \sigma\widetilde{\kappa_I}\,\widetilde{\mathbf{n}_I}\Sigma + \sigma\frac{d\Sigma}{d\alpha_\varphi}\nabla\alpha_\varphi \\ &\approx \sigma\left(\nabla_\bullet\left(\frac{\nabla\alpha_\varphi}{|\nabla\alpha_\varphi|}\right) + 4\Sigma_0\,(1-2\alpha_\varphi)\right)\nabla\alpha_\varphi.\end{aligned} \tag{8.61}$$

The model assumption according to equation 8.59 is rational, since $d\Sigma/d\alpha_\varphi$ is identified to provide the contribution from the microscopic

unresolved curvature and $\widehat{\kappa_I^\sharp \mathbf{n}_I^\sharp}^{\Sigma}$ is interpreted as the mean effect of this microscopic unresolved curvature. Thus,

$$\mathbf{M}_{\varphi,\sigma} \approx \alpha_\varphi \cdot 4\alpha_\varphi\alpha_\phi\,\sigma\left(\nabla\bullet\left(\frac{\nabla\alpha_\varphi}{|\nabla\alpha_\varphi|}\right)+4\Sigma_0\left(1-2\alpha_\varphi\right)\right)\nabla\alpha_\varphi,$$
$$\mathbf{M}_{\phi,\sigma} \approx \alpha_\phi \cdot 4\alpha_\varphi\alpha_\phi\,\sigma\left(\nabla\bullet\left(\frac{\nabla\alpha_\varphi}{|\nabla\alpha_\varphi|}\right)+4\Sigma_0\left(1-2\alpha_\varphi\right)\right)\nabla\alpha_\varphi. \quad (8.62)$$

Taking advantage of the product rule, the term $\nabla\left(\alpha_\varphi\,\overline{p}^{\varphi}\right)$ in the conditional volume-averaged momentum equation 8.29 is expanded towards $\alpha_\varphi\nabla\,\overline{p}^{\varphi}+\overline{p}^{\varphi}\nabla\alpha_\varphi$. This allow us to isolate a net interfacial pressure force density $\mathbf{M}_{\varphi,p}\equiv\left(\widehat{p}^{\varphi}-\overline{p}^{\varphi}\right)\nabla\alpha_\varphi$, accounting for the pressure difference $\widehat{p}^{\varphi}-\overline{p}^{\varphi}$ due to phase slip. For segregated flow from equation 8.55 it follows

$$\mathbf{M}_{\varphi,p}=-\frac{\alpha_\varphi\alpha_\phi\,\overline{\rho}^{\varphi}\,\overline{\rho}^{\phi}}{\alpha_\varphi\,\overline{\rho}^{\phi}+\alpha_\phi\,\overline{\rho}^{\varphi}}|\,\overline{\mathbf{U}}^{\phi}-\,\overline{\mathbf{U}}^{\varphi}|^2\,\nabla\alpha_\varphi. \quad (8.63)$$

The final form of the conditional volume-averaged momentum equation reads:

$$\frac{\partial\alpha_\varphi\,\overline{\mathbf{U}}^{\varphi}}{\partial t}+\nabla\bullet\left(\alpha_\varphi\,\overline{\mathbf{U}}^{\varphi}\,\overline{\mathbf{U}}^{\varphi}\right)=-\frac{\alpha_\varphi\nabla\,\overline{p}^{\varphi}}{\overline{\rho}^{\varphi}}-\frac{\nabla\bullet\left(\alpha_\varphi\,\overline{\boldsymbol{\tau}}^{\varphi}\right)}{\overline{\rho}^{\varphi}}$$
$$+\alpha_\varphi\mathbf{g}+\frac{\mathbf{M}_{\varphi,h}+\mathbf{M}_{\varphi,p}+\mathbf{M}_{\varphi,\sigma}}{\overline{\rho}^{\varphi}}. \quad (8.64)$$

It is left to consider the unbalanced interfacial pressure and shear stress contribution, $\mathbf{M}_{\varphi,h}$.

Unbalanced interfacial pressure and shear stress contribution. In the concept of partially penetrating continua $\mathbf{M}_{\varphi,h}$ in the interfacial transition region is identified as the interfacial force density due to unbalanced pressure and viscous stresses, which manifests itself in a dissipative drag due to interfacial friction in the presence of phase slip.

With $\widehat{\mu}^{\varphi}=\overline{\mu}^{\varphi}$ the following relation is proposed:

$$\mathbf{M}_{\varphi,h}\sim\frac{\Sigma}{\delta}\,\overline{\mu}^{\varphi}\left(\overline{\mathbf{U}}^{\varphi}-\widehat{\mathbf{U}}^{\varphi}\right), \quad (8.65)$$

where Σ denotes the interfacial area density that varies across the interfacial transition region of width δ.

Rewriting relation 8.65 by use of equation 8.44 (model for $\widehat{\mathbf{U}}^{\varphi}$), 8.37 (model for Σ), and equation 8.50 (model for δ) yields:

$$\mathbf{M}_{\varphi,h}\sim\frac{|\nabla\alpha_\varphi|}{\delta}\frac{\overline{\mu}^{\varphi}\,\overline{\mu}^{\phi}}{\overline{\mu}^{\varphi}+\overline{\mu}^{\phi}}\left(\overline{\mathbf{U}}^{\varphi}-\overline{\mathbf{U}}^{\phi}\right), \quad (8.66)$$

which is further written into a more exploitable form:

$$\mathbf{M}_{\varphi,h} = \lambda\left(Re_I, \pi_\mu\right) \frac{|\nabla \alpha_\varphi|}{\delta} \frac{\overline{\mu}^\varphi \, \overline{\mu}^\phi}{\overline{\mu}^\varphi + \overline{\mu}^\phi} \left(\overline{\mathbf{U}}^\varphi - \overline{\mathbf{U}}^\phi \right), \tag{8.67}$$

where the proportionality factor has been denoted as $\lambda\left(Re_I, \pi_\mu\right)$, representing a dimensionless friction coefficient which holds (unbalanced) tangential inertia and tangential shear contributions:

$$\lambda\left(Re_I, \pi_\mu\right) = m\, Re_I + n\, \pi_\mu, \tag{8.68}$$

where the parameters m and n have to be chosen appropriately; $m = 0.1 \ldots 1.5$ and $n \approx 8$ have proven adequate. From this, it is evident that the dissipative drag is a function of the relative phase velocity, that is the averaged slip velocity between the phases. Note that the interfacial Reynolds number is defined as

$$Re_I \equiv \frac{\rho\, \delta\, |\, \overline{\mathbf{U}}^\varphi - \overline{\mathbf{U}}^\phi |}{\alpha_\varphi \alpha_\phi \; \overline{\mu}^\varphi \, \overline{\mu}^\phi / (\, \overline{\mu}^\varphi + \overline{\mu}^\phi)}. \tag{8.69}$$

For the dimensionless group π_μ (viscous shear contribution), it is suggested:

$$\pi_\mu \equiv \frac{\alpha_\varphi \alpha_\phi \, \overline{\mu}^\varphi \, \overline{\mu}^\phi / \left(\alpha_\phi \, \overline{\mu}^\varphi + \alpha_\varphi \, \overline{\mu}^\phi \right)}{\overline{\mu}^\varphi \, \overline{\mu}^\phi / \left(\overline{\mu}^\varphi + \overline{\mu}^\phi \right)}. \tag{8.70}$$

In the view of the underlying microscopic shear flow scenario for closure – the numerator of the above expression has been chosen as the harmonic mean of the phase viscosities weighted with the respective volumetric phase fractions. This in fact is the correct viscosity value when the flow velocity is parallel to the interface. For the denominator, the corresponding local instantaneous analogue at the interface ($I_\varphi = I_\phi = 0.5$) has been chosen as dimensionless viscosity term. Note that this term is also present within our approach as given by equation 8.67.

Self-interaction Terms – $\overline{\boldsymbol{\tau}}^\varphi$ and $\overline{\boldsymbol{\tau}}^\phi$

A closure model for the conditional volume-averaged (viscous) shear stress tensor $\overline{\boldsymbol{\tau}}^\varphi$ is obtained by examining the conditional volume-averaged constitutive equation of the *local* shear stress tensor. For incompressible Newtonian fluids it is:

$$\boldsymbol{\tau} = -\mu \left(\nabla \mathbf{U} + (\nabla \mathbf{U})^T \right). \tag{8.71}$$

Conditional volume-averaging of equation 8.71 yields for phase φ:

$$\begin{aligned} \alpha_\varphi \, \overline{\boldsymbol{\tau}}^\varphi &= -\overline{I_\varphi \mu \left(\nabla \mathbf{U} + (\nabla \mathbf{U})^T \right)} = -\overline{I_\varphi \mu \nabla \mathbf{U}} - \overline{I_\varphi \mu \nabla \mathbf{U}^T} \\ &= -\nabla \left(\alpha_\varphi \, \overline{\mu \mathbf{U}}^\varphi \right) - \overbrace{(\mu \mathbf{U})\, \mathbf{n}_I}^{\varphi} \Sigma - \nabla \left(\alpha_\varphi \, \overline{\mu \mathbf{U}}^\varphi \right)^T - \overbrace{\mathbf{n}_I \, (\mu \mathbf{U})}^{\varphi} \Sigma. \end{aligned} \tag{8.72}$$

Thus, it follows with the decomposition for the local-instantaneous velocity into an interfacial averaged and an interface fluctuating velocity and using the product rule

$$\begin{aligned}\alpha_\varphi \overline{\boldsymbol{\tau}}^\varphi = &- \overline{\mu}^\varphi \nabla \left(\alpha_\varphi \overline{\mathbf{U}}^\varphi\right) - \overline{\mu}^\varphi \nabla \left(\alpha_\varphi \overline{\mathbf{U}}^\varphi\right)^T \\ &- \overbrace{\left(\mu \left(\widetilde{\mathbf{U}}^\varphi + \mathbf{U}^\sharp_{I,\varphi}\right)\right) \mathbf{n}_I}^{\varphi} \, \Sigma - \overbrace{\mathbf{n}_I \left(\mu \left(\widetilde{\mathbf{U}}^\varphi + \mathbf{U}^\sharp_{I,\varphi}\right)\right)}^{\varphi} \, \Sigma,\end{aligned} \tag{8.73}$$

For the first term it is

$$\begin{aligned}\overbrace{\left(\mu \left(\widetilde{\mathbf{U}}^\varphi + \mathbf{U}^\sharp_{I,\varphi}\right)\right) \mathbf{n}_I}^{\varphi} \, \Sigma &= \overbrace{\mu \widetilde{\mathbf{U}}^\varphi}^{\varphi} \widetilde{\mathbf{n}_I} \Sigma + \underbrace{\overbrace{\mu \mathbf{U}^\sharp_{I,\varphi}}^{\varphi}}_{=\mathbf{0}} \widetilde{\mathbf{n}_I} \Sigma \\ &= - \widetilde{\mu}^\varphi \, \widetilde{\mathbf{U}}^\varphi \nabla \alpha_\varphi.\end{aligned} \tag{8.74}$$

Finally:

$$\begin{aligned}\alpha_\varphi \overline{\boldsymbol{\tau}}^\varphi = &- \alpha_\varphi \overline{\mu}^\varphi \nabla \overline{\mathbf{U}}^\varphi - \overline{\mu}^\varphi \overline{\mathbf{U}}^\varphi \nabla \alpha_\varphi - \alpha_\varphi \overline{\mu}^\varphi \nabla \overline{\mathbf{U}}^{\varphi T} - \nabla \alpha_\varphi \overline{\mu}^\varphi \overline{\mathbf{U}}^\varphi \\ &+ \widetilde{\mu}^\varphi \widetilde{\mathbf{U}}^\varphi \nabla \alpha_\varphi + \widetilde{\mu}^\varphi \nabla \alpha_\varphi \widetilde{\mathbf{U}}^\varphi \\ \Rightarrow \quad \alpha_\varphi \overline{\boldsymbol{\tau}}^\varphi = &- \left(\alpha_\varphi \overline{\mu}^\varphi \left(\nabla \overline{\mathbf{U}}^\varphi + \nabla \overline{\mathbf{U}}^{\varphi T}\right)\right) \\ &- \left(\left(\overline{\mu}^\varphi \overline{\mathbf{U}}^\varphi - \widetilde{\mu}^\varphi \widetilde{\mathbf{U}}^\varphi\right) \nabla \alpha_\varphi + \nabla \alpha_\varphi \left(\overline{\mu}^\varphi \overline{\mathbf{U}}^\varphi - \widetilde{\mu}^\varphi \widetilde{\mathbf{U}}^\varphi\right)\right).\end{aligned} \tag{8.75}$$

By substituting closure models for $\widetilde{\mathbf{U}}^\varphi$ and with $\widetilde{\mu}^\varphi = \overline{\mu}^\varphi$, the conditional volume-averaged shear stress tensor $\overline{\boldsymbol{\tau}}^\varphi$ might be expressed in terms of averaged flow quantities for different flow types.

Substituting equation 8.44 for $\widetilde{\mathbf{U}}^\varphi$ into equation 8.75 yields

$$\begin{aligned}\alpha_\varphi \overline{\boldsymbol{\tau}}^\varphi = &- \left(\alpha_\varphi \overline{\mu}^\varphi \left(\nabla \overline{\mathbf{U}}^\varphi + \nabla \overline{\mathbf{U}}^{\varphi T}\right)\right) \\ &- \frac{\overline{\mu}^\varphi \overline{\mu}^\phi}{\overline{\mu}^\varphi + \overline{\mu}^\phi} \left(\left(\overline{\mathbf{U}}^\varphi - \overline{\mathbf{U}}^\phi\right) \nabla \alpha_\varphi + \nabla \alpha_\varphi \left(\overline{\mathbf{U}}^\varphi - \overline{\mathbf{U}}^\phi\right)\right).\end{aligned} \tag{8.76}$$

The first term holds the viscous stress contributions of the phase φ to itself, and the second accounts for phase slip, inducing viscous stress in phase φ due to relative motion with respect to phase ϕ. Note that $\nabla \alpha_\varphi$ ensures the latter contribution to be non-zero only inside the interfacial region.

It is interesting to note that Sun and Beckermann [49] found a similar term. However, it seems neither rational nor plausible that their phase slip contribution is proportional to the phase fraction α_φ, since strictly decomposing into terms $\sim \alpha_\varphi$ (i.e., bulk contribution) and terms $\sim \nabla \alpha_\varphi$ (i.e., a interfacial contribution) – as shown in equation 8.75 and its derivation – does not result in such an outcome. Drew and Passman [47] also proposed another closure for $\overline{\boldsymbol{\tau}}^\varphi$. However, their approach is case-sensitive, as it holds several *effective viscosities* for different flow scenarios, which is rather ponderous and avoided by the above approach.

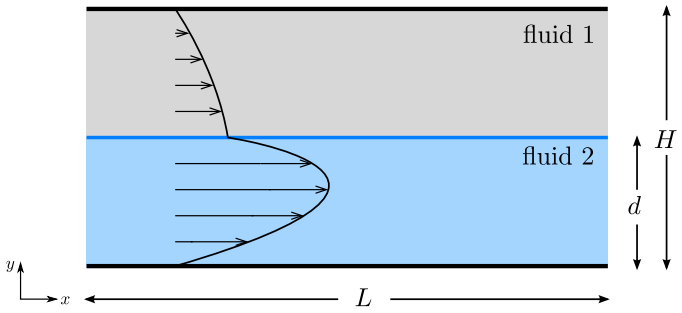

Figure 8.7: Stratified two-phase shear flow.

8.4. Simulation Results

The novel Eulerian-Eulerian multi-scale two-phase model will be validated for segregated flows against different pseudo-2D test cases at varying spatial resolutions. In doing so, the quality of the sub-grid closure models shall be assessed, as the role of modeled terms will become predominant with coarser meshes.

The implementation has been done in OpenFOAM v. 1.5-ext, a general purpose Open Source CFD tool providing a comprehensive C++ library for all kind of problems in computational continuum mechanics (CCM), [50, 51].

8.4.1. Tangential Interfacial Coupling – Stratified Two-Phase Shear Flow

A stratified flow scenario is examined in order to assess the *tangential interfacial coupling*. We shall examine the velocity profiles within both fluids that constitute the stratified two-phase flow. Due to continuity of shear stresses across the interface and different viscosities of the two fluids, the velocity profile will exhibit a sharp bend at the interface.

The flow domain under consideration is shown in figure 8.7. Two fluids are encompassed by two horizontal plates of length L at a distance H. The interface is at height d and parallel to the walls. For this simple duct flow we employ constant pressure boundary conditions [52], i.e., the pressure drop is fixed and given by $\Delta p = p(x = L) - p(x = 0)$. No-slip boundary conditions for the velocities are imposed on the walls and zero-gradient boundary conditions on the left side (inlet) and the right side (outlet). For the pressure, zero gradient boundary conditions are imposed on the walls, while fixed values are imposed on the inlet ($p(x = 0)$) and outlet ($p(x = L)$), respectively.

The material properties of the two-phase system are $\rho_1 = 1\,\mathrm{kg\,m^{-3}}$, $\rho_2 = 1\,\mathrm{kg\,m^{-3}}$, $\eta_1 = 1.85 \cdot 10^{-5}\,\mathrm{Pa\,s}$ and $\eta_2 = 5 \cdot 10^{-4}\,\mathrm{Pa\,s}$. The buoyancy and surface tension force have been neglected. The channel's length and height are $L = 0.04\,\mathrm{m}$ and $H = 0.02\,\mathrm{m}$ with the interface being positioned at $d = 0.01\,\mathrm{m}$. The pressure difference is $\Delta p = 0.0021\,\mathrm{Pa}$. The grid resolution in y-direction was varied from 15 over 20 to 25 cells. Model parameters for the unbalanced interfacial pressure and shear stress contributions have been set to $n = 0.13$, $n = 0.27$ and $n = 0.50$ for the coarse, mid and fine spatial resolution, respectively. The parameter m has been set constant: $m = 8.5$.

This test case is useful, since there is an analytical solution, derived in [53] and recapitulated in 8.A:

$$\mathbf{U}_{x,1}(y) = \frac{1}{2\eta_1}\frac{\partial p}{\partial x}\left(y^2 - \frac{H^2 + d^2\,(\eta_2/\eta_1 - 1)}{H + d\,(\eta_2/\eta_1 - 1)}\,y\right), \tag{8.77}$$

$$\mathbf{U}_{x,2}(y) = \frac{1}{2\eta_2}\frac{\partial p}{\partial x}\left(y^2 - \frac{H^2 + d^2\,(\eta_2/\eta_1 - 1)}{H + d\,(\eta_2/\eta_1 - 1)}\,y + \frac{(\eta_2/\eta_1 - 1)\,(Hd^2 - H^2 d)}{H + d\,(\eta_2/\eta_1 - 1)}\right). \tag{8.78}$$

Results of CFD simulations are shown in figure 8.8. In order to examine the quality of the results we perform a quantitative comparison of the simulation results with the corresponding reference solution as given by the equations 8.77 and 8.78. For this purpose, a percentage normalized error (PNE) is defined according to

$$PNE \equiv \max_{k=1}^{N}\left(\frac{\left|\phi_k - \phi_k^{\mathrm{ref}}\right|}{\max\left|\phi^{\mathrm{ref}}\right|}\right), \tag{8.79}$$

where ϕ_k denotes the respective quantity under consideration, c.q. $\mathbf{U}_x$. In doing so, we obtain a PNE of 2.69%, 1.22% and 1.69% for the coarse, intermediate and fine mesh resolution, respectively. Evidently, the PNE is higher for the finest spatial resolution than it is for both the intermediate and coarse one. An inherent error might arise from the fact that the interface position can only be *approximated* by an iso-surface, which is neither justified per se within an conditional volume-averaged framework nor exact in terms of phase volume conservation. Moreover, since the presented model framework is new, model uncertainties still have to be addressed, which is left for forthcoming studies. Using the standard solver *interFoam* as provided in OpenFOAM results in a PNE of 17.5% for a spatial resolution of 20 cells over the channel's height, for instance. Hence, our Eulerian-Eulerian multi-scale two-phase model HIRES-TFM has been found to outperform the state-of-the-art interface capturing model.

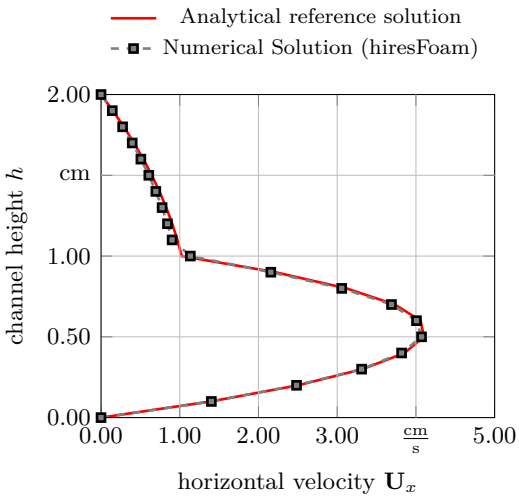

(a) coarse spatial resolution (60 x 15 mesh cells).

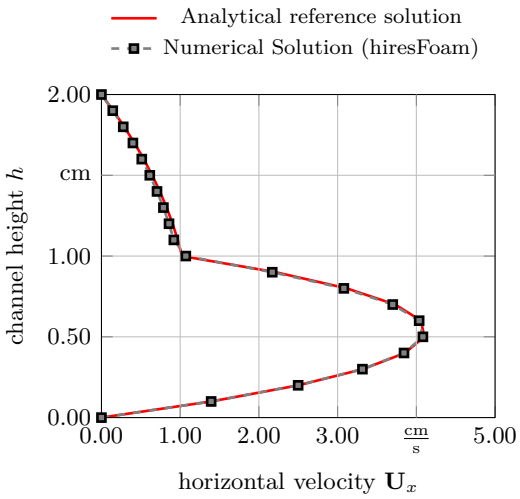

(b) intermediate spatial resolution (80 x 20 mesh cells).

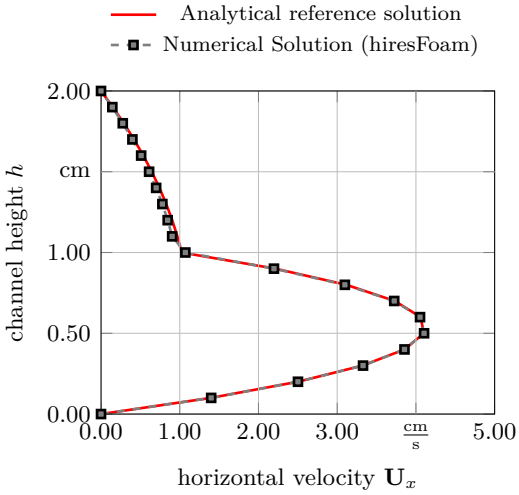

(c) fine spatial resolution (100 x 25 cells).

Figure 8.8: Velocity profile over channel height for stratified two-phase shear flow scenario.

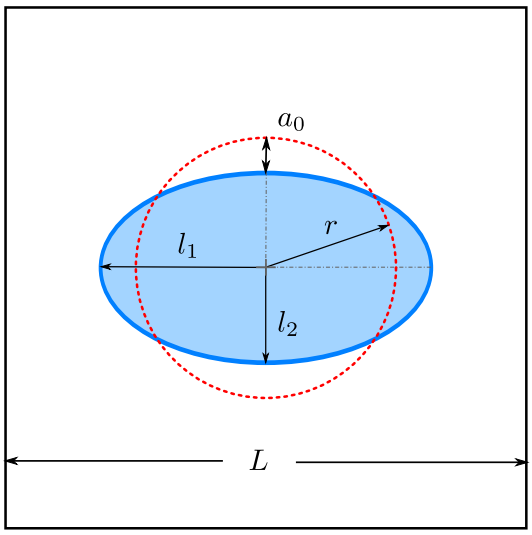

Figure 8.9: Oscillating viscous droplet.

8.4.2. Normal Interfacial Coupling – Oscillating Viscous Cylinder

The second test case deals with the *coupling in interfacial normal direction*. Consider an oscillating droplet in two dimensions under zero-gravity conditions. The oscillation is caused by surface tension and induced by an initial perturbation of the droplet shape: a ellipsoidal droplet. Due to its viscosity, the droplet will experience a damped oscillatory movement. The interplay of pressure and surface tension, and the influence of viscosity on the interface dynamics state the subject of the present test case.

The flow domain is shown in figure 8.9. Material properties of the two-phase system are $\rho_1 = 797.88\,\mathrm{kg\,m^{-3}}$, $\rho_2 = 1.1768\,\mathrm{kg\,m^{-3}}$, $\nu_1 = 1.346 \cdot 10^{-5}\,\mathrm{m^2\,s^{-1}}$ and $\nu_2 = 1.581 \cdot 10^{-5}\,\mathrm{m^2\,s^{-1}}$, corresponding to a methanol droplet (phase 1) in air (phase 2). The droplet with $r = 8.18535\,\mathrm{mm}$ equilibrium radius and $a_0 = 1.81465\,\mathrm{mm}$ initial distortion (corresponding to an initial major axis of $l_1 = 5 \cdot 10^{-3}\,\mathrm{m}$ and an aspect ratio equal to 0.667) has been placed into a squared cavity of $L = 75\,\mathrm{mm}$ edge length at zero-gravity condition. Note that the viscosity of the liquid phase has been increased artificially in order to pronounce viscous damping. Surface tension coefficient has been set to $\sigma = 0.02361\,\mathrm{kg\,s^{-2}}$. Numerical simulations have been performed for different spatial resolution, i.e., mesh densities of $48\,\mathrm{x}\,48$, $64\,\mathrm{x}\,64$ and $80\,\mathrm{x}\,80$ cells. In the remainder we will refer to these mesh resolutions as coarse, intermediate and fine. Model parameters for the unbalanced interfacial pressure and shear stress contributions have been set to $n = 1.60$, $n = 0.60$ and $n = 0.33$ for the coarse, intermediate and fine spatial resolution, respectively. The parameter m

has been set constant as for the previous case: $m = 8.5$. For the velocities, free-slip boundary conditions are imposed on the walls, while a total pressure boundary condition is utilized for the pressure.

Let r and a_0 be the radius of the spherical droplet in equilibrium and the magnitude of the initial distortion from this shape at the pole interface position as illustrated in figure 8.9. The oscillation frequency is given by [54, 55]

$$\omega_n = \sqrt{\frac{n(n+1)(n+2)\sigma}{((n+1)\rho_l + n\rho_g)\, r^3}}, \tag{8.80}$$

with the corresponding oscillation time period

$$\tau_n = \frac{2\pi}{\omega_n}, \tag{8.81}$$

where n denotes the mode of oscillation. Here, the primary mode ($n = 2$) applies.

Neglecting the viscosity of the ambient gas phase the viscous damping or decay factor might be written as reciprocal of the viscous damping time constant

$$\beta_\nu = 1/\tau_\nu \equiv (n-1)(2n+1)\frac{\nu_l}{r^2}. \tag{8.82}$$

A damped oscillatory motion for the temporal evolution of the envelope $e(t)$ of the amplitude distortion a(t) reads

$$e(t) = \pm\, a_0 e^{-t/\tau_\nu}, \tag{8.83}$$

which can be used for a quantitative assessment of numerical results.

Comparing the oscillation time period and viscous damping behavior with theoretical values according to equations 8.81 and 8.83 indicates a acceptable agreement as illustrated in figure 8.10. Approximating the interface position by an iso-surface at value $\alpha_\varphi = 0.5$, the normalized errors according to equation 8.79 for the maxima in the distortion amplitude and corresponding envelope values are 7.56%, 5.07% and 9.75% for the coarse, intermediate and fine resolution. The higher discrepancy for fine mesh resolution shows clearly that the presented models for the surface tension force density needs to be considered as a model framework; however, submodels – such as the algebraic model for the interfacial area density Σ – are subject to further research. This can be also seen from the deviation at early stages of the droplet's oscillatory movement on fine meshes. However, both the oscillation time period and the viscous damping behavior has been shown to reasonably match the expected values. Note that an inherent error might arise from the fact that the interface position can only be *approximated* by an iso-surface, which is neither justified per se within a conditional volume-averaged framework nor exact in terms of phase volume conservation.

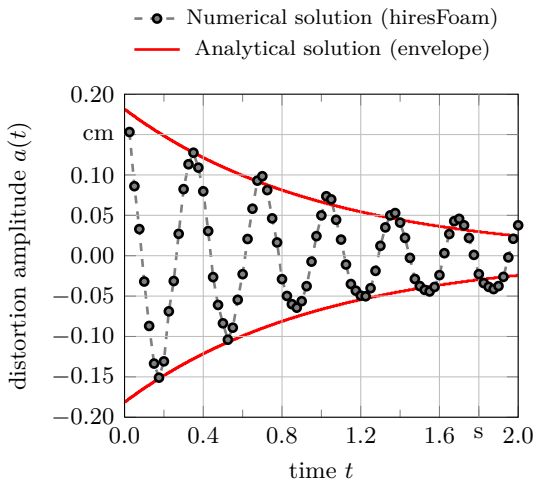

(a) coarse spatial resolution (48 x 48 cells).

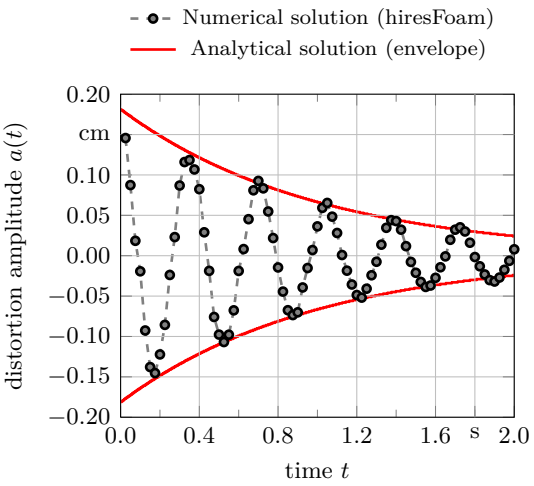

(b) intermediate spatial resolution (64 x 64 cells).

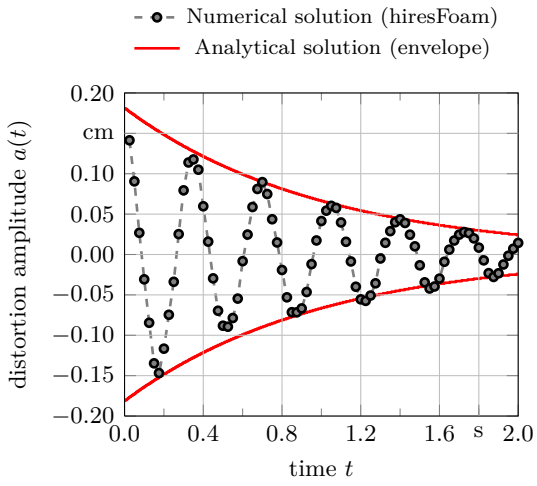

(c) fine spatial resolution (80 x 80 cells).

Figure 8.10: Temporal evolution of distortion amplitude for an oscillating viscous droplet.

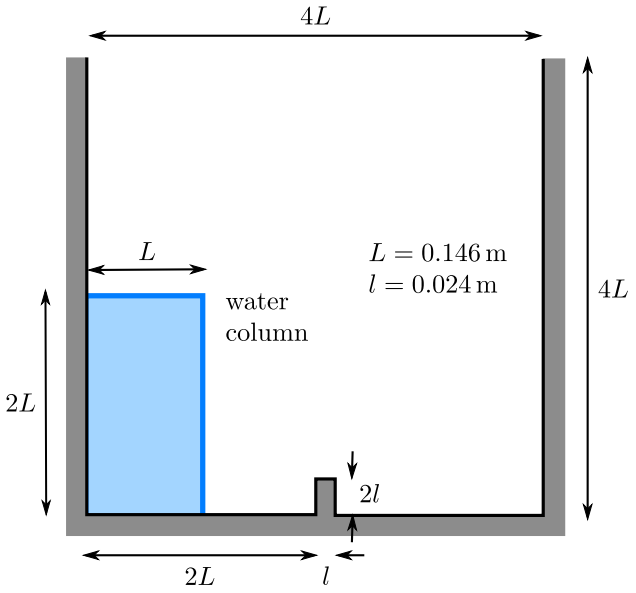

Figure 8.11: Dambreak with obstacle.

8.4.3. Inertia-dominated – Dambreak with Obstacle

Eventually, we consider a rather classical yet demanding test case for two-phase flow validation which combines the subject of interest of the previous ones: it involves both tangential and normal interfacial coupling, however, pronouncing the influence of inertia on interfacial dynamics, while additionally the flow morphology is subject to cross changes. We consider a water column, which initially is held back by a barrier. The initial setup and the geometry is shown in figure 8.11. Suddenly removing this barrier will cause the water to collapse, i.e., flow to the right, hitting the obstacle, flowing over it and finally hitting the opposite wall.

Numerical simulations have been performed at different spatial resolutions, that is for meshes of 23×23, 46×46 and 69×69 cells. We consider the air-water system with the following material properties: $\rho_1 = 1.0 \cdot 10^3\,\mathrm{kg\,m^{-3}}$, $\rho_2 = 1.0\,\mathrm{kg\,m^{-3}}$, $\nu_1 = 1.0 \cdot 10^{-6}\,\mathrm{m^2\,s^{-1}}$ and $\nu_2 = 1.48 \cdot 10^{-5}\,\mathrm{m^2\,s^{-1}}$. As illustrated in figure 8.11 the flow domain is bounded by walls except at its top boundary, where it is free to the atmosphere. At walls a Neumann boundary condition is imposed for the pressure, evaluating the normal pressure gradient from the local density gradient. As for the wall velocities, no-slip Dirichlet boundary conditions are imposed. At the top boundary of the flow domain both inflow and outflow is permitted – according to the internal flow within its interior. This is accomplished by a combination of boundary conditions for pressure and velocities in a way maintaining stability: for the velocities, a zero-gradient Neumann boundary condition is adopted, except where

there is an inflow, in which case the tangential velocity components are set to zero. The pressure is evaluated according to a fixed-value Dirichlet condition, which adjusts the pressure according to the local mixture velocity and a fixed total pressure. For turbulence modeling a simple $k-\epsilon$ model has been adopted.

A comparison with experimental results obtained by Koshizuka et al. [56] shows a good agreement – both qualitatively (figures 8.12 and 8.13) and quantitatively (figure 8.14). The water creates a complicated flow structure after subsequently hitting the obstacle and the opposite wall. Eventually, several pockets of captured air are formed, whereupon the water falls onto the floor letting the confined air escape upwards. During the entire process small droplets and bubbles are entrained from the continuous liquid phase and the continuous gas phase, respectively. However, since the applied model only involves closure terms for the segregated flow type, droplets or bubbles are not captured adequately. Only the main dynamics of the resolved interfacial structures of segregated type is captured. A generalization towards a full multi-scale two-phase flow model that is involving both dispersed flow types and segregated flow types will be presented in a forthcoming publication.

8.5. Conclusions & Outlook

A general multi-scale two-phase flow model framework is presented, that not only inherently encompasses both interfacial scale resolving and interfacial scale averaging approaches, but also consistently involves intermediate scale situations. By conditional volume-averaging the two-phase flow features are divided into an unresolved (averaged) and a resolved portion, in the same manner as this is accomplished by spatial filtering – known from single phase turbulence modeling when underlying the Large Eddy Simulation (LES) methodology. It is shown that the terms accounting for the unresolved portions can be grouped to additional terms within the set of governing equations. For closure these terms are to be interpreted according to the specific flow type under consideration and the averaging procedure applied. In doing so, two-phase flows of both dispersed and segregated type can be captured in one generalized Eulerian-Eulerian multi-scale two-phase model framework. This is accomplished by means of two conceptual approaches that enable us to describe transitions of flow regimes in a scale-consistent manner, namely the well-known '*concept of interpenetrating continua*' and the novel '*concept of partially penetrating continua*'.

This work focuses on modeling of two-phase systems of segregated flow type, presenting the development and validation of the concept of partially penetrating continua. One outstanding benefit of this practice is that one general form of the governing equation is retained, that is independent on the nature of the underlying two-phase flow type, while exhibiting the same basic structure as found for single-phase flows. This enables us to reuse numerical methodologies that originally have been developed

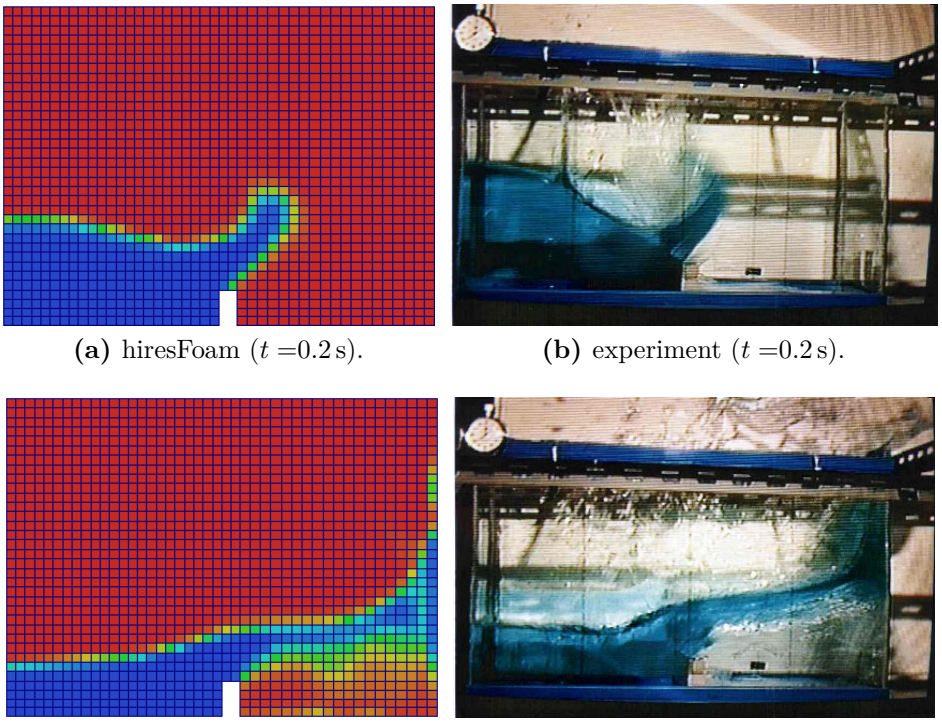

(a) hiresFoam (t =0.2 s). **(b)** experiment (t =0.2 s).

(c) hiresFoam (t =0.4 s). **(d)** experiment (t =0.4 s).

Figure 8.12: Qualitative comparison of numerical results with dambreak experiment – left: numerical results showing the phase fraction distribution (hiresFoam, 46 x 46 cells), right: high-speed imaging (experiment, Koshizuka et al. [56]).

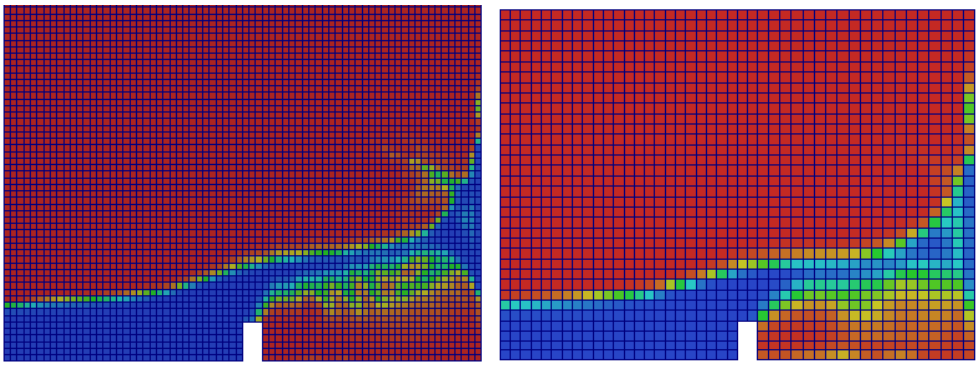

(a) 69 x 69 cells.

(b) 46 x 46 cells.

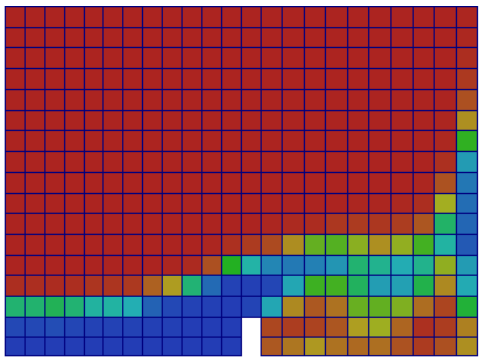

(c) 23 x 23 cells.

Figure 8.13: Qualitative comparison of numerical results showing the phase fraction at different spatial resolutions for the dambreak scenario with obstacle at t =0.4 s.

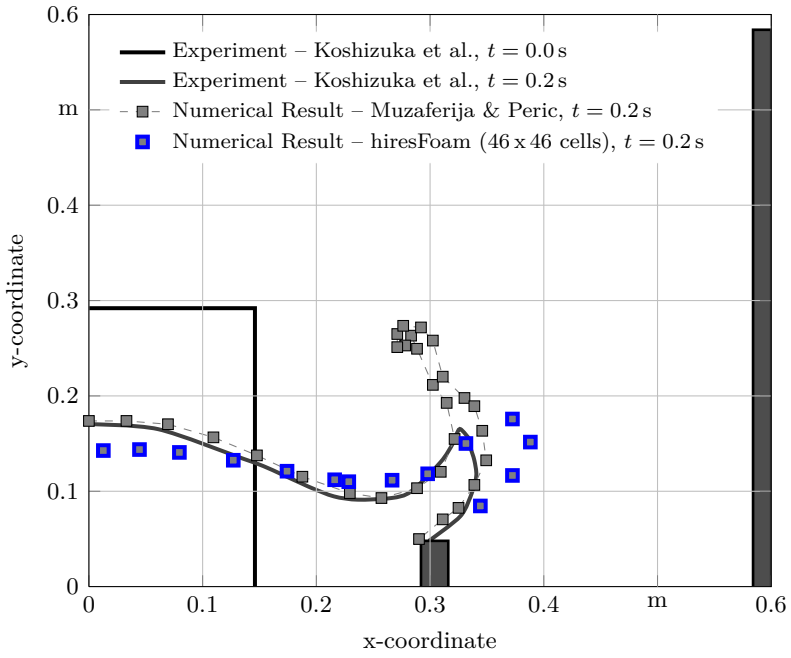

(a) 0.2 s.

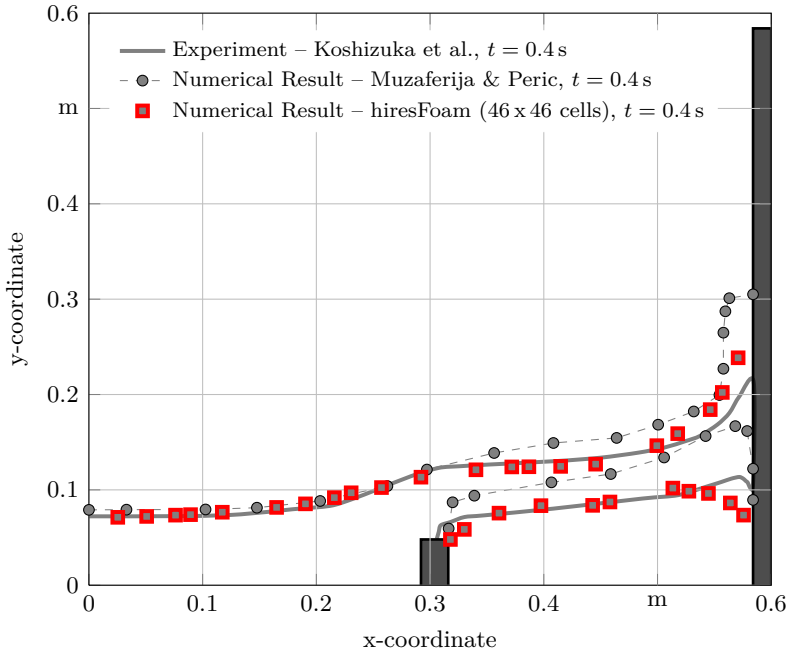

(b) 0.4 s.

Figure 8.14: Quantitative assessment of numerical results showing the interface position during a dambreak scenario with obstacle.

for single-phase flows for several broad classes of problems. Due to averaging the *resolved portions* of the two-phase flow are continuous and smooth (on the resolved scale), resulting in a robust and consistent representation of interfacial structures within the Eulerian framework. Another noteworthy remark needs to be made about the expectations: the presented two-phase model framework potentially opens up new avenues towards the simulation of turbulent two-phase flow systems due to the conceptual proximity to the well-established LES method.

The present model has been tested at different spatial resolutions considering benchmarks for two-phase flows of segregated type, in order to assess the quality of the corresponding closure. Two basic test cases have been examined covering the validation of coupling of phase momenta in tangential and normal direction to the interface – namely the *stratified shear flow* and the *oscillating viscous cylinder*. For each case, the numerical results are compared to analytical reference solutions. Good agreement is observed, which provides a solid base for assessing the potential of the model. The model framework is expected to be (at least more) general and applicable to a broad range of fundamental two-phase flow types. For this reason, another standard test case, that is a *dambreak with obstacle*, has been examined, in order to assess the model's reliability when being adopted to a two-phase flow with a greater scope of complexity than exposed by the above basic test cases. Owing to the complexity, there is no analytical solution to compare with and the comparison now needs to be based on experimental results. However, still a good agreement is observed.

The applicability of the Eulerian-Eulerian two-fluid approach has been found to be solely limited by its ability to accurately capture the characteristic features of the particular flow type under consideration. However, this eventually depends on the physical interpretation of closure terms, representing portions of the flow type that have become unresolved due to averaging. On the basis of the presented model framework, it is possible to realize the closure modeling for different flow types in *one generalized*, consistent and physically meaningful manner. In effect, such a model enables us to deal with two-phase flows of both dispersed type *and* segregated type, which is to be further developed in future publications.

8.A. Derivation of Analytical Validation Base

Stratified Two-Phase Shear Flow

The two-dimensional, incompressible continuity and momentum balance in x- and y-direction read:

$$\frac{\partial \mathbf{U}_x}{\partial x} + \frac{\partial \mathbf{U}_y}{\partial y} = 0 \tag{8.84}$$

$$\frac{\partial \mathbf{U}_x}{\partial t} + \mathbf{U}_x \frac{\partial \mathbf{U}_x}{\partial x} + \mathbf{U}_y \frac{\partial \mathbf{U}_x}{\partial y} = -\frac{1}{\rho}\frac{\partial p}{\partial x} + \frac{\eta}{\rho}\left(\frac{\partial^2 \mathbf{U}_x}{\partial x^2} + \frac{\partial^2 \mathbf{U}_x}{\partial y^2}\right) \tag{8.85}$$

$$\frac{\partial \mathbf{U}_y}{\partial t} + \mathbf{U}_x \frac{\partial \mathbf{U}_y}{\partial x} + \mathbf{U}_y \frac{\partial \mathbf{U}_y}{\partial y} = -\frac{1}{\rho}\frac{\partial p}{\partial y} + \frac{\eta}{\rho}\left(\frac{\partial^2 \mathbf{U}_y}{\partial x^2} + \frac{\partial^2 \mathbf{U}_y}{\partial y^2}\right) \tag{8.86}$$

The flow under consideration is an incompressible, two-dimensional, steady-state, developed channel flow (Poiseuille flow). Furthermore, it holds that $\mathbf{U}_y = 0$, resulting in $\frac{\partial \mathbf{U}_y}{\partial x} = 0$ and $\frac{\partial \mathbf{U}_y}{\partial y} = 0$. From continuity it follows that $\frac{\partial \mathbf{U}_x}{\partial x} = 0$, so that the only non-zero component of the velocity is $\mathbf{U}_x \neq 0$ and the only nonzero component of the velocity-gradient is $\frac{\partial \mathbf{U}_x}{\partial y} \neq 0$. Therefore, the momentum balances reduce to:

$$\eta\left(\frac{\partial^2 \mathbf{U}_x}{\partial y^2}\right) = \frac{\partial p}{\partial x} \quad \text{and} \tag{8.87}$$

$$\frac{\partial p}{\partial y} = 0. \tag{8.88}$$

From Eq. 8.88 it follows, that the pressure is only a function of the coordinate x: $p = p\,(x)$. Considering Eq. 8.87, the l.h.s. is only a function of y-coordinate, while the right hand side is only a function of x-coordinate. Consequently, Eq. 8.87 can only hold if both sides are constants:

$$\eta\left(\frac{\partial^2 \mathbf{U}_x}{\partial y^2}\right) = \frac{\partial p}{\partial x} = \mathbb{C}. \tag{8.89}$$

Integration results in:

$$\mathbf{U}_x(y) = \frac{1}{2\eta}\frac{\partial p}{\partial x} y^2 + \mathbb{C}_a y + \mathbb{C}_b. \tag{8.90}$$

Considering two fluids being separated by the horizontal interface at height $y = d$, as depicted in Fig. 8.7, results in:

$$\mathbf{U}_{x,1}(y) = \frac{1}{2\eta_1}\frac{\partial p}{\partial x}y^2 + \mathbb{C}_1 y + \mathbb{C}_2, \tag{8.91}$$

$$\mathbf{U}_{x,2}(y) = \frac{1}{2\eta_2}\frac{\partial p}{\partial x}y^2 + \mathbb{C}_3 y + \mathbb{C}_4. \tag{8.92}$$

The boundary conditions to determine the four constants are:

$$\mathbf{U}_{x,1}(y = 0) = 0, \tag{8.93}$$

$$\mathbf{U}_{x,2}(y = H) = 0, \tag{8.94}$$

$$\mathbf{U}_{x,1}(y = d) = \mathbf{U}_{x,2}(y = d) \text{ and} \tag{8.95}$$

$$\eta_1 \frac{\partial \mathbf{U}_{x,1}}{\partial y}|_{y=d} = \eta_2 \frac{\partial \mathbf{U}_{x,2}}{\partial y}|_{y=d}, \tag{8.96}$$

where the latter equation 8.96 follows from the condition $\tau_1|_{y=d} = \tau_2|_{y=d}$ at the interface. This results in:

$$\mathbb{C}_1 = \frac{-\frac{1}{2\eta_1}\frac{\partial p}{\partial x}\left(H^2 + d^2\left(\frac{\eta_2}{\eta_1} - 1\right)\right)}{H + d\left(\frac{\eta_2}{\eta_1} - 1\right)}, \tag{8.97}$$

$$\mathbb{C}_2 = 0, \tag{8.98}$$

$$\mathbb{C}_3 = \frac{-\frac{1}{2\eta_2}\frac{\partial p}{\partial x}\left(H^2 + d^2\left(\frac{\eta_2}{\eta_1} - 1\right)\right)}{H + d\left(\frac{\eta_2}{\eta_1} - 1\right)} \text{ and} \tag{8.99}$$

$$\mathbb{C}_4 = \frac{\frac{1}{2\eta_2}\frac{\partial p}{\partial x}\left(\frac{\eta_2}{\eta_1} - 1\right)(Hd^2 - H^2 d)}{H + d\left(\frac{\eta_2}{\eta_1} - 1\right)}. \tag{8.100}$$

References

[1] M. Wörner, W. Sabisch, G. Grötzbach, and D. G. Cacuci. Volume-averaged conservation equations for volume-of-fluid interface tracking. In *4th Int. Conf. on Multiphase Flow, ICMF 2001*, New Orleans, Louisiana, U.S.A, May 27 – June 1 2001. Michaelides, E. E. CD-ROM. 229

[2] W. Sabisch. *Dreidimensionale numerische Simulation der Dynamik von aufsteigenden Einzelblasen und Blasenschwärmen mit einer Volume-of-Fluid-Methode*. PhD thesis, Universität Karlsruhe, 2000. 229

[3] Y. Sun and C. Beckermann. Diffuse interface modeling of two-phase flows based on averaging: mass and momentum equations. *Physica D: Nonlin. Phenomena*, 198(3-4):281–308, 2004. 230

[4] Ronald P. Fedkiw, Tariq Aslam, Barry Merriman, and Stanley Osher. A non-oscillatory eulerian approach to interfaces in multimaterial flows (the ghost fluid method). *J. Comput. Phys.*, 152:457–492, July 1999. 230

[5] S. O. Unverdi and G. Tryggvason. A front tracking method for viscous incompressible flows. *J. Comp. Phys.*, 100:25–37, 1992. 230

[6] S. O. Unverdi and G. Tryggvason. Computations of multi-fluid flows. *Physica D: Nonlin. Phenomena*, 60:70–83, 1992. 230

[7] C. W. Hirt and B. D. Nichols. Volume Of Fluid (VOF) method for the dynamics of free boundaries. *J. Comput. Phys.*, 39(1):201–225, 1981. 230, 241

[8] F. H. Harlow and J. E. Welch. Numerical calculation of time-dependent viscous incompressible flow of fluid with free surface. *Phys. Fluids*, 8(12):2182–2189, 1965. 230, 241

[9] J. A. Sethian. *Level Set Mehods: Evolving interfaces in geometry, Fluid mechanics, computer vision, and material science*. Cambridge Univ. Press, 1996. 230, 241

[10] G. Černe. *Two-Fluid Flow Simulation with the Coupling of Volume-Of-Fluid Model and Two-Fluid Model*. PhD thesis, University of Ljubljana, Faculty of Mathematics and Physics (Department of Physics), 2001. 230

[11] G. Černe, S. Petelin, and I. Tiselj. Upgrade of the VOF method for the simulation of the dispersed flow. In *ASME Fluids Eng. Division Summer Meeting*, Boston, Massachusetts, 2000. 230

[12] G. Černe, S. Petelin, and I. Tiselj. Coupling of the interface tracking and the two-fluid models for the simulation of incompressible two-phase flow. *J. Comput. Phys.*, 171(2):776–804, 2001. 230

[13] G. Černe, S. Petelin, and I. Tiselj. Numerical errors of the volume-of-fluid interface tracking algorithm. *Int. J. Numer. Meth. Fluids*, 38:329–350, 2002. 230

[14] A. Tomiyama and N. Shimada. (N+2)-field modeling for bubbly flow simulation. *Comp. Fluid Dyn. J.*, 9(4):418–426, 2001. 230

[15] A. Tomiyama and N. Shimada. A numerical method for bubbly flow simulation based on a multi-fluid model. *J. of Pressure Vessel Technology*, 123(4):510–516, 2001. 230

[16] A. Tomiyama, N. Shimada, I. Zun, T. Noguchi, and T. Yakawa. NP2-3D: An (N+2)-field model for computing mesoscale and macroscale multiphase flows. In *ASME FEDSM2001-18191*, 2001. 230

[17] A. Tomiyama, N. Shimada, and H. Asano. Application of number density transport equation for the recovery of consistency in multi-fluid model. In *4th ASMER-JSME Joint Fluids Eng. Conf. (CD-ROM)*, pages 1–7, 2003. FEDSM'03 No.45168. 230

[18] A. Tomiyama, K. Sakoda, K. Hayashi, A. Sou, N. Shimada, and S. Hosokawa. Modeling and hybrid simulation of bubbly flow. In *Japan-US Sem. on Two-Phase Flow Dynamics*, December 6-11 2004. 230

[19] A. Tomiyama, K. Sakoda, K. Hayashi, A. Sou, N. Shimada, and S. Hosokawa. Modeling and hybrid simulation of bubbly flow. *Multiphase. Sci. Tech.*, 18(1):73–110, 2006. 230

[20] A. Alajbegovic and J. Han. Simulation of multiphase flows in complex geometry using a hybrid method combining the multi-fluid and the Volume-of-Fluid (VOF) approaches. In *ASME Joint U.S.-European Fluids Eng. Conf. (Fluids2002)*, pages 887–892, Montreal, Quebec, Canada, July 14-18 2002. 230

[21] H. Yoshida, A. Ohnuki, K. Takase, M. Kureta, H. Akimoto, H. Okada, and K. Yamamoto. Development of mechanistic boiling transition model in rod bundles. In *11th Int. Conf. Nucl. Eng.*, April 20-23 2003. ICONE-11-36097. 230

[22] H. Yoshida, H. Tamai, K. Takase, T. Nagayoshi, and H. Akimoto. Development of predictable technology for thermal/hydraulic performance of reduced-moderation water reactors (3) – Current status of development of three-dimensional two-phase flow simulation method. In *Int. Congr. on Adv. Nucl. Power Plants - ICAPP 2004*, 2004. 230

[23] H. Yoshida, A. Ohnuki, T. Misawa, K. Takase, and H. Akimoto. Development of analytical procedures on two-phase flow in tight-lattice fuel bundles for innovative water reactor for flexible fuel cycle (FLWR). In *Int. Congr. Adv. Nucl. Power Plants - ICAPP 2006*, pages 1593–1600. American Nuclear Society, 555 North Kensington Avenue, La Grange Park, IL 60526 (United States), American Nuclear Society - ANS, La Grange Park (United States), 2006. 230

[24] H. Yoshida. Draft Report – Development of analytical procedures on two-phase flow in tight-lattice fuel bundles for innovative water reactor for flexible fuel cycle (FLWR). Personal Communication, July 2007. 230

[25] A. Minato, K. Takamori, and N. Ishida. An extended two-fluid model for interface behavior in gas-liquid two-phase flow. In *8th Int. Conf. Nucl. Eng., ICONE 8*, volume 6 of *Part A*, pages 27–35, April 2-6 2000. 230

[26] A. Minato, T. Nagayoshi, M. Misawa, A. Suzuki, H. Ninokato, and S. Koshizuka. Numerical simulation method of complex 3D gas-liquid two-phase flow. In *5th Int. Conf. Multiphase Flow, ICMF 2004*, pages 1–11, May 30 - June 4 2004. 230

[27] A. Minato, T. Nagayoshi, and K. Takamori. Numerical simulation of gas-liquid two-phase flow in siphon outlets of pumping plants. available online at http://www.hitachi-pt.com/products/si/pump/pdf/pump_04.pdf, January 2008. 230

[28] A. Minato, N. Nakajima, and T. Nagahara. Simulation of two-phase flow in pumping stations. In *Advances in the Modeling Methodologies of Two-Phase Flows*, 2004. 230

[29] A. Minato, N. Nakajima, and T. Nagahara. Simulation of two-phase flow in pumping stations. *La Houille Blaunche*, 1:59–64, 2006. 230

[30] A. Minato, N. Nakajima, T. Nagahara, and K. Kariya. Three-dimensional two-phase flow simulation of siphon self-priming in pumping stations. In *23rd IAHR Symp. Hydraulic Machinery and Systems*, pages 1–6, 2006. 230

[31] T. Nagayoshi, A. Minato, M. Misawa, A. Suzuki, M. Kuroda, and N. Ichikawa. Simulation of multi-dimensional heterogeneous and intermittent two-phase flow by using an extended Two-Fluid Model. *J. Nucl. Sci. Technol.*, 40(10):827–833, 2003. 230

[32] L. Štrubelj. *Numerical Simulations of Stratified Two-Phase Flows with Two-Fluid Model and Interface Sharpening*. PhD thesis, University of Ljubljana, Faculty of Mathematics and Physics (Department of Physics), 2009. 230

[33] L. Štrubelj, I. Tiselj, and B. Mavko. Simulations of free surface flows with implementation of surface tension and interface sharpening in the two-fluid model. *Int. J. Heat Fluid Flow*, 30(4):741–750, 2009. 230

[34] C. Morel. Modeling approaches for strongly non-homogeneous two-phase flows. *Nucl. Eng. Des.*, 237(11):1107–1127, 2007. 230

[35] M. Ishii. Two-Fluid Model for two-phase flow. *Multiphase. Sci. Tech.*, 5(1-4):1–63, 1990. 231, 241

[36] H. G. Weller. The Development of a New Flame Area Combustion Model Using Conditional Averaging. Technical report, Thermo-Fluids Section Report TF 9307, Imperial College of Science, Technology and Medicine, 1993. 235, 236

[37] H. G. Weller. Derivation, Modelling and Solution of the Conditionally Averaged Two-Phase Flow Equations. Technical report, OpenCFD Limited, 2005. 235

[38] C. Dopazo. On conditioned averages for intermittent turbulent flows. *J. Fluid Mech.*, 81(03):433–438, 1977. 235

[39] A. Toutant. *Physical Modelling of Interactions between Interfaces and Turbulence*. PhD thesis, CEA-Grenoble and IMF-Toulouse, 2006. 240

[40] A. Toutant, E. Labourasse, O. Lebaigue, and O. Simonin. DNS of the interaction between a deformable buoyant bubble and a spatially decaying turbulence: A priori tests for LES two-phase flow modelling. *Comput. Fluids*, 37(7):877–886, 2008. 240

[41] A. Toutant, M. Chandesris, D. Jamet, and O. Lebaigue. Jump conditions for filtered quantities at an under-resolved discontinuous interface. Part 1: Theoretical development. *Int. J. Multiphase Flow*, 35(12):1100–1118, 2009. 240

[42] A. Toutant, M. Chandesris, D. Jamet, and O. Lebaigue. Jump conditions for filtered

quantities at an under-resolved discontinuous interface. Part 2: A priori tests. *Int. J. Multiphase Flow*, 35(12):1119–1129, 2009. 240

[43] Sarah Monahan. *Computational Fluid Dynamics Analysis of Air-Water Bubble Columns*. PhD thesis, Iowa State University, 2007. 242

[44] Dongsheng Zhang. *Eulerian Modeling of Reactive Gas-Liquid Flow in a Bubble Column*. PhD thesis, University Twente, 2007. 242

[45] J. M. Donbar, J. F. Driscoll, and C. D. Carter. Reaction zone structure in turbulent nonpremixed jet flames. *Combustion and Flame*, 122:1–19, 2000. 248

[46] D. Bestion. The physical closure laws in the CATHARE code. *Nucl. Eng. Des.*, 124(3):229–245, 1990. 249

[47] D. A. Drew and S. L. Passman. *Theory of Multicomponent Fluids*. Number 135 in Applied mathematical sciences. Springer, New York, NY [u.a.], 1999. 249, 253

[48] S. T. Munkejord. *Analysis of the Two-Fluid Model and the Drift-Flux Model for Numerical Calculation of Two-Phase Flow*. PhD thesis, Norwegian University of Science and Technology, 2005. 249

[49] C. Beckermann and Y. Sun. Diffuse interface modeling of two-phase flows based on averaging: Mass and momentum equations. *Physica D: Nonlinear Phenomena*, 198(3-4):281–308, 2004. 253

[50] H. G. Weller, G. Tabor, H. Jasak, and C. Fureby. A tensorial approach to computational continuum mechanics using object orientated techniques. *Comput. Phys.*, 12(6):620–631, 1998. 254

[51] H. Jasak, A. Jemcov, and Ž Tuković. OpenFOAM: A C++ library for complex physics simulations. In *International Workshop on Coupled Methods in Numerical Dynamics IUC*, Dubrovnik, Croatia, September, 19-21 2007. 254

[52] Henk Kaarle Versteeg and Weeratunge Malalasekera. *An introduction to computational fluid dynamics: the finite volume method*. Pearson Education, January 2007. 254

[53] N. Coutris, J.M. Delhaye, and R. Nakach. Two-phase flow modelling: the closure issue for a two-layer flow. *International Journal of Multiphase Flow*, 15(6):977 – 983, 1989. 255

[54] H. Lamb. *Hydrodynamics*. Oxford Univ. Press, Oxford, 6. ed. edition, 1932. 258

[55] A. Prosperetti. Free oscillations of drops and bubbles: the initial-value problem. *J. Fluid Mech.*, 100:333–347, 1980. 258

[56] S. Koshizuka, H. Tamako, and Y. Oka. A particle method for incompressible viscous flow with fluid fragmentation. *Comp. Fluid Dyn. J.*, 4:29–46, 1995. 261, 262

Closure

9

Summary & Outlook

9.1. Summary and Closing Comments

Many applications in chemical and process engineering possess two-phase flows of different types – often involving both a continuous cascade of temporal and spatial scales varying over orders of magnitude (multi-scale) and multiple coupled phenomena (multiphysics).

The Eulerian-Eulerian two-fluid approach certainly exhibits the most promising and developable features to treat these kinds of flows in one generalized and consistent model framework. It is rooted in fundamental local-instantaneous conservation equations, i.e., the Navier-Stokes equations, that themselves are valid within each phase up to the interface separating the phases. An appropriate conditional averaging procedure (based on the immersed interface concept) and subsequent closure modeling on a sound physical basis constitute the steps of a clear and mathematical rigour derivation procedure, the two-fluid approach relies upon. By conditional volume-averaging, the two-phase flow features are divided into an *unresolved (averaged)* and a *resolved portion*, in the *same manner* as this is accomplished by spatial filtering – known from single phase turbulence modeling when underlying the Large Eddy Simulation (LES) methodology.

In this work, it is shown that all model terms that account for *unresolved portions* can be grouped to additional terms within the set of governing equations. For closure these terms are to be interpreted according to the specific flow type under consideration *and* the averaging procedure applied. In doing so, one general form of the governing equations is retained, that is not depending on the nature of the underlying two-phase flow type while exhibiting the same basic structure as found for single-phase flows. It is on this general equation structure that numerical methods in the field of CMFD hinge. Advantageously, this enables us to reuse numerical

methodologies that originally have been developed for single-phase flows for several broad classes of problems. Moreover, due to averaging the *resolved portions* of the two-phase flow are found to be continuous and smooth (on the resolved scale), inherently resulting in a robust and consistent representation of interfacial structures within the Eulerian framework. This is independent of the flow type. However, the physical interpretation of closure terms, and thus, their concrete forms and treatments might change significantly for different flow types. Through the course of this study it has become clear that applying conditional volume-averaging (adopting the immersed interface concept) for some cases just yields well-established models, namely the two-fluid model for dispersed two-phase flows (concept of interpenetrating continua), while others correspond to entirely unexplored two-phases flow scenarios which yet have not been treated with the two-fluid approach (concept of partially penetrating continua), as for instance under-resolved free-surface flows of segregated flow type.

The applicability of the employed Eulerian two-fluid approach has been found to be solely limited by its ability to accurately capture the characteristic features of the particular flow type under consideration. However, this eventually depends on the physical interpretation of closure terms, representing portions of the flow type that have become unresolved due to averaging. On the basis of the presented model framework, it is possible to realize the closure modeling in *one generalized (common)*, consistent and physical meaningful (averaged) manner.

9.2. Outlook and Future Work

Certainly, the novel field of research stating the scientific subject of this thesis has just evolved and leaves much to be examined. In this view, further developments should aim at

analysis and recapitulation of well-established models allowing further insights and enabling to physical interpretations: For example, the Continuous-Surface-Force (CSF) method of Brackbill for surface tension modeling in an Eulerian framework, indeed relies upon the assumption that the radius of the interfacial curvature is larger than the interfacial filter width (length scale characterizing the averaging volume). Hence the CSF is not capable of capturing non-resolved interfacial features being beyond the applied filter scale – in the sub-filter scale (SFS) region. However, in this view, the application of the CSF method is *not restricted* to local-instantaneous formulations being treated within an Eulerian framework. It is rather about complementing the CSF methodology by SFS models taking into account unresolved portions of the interfacial structure under consideration by underlying the presented generalized model framework. This in turn already means an extension towards multi-scale two-phase flow scenarios, since the features have been divided into resolved and unresolved components by use of conditional volume-averaging.

extension and enhancement of novel model approaches that have educed from the adoption of the model framework to flow types that have been unexplored in this context up to now. As the consistent model framework enables us to examine its extremes of applicability, that is the interfacial scale being fully resolved and the interfacial scale being completely unresolved, model enhancements can be achieved by analyzing results and comparing them with results from simulations performed for these extremes – however, by established approaches with known closure quality.

Furthermore, physical assumptions that have been inherently presumed when stating the local-instantaneous conservation equations and corresponding jump conditions should be varied in a subsequent step. For instance, the assessment of viscosity obeying Newton's law or the existence of a sharp interface under surface tension might be altered in order to examine Non-Newtonian two-phase flows or to revisit diffuse interface models being thermodynamically motivated (e.g., phase-field methods). This certainly would reveal new insights into both the numerical treatment and the physical significance of model approaches being currently state-of-the-art.

Lastly, other flow variables such as energy, for instance, should be taken into account. Along with models for mass, momentum and chemical species, which have been presented in this thesis, reacting two-phase system could be addressed and examined at different scales of interest – micro-, meso- and macroscale.

full multi-scale two-fluid model that is able to simultaneously capture dispersed and segregated flow types in one flow domain (mixed flow type). The governing equations of the multi-scale model framework, that has been developed in this study, have one general form which is independent from the underlying two-phase flow type. Nevertheless, model terms are to be interpreted according to the specific flow type under consideration. However, since the model terms are based on the same conditional averaging procedure (same spatial filter), the treatment of mixed flow types can be accomplished in a scale-consistent manner, which means that flow regime transitions (from dispersed to segregated flow type, or vice versa) can be dealt with by a switch or transition factor in front of these model terms. It is surely necessary to do further research in order to arrive at such a *flow regime discrimination* practice that is both reliable and consistent. It is the author's belief that this has to be based upon the same conceptual approach (immersed interface concept) and the same methodology (conditional volume-averaging / spatial filtering) as for the underlying model framework.

Appendix

A

Subject Index

A

algorithm
- PISO 127
- PISO, single-phase 129
- PISO, two-phase 131
- pressure equation 129
- Rhie-Chow interpolation ... 128

averaging rules
- commutation 39
- idempotence 39
- linearity 39

B

boundary condition
- Dirichlet 113
- von Neumann 114

C

closure modeling 36, 60
- interfacial area density 66
- interfacial averaged curvature 66
- interfacial averaged unit normal 66
- interfacial averaged velocity . 67
- interfacial transport 84
- interfacial width 80
- momentum transfer 71
- phase-interaction terms 71
- self-interaction terms 82

closure terms
- phase-interaction terms 60
- self-interaction terms 60
- turbulence terms 60

concept of immersed interfaces ... 3
concept of interpenetrating continua 64, 69
concept of partially penetrating continua 64
conditional volume-averaged
- continuity equation 53
- interfacial mass jump condition 55
- interfacial momentum jump condition 55
- interfacial species jump conditions 56
- momentum equation 53
- species equation 54

conditional volume-averaging 44
conditioned interface-average 51
conditioning 32
consistency requirement 99
constitutive model ..... *see* closure modeling

D

density-weighted average 47
density-weighted volume fraction 48

domain discretization 96

E

ensemble-averaging 38
equation discretization 96, 98
  central differencing 101
  convection boundedness criterion 103
  convection term 101
  differencing scheme 101
  diffusion term 106
  Gamma scheme 104
  inter-Gamma scheme 104
  non-orthogonal correction .. 107
  Normalised Variable Approach . 103
  source term 108
  upwind differencing 102

G

Gauss' theorem 25, 100
general balance
  single-phase flow 25
  two-phase flow 29
generic interfacial jump condition 30
generic transport equation 26
governing equations
  single-field equations 88
  two-field equations 85

I

immersed interface concept 32
interface average 51
interface delta function 34
interface transport equation
  local instantaneous 34
  volume-averaged 56
interfacial area density 51
interfacial momentum transfer ... 54
interfacial scale averaging 3, 60
interfacial scale resolving 3, 60
isotropic interfacial morphology . 66

J

jump notation 31

L

Leibniz' theorem 25
local instantaneous
  continuity equation 27
  interfacial jump condition for mass 31
  interfacial jump condition for momentum 31
  interfacial jump condition for species 32
  momentum equation 27
  species equation 28

M

matrix
  diagonal dominance 125
  diagonal equality 125
mixture quantities 88
  center-of-mass velocity 88
  interfacial friction tensor 91
  mixture density 88
  mixture pressure 88, 121
  mixture viscosity 88
  momentum drift-flux term ... 91
  phase relative velocity 88

O

OpenFOAM 97

P

phase discrimination 32
phase distribution function 33
phase indicator function 32
phase mass fraction 48
phase volume fraction 44, 48
phase-weighted average 47
phasic or intrinsic average 44

R

Reynolds decomposition 46

Reynolds stress 54

S

scale similarity hypothesis 61
solution method
    explicit 124
    implicit 125
spatial discretization 97
    cell face 97
    control volume 97
spatial filtering
    box filter 45
    Gaussian filter 45
    top-hat filter 45
surface average 52
surface fluctuation 52

T

temporal discretion 98
    time step 98
tensor notation xi
time integration
    backward differencing method 112
    Crank-Nicholson method ... 111
    Euler explicit method 111
    Euler implicit method 111
    time level 109
time-averaging 38

V

volume-averaging 37
volumetric phase fraction 44, 48

B

Declaration

This work has been supervised and reviewed by Prof. Dr.-Ing. Kai-Olaf Hinrichsen (Technische Universität München – Lehrstuhl I für Technische Chemie).

Hereby, I declare that this document and the accompanying code has been composed by myself and describes my own work, unless otherwise acknowledged in the text by clear cross-referencing to author, work and page(s). No other person's work has been used without due acknowledgement and/or prior permission. All verbatim extracts have been distinguished by quotation marks. Any illustrations which are not the work of the author of this dissertation have been used with the explicit permission of the originator. All sources of information have been specifically acknowledged.

Furthermore, I certify that I have not submitted the same, a substantially similar, or a different document to another postsecondary school or any other tertiary institution as dissertation or as thesis for evaluation in a similar context.

I am familiar with the relevant course of examination for doctoral candidates at the Technische Universität München (Promotionsordnung). I hereby affirm the above statements to be complete and true to the best of my knowledge.

Garching, December 20, 2011 Holger Marschall

C

List of Publications

Results of this work have partly been published in or submitted for peer-review to international journals and proceedings of international conferences. As of December 20, 2011, there are the following publications related to this thesis and included as individual chapters (in *Results & Publications*):

[1] H. Marschall, R. Mornhinweg, A. Kossmann, S. Oberhauser, K. Langbein, and O. Hinrichsen. Numerical simulation of dispersed gas/liquid flows in bubble columns at high phase fractions using OpenFOAM®. Part I – Modeling basics. *Chem. Eng. Technol.*, 34(8):1311–1320, 2011.

[2] H. Marschall, R. Mornhinweg, A. Kossmann, S. Oberhauser, K. Langbein, and O. Hinrichsen. Numerical simulation of dispersed gas/liquid flows in bubble columns at high phase fractions using OpenFOAM®. Part II – Numerical simulations and results. *Chem. Eng. Technol.*, 34(8):1321–1327, 2011.

[3] H. Marschall, K. Hinterberger, C. Schüler, and O. Hinrichsen. Numerical simulation of species transfer across fluid interfaces in free-surface flows using OpenFOAM®. submitted to Chem. Eng. Sci., 2011.

[4] H. Marschall and O. Hinrichsen. Numerical simulation of multi-scale two-phase flows using a hybrid interface-resolving two-fluid model (HIRES-TFM). In *Proceedings of 1st Symposium on Multi-scale Multiphase Process Engineering*, Kanazawa, Japan, 2011.

[5] H. Marschall, H. Jasak, F. Habla, and O. Hinrichsen. Towards the numerical simulation of multi-scale two-phase flows – Hybrid Interface-Resolving Two-Fluid Model (HIRES-TFM). to be submitted, 2011.